Development of lanthanide probes for cellular imaging

Kielar, Filip

Development of Lanthanide Probes for Cellular Imaging

Filip Kielar

A thesis submitted for the degree of Doctor of Philosophy

Department of Chemistry

Durham University

2008

I may be wrong and you may be right, and by an effort, we may get nearer to truth.

Karl R. Popper

Abstract

Luminescent complexes of europium and terbium, incorporating new sensitizing chromophore moieties containing carboxylic acid functional groups, have been synthesised. It has been shown that the new tetraazatriphenylene chromophore leads to highly emissive complexes. A thiaxanthone chromophore, despite sensitizing lanthanide emission, results in complexes with lower quantum yields and is only practically useful for europium.

Modification of the azaxanthone chromophore by formation of its N-oxide was investigated as a possibility of extending its longest wavelength absorption maximum beyond 340 nm.

Phosphinate pendant arms were introduced into complexes containing the azaxanthone chromophore and resulted in highly emissive complexes

Complexes of the new chromophores were investigated, together with numerous further examples, in terms of their susceptibility to quenching by electron rich species (iodide, ascorbate, urate). These experiments enhanced the mechanistic understanding of this process.

Complexes using an azaxanthone chromophore with a carboxylic function and phenyl amide arms were used in coupling reactions. The coupling reactions involved isolation of the NHS ester of the complex. Cellular uptake and cytotoxicity experiments were carried out with several of these conjugate complexes. The possibility to observe these complexes using two photon excitation fluorescence microscopy was demonstrated.

Declaration

The work described herein was carried out in the Department of Chemistry, University of Durham between October 2004 and December 2007. All of the work is my own; no part has previously been submitted for a degree at this or any other university.

Statement of Copyright

Acknowledgements

I would like to thank my supervisor Prof. David Parker, for giving me the opportunity to conduct my PhD research in his group. Furthermore, I would like to thank him for all the help and support he has given me, as well as for the knowledge and experience that I have gained over the last three years.

I would also like to thank all the members of analytical services of Chemistry Department of Durham University. In particular I would like to thank Dr. Alan Kenwright, Catherine Hefferman and Ian McKeag for their assistance with NMR spectroscopy and to Dr. Mike Jones, Dr Jackie A. Mosely and Lara Turner for their advice and assistance with mass spectrometry measurements. Thanks also to Jarka Dostal for measurement of C, H, N microanalysis.

I would like to thank Dr. Andrew Beeby and his group for the measurement of low temperature phosphorescence spectra. I would like to thank Dr. Aileen Congreve for the flow cytometry measurements. I would like to thank Dr. Olof Pålsson for the measurement of two photon excitation spectra and quantum yields.

Outside of the department I would like to thank Dr. Chriss Ottley for the ICP-MS measurements and Dr. R. D. Peacock for the measurement of the CPL spectra.

I am also very grateful to our collaborators Prof. Ivan Lukeš, Dr. Petr Herman and Zuzana Jandurová from Prague as well as Dr. Javier de Mendoza and Dr. Pilar Prados from Barcelona, with whom we have embarked on interesting research projects.

I would like to also thank some of the present and past members of our group for their contribution to my research. I would like to thank Dr. Robert A. Poole for his assistance during his time in Durham and for the continued collaboration after his move to CisBio international in France. I would like to thank Dr. Phillip Stenson for cyclic voltametry measurements. I would like to thank Dr. Ga-Lai Law for her help especially for the two photon microscopy work she has done in Hong-Kong. I would also like to thank Elizabeth J. New for her help especially for the measurements of the IC_{50} values and for the flow cytometry experiments.

I would like to thank the past and present members of the Parker group for creating a good and friendly working atmosphere. Here I would like to especially thank Elisa M. Elemento, who has been the closest friend with whom I have shared the ups and downs of my time in Durham in and out of the laboratory.

I would like to thank my parents, Ljuba and Pavel Kielarovi, for their continued support during my PhD. studies.

Abreviations

ATP	Adenosine triphosphate
Arg	Arginine
BODIPY	Boron, difluoro[2-[(2H-pyrrol-2-ylidene-κN)methyl]-1H-pyrrolato-κN]-
CoA	Coenzyme A
CPL	Circularly Polarized Luminescence
CPP	Cell Penetrating Peptide
DCM	Dichloromethane
DMF	Dimethylformamide
DMSO	Dimethylsulphoxide
DO3A	1,4,7-*tris*(*tert*butoxycarbonylmethyl)-1,4,7,10-tetraazacyclododecane
dpq	Dipyrido[3,2-f:2',3'-h]quinoxaline
dpqC	3-Methyl-10,11,12,13-tetrahydrodipyrido-[3,2*a*:2_,3_-*c*]phenazine
EDC	*N*-(3-Dimethylaminopropyl)-*N'*-ethylcarbodiimide hydrochloride
EDTA	Ethylenediamine tetraacetic acid
EPA	Diethyl ether-ethanol-isopentane glass
ER	Endoplasmic reticulum
ES	Electrospray
FCS	Fluorescence Correlation Spectroscopy
FITC	Fluorescein Isothiocyanate
FLIM	Fluorescence Lifetime Imaging
FLIP	Fluorescence Loss In Photobleaching
FP	Fluorescent Protein
FRAP	Fluorescence Recovery After Photobleaching
FRET	Fluorescence Resoance Energy Transfer
GFP	Green Fluorescent Protein
HEPES	4-(2-Hydroxyethyl)piperazine-1-ethanesulfonic acid
HOBt	1-Hydroxybenzotriazole hydrate
HPLC	High performance liquid chromatography
HSA	Human Serum Albumin
IR	Infrared
ISC	Intersystem Crossing
Lys	Lysine
MALDI	Matrix assisted laser desorption ionization
MLCT	Metal to Ligand Charge Transfer
MRI	Magnetic Resonance Imaging
MS	Mass spectrometry
MTT	3-(4,5-dimethylthiazol-2-yl)-2,5-

	diphenyltetrazolium bromide
NBD	4-Chloro-7-nitro-1,2,3-benzoxadiazole
NBS	N-bromosuccinimide
NHS	N-hydroxysuccinimide
NIR	Near Infra Red
NMR	Nuclear Magnetic Resonance
PAMAM	Dendrimer based on ethylene diamine and acrylic acid building blocks
PBR	Peripheral type benzodiazepine receptor
PBS	Phosphate Buffered Saline
PPA	Polyphosphoric acid
STED	Stimulated Emission Depletion
STIM	Stromal Interaction Molecule
TAT	*trans*-activating transcriptional activator
TFA	Trifluoroacetic acid
THF	Tetrahydrofuran
TIRF	Total Internal Reflection Fluorescence
TOF	Time of flight
UV	Ultra violet
Vis	Visible

Table of Contents

CHAPTER 1

Introduction

1 Introduction

The importance of the phenomenon of fluorescence, first described by Sir George Gabriel Stokes in 1852, has grown from a simple and intriguing observation into a very widely used technique. Fluorescence based techniques are now amongst the principal tools used in biological research, especially in the fields of microscopy and cell imaging The high intrinsic sensitivity and modality of fluorescence had predestined it for this role, and its realisation comes through endless amounts of research and development.[1, 2, 3]

The development has two principal aspects: instrumental development on the one hand and new fluorescent probes on the other. Confocal and multiphoton microscopy procedures are just some of the major advancements in instrumental development over recent years, each of which is being refined and improved constantly.[4]

Many fluorophore molecules have been developed and are being used for more specific and intriguing observations. The vast selection of small organic fluorophores[5] is accompanied by several other types of fluorescent label. The group of fluorescent proteins probably constitutes the major one. Isolation and cloning of the Green Fluorescent Protein from the jellyfish *Aequorea Victoria* initiated the development of this field. Since then, many new variants of the protein have been developed with improved photophysical, stability and functionality properties.[6] Recent years have also seen a boom in the use of quantum dots. This advance is much more recent and hence not so well developed.[7]

Receiving less attention from the biological community are luminescent metal complexes, whether based on a transition metal or a lanthanide (III) ion. These possess unique properties, which make them particularly attractive for cellular imaging. Namely, their long luminescent lifetimes making time gated experiments possible and large Stokes' shifts, especially useful in FRET based experiments. Lanthanide emission further offers a sharp, line-like spectrum, which can even exhibit ratiometric sensitivity to its environment.[8]

The development of highly specific probes, capable of directed localization and reporting on cell status and activity, is happening for each class of fluorophore.

In vivo imaging in small animals is slowly being made possible by the development of NIR probes and multiphoton excitation techniques, as the problems associated with light propagation in tissue are decreased in these cases.[9, 10]

1.1 Development of Imaging Instrumentation

Whilst this thesis deals with the development of new fluorescent probes, it is fitting to mention some of the current technological advances in the field of fluorescence microscopy, as these have implication for the design and structure of the new fluorophores.

Instrument	*Key application*	*Advantage*	*Disadvantage*
Scanning confocal	Core confocal microscope suitable for most applications including imaging of fixed and living specimens. Can be used for many techniques including FRAP and FLIP. Add-ons enable FLIM and multiphoton.	Highly flexible core technology, widely available in many institutions	Expensive. Notwell suited to longer-term live cell imaging. Generally slow scanning except of the less flexible fast-scanning variations (e.g. resonant scanners).
Scanning disk confocal	Live cell imaging confocal.	Less photobleaching, faster acquisition rates.	Not suitable for photobleaching, and can have lower resolution than scanning systems, e.g., less amenable to imaging of multiple fluorophores, or more limited scan orientations during acquisition.
Multi-photon	Imaging thicker tissue specimens.	Can be used to image deep inside tissues and model organisms.	Expensive. Requires specialised equipment and maintenance. Axial resolution inferior to scanning confocals.
Wide-field	General 'work horse' in imaging that is available in most departments.	Fast, flexible data acquisition, with high spatial and temporal resolution; multidimensional data can be processed using deconvolution.	Not confocal so z-information really requires deconvolution which is a complex issue. Photobleaching techniques require laser coupling.

Table 1.1 – Instrumentation of fluorescence microscopy[4]

1.1.1 Confocal Microscopy

The aim of obtaining images with the best possible resolution and contrast is omnipresent in any imaging technique. One of the reasons for loss of these in normal (Epi-illumination, widefield) fluorescence microscopy set ups, is the fact that light emitted out of focus reaches the detector as well as light that is in focus. Confocal microscopy offers significant improvement to the image contrast and resolution, as only light coming from the plane of focus is allowed to reach the detector.[11]

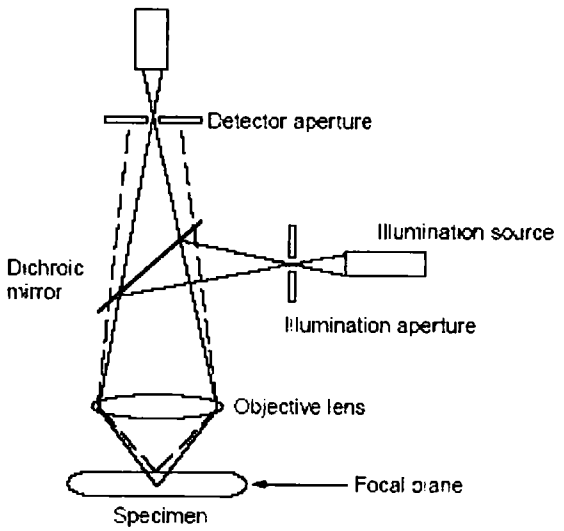

Figure 1.1 – Schematic representation of a confocal microscope[11]

This is achieved by placing a pinhole between the specimen and the detector, which allows only the in-focus light (solid line, **Figure 1.1**) to reach the detector, rejecting the out-of-focus light (dashed line, **Figure 1.1**). This, however, creates new problems as spectral acquisition is much slower. Hence, more extended illumination of the sample is needed, leading to the danger of photobleaching and photodamage. These disadvantages are effectively removed by the use of spinning disk confocal microscopy, where a disc with multiple pinholes is used instead of a single one. Thus, a confocal image of the field of view can be generated in a much shorter time, furthermore a camera can be used instead of a photomultiplier tube. Recent advances include the use of high sensitivity cameras, which leads to a decrease in the excitation intensity needed and a lessening of induced photodamage.[12]

1.1.2 Multiphoton microscopy

An alternative way of reducing the amount of light coming from planes out of focus is to reduce the amount of specimen being excited. Two-photon excitation procedures, using a pulsed laser as a light source offer one possible solution. Under these conditions, the excitation of the fluorophore is achieved by the concomitant absorption of two "low energy" (IR) photons (**Figure 1.2**).

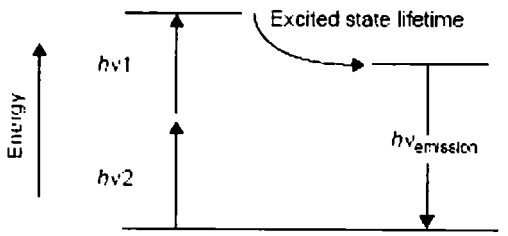

Figure 1.2 – Energy diagram describing two photon excitation in fluorescence spectroscopy[11]

The reduced number of excited fluorophore molecules results from the fact that it is the square of the intensity of the light that determines the probability of excitation. So, the number of excited fluorophores falls non-linearly as a function of the distance from the plane of focus. Thus, not only light generated from out of focus fluorophores is diminished, but also photobleaching and photodamage are significantly reduced. Moreover, the long wavelength (NIR) excitation wavelength suffers less scattering in the biological sample, leading to the possibility to collect information from within a tissue. The long wavelength, however, brings decreased spatial resolution.

1.1.3 4Pi and I^{5}M microscopy[13]

The 4Pi microscopy is a modification of confocal microscopy experiment, which improves its axial (z-axis) resolution. The sample is however illuminated by light focused onto it from two opposing objectives. The fluorescence light is also collected using these two objectives (**Figure 1.3**). This is in principle equivalent to increasing

the numerical aperture value of the system, thus making the focal spot 3-4 times narrower than that of a single objective.

The I^{5}M microscopy set up replaces the laser excitation with a spatially coherent source such as an arc lamp. Once again the sample is illuminated through two objectives but Köhler illumination should preferably be used (**Figure 1.3**). An interference pattern is created and its modulation rapidly falls off to constant intensity outside the common focal plane of the lenses. The signal collection is similar to that of the 4Pi experiment.

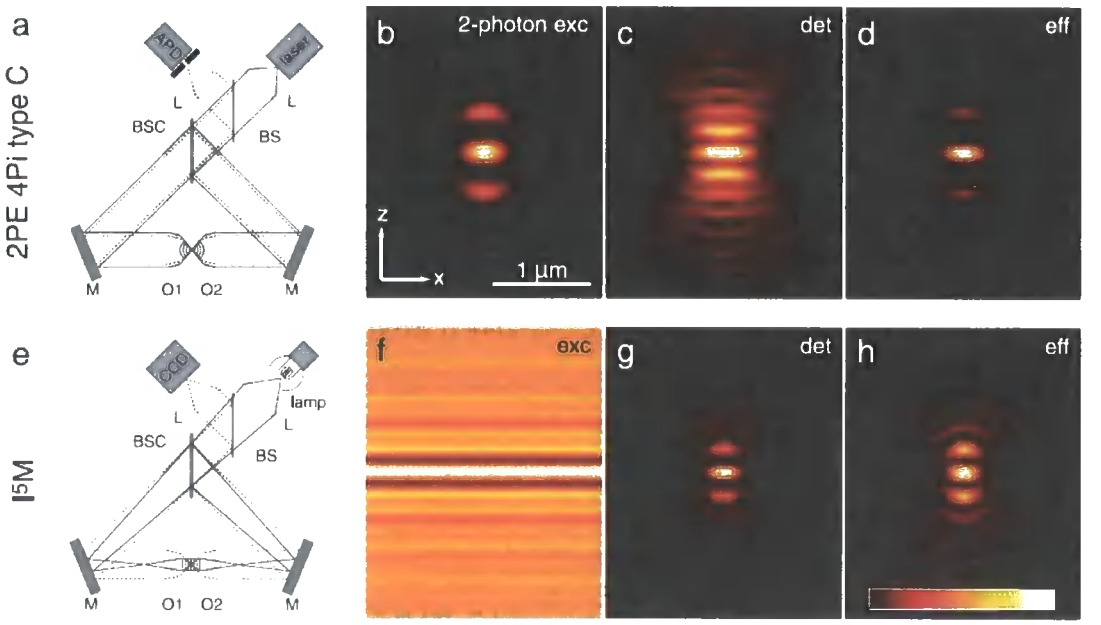

Figure 1.3 – 4Pi and I^{5}M microscopy set ups and excitation light patterns[13]

Both techniques thus achieve narrowing of the central excitation spot to approximately 100 nm. Further developments are needed however, for more practicable application of these principles.

1.2 Developments of Imaging Techniques

Developments are being made not only in the instrumentation for fluorescence microscopy, but also with new experimental techniques.

Technique	*Key application*	*Advantage*	*Disadvantage*
Fluorescence Recovery After Photobleaching (FRAP)	Monitoring diffusion rates of fluorescent species in cells.	Simple. Implemented in most confocal microscopes very easily.	Data analysis can be complex.
Fluorescence Loss In Photobleaching (FLIP)	Monitoring diffusion rates of fluorescent species in cells.	More appropriate for longer time frames than FRAP. Very useful validation of FRAP kinetics and additionally indicates connectivity of fluorophore pools.	Continual illumination required can lead to more photodamage.
Photoactivation	Selective illumination of a fraction of cell/organelle. Similar in many ways to a pulse-chase experiment.	Simple, allows selective imaging of subpopulation of structures/proteins.	Only applicable to a limited number of photoactivatable fluorophores and nonstandard lasers.
Fluorescence Resonance Energy Transfer (FRET)	Monitoring protein-protein (or protein-lipid) interactions in live and fixed cells.	Multiple methods can be used to verify experiments. Can be implemented on both confocal and wide-field systems.	Data analysis can be complex, careful correction for bleed-through and/or cross-talk required. Absolutely dependent on the orientation as well as proximity of fluorophores.
Fluorescence Lifetime Imaging	A key technology for FRET measurement as it is concentration independent.	Concentration-independent FRET measurements. Can also give useful data on the microenvironment of a fluorescent probe. Can be used for separation of closely related fluorophores.	Technically demanding, complex data analysis, difficult to apply to living cells.
Total Internal Reflection Fluorescence Microscopy (TIR-FM)	Monitoring fluorophore mobility close to the coverslip-sample interface.	Excellent for monitoring dynamics of exo- and endocytosis, and plasma membrane events.	Requires careful alignment of illumination using specialise quipment. Can only by used for events 50-200 nm from the coverslip.
Fluorescence Correlation Spectroscopy (FCS)	Monitoring diffusion dynamics in solution and in cells by measuring small changes in fluorescence caused by changes in microenvironment.	Applicable to the analysis of size distributions (e.g., ligand binging, complex formation).	Complex mathematical analyses required.

Table 1.2 – Experimental techniques for fluorescence microscopy[4]

Some of the more common protocols for fluorescence microscopy are described in **Table 1.2**.[14]

1.2.1 Total Internal Reflection Fluorescence Microscopy (Evanescent Wave Microscopy)

The principle of this technique arises from the formation of a standing (evanescent) wave during total internal reflection of light. Total internal reflection happens when light reaches an interface of high (glass) and low (water) refractive index media, in the medium with high refractive index, above a critical angle. The intensity of the new field ('evanescent wave'), which is formed in the medium of low refractive index, decreases exponentially with distance from the interface.

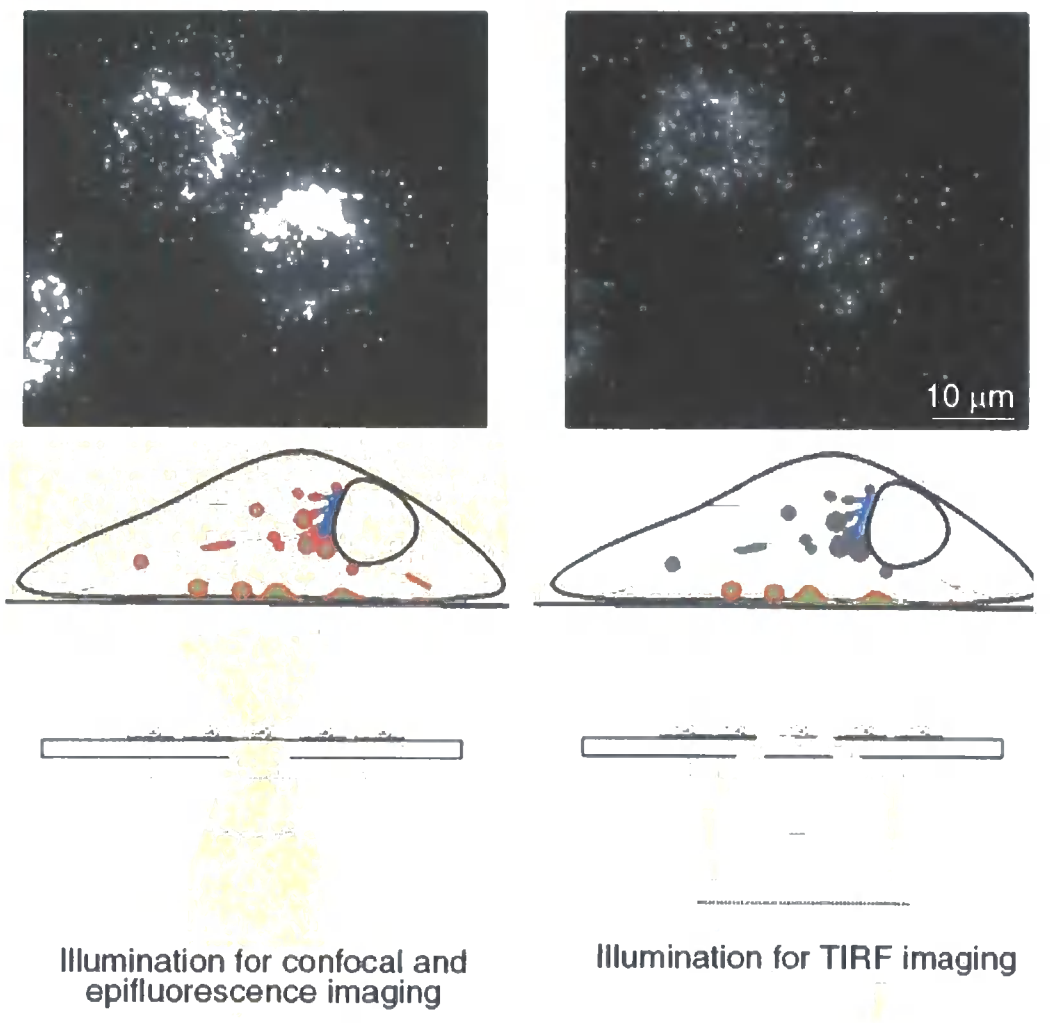

Figure 1.4 – Differences in confocal and total internal reflection illumination and images obtained[12]

Thus, only fluorophores close to the interface are excited. The depth of excitation can be varied with the angle of incidence and can range from 50 nm to 150 nm (**Figure 1.4**). Once again the exposure of the cell to the excitation beam is significantly reduced, minimizing photobleaching and photodamage.

1.2.2 Fluorescence Correlation Spectroscopy

Fluorescence correlation spectroscopy (FCS) is a more specialised technique based on the observation and measurement of the fluorescence intensity fluctuation in a small volume (10^{-15} l), arising from the diffusion of fluorophores in and out of the illuminated region as well as changes in their emission spectra. Its main use is in the study of events at cell membranes, where the diffusion is much slower than in the cytoplasm and, within the cellular compartments. Better resolution of this technique can be achieved with two photon excitation or by using total internal reflection fluorescence microscopy (TIRFM).

1.2.3 Fluorescence (Förster) Resonance Energy Transfer (FRET)

FRET is a process whereby energy of an excited chromophore (donor) is non-radiatively transferred to another chromophore (acceptor) that is in close proximity (**Figure 1.5**). The transfer process involves a long range dipole-dipole coupling. The acceptor chromophore may subsequently emit the gained energy as fluorescence. The efficiency of this process is inversely proportional to the 6^{th} power of the distance between the donor and the acceptor. Thus, observation of FRET implies that these two chromophores are within the range of 1-10 nm. Ranges of this order of magnitude are common in many biomolecules, their domains, complexes and conformational transitions and are far below the diffraction limits of optical microscopy. Further parameters, determining the efficiency of FRET are; spectral overlap of donor emission and acceptor absorption spectra, the relative-orientations of the donor absorption and acceptor transition moments and the refractive index.[15, 16, 17]

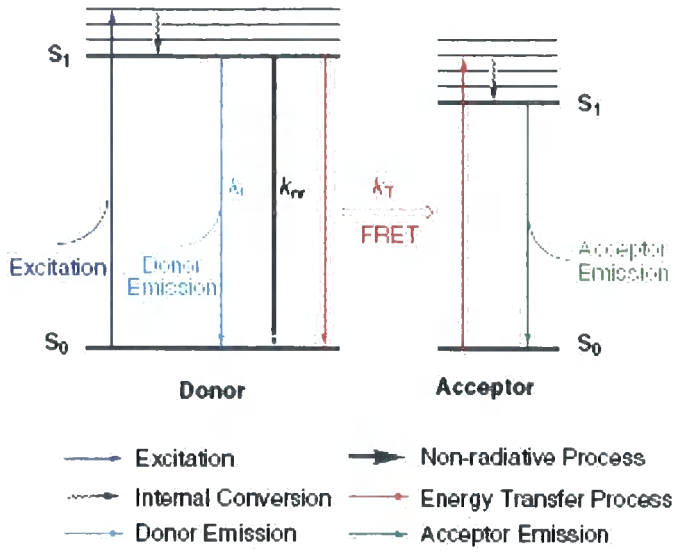

Figure 1.5 – Schematic energy diagram representing Fluorescence Resonance Energy Transfer (FRET)[15]

Therefore, it comes as no surprise that FRET based experiments have been widely used in many fluorescence microscopy experiments. Schematic examples of two ideas using FRET principles are shown in **Figure 1.6**.

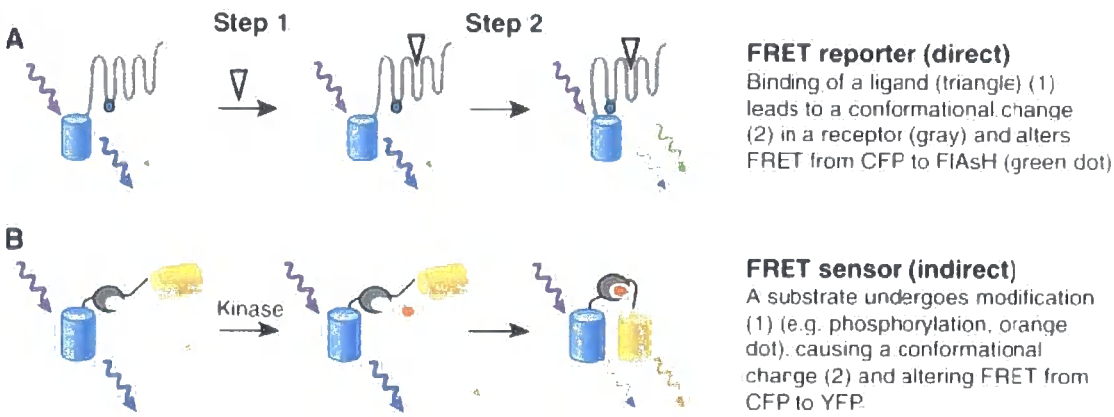

Figure 1.6 – Use of FRET between a fluorescent protein and an organic dye or two fluorescent proteins to observe a conformational change in a peptide chain[18]

Metal complexes and quantum dots can also be part of FRET pairs. Work by Mathis *et. al.*, for example, uses a europium cryptate complex as a donor for Alexa Fluor 647, in experiments aimed at cell surface detection of membrane protein interactions.[19]

1.2.4 Fluorescence Lifetime Imaging Microscopy

Fluorescence Lifetime Imaging Microscopy (FLIM) is based on the observation and determination of fluorescent lifetimes of probes in cellular media, instead of measuring emission intensity. The major advantage of measuring the fluorescent lifetime instead of the intensity is the fact that this measurement is independent of the probe's concentration and the light path length. Thus, a direct measurement of excited-state dynamics and reaction kinetics can be obtained, in suitable cases.[20, 21]

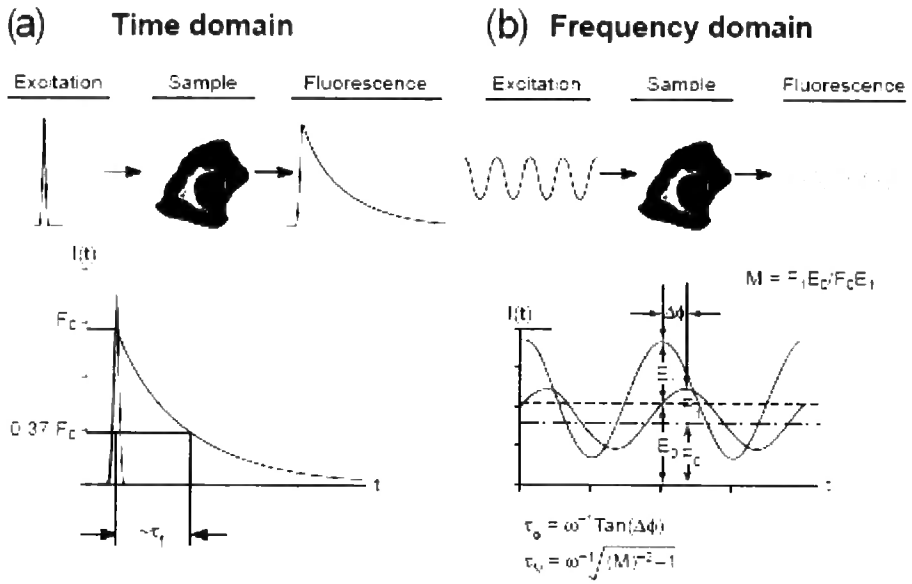

Figure 1.7 – Two ways of measuring fluorescence lifetime; a) in the time domain and b) in the frequency domain[20]

The measurement of the lifetime can be undertaken using two different procedures (**Figure 1.7**). One is the time domain measurement and the second is a frequency domain measurement. It is the exponential decay after a single pulse excitation of the fluorescence intensity that is recorded and used for the lifetime calculation in the time domain experiment. In the frequency domain experiment, it is the modulation of the fluorescence signal from the probe, as a response to time modulated excitation, which forms the basis of the lifetime measurement.

1.2.5 Fluorescence Recovery After Photobleaching (FRAP) and Fluorescence Loss in Photobleaching (FLIP)

Fluorescence recovery after photobleaching is a technique used to investigate the mobility of fluorescent probes in cellular media. It is based on the photobleaching of a defined space within the studied region and subsequent observation of the recovery of the signal, arising from new (unbleached) fluorophores diffusing into the bleached region (**Figure 1.8**).[22]

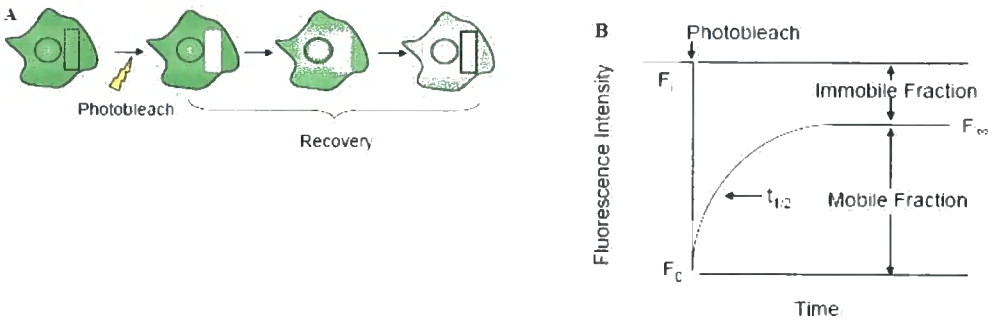

Figure 1.8 – Schematic representation of Fluorescence Recovery After Photobleaching[22]

Fluorescence loss in photobleaching is a complementary method, in which a specific region is photobleached repeatedly and the effect on the overall emission intensity from the given cell is observed. The decrease of the overall emission intensity is interpreted as evidence of free interchange of fluorophores between different regions of the cell. The failure to photobleach the entire population of chromophores in the given cell indicates isolation of different sub-populations and restricted exchange between them (**Figure 1.9**).

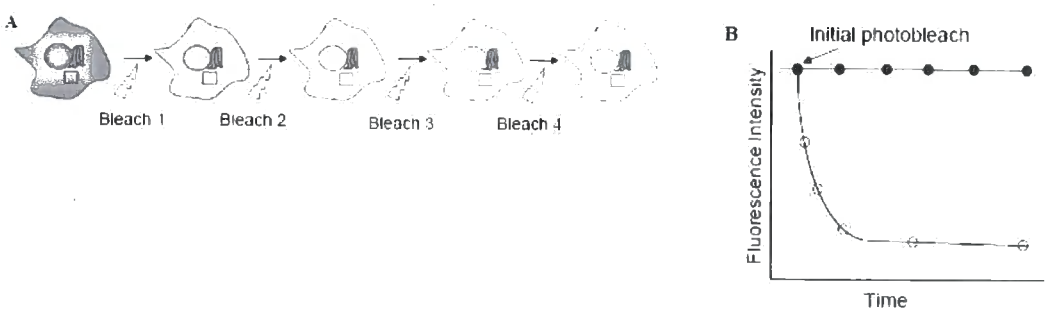

Figure 1.9 – Schematic representation of Fluorescence Loss In Photobleaching[22]

1.2.6 Stimulated Emission Depletion (STED)[23]

Stimulated emission depletion microscopy is based on a forced relaxation of the excited fluorophore back to the ground state by a means of a second light pulse. A photon of energy corresponding to the depleting beam is emitted. This deactivation is, however, carried out with a pulse having a "doughnut-shaped" intensity profile. Thus, only molecules in the periphery of the excitation focal spot are deactivated and a very sharp excitation is achieved (**Figure 1.10**).

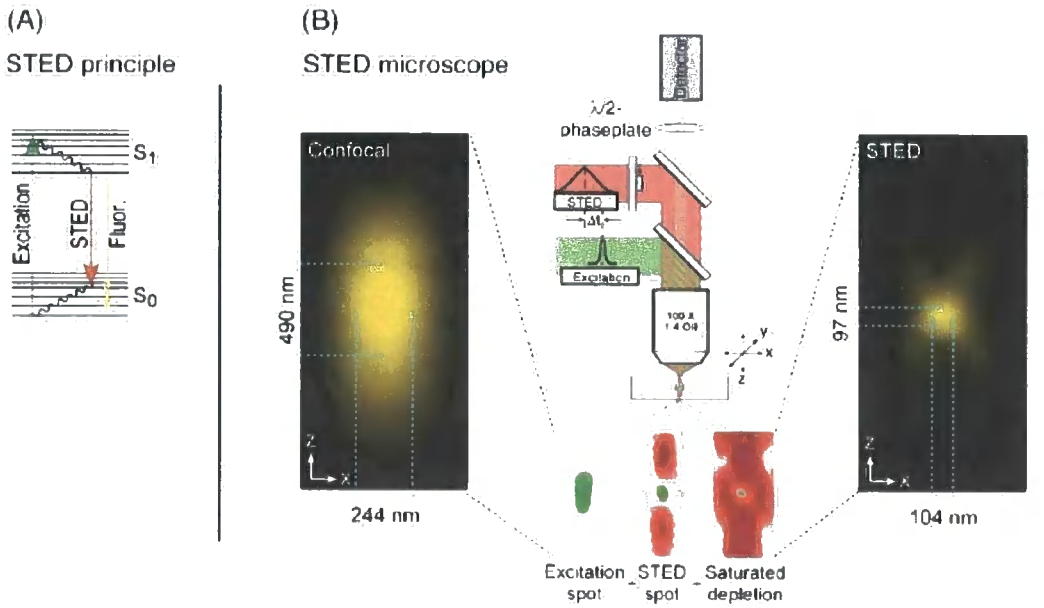

Figure 1.10 – Principle and experimental set up of Stimulated Emission Depletion Microscopy[23]

1.2.7 Fluorescence Speckle Microscopy[24, 25]

Fluorescence speckle microscopy is a method to analyse the movement, assembly and disassembly dynamics of macromolecular structures. It was established during the study of cytoskeleton, for which it is very well suited. It uses covalently labelled macromolecules, which appear to be "speckled" when observed by flurorescence microscopy. The dynamics of the each macromolecule can then be deduced from the changes in the speckle patterns (**Figure 1.11**).

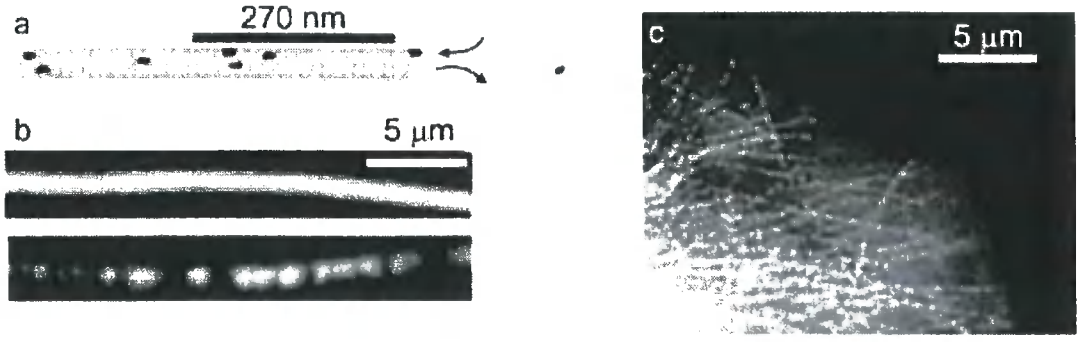

Figure 1.11 – Images demonstrating the principles of Fluorescence Speckle Microscopy[25]

1.3 Classes of Fluorophore

As mentioned earlier, the fluorophores used for cellular imaging may be divided into four distinct classes. The two more established ones are small organic dyes and fluorescent proteins, whereas the less common ones are quantum dots and luminescent metal complexes.

1.3.1 Small Organic Dyes

The list of small organic dyes that have found application in cellular imaging is very long. Fluorescein, DAPI, ethidium bromide, Hoechst 33342 or rhodamines are just a few of the classical examples of these.[2]

The most powerful demonstration of the level of development in this field can almost certainly be obtained from Invitrogen's Handbook of Fluorescent Probes (The Handbook-A Guide to Fluorescent Probes and Labeling Technologies; http://probes.invitrogen.com/handbook/).[5] It describes about 3000 fluorescent probes, designed and developed for use in cellular imaging.

The major strength of small organic dyes is that they can be engineered and adapted for a particular purpose. Hence, series such as the 'Alexa'[26] or 'Cyanine'[27] (**Figure 1. 12**) dyes have been developed where the excitation/emission wavelength is systematically changed by the changes in the structure of the fluorophore[28], thus

covering large parts of the visible and near infra-red regions of the spectrum (**Figure 1.13**). Inclusion of reactive functional groups which enable conjugation of these probes to biologically relevant macromolecules is an integral part of the development in this field.

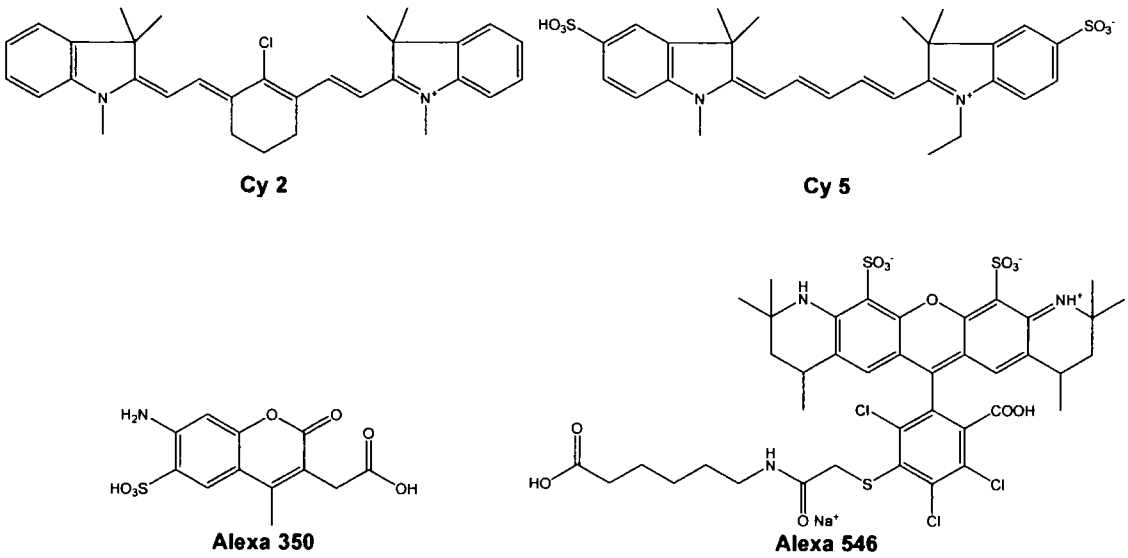

Figure 1.12 – Examples of small organic fluorescent molecules used in cellular imaging; the 'Cyanine Cy' and 'Alexa Fluor' series[5, 26, 27]

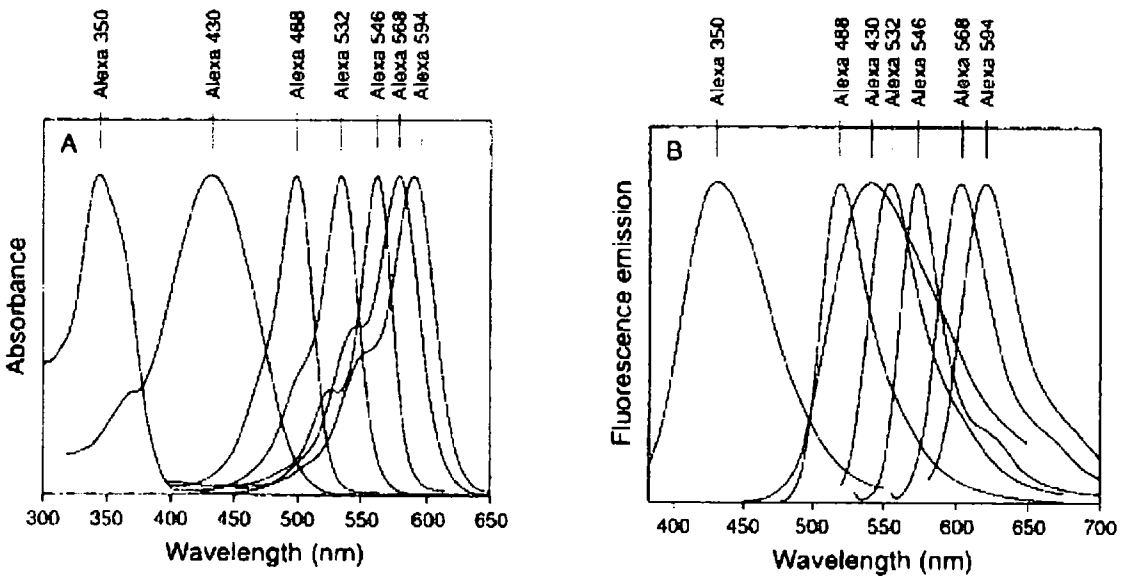

Figure 1.13 – Absorption (A) and emission spectra (B) of selected dyes from the 'Alexa Fluor' series[26]

The emergence of new series of dyes, such as the DyLight, BODIPY and Nile blue derived dyes suggests that developments in this field are still ongoing.[29]

The main drive at the moment is the development of probes emitting in the red and near infra-red end of the spectrum. These can be used for *in-vivo* imaging, as well as fluorescence microscopy at the cellular level.

Short luminescence lifetimes (typically 1-10 ns), of the same order as endogenous fluorophores, and poor spectral separation of the excitation and emission bands (e.g. <50 nm) are the most common disadvantages of the low MW organic fluorophores.

1.3.2 Fluorescent Proteins[18, 30]

The use of fluorescent proteins in cellular imaging was initiated by the discovery of Green Fluorescent Protein from the jellyfish, *Aequorea Victoria.*

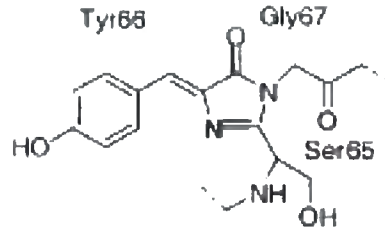

Figure 1.14 – Image of the barrel structure protecting the GFP florophore and the structure of the fluorophore indicating the amino acids it has formed from[6]

It was the observation that the protein expressed outside of the original organism remains fluorescent, which led to the realisation that the fluorophore (**Figure 1.14**) assembles in an autocatalytic reaction of the polypeptide chain.

The possibility to fluorescently tag proteins of choice by the hybridization of the native genome with the gene for FP production thus became apparent and has been exploited in many experiments.[31, 32, 33]

Figure 1.15 – Structure of the fluorophore of GFP and its mutated variant DsRed[34]

The fluorescent proteins have been further developed by mutation. The primary aim was creation of proteins with different excitation/emission profiles to the original GFP (**Figure 1.15**). Thus, proteins emitting from the blue to the far red are now available (**Figure 1.16**).

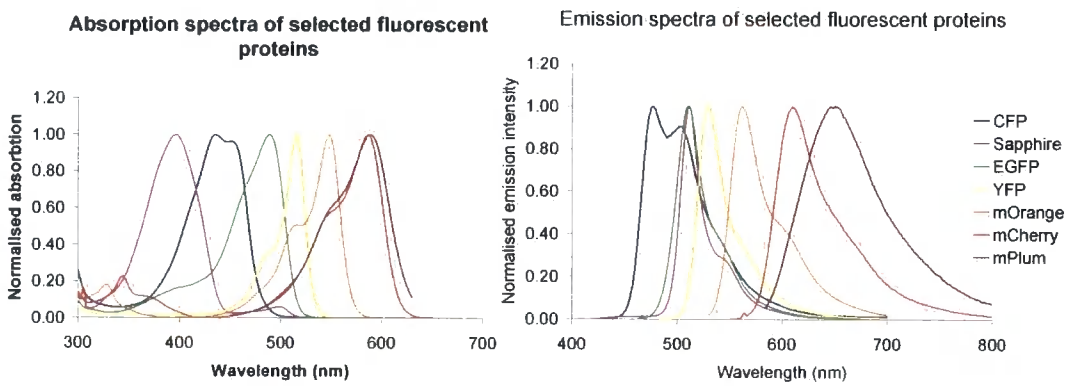

Figure 1.16 – Absorption and mission spectra of selected fluorescent proteins (FPs)[35]

Further developments have been aimed at removing the tendency of FPs to oligomerise, optimizing the folding efficiency at 37 °C and increasing their photostability and optical brightness. These developments are expected to extend the

usefulness of FPs in cellular imaging even further (**Table 1.3**). Nevertheless, the problem of labelling proteins with an allegedly "non-invasive" label of the same order of molecular volume and molecular weight, will always be present.

Class	Protein	Source laboratory (references)	Excitation[c] (nm)	Emission[d] (nm)	Brightness[e]	Photostability[f]	pKa	Oligomerization
Far-red	mPlum[g]	Tsien (5)	590	649	4.1	53	<4.5	Monomer
Red	mCherry[g]	Tsien (4)	587	610	16	96	<4.5	Monomer
	tdTomato[g]	Tsien (4)	554	581	95	98	4.7	Tandem dimer
	mStrawberry[g]	Tsien (4)	574	596	26	15	<4.5	Monomer
	J-Red[h]	Evrogen	584	610	8.8*	13	5.0	Dimer
	DsRed-monomer[h]	Clontech	556	586	3.5	16	4.5	Monomer
Orange	mOrange[g]	Tsien (4)	548	562	49	9.0	6.5	Monomer
	mKO	MBL Intl. (10)	548	559	31*	122	5.0	Monomer
Yellow-green	mCitrine[i]	Tsien (16,23)	516	529	59	49	5.7	Monomer
	Venus	Miyawaki (1)	515	528	53*	15	6.0	Weak dimer[j]
	YPet[g]	Daugherty (2)	517	530	80*	49	5.6	Weak dimer[j]
	EYFP	Invitrogen (18)	514	527	51	60	6.9	Weak dimer[j]
Green	Emerald[g]	Invitrogen (18)	487	509	39	0.69[k]	6.0	Weak dimer[j]
	EGFP	Clontech[l]	488	507	34	174	6.0	Weak dimer[j]
Cyan	CyPet	Daugherty (2)	435	477	18*	59	5.0	Weak dimer[j]
	mCFPm[m]	Tsien (23)	433	475	13	64	4.7	Monomer
	Cerulean[g]	Piston (3)	433	475	27*	36	4.7	Weak dimer[j]
UV-excitable green	T-Sapphire[g]	Griesbeck (6)	399	511	26*	25	4.9	Weak dimer[j]

Table 1.3 – Classification of the most useful fluorescent proteins[30]

1.3.3 Quantum Dots[36]

Quantum dots constitute the most recent addition to the range of fluorescent probes suitable for cellular imaging. They started off as a curiosity in materials science little more than two decades ago and have developed into a useful tool for biological science, particularly for cell labelling studies.[7]

The photochemical basis comes from the luminescence observed from colloidal suspension of monocrystals of semiconductors such as CdSe or CdTe. They typically consist of a protective ZnS shell. The surface layer may be coated to provide water solubility and functionality for conjugation or interaction with biological systems. (**Figure 1.18**)

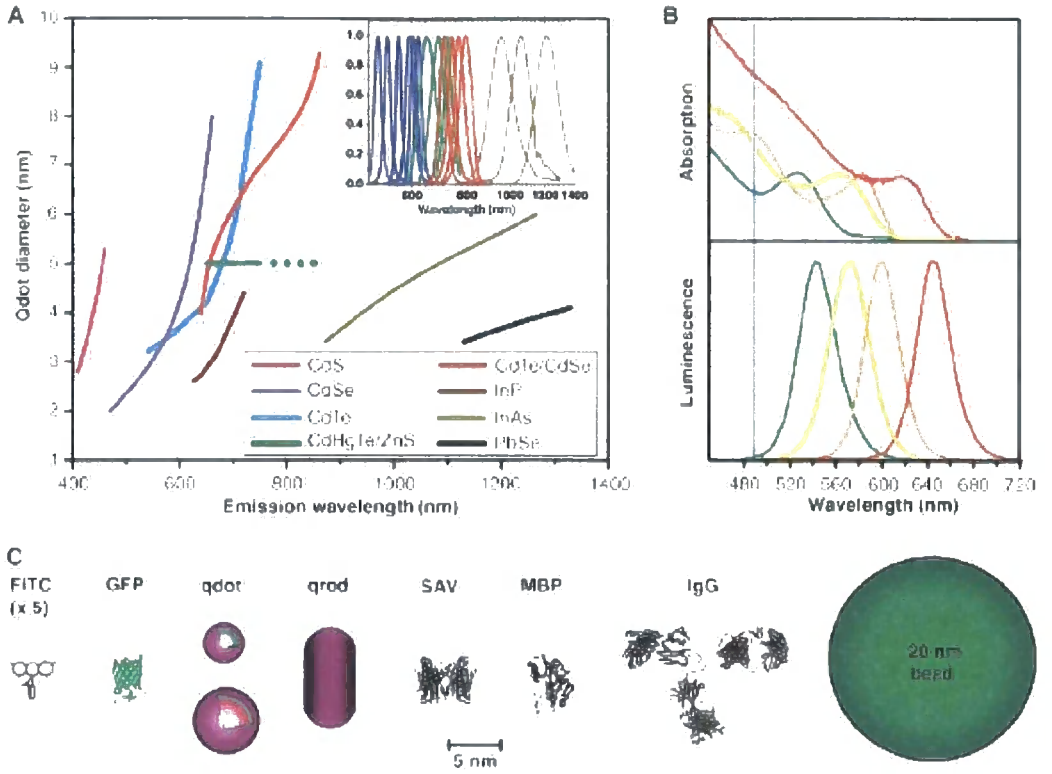

Figure 1.18 – Characteristics of quantum dots; A) dependence of emission wavelength on material and size; B) excitation and emission spectra; C) size comparison to other fluorescent probes or proteins[7]

The interesting properties of quantum dots relate to the possibility of obtaining different emission/excitation wavelengths based on the size of the semiconductor core which, in turn, can be tuned by the conditions of its synthesis. Furthermore, quantum dots have 10 to 100 times higher extinction coefficients, compared to simple organic fluorophores and fluorescent proteins, as well as very high photostabilities. Quantum dots also possess luminescent lifetimes longer than 10 ns, which makes them suitable for time-resolved microscopy, where the fluorescence of endogenous fluorophores is eliminated from the signal observed. Their size however does make it difficult for them to cross the cellular membrane. Thus, they can be used mainly for membrane staining or in fixed or permeabilised cells. On the other hand, their size and electron density makes them suitable for use in correlated electron microscopy.[7]

1.3.4 Metal Complexes

Luminescent metal complexes offer an alternative to entirely organic fluorophores. There are two major categories of luminescent metal complexes (**Figure 1.19**); luminescent transition metal complexes (e.g. Ru, Re, Os) and luminescent lanthanide complexes (Tb, Eu, Sm, Nd, Er, Yb).[2, 8, 37]

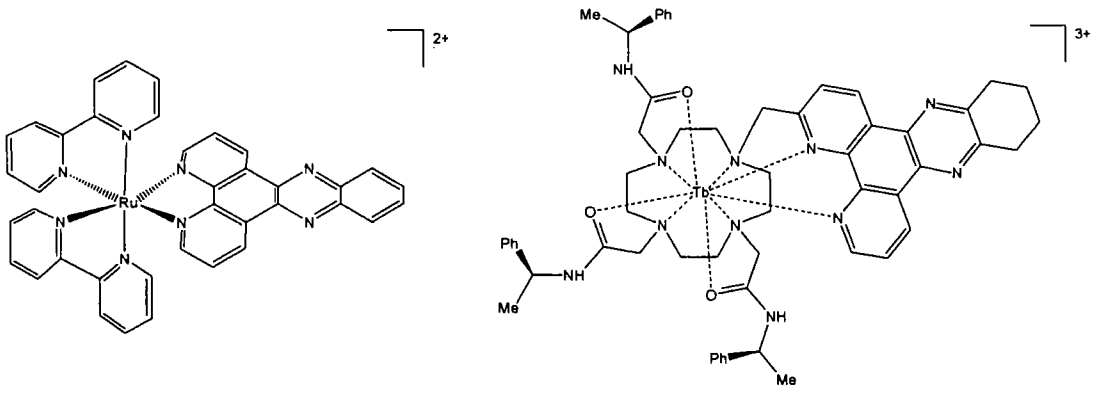

Figure 1.19 – Examples of emissive transition metal and lanthanide complexes

The two common features that give these compounds advantages as fluorescent dyes for biological applications are their large Stokes' shifts and long lifetimes of luminescence (up to microseconds for transition metal complexes and up to several milliseconds for lanthanide comlexes). The large Stokes' shifts ensure sufficient separation of excitation and emission spectra, which is most useful in FRET measurements. The long lifetimes of luminescence, on the other hand, enable time gated experiments that remove the background fluorescence from the signal observed.

The nature of the excited state is what distinguishes these two types of metal complexes from the photophysical perspective. The transition metal complexes generally emit from an MLCT based excited state, whereas the lanthanide (III) ions all emit from a metal based excited state. The luminescence observed can be modulated by the design of the ligand structures in each case.

1.4 Applications of Fluorescent Probes

The cellular medium is a very complex system, divided into numerous compartments (organelles), with an enormous number of events (chemical reactions, transport of compounds across membranes and supramolecular interactions) happening at any given time. Fluorescent compounds used in cellular imaging are expected to convey information about the condition of the biological system into which they are introduced. Therefore, further requirements are placed upon fluorophore molecules apart from the ability to enter the biological system and maintaining their fluorescence in a cellular medium.

Hence, another way of classifying fluorescent probes is by their intended use and the information they should deliver. Some of the tasks that fluorescent molecules in cellular imaging are expected to perform are: selective staining of a particular cellular compartment, reporting on the concentration of ions (Ca^{2+}, H^{+}) and molecules, measuring enzyme activity or monitoring the synthesis transfer and interactions of biological macromolecules, such as proteins and nucleic acids.

1.4.1 Compartment Staining

Cells, especially eukaryotic ones, are divided into many different compartments. Being able to visualize these selectively is of interest to the biologist, as morphologies of different organelles can be indicative of the state of the cell.

The compartments of greatest interest for observation are nucleus, mitochondria, Golgi complex, endoplastic reticulum, endosomes/lysosomes and cellular membranes (**Figure 1.20**).[38, 39] Structures of the cytoskeleton such as tubulin and actin are also common targets for visualisation using fluorescent probes.

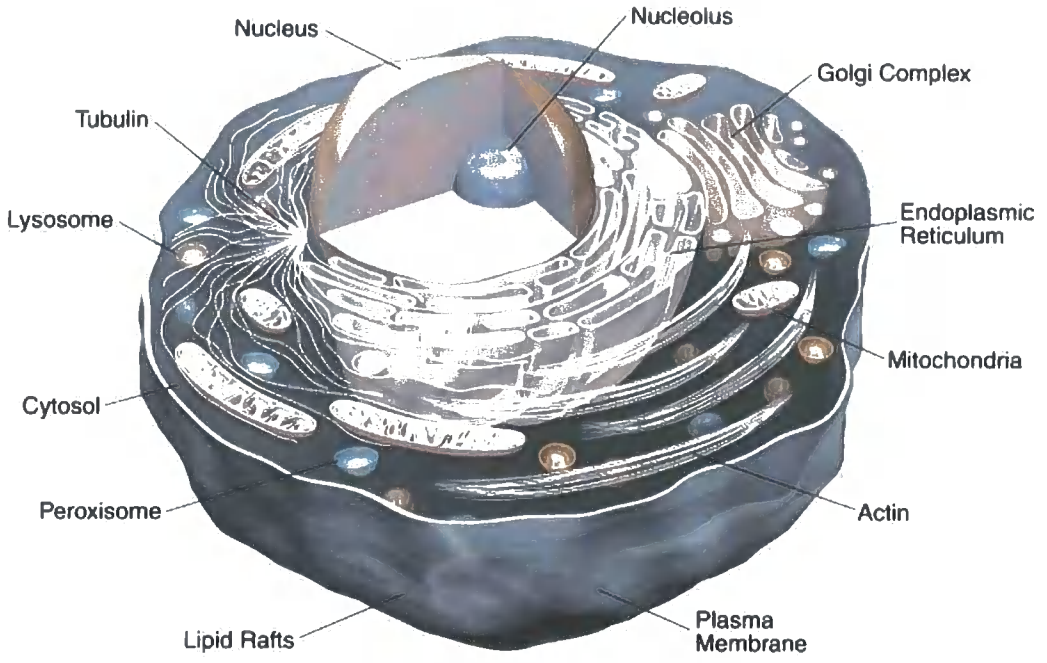

Figure 1.20 – Image of an animal cell showing its different compartments[5]

The staining of organelles is currently dominated by low MW organic dyes. With traditional, empirically identified dyes being replaced by dyes made for specific purposes.

1.4.1.1 Nuclear Probes

The cell nucleus (**Figure 1.21**) is an organelle of paramount importance, storing, reproducing and bringing into life the genetic information of the cell. Hence, visualisation of the nucleus, its substructures and dynamics is highly desirable.

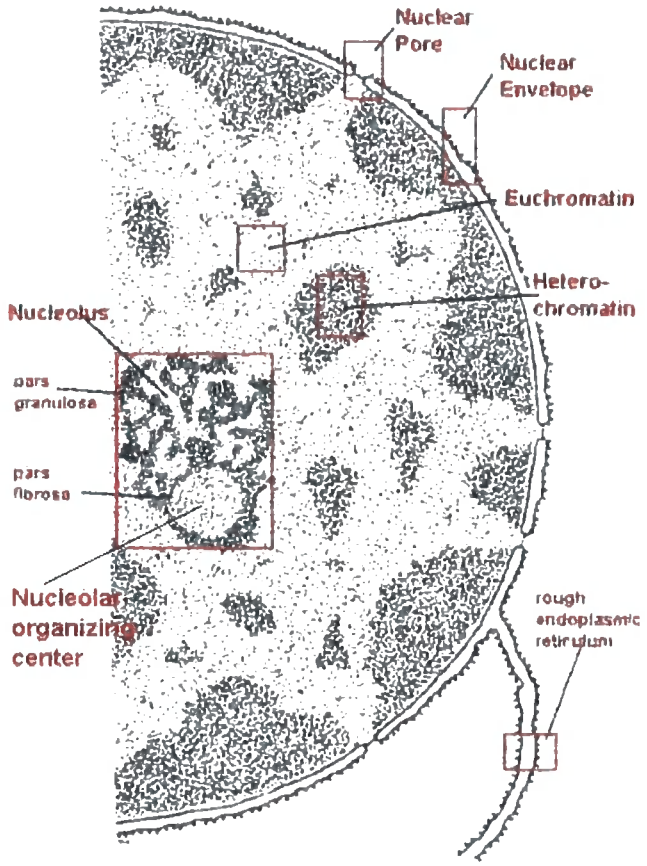

Figure 1.21 – Micrograph of the cell nucleus[39]

Ethidium bromide, DAPI, Acridine orange, Hoechst dyes (**Figure 1.22**) and their derivatives are the classical examples of fluorescent dyes that interact with DNA. They are also capable of traversing the cellular and the nuclear membrane, hence staining the regions where most of the DNA resides.

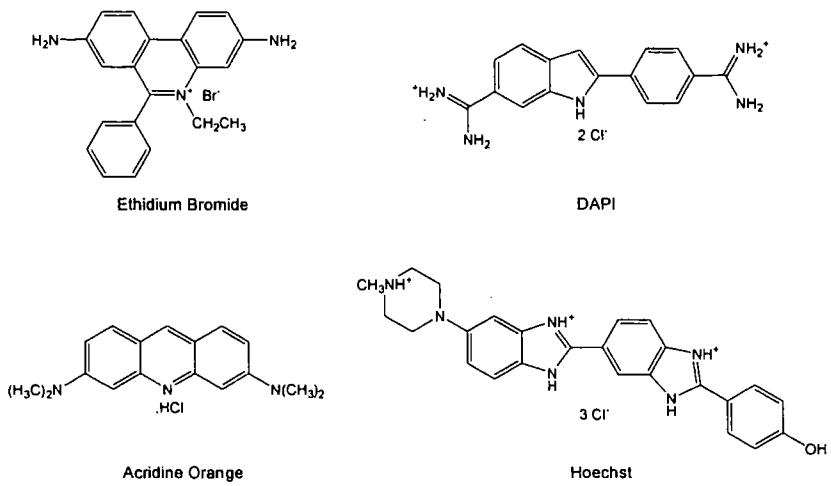

Figure 1.22 – Examples of traditional fluorophores that stain the nucleus[2, 5]

Ethidium bromide itself does not cross cellular membranes; only structurally related compounds such as Hexidium Iodide and Dihydroethidum are able to do that.[5]

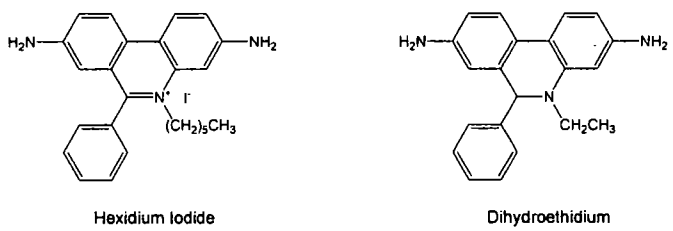

Figure 1.23 – Cell permeable derivatives of Ethidium bromide[5]

Dihydroethidium (**Figure 1.23**) fluoresces in the blue and stains the cytosol. In many viable cells, however, it gets oxidised to ethidium, which gives a red fluorescence only after intercalating into DNA.[40] Hexidium iodide (**Figure 1.23**), which upon DNA binding has a shorter wavelength of emission compared to ethidium, stains the nuclei and cytosol of eukaryotic cells and it has been observed to stain mitochondria and nucleoli in certain instances.

Both DAPI and Hoechst dyes exhibit blue fluorescence upon binding into the minor groove of DNA. DAPI shows selectivity for AT base pairs[41] and possesses a higher photostability but lower brightness. The selectivity of DAPI for DNA binding over RNA binding is more pronounced than for Ethidium bromide and related probes.

Acridine orange is another intercalating DNA stain, which undergoes emission wavelength changes from 525 nm to 650 nm, upon binding.

Another long wavelength emitting, cell permanent dye that targets the nucleus is LDS 751 (**Figure 1.24**). It undergoes fluorescence intensity enhancement upon DNA binding. It can be used to discriminate between intact nucleated, damaged nucleated and non-nucleated cells.[42]

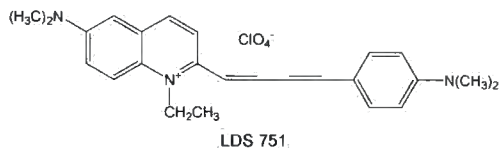

Figure 1.24 – Structure nuclear probe LDS 751[5]

Further fluorescent probes for the nucleus have been developed by Invitrogen in their SYTO® range (**Figure 1.25**).

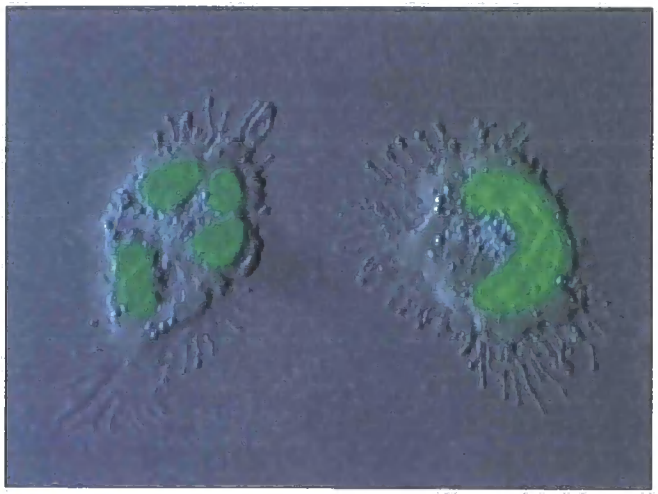

Figure 1.25 – Overlay of brightfield and fluorescence images of human neutrophil nuclei stained with SYTO® dyes[5]

Most of the SYTO dyes stain both DNA and RNA. The SYTO™RNASelect dye is claimed to stain RNA selectively.[43] The usefulness of this series has yet to be fully tested.

Chang *et. al.* have recently published the synthesis and cellular localisation of a library of styryl based fluorescent probes (**Fig 1.26**).[44]

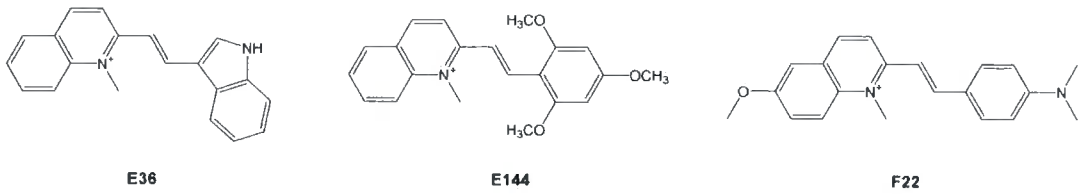

Figure 1.26 – Structures of styryl based fluorescent nuclear probes[44]

These fluorophores show an increase of emission quantum yield as well as a red shift of excitation wavelength, upon binding to RNA and DNA (**Figure 1.27**). The increase in the emission intensity is larger in the case of RNA binding.

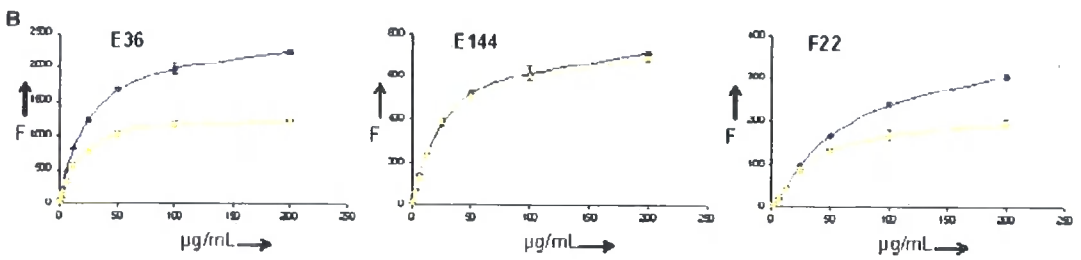

Figure 1.27 – Titration curves for the styryl dyes with RNA (blue) and DNA (yellow)[44]

The probes show strong nucleolus staining in cell labelling experiments, which is interpreted in terms of their selectivity for RNA. The authors claim better results in the live cell experiments (**Figure 1.28**) than with the commercially available SYTORNA™Select dyes.

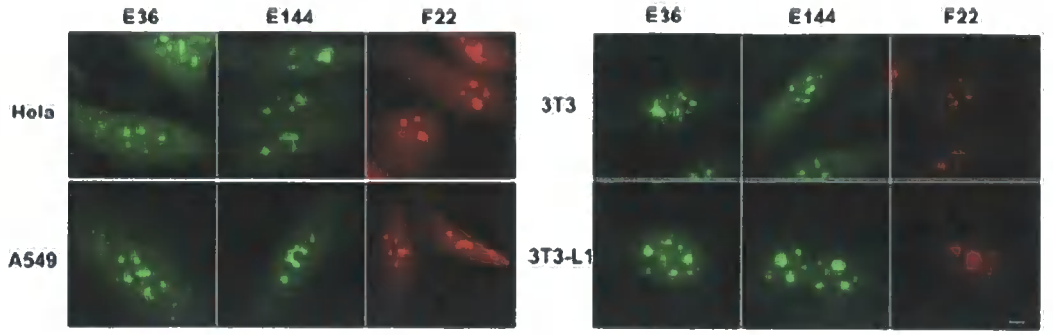

Figure 1.28 – Fluorescence images obtained with the styryl dyes in different cell types[44]

GFP and its variants are also used in nuclear staining. The motive is, however, to determine the localisation of a protein to which the GFP is fused. Thus, a GFP fused to DNA binding proteins was used to visualise structures such as centromers and histones in live cells (**Figure 1.29**).[45, 46]

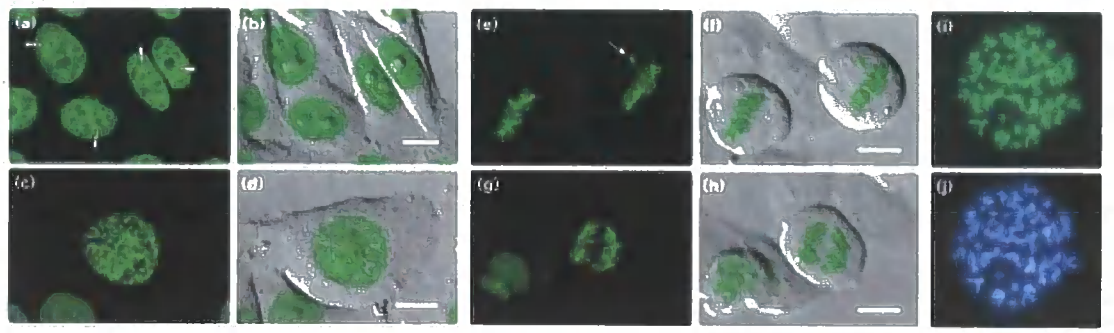

Figure 1.29 – Fluorescence images obtained with GFP expressing together with a nuclear localizing protein in HeLa cells in different cell cycle phases[45]

Nuclear localisation was observed in Durham with cyclen based complexes of terbium and europium, in experiments with live NIH 3T3 and CHO cells.

Complexes containing a tetraazatriphenylene moiety were observed to reversibly stain the nucleus if a high concentration gradient was maintained (0.2 to 1 mM complex in growth medium, **Figure 1.30**).[47]

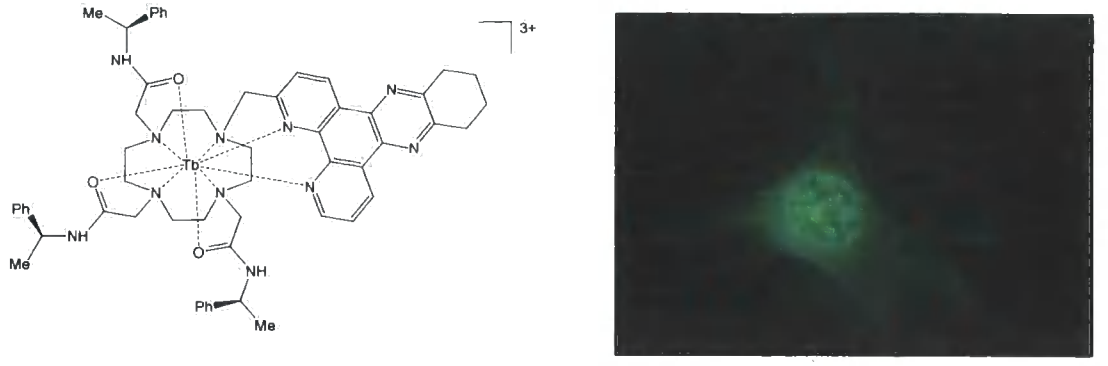

Figure 1.30 – Lanthanide complex and the fluorescence image obtained in NIH 3T3 cells[47]

A similar complex, bearing an azathioxanthone moiety, was shown to localise in the nucleolus by co-staining with SYTO-RNA dye (**Figure 1.31**).[48]

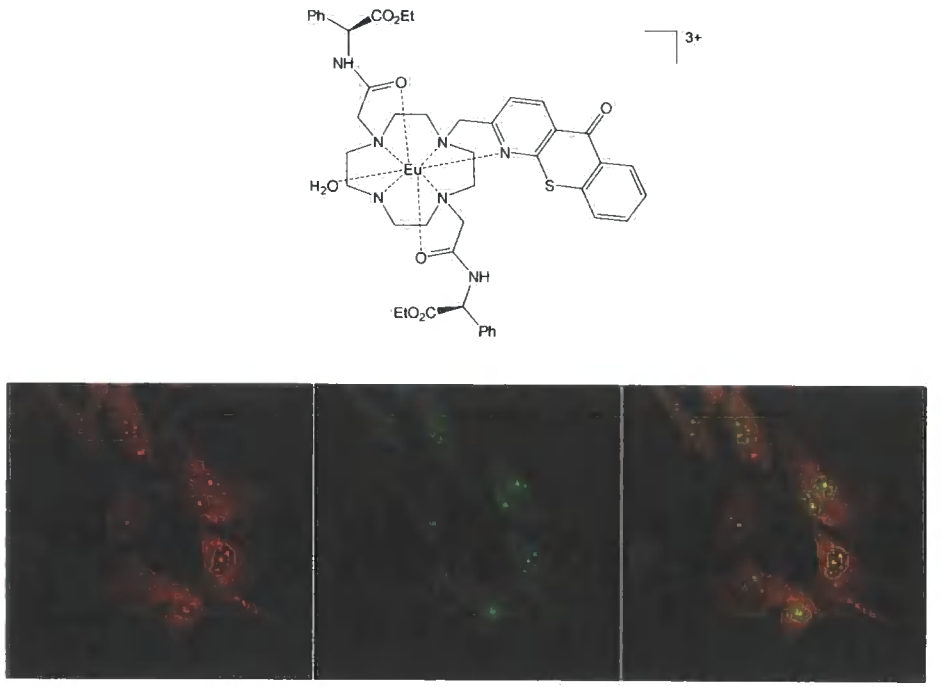

Figure 1.31 – The fluorescence image showing the staining of NIH 3T3 cells with the Europium complex (red), SYTO-RNA dye (green) and a merged image[48]

1.4.1.2 Mitochondrial Probes

Mitochondria are vitally important organelles of eukaryotic cells (**Figure 1.32**). Their key function is performing the energy transforming/producing reactions based

on oxidative phosphorylation and lipid oxidation. Further functions of the mitochondria involve urea, heme and non-heme iron production, steroid biogenesis and intracellular Ca^{2+} homeostasis. Mitochondria also play a key role in cell apoptosis. The morphology of mitochondria is highly variable across cell types and during the cell cycle.

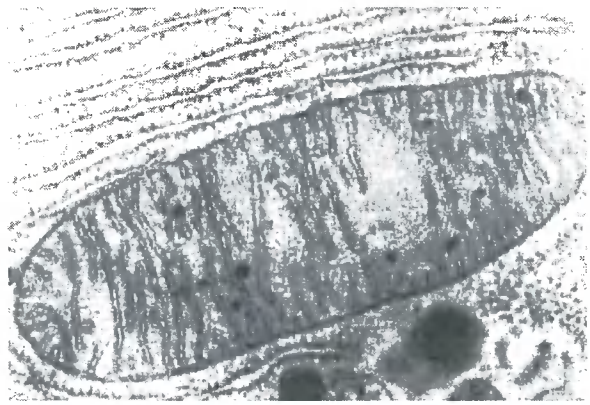

Figure 1.32 – Electron micrograph of a mitochondrion[39]

The traditional fluorophores that stain mitochondria in live cells are Rhodamine 123 and Tetramethyl rosamine (**Figure 1.33**).

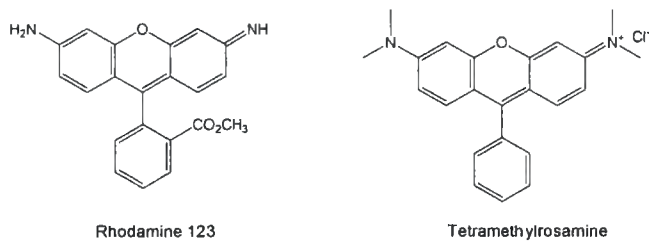

Figure 1.33 – Structures of classical fluorescence probes for mitochondria[5]

Derived from the tetramethylrosamine and X-rosamine structures are the commercially available mictochondrial probes MitoTracker Orange and MitoTracker Red (**Figure 1.34**). They incorporate choromethyl groups that are assumed to react with thiol groups to link the probe covalently to proteins in the mitochondria.[5, 49] This improves the retention of the probe for the work with fixed cells. However, subjecting cells to alkylating reagents can lead to damage and mutations. Phototoxicity of the MitoTracker dyes has been observed as well.[50]

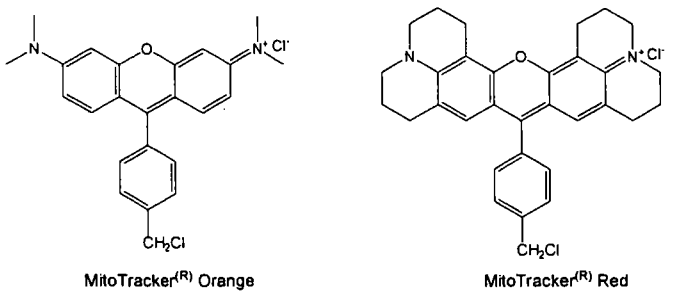

Figure 1.34 - Structures of Mitotracker® probes[5]

In addition, partially reduced forms of these fluorescent probes are available as well (**Figure 1.35**). They are non-fluorescent and become fluorescent only upon oxidation inside normally respiring cells.

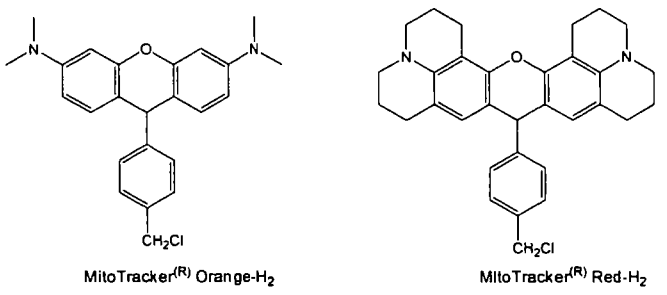

Figure 1.35 – Structures of reduced mitochondrial probes[5]

Also available are the MitoTacker® Green and MitoFluor™ Green mitochondrial probes (**Figure 1.36**).[51] Their major advantage is the fact that they are non-fluorescent in aqueous media and only become fluorescent upon being taken into the less polar 'lipid'-like environment of the mitochondria. This practically eliminates background luminescence from the probe.[5]

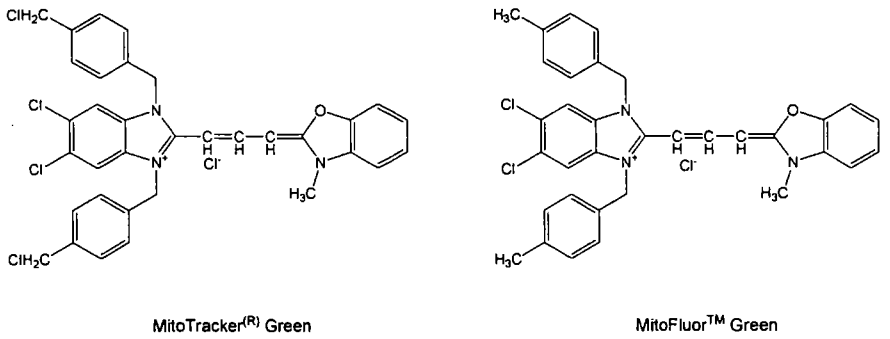

Figure 1.36 – Structures of green fluorescent mitochondrial probes[5]

Furthermore, probes with a degree of responsiveness have been developed as well. Examples of these include RedoxSensor™ Red (2,3,4,5,6-pentafluorotetramethyldihydrorosamine) and the JC-1 probe (5,5',6,6'-tetrachloro-1,1',3,3'-tetraethylbenzimidazoylcarbocyanine iodide) (**Figure 1.37**).

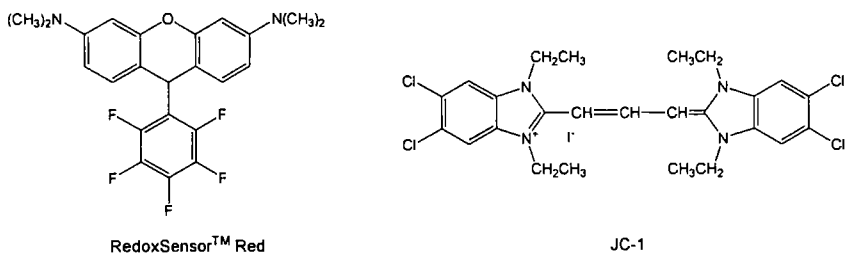

Figure 1.37 – Structures of responsive mitochondrial probes[5]

The RedoxSensor™ is introduced into the cell in its reduced non-fluorescent form. Depending on the reduction potential of the cytosol, it might be oxidised to its fluorescent form (excitation/emission 540 nm/600 nm) and then be taken up by mitochondria.[52] Alternatively, the reduced form is taken up by lysosomes and oxidised to the fluorescent probe there. Co-staining with MitoTracker® Green is beneficial for quantitative measurement of this distribution (**Figure 1.38**).

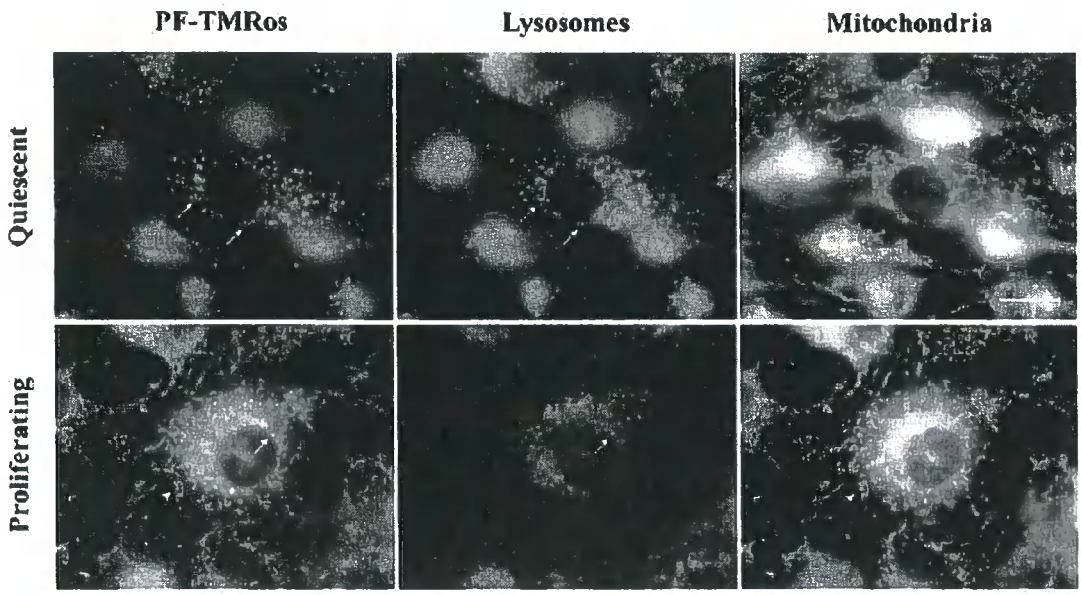

Figure 1.38 – Live cell experiments with the RedoxSensor™ in NRK cells; upper row showing cells stained by the RedoxSensor during quinescent time (showing lysosomal localisation) where as lower row shows staining with RedoxSensor for proliferating cells. Lysosomes are stained by cascade blue conjugated dextran and mitochondria by MitoTracker green. [52]

The JC-1 probe displays concentration and potential (membrane) dependent excitation/emission profiles, which are attributed to its monomer (low concentration, low potential) and "J-aggregate" (high concentration, high potential). The momomer absorption and emission maxima are at 514 and 529 nm respectively. The aggregate on the other hand exhibits broad absorption and emission spectra with maxima around 590 nm (effective excitation can be achieved between 485 and 585 nm). The ratio of the two emissions is claimed to be dependent only upon the membrane potential. The spectral overlap of the emission of the monomer and absorption of the aggregate can, however, lead to problematic signal deconvolution.

Carbocyanine dyes (**Figure 1.39**) with short chains (up to hexyl) stain mitochondria as well.

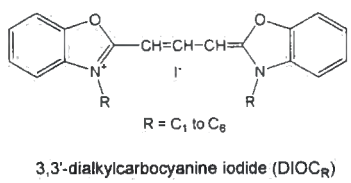

3,3'-dialkylcarbocyanine iodide ($DIOC_R$)

Figure 1.39 – Short chain carbocyanine dye staining mitochondria[5]

The pentyl and hexyl derivatives stain the endoplasmic reticulum as well, at higher concentrations.

A new mitochondrial probe MitoSOX red (**Figure 1.40**), capable of detecting superoxide production, has been developed by Invitrogen.[53]

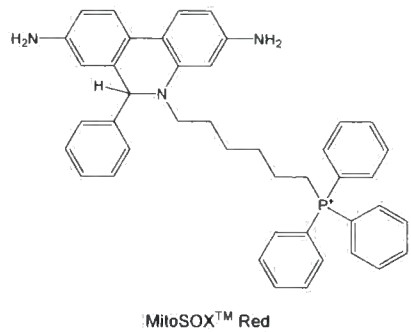

Figure 1.40 – Novel mitochondrial probe for superoxide detection[53]

Mukhopadhyay *et. al.* have used this fluorescent dye to monitor superoxide production in rat cardic-derived H9c2 myocytes and in human coronary artery endothelial cells (**Figure 1.41**). Antimycin A, Paraquat, Doxorubicin or high glucose were used as triggering compounds. The response was observed using confocal fluorescence microscopy as well as flow cytometry.[54]

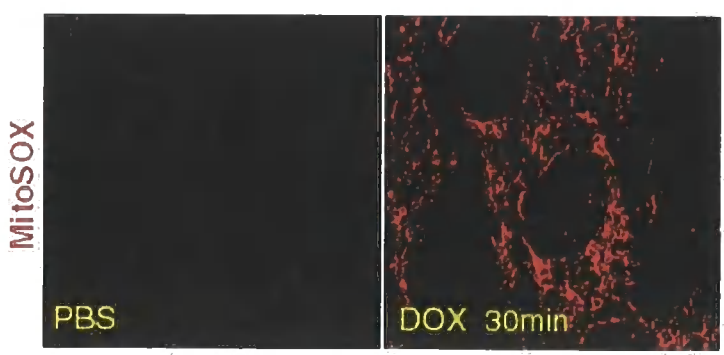

Figure 1.41 – Change in fluorescence of the MitoSOX™ probe upon addition of Doxorubicin[54]

Taliani *et. al.* have recently published the synthesis of a new fluorescent probe selective for mitochondria. The probe contains a ligand for the peripheral type

benzodiazepine receptor (PBR), which is expressed on the outer mitochondrial membrane. This receptor is believed to be involved in many of the biological functions of the mitochondria. Furthemore, its over-expression should mark a pathological state of the cells such as variety of tumours or neurodegenerative diseases (Huntington's and Alzheimer's disease, as well as multiple sclerosis). The fluorophore in this probe is the 7-nitrobenz-2-oxa-1,3-diazol-4-yl (NBD) moiety (**Figure 1.42**).[55]

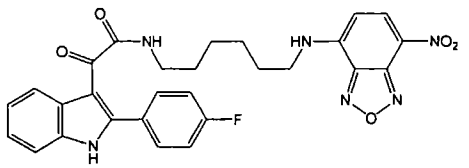

Figure 1.42 – Fluorescent probe for the Peripheral Benxodiazepine Receptor expressed on the mitochondrial surface[55]

Selective mitochondrial staining was also reported by Koide et. al. with their modified rhodamine fluorophore MitoAR (**Figure 1.43**). The MitoAR probe is faintly fluorescent due to the quenching by intramolecular photoinduced electron transfer. The fluorescence is "switched on" by the reaction of the probe with highly reactive oxygen species (hROS) such as hypochlorite or hydroxyl radical, which are formed *in cellulo* under oxidative stress conditions. The strongly fluorescent HMTMR (**Figure 1.43**) fluorophore is formed in this reaction.[56]

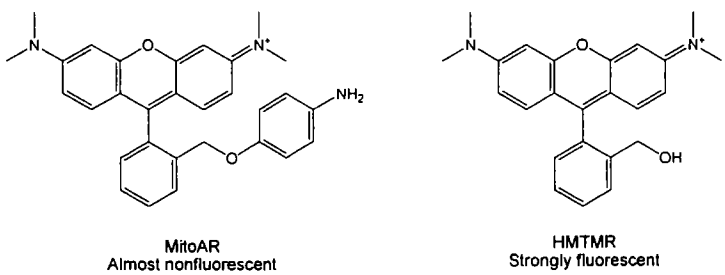

Figure 1.43 – Modified rhodamines as mitochondrial probes[56]

The localisation of the MitoAR was shown to be equivalent to that of the commercially available MitroTracker in a co-localisation experiment, despite the low emission intensity of MitoAR (**Figure 1.44**).

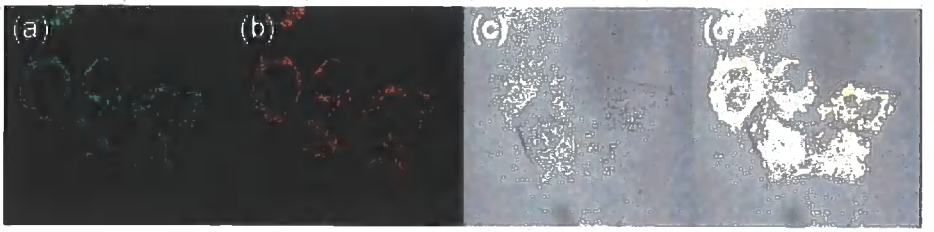

Figure 1.44 – Fluorescence microscopy images for MitoAR probes[56]

An increase in the emission intensity of the complex taken into HL-60 cells was observed, following addition of H_2O_2 (100 μM) to the growth medium (**Figure 1.45**).

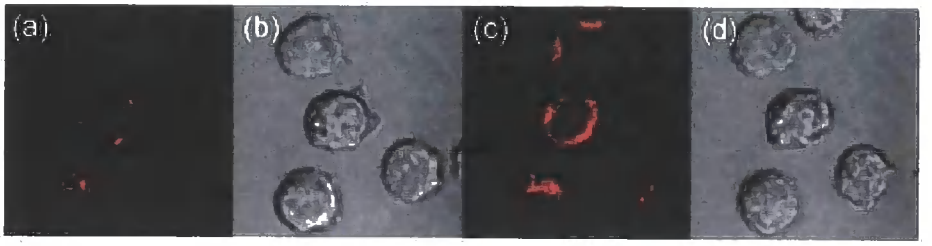

Figure 1.45 – Response of MitoAR probe to H_2O_2 oxidative stress[56]

In recent work, deriving from the work on cell penetrating peptides, two examples of mitochondria selective stains, based on guanidinium vectors, have been reported.

Mendoza *et. al.* have syntheised a tetraguanidium, non-peptidic vector and labelled it with fluorescein (**Figure 1.46**).[57]

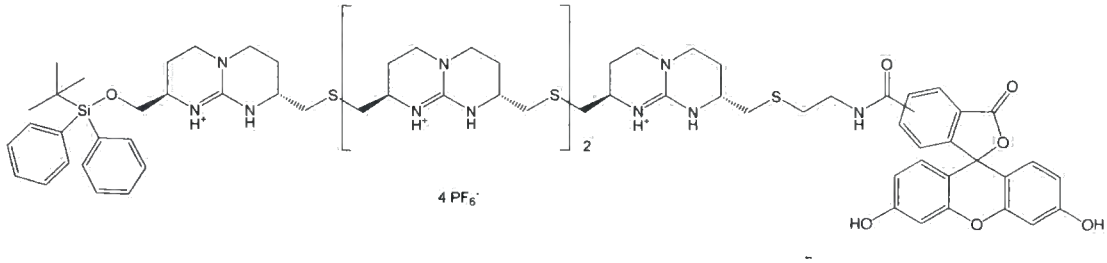

Figure 1.46 – Tetraguanidinum vector labelled with fluorescein[57]

In cellular experiments, with HeLa cells, mitochondrial localisation was observed and confirmed by colocalisation with MitoTracker dye (**Figure 1.47**).

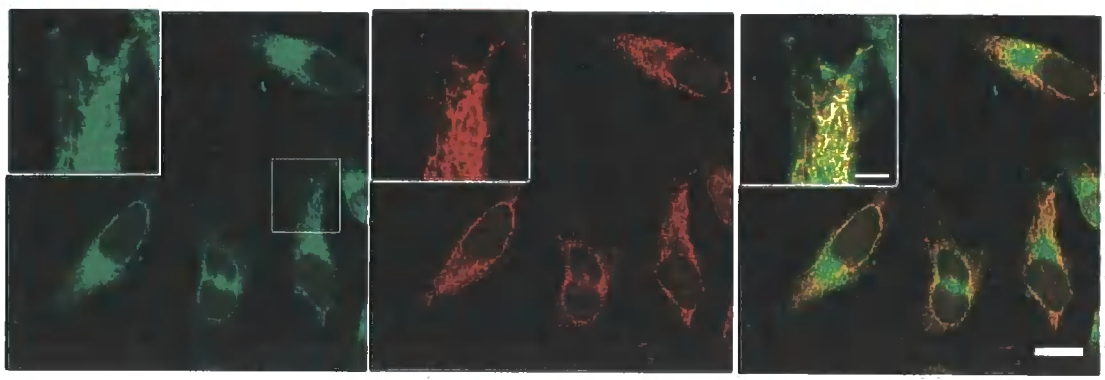

Figure 1.47 – HeLa cells fluorescently labelled with the guanidinium probe (green), MitoTracker (red) and a merged image[57]

Matiti *et. al.* have based their probe on sorbitol, once again using fluorescein as the label and guanidinium groups for targeting (**Figure 1.48**).[58]

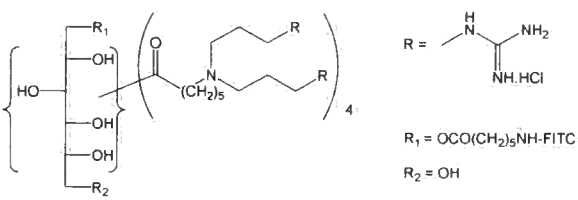

Figure 1.48 – Sorbitol based polyguanidium fluorescent probe[58]

Cellular experiments, involving colocalisation with MitoTracker probe, in HeLa cells were consistent with mitochondrial localisation (**Figure 1.49**).

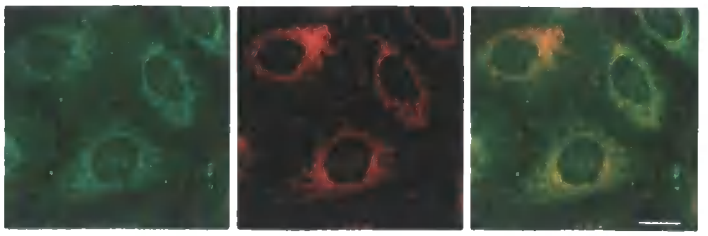

Figure 1.49 – HeLa cells imagined with the sorbitol based probe (gree), MitoTracker (red) and a merged image[58]

Tsien et. al. have made an interesting GFP based probe for the mitochondrial redox potential. They have obtained a GFP (roGFP) variant containing two cysteines in close proximity, on the surface of the barrel structure incorporating the fluorophore (**Figure 1.50**).[59]

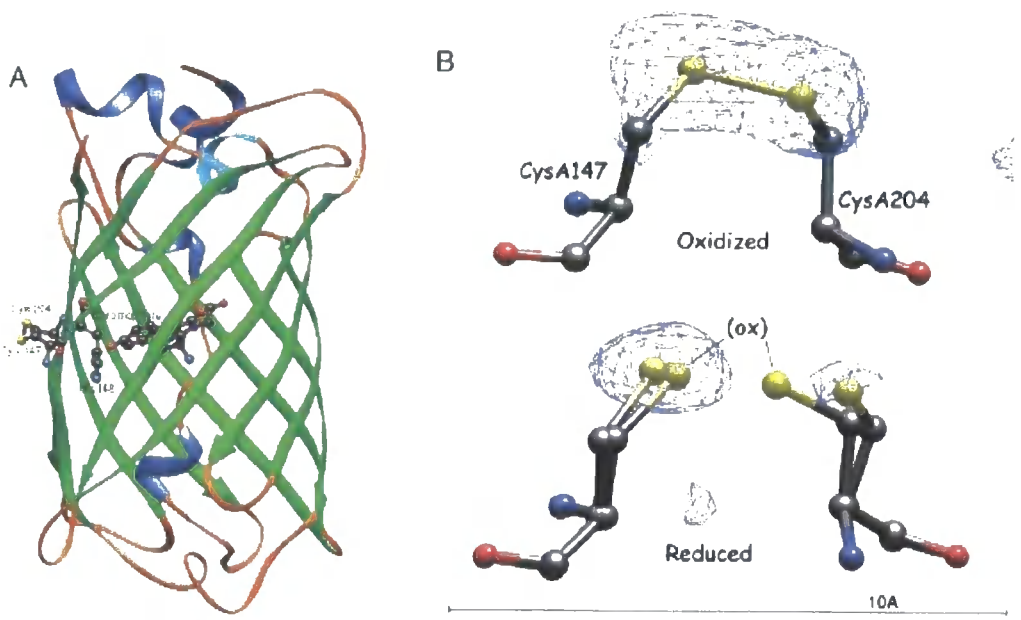

Figure 1.50 – Structures of RoGFP[59]

The formation and cleavage of the corresponding disulfide bridge induces changes in the emission intensity of the protein.

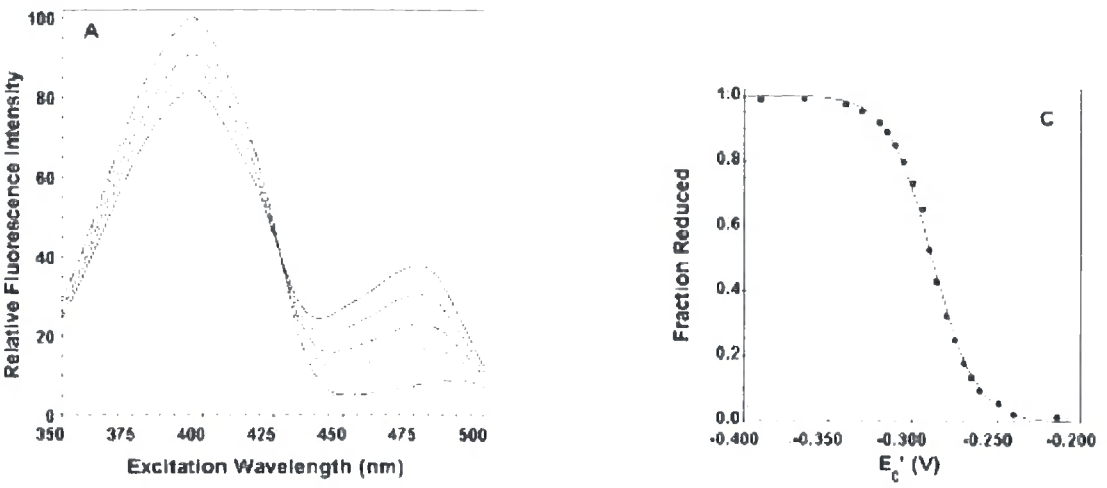

Figure 1.51 – Redox response of roGFP[59]

Furthermore, as the excitation spectra show an isosbestic point, a ratiometric measurement is possible with this probe (**Figure 1.51**).

The cellular localisation of the roGFP was achieved by its expression with the E1α subunit of pyruvate dehydrogenase, which is located in the mitochondrial matrix (**Figure 1.52**).

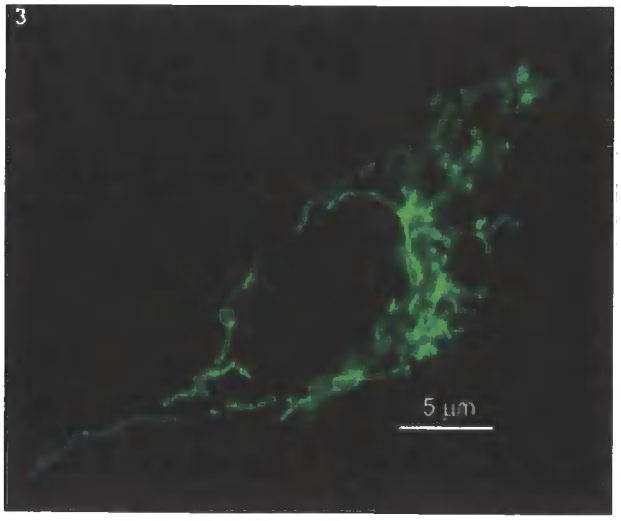

Figure 1.52 – Fluorescence microscopy image obtained with roGFP[59]

1.4.1.3 Probes for the Endoplasmic Reticulum and Golgi apparatus

The endoplasmic reticulum and Golgi apparatus (**Figure 1.53**) are two closely linked organelles. They are the key biosynthetic compartments of the cell. Proteins are synthesised in the translation process in the ribosomes associated with the rough endoplasmic reticulum. Lipid biosyntheis also takes place here. The Golgi apparatus continues the biosynthesis by further transformations of these biological macromolecules and their packaging before being dispatched to other parts of the cell to fulfil their roles.[38,39]

The principal component of Endoplasmic reticulum and Golgi apparatus is a lipid membrane. Thus, the majority of the probes are highly lipophilic or lipid based. Others are molecules that affect protein movement, as this interferes with the function of these organelles.

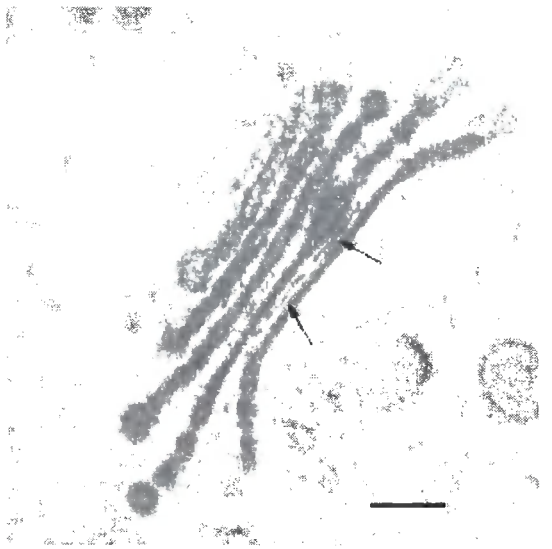

Figure 1.53 – An electron micrograph of the Golgi apparatus[39]

Some of the carbocyanine dyes, such as $DiOC_6$, stain the endoplasmic reticulum as well as mitochondria, as mentioned in the previous section. The ER-Tracker™ Blue-White DPX dye is claimed to be exclusively selective for endoplasmic reticulum (**Figure 1.54**).[60]

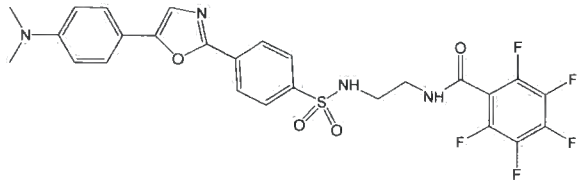

ER-Tracker™ Blue-White DPX

Figure 1.54 – Structure of ER-Tracker™ probe[5]

This dye possesses several interesting properties, such as a large Stokes' shift, high extinction coefficient and solvatochromic dependence of emission wavelength and quantum yield. The emission wavelengths maximum exhibits a red shift with increasing solvent polarity in the range from 430 to 640 nm. The emission quantum yield decreases with increasing solvent polarity. Furthermore, two-photon fluorescence microscopy has been performed with this dye (**Figure 1.55**).[61]

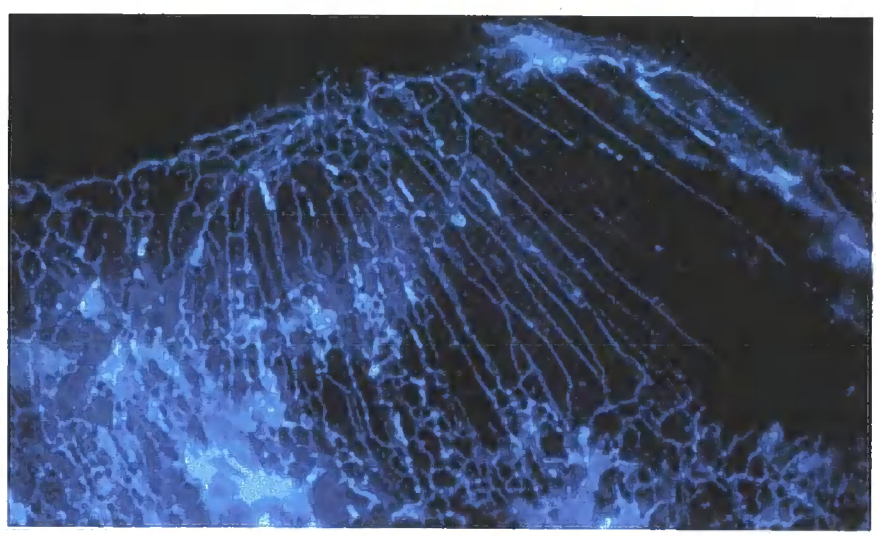

Figure 1.55 – Fluorescence microscopy image obtained with ER-Tracker probe in bovine pulmonary artery endothelial cells[5]

The commercially available probes for the Golgi apparatus are based on two fluorophores NBD and BODIPY and their conjugates with ceramide and sphingomyelin (**Figure 1.56**). They are usually used in solution with bovine serum albumin, which helps to dissolve these highly lipophilic molecules.

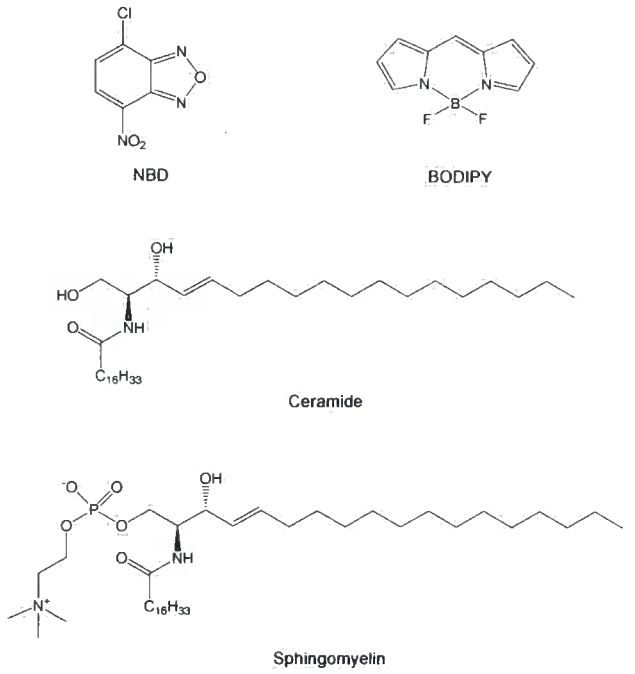

Figure 1.56 – Fluorophore and lipid constituents of ER probes[5]

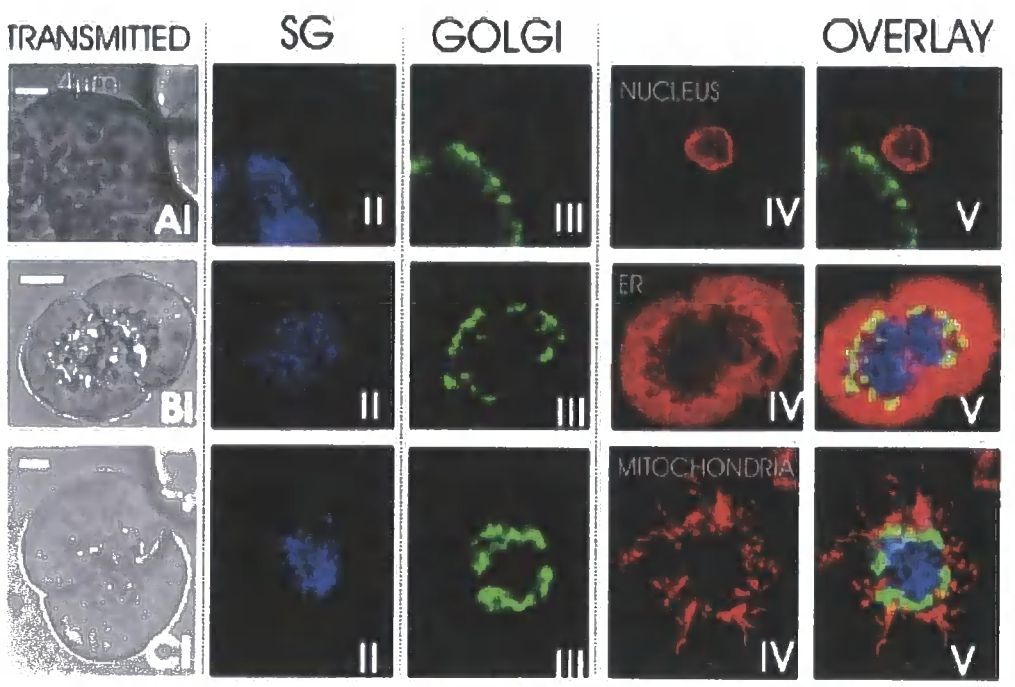

Figure 1.57 – Fluorescence microscopy images showing the location of the Golgi apparatus in relation to other organelles[62]

Such a probe (NBD C_6-ceraminde) has been used in a study, together with Mito-Tracker deep red (mitochondria staining) and BODIPY Texas Red thapsigargin (endoplasmic reticulum staining), investigating the juxtaposition of these organelles in pancreatic acinar cells and their responses to acetocholine-induced signals using Ca^{2+} ions (**Figure 1.57**).[62]

Fluorescently labelled derivatives of Brefeldin **A**, which is a fungal metabolite, are also available for staining the Endoplasmic reticulum and Golgi apparatus.

An interesting result in staining the Endoplasmic reticulum and Golgi apparatus has recently been reported by Villa *et. al.*. They have published the preparation of NBD labelled choline (**Figure 1.58**) and described its use for fluorescence microscopy, in a study using commercially available C_6-NBD-phosphatidylcholine as well.[63]

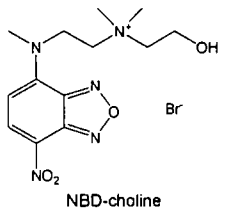

NBD-choline

Figure 1.58 – NBD-choline[63]

These dyes have shown differential localisation profiles in three related cell lines; drug sensitive carcinoma MCF-7 cells, multidrug resistant carcinoma MCF-7/DX cells and normal immortalized MCF10A cells.

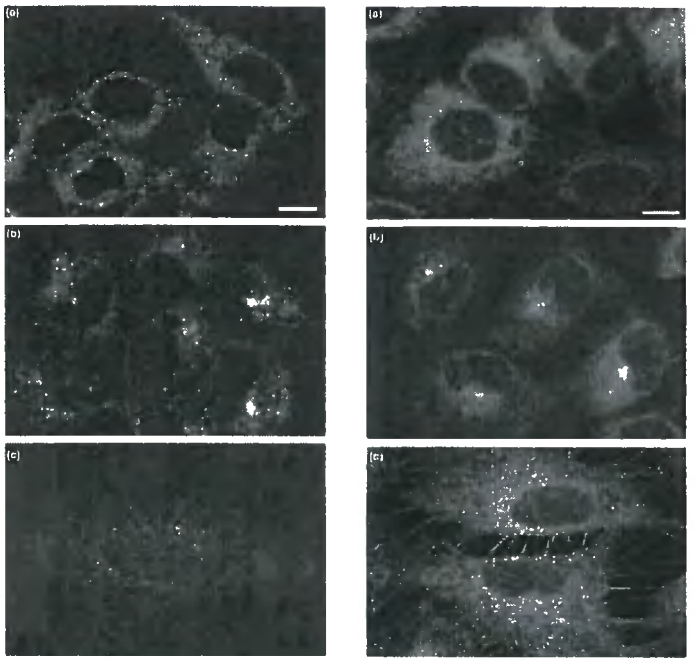

Figure 1.59 – NBD-choline fluorescence images in different cell types a) drug sensitive MCF-7 cells, b) multidrug resistant MCF-7/DX cells, c) normal immortalised MCF10A cells[63]

Both probes localised in the Endoplasmic reticulum of the drug sensitive MCF-7 cells. Predominant staining of the Golgi apparatus was observed with the two probes for the resistant MCF-7/DX cells, with partial ER staining especially with the C_6-NBD-phosphatidylcholine probe. Virtually no staining was observed in the normal MCF10A cells with NBD-choline, but a diffuse signal from the cytosol was observed for C_6-NBD-phosphatidyl choline (**Figure 1.59**).[63]

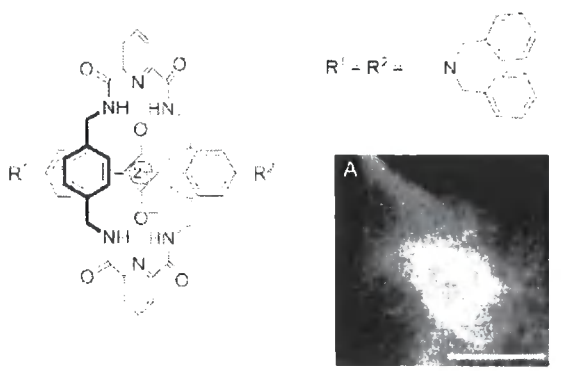

Figure 1.60 – Squaraine rotaxane fluorescent probe and a fluorescence microscopy image[64]

An interesting result has been reported by Smith *et.al.* using squaraine rotaxanes as fluorescent probes (**Figure 1.60**). They have prepared a rotaxane with the squaraine anion, as the fluorophore in the thread being protected by the macrocyclic ring to improve the chemical stability of the fluorophore. Different cellular profiles are observed with this fluorophore in different cell lines, with endoplasmic reticulum staining being observed in CHO cells (**Figure 1.60**).[64]

A europium complex with an acridone moiety has been observed to have cytosolic as well as ER localisation in experiments carried out in Durham (**Figure 1.61**).[65]

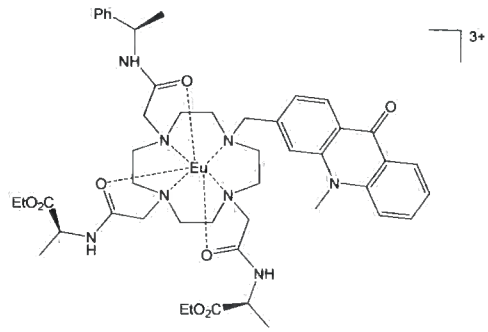

Figure 1.61 – Sturcture of europium complex exhibiting ER localisation[65]

The cell experiments were carried out in NIH 3T3 cells and the localisation was confirmed by costaining with labelled Brefeldin A (**Figure 1.62**).

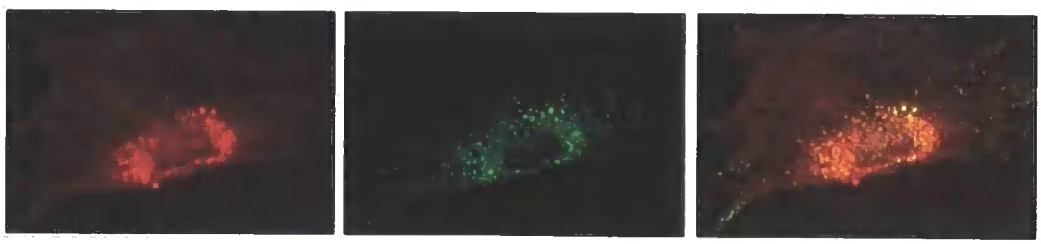

Figure 1.62 – Fluorescence images of NIH 3T3 cells stained with the europium complex (red), labelled Brefeldin A (green) and the colocalisation image[65]

A GFP that localises in the endoplasmic reticulum has been used by Irvine *et. al.* in a study of ER and mitochondrial motility. The study was performed with HEK-293

cells and the authors observed the effect of Ca^{2+} and ATP on the motility of the organelles (**Figure 1.63**).[66]

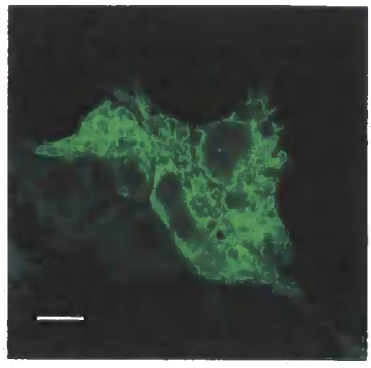

Figure 1.63 – Fluorescence image for an ER localising GFP[66]

The GFP technique was recently used by Garstka *et. al.* in a study on the post translational processes and packing of the 'Major Histocompatibility Complex Class I' molecules in the endoplasmic reticulum and Golgi of wild-type lymphocytes (**Figure 1.64**).[67]

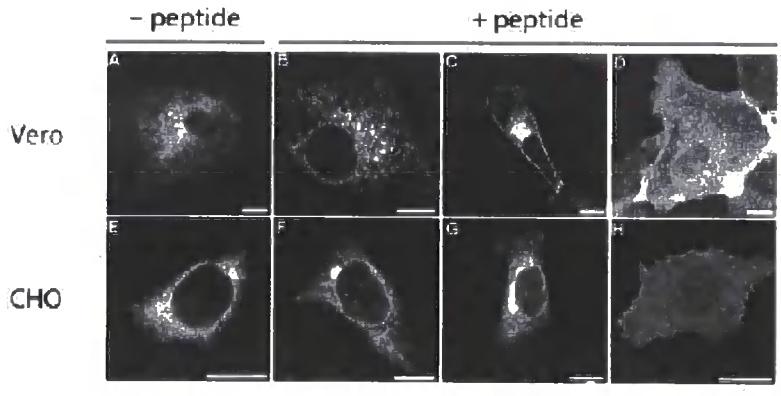

Figure 1.64 – Fluorescence images of H-2D-GFP in Vero and CHO cells showing the translocation of the protein from ER to Golgi in the absence and presence of a peptide that disturbs this cycling[67]

1.4.1.4 Probes for Lysosomes

Lysosomes are the digestive compartments of cells, involved in the processing of material taken up by cells in autophagy and endocytosis. They contain over 50 different hydrolases (e.g. nucleases, proteases, glycosidases, lipases, phosphatases and sulphatases) that operate in acidic conditions. Therefore, the pH of lysosomes is kept at 5.[38, 39]

The lower pH of lysosomes is also used as a means for their labelling with some fluorescent dyes. This, for example is the case for the LysoTracker®[68] dyes from Invitrogen, where a weakly basic amine is linked to the fluorophore. Only a small portion of the probe is thus *N*-protonated at the neutral pH of most of the cell compartments. The amine group gets substantially protonated in the acidic organelles, such as the lysosomes, switching off the photoinduced electron transfer process that quenches the singlet excited state.[5]

Also available are the LysoSensor™ dyes, which show pH dependent changes in their emission spectra. The fluorophore in these probes is quenched by the amino group side chain. This quenching is effectively removed by the protonation of the amino group in weakly acidic compartments. Dyes with different emission maxima and pK_a values are available (**Table 1.4**).

Dye	λ_{Abs} *(nm)*	λ_{Em} *(nm)*	*pKa*
LysoSensor Blue DND-167	373	425	5.1
LysoSensor Green DND-189	443	505	5.2
LysoSensor Green DND-153	442	505	7.5
LysoSensor Yellow/Blue DND-160	384	540[a]	3.9
	329	440[b]	
LysoSensor Yellow/Blue 10000 MW Dextran	381	540[a]	4.2
	335	440[b]	

Table 1.4 – Properties of different LysoSensor dyes (a: pH 3; b: pH 7)[5]

The 2,3,4,5,6-pentafluorotetramethyldihydrorosamine, mentioned in the section on mitochondrial staining, can also stain lysosomes. The compartmental selectivity appears to be dependent on cytosolic redox potential, as mentioned above. Also the (2-aminoethyl)sulphonamide derivative of Dapoxyl® [69] (**Figure 1.65**) shows accumulation in acidic organelles.

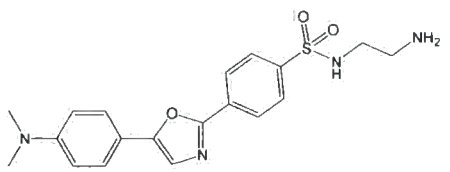

Dapoxyl(R) (2-aminomethyl)sulfonamide

Figure 1.65 – Dapoxyl® lysosomal fluorescence probe[5]

Lysosomal staining has been observed for compounds synthesised as Cathepsin K inhibitors (**Figure 1.66**) containing the piperazine-thiazol-phenyl fluorophore.[70]

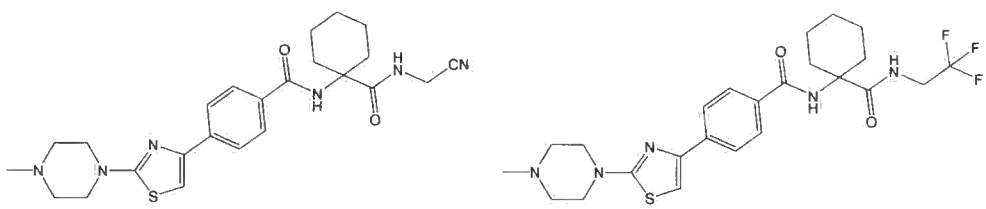

Figure 1.66 – Fluorescent Cathepsin K inhibitors exhibiting lysosomal localisation[70]

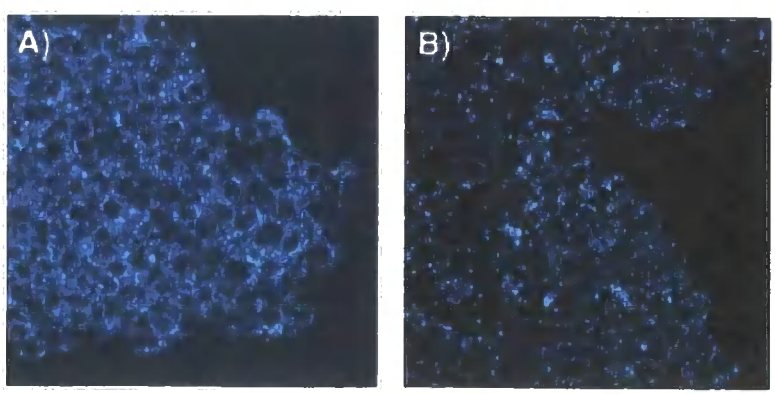

Figure 1.67 – Two photon fluorescence microscopy images of HepG2 cells loaded with Cathepsin K inhibitors showing lysosomal localisation [70]

An analogous Eu complex to that mentioned in the section on endoplasmic reticulum, indeed its constitutional isomer, has been found to localise in lysosomes (**Figure 1.68**).

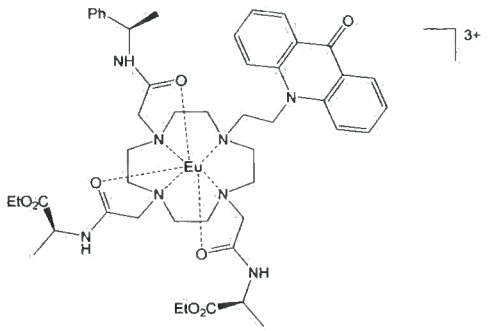

Figure 1.68 – Europium complex localising in lysosomes [8, 65]

The localisation was confirmed in NIH 3T3 cells by co-staining experiments with Lysotracker green (**Figure 1.69**).

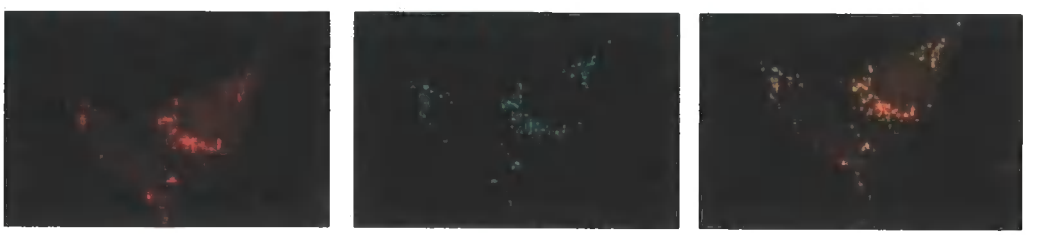

Figure 1.69 – Images of NIH 3T3 cells labelled with the europium complex (red), LysoTracker (green) and the merged image[8, 65]

Further lanthanide complexes were seen to be cell permeant in the work in Durham, and late endosomal or lysosomal localisation is suspected. This has yet to be verified in co-localisation studies.[71, 72]

1.4.1.5 Probes for cellular membranes

Biological membranes are not organelles, as such, but are of paramount importance to the living system. They define the boundaries of cells and organelles, separating

their contents from the surroundings. Their structure does not permit free diffusion of matter from one side to the other. Their basic lipid bilayer structure is enhanced by incorporation of many membrane peptides. These are involved in reactions at the membrane, transport of chemical substances across the membrane or the receipt of chemical information from the surroundings.[38, 39]

The lipid constituents of biological membranes can be sorted into several groups. The major structural theme is their amphiphilicity, meaning that they contain a polar head group and a non-polar (hydrocarbon) tail. There are three major classes of molecules of membrane lipids: phospholipids, sphingolipids and cholesterol and its derivatives.[38,39] Many experiments carried out to enhance the understanding of biological membranes are carried out using models such as vesicles, which range immensely in size and composition.[73]

Many available fluorescent probes, localising into biological membranes, are derived from lipid molecules by the incorporation of fluorophores into the lipid structures. The fluorophores can be incorporated both into the long chain acid tails, as well as the head-groups for phospholipids.

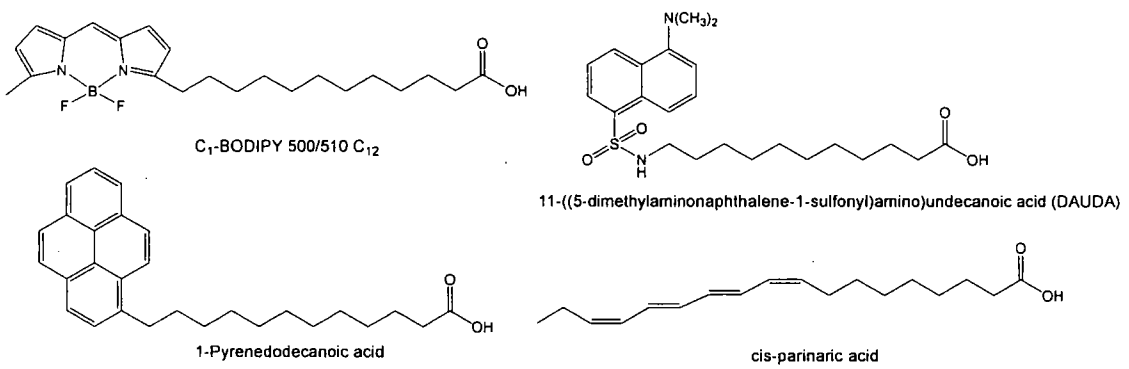

Figure 1.70 – Fluorescently labelled fatty acids[5]

Fluorescently labelled fatty acids (**Figure 1.70**) are available, even though their main use is for incorporation into fluorescent lipid molecules. They are also used directly

as probes for membranes and liposomes as well as in live cell experiments, concerning their metabolic fate.

Phospholipid molecules, fluorescently labelled in the fatty acid part of the molecule (**Figure 1.71**), usually contain the probe in one chain of the acid, acylating position two of glycerol. The most common fluorophores are BODIPY and pyrene molecules. Diphenyl hexatrienyl and NBD fluorophores are used as well. It is, however, suspected that the NBD fluorophore is too polar, and therefore it localises in the head group region rather than deep in the phospholipid bilayer.

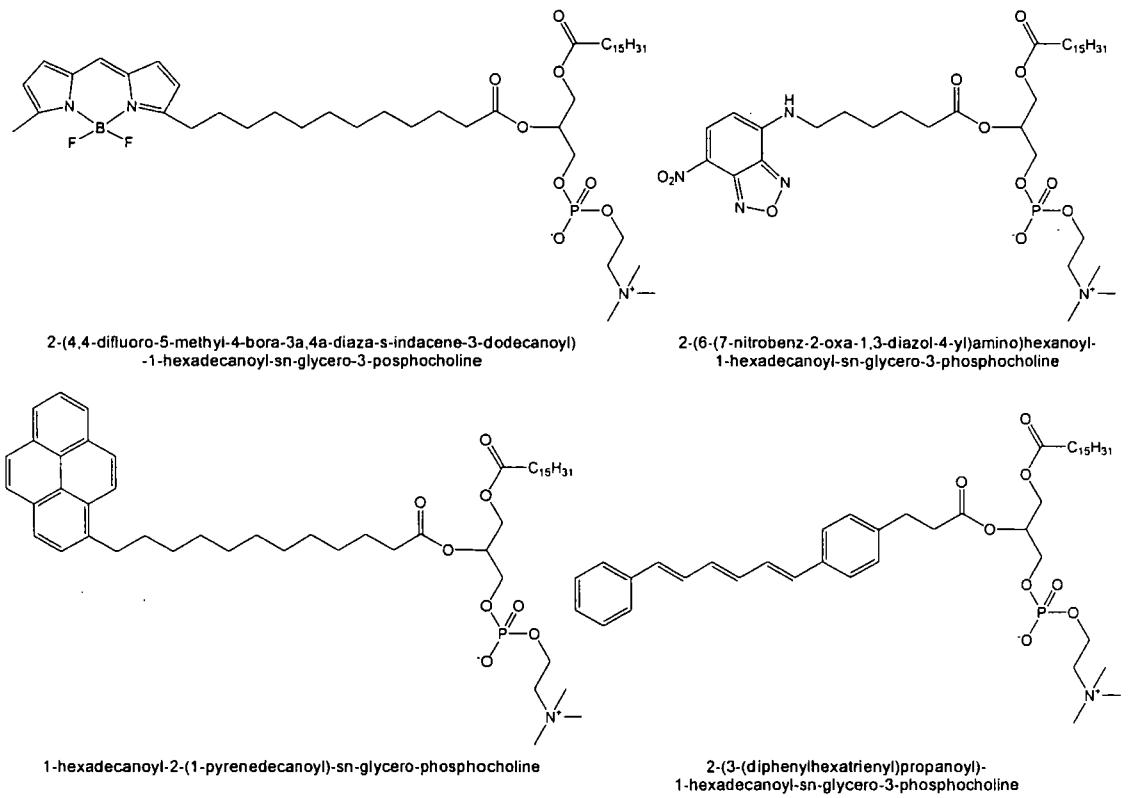

Figure 1.71 – Phospholipids with fluorescent label in fatty acid residues[5]

Both fatty acid residues of the phospholipid molecules may be labelled as well.

NBD labelled phosphatydyl inositol was used in a study of cellular delivery of fluorescently labelled inositol derivatives by polyamine shuttles (**Figure 1.72**).[74]

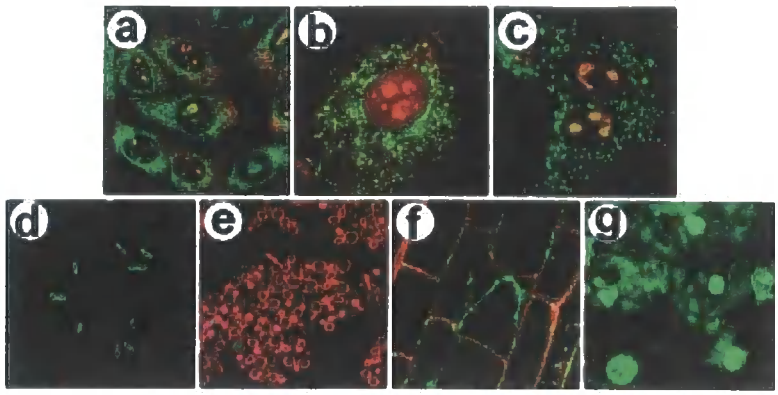

Figure 1.72 – Fluorescent staining by NBD labelled phophatidyl inositol in different cell lines; a) CHO cells, b) 3T3-L1 preadipocyte cells, c) MDCK cells, d) *E. Coli* cells, e) *S. cerevisiae* cells, f) *A. Thaliana* root tip cells and g) *C. Parvum* cells[74]

Head group labelling needs to be carried out with more polar fluorophores such as Marina Blue®, NBD, Fluorescein or Rhodamine (**Figure 1.73**).[75]

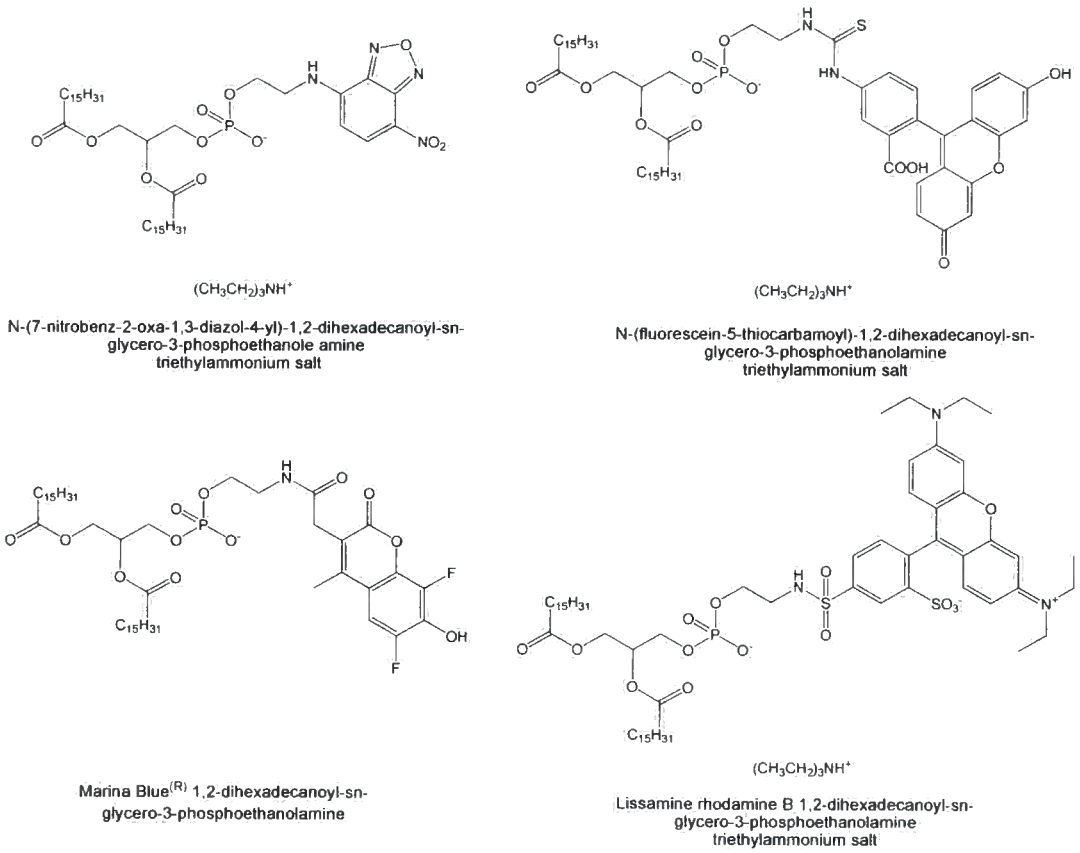

Figure 1.73 – Head group labelled phospholipids[5]

Sphingolipids are important components of biological membranes, especially for eukaryotes. Both sphingomyelin and glycosylsphingolipids, that contain fluorophores are therefore available (**Figure 1.74**). The BODIPY fluorophore is the most common label in these probes.

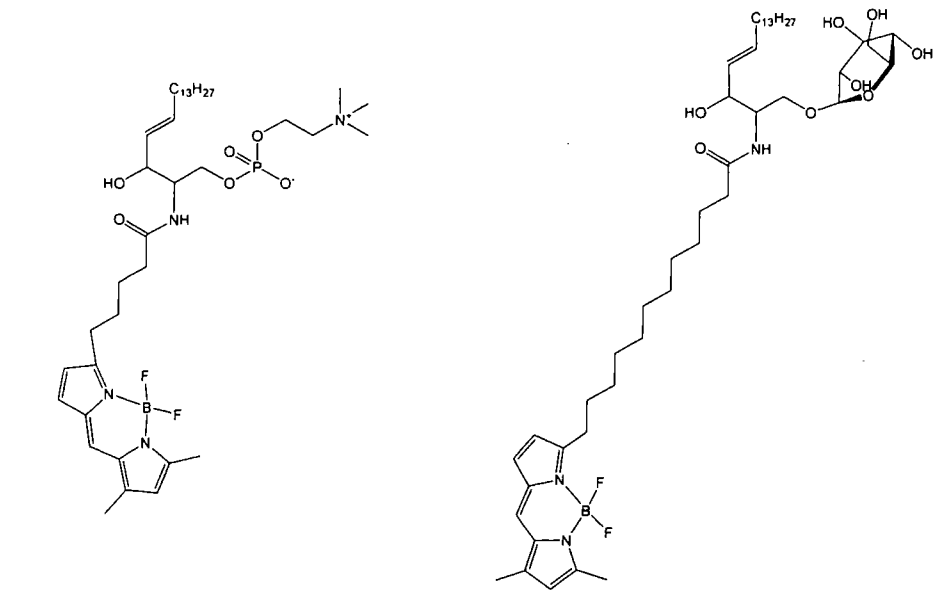

N-(4,4-difluoro-5,7-dimethyl-4-bora-3a,4a-diaza-s-indacene-3-pentanoyl) sphingosyl phosphocholine

N-(4,4-difluoro-5,7-dimethyl-4-bora-3a,4a-diaza-s-indacene-3-dodecanoyl) sphigosyl-1-b-glucopyranoside

Figure 1.74– Fluorescently labelled sphingolipids[5]

Sphingolipids labelled with an NBD fluorophore, such as NBD C_6-ceramide, were extensively used, prior to the development of the BODIPY chromophore.

Cholesteryl esters, where the 3β-hydroxyl group of cholesterol is acylated with a fatty acid incorporating a fluorescent probe, can be used to study the transport of cholesterol in cells or the receptor-mediated endocytosis of lipoproteins. The BODIPY labelled cholesteryl ester is available commercially (**Figure 1.75**). Fluorescent cholesterol derivatives as membrane probes have recently been reviewed by Wüstner.[76]

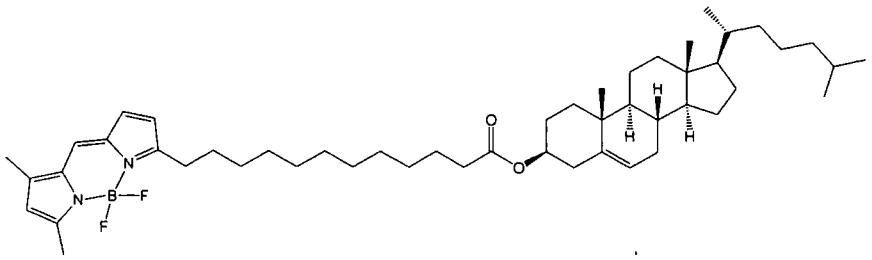

Figure 1.75 – Fluorescently labelled cholesteryl ester[5]

Probes for biological membranes that are not structurally related to their lipid components are available as well. Examples of these are long chain dialkylcarbocyanines, lipophilic coumarines (fluoresceins, rhodamines), diphenyl hexatrienyls, Nile red, prodan, laurdan and anilinonapthalene sulfonates (**Figure 1.76**).[5]

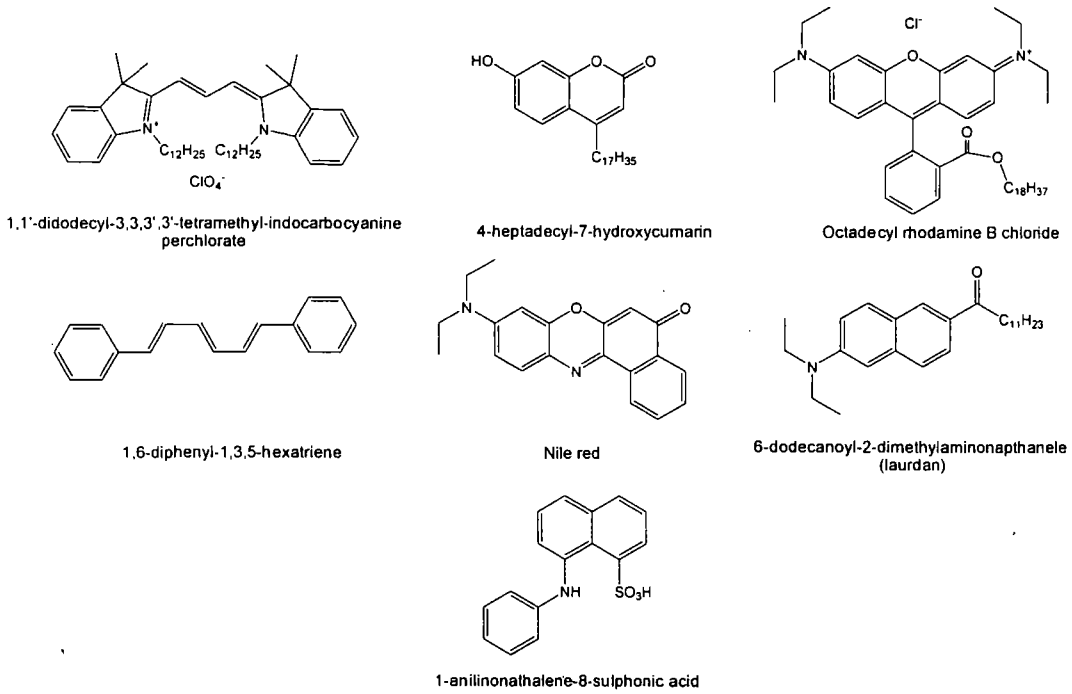

Figure 1.76 – Non-lipid probes for cellular membranes[5]

A range of these probes as well as GFP labelled α-synuclein have been used in the studies of membrane interactions of amyloid fibril forming proteins. These are

summarised in a review by Munishkina and Fink.[77] A further review by Johnson discusses the studies of protein conformations and interactions at membranes.[78]

Traffic of lipid molecules has also been observed by Pagano et al, using BODIPY labelled sphinogmyelin (N-[5-(5,7-dimethyl boron dipyrromethene difluoride)-1-pentanoyl)]-D-*erythro*-sphingosylphosphorylcholine). [79] They have observed the internalisation of the probe from the cellular membrane into endosomes, through endocytosis, and later incorporation into the Golgi apparatus (**Figure 1.77**).

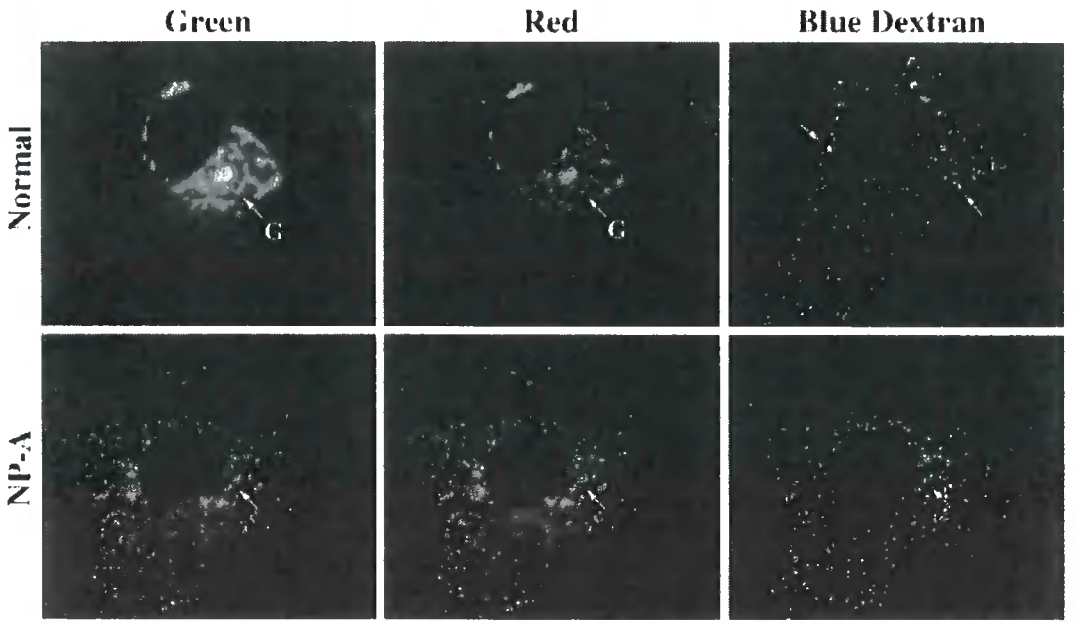

Figure 1.77 – Fluorescent images of normal and Nieman-Pick, Type A human fibroplasts with lysosomes stained by blue fluorescent dextran. The fluorescent probes exhibit concentration dependent emission profiles, emitting in red at high concentration and in green in low concentration[79]

Labelling on the outer side of cellular membranes can be achieved by non-permeant dyes, which can associate with transmembrane proteins. Such an approach was used by Tsien and Hauser, to label the stromal interaction molecule STIM 1 co-expressed with a hexahistidine tag (**Figure 1.78**).[80]

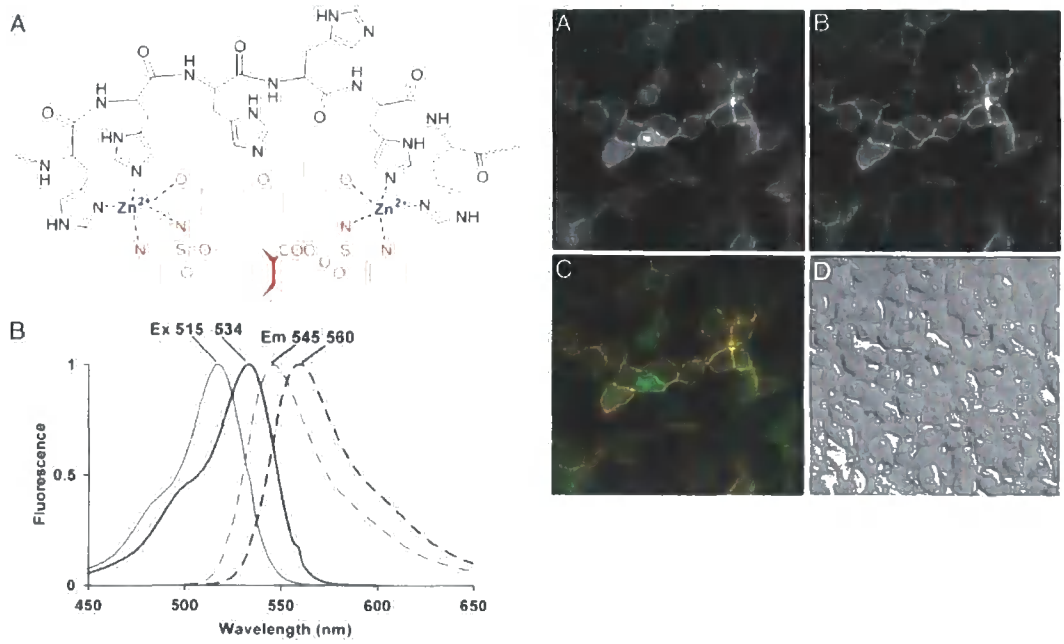

Figure 1.78 – Fluorescence images of cell surface of HEK293T cells coming from the association of the fluorescein probe with the hexahistidine tag by Zn^{2+} complexation[80]

They have achieved labelling of the cellular membrane of HEK293T cells, expressing the given peptide, using the affinity of Zn^{2+} ion for the hexahistidine moiety and a suitably modified fluorescein derivative (**Figure 1.78**).

1.4.1.6 Probes for the cytoskeleton

The cytoskeleton is composed of fibres of cytoskeletal proteins, such as actin and tubulin, which form a network throughout the cytoplasm. Cytoskeletal proteins fulfil many important functions, such as maintaining the shape of the cell, the spatial organisation of organelles and the movement of vesicles within the cell.

Most commercially available probes for the cytoskeleton are based on proteins and antibodies and thus are not usable for live cell imaging. The fluorescent derivatives of Paclitaxel (anticancer drug Taxol) (**Figure 1.79**) and vinblastine (**Figure 1.80**) are some of the exceptions. Oreon Green dye is used for labelling of Paclitaxel and a BODIPY fluorophore for both Paclitaxel and vinblastine.[81, 82]

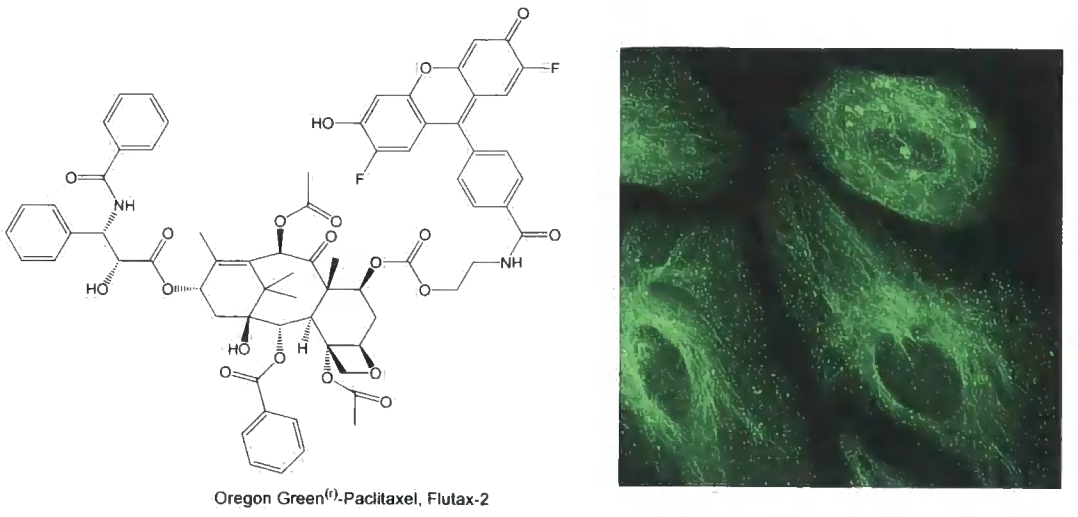

Figure 1.79 - Oregon Green® labelled Taxol (Flutax-2) and a fluorescent image of microtubules of HeLa cells[5, 81]

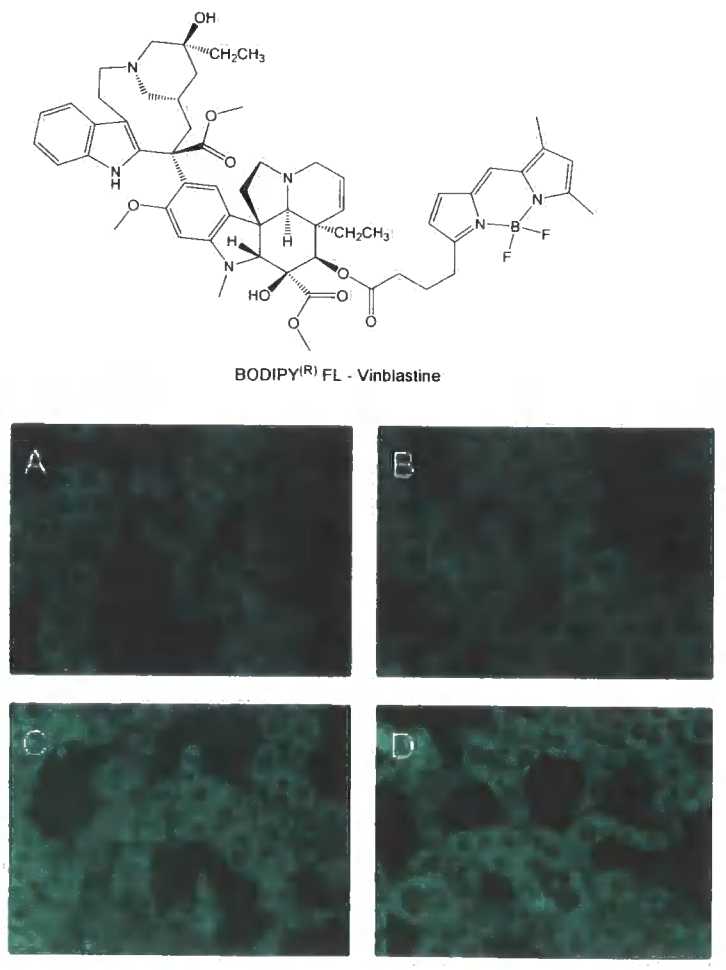

Figure 1.80 – BODIPY® FL labelled Vinblastine and images obtained with Vinblastine-Fluorescein conjugate[5, 82]

The technique of Fluorescent Speckle Microscopy has been used in the analysis of cytoskeleton dynamics as has been discussed in section 1.2.7.

1.4.2 Targeted imaging

Following analysis of the fluorescent molecules, fluorescent proteins apart, mentioned in the preceding brief overview of probes for cellular organelles, it becomes apparent that another classification is possible. Two fluorophore groups can be identified. The first group are molecules where the fluorophore itself is also the moiety determining the fate of the probe *in cellulo* (e.g. Ethidium, Hoechst or MitoTracker). The other group is comprised of probes, where a clear breakdown of the structure to a fluorophore and a localising vector is possible (e.g. lipid based membrane probes, guanidinium mitochondrial probe or fluorescently labelled Taxol and Vinblastine).

The idea of making targeted or specific fluorescent probes by combining a fluorophore and a targeting vector will be discussed further. Preparation of targeted fluorescent probes was one of the major aims of the work presented in this thesis, using luminescent lanthanide complexes as the lumophore.

1.4.2.1 Organelle Targeting

Several conclusions for organelle targeting can be inferred from preceding sections. These should however be treated as guidelines rather than 'hard' rules.

- Nuclear localisation can be expected for molecules including flat aromatic moieties, as these tend to intercalate the DNA and RNA.
- High positive charge favours mitochondrial localisation due to the highly negative potential of the mitochondrial membrane.

- Incorporating the fluorophore into a lipid like structure can enhance localisation into endoplasmic reticulum and Golgi apparatus as they are highly membraneous oranelles.
- Incorporation of weakly basic amino groups into the probe structure should enhance localisation into acidic organelles such as lysosomes

Further developments of targeting vectors, especially of those with low molecular weights, are however needed, to achieve a state where a "toolbox" of such agents would be available.

One possible base for development could be the cell penetrating peptides (CPPs). The permeation and localisation of small molecules and macromolecules alike can be enhanced by conjugation to certain oligopeptide sequences. The seminal work in the field was carried out with the *trans*-activating transcriptional activator (TAT) from HIV-1. Many more CPPs have been identified to date.[83, 84]

Despite having been developed mainly to enhance cellular penetration, they can impart effects on localisation as well. Some of the TAT sequences can impart nuclear localisation.[85] Some of the arginine rich sequences can target mitochondria due to their high positive charge.

The success of the CPPs has been a starting point for the development of new localisation vectors, such as the oligoarginine vector developed by de Mendoza et. al..[57] The aim was to maintain the localisation profile due to the high positive charge imparted by the guanidinium groups, but to remove deficiencies such as the danger of hydrolysis imminent for the peptide chains.

Targeting by means of complex molecules such as taxol or vinblastine as the targeting vectors is also possible.[86] It, however, is a case to case approach rather than a general tool, as targeting based on guests for specific receptors.[87]

1.4.2.2 Macromolecular targeting

Targeting and fluorescently labelling any given macromolecule of choice in the living system can be seen as one of ultimate goals for fluorescent imaging. The most obvious example of coming very close to this aim are the fluorescent proteins, which can be tagged by co-expression to many endogenous peptides.[88] This, however, is not without problems. The major issue is that fluorescent protein probe is the same size as the protein it is reporting. Thus, the localisation and function of the protein monitored may be altered significantly. The development of specific labelling of macromolecules with low molecular weight fluorescent probes is thus necessary, and the goal is still far from being achieved.

A way of labelling the macromolecule in question by the probe needs to be established. Several bioorthogonal reactions have been identified for this purpose. These include formation of hydrazides, the Staudinger ligation and reaction of azides with alkynes.[89] The benefit of these reactions is that they do not need the biological machinery of the cell to make them happen. They still have their drawbacks. To achieve labelling, the cells have to be fed unnatural monomers of macromolecules bearing one of the reactants (eg. azide). In the simplest scenario, these would then be nonspecifically incorporated into the biological macromolecule, which would become labelled reacting with the probe incorporating the other reactant (e.g. triphenyl phosphine) (**Figure 1.81**).[90] This approach is however non-specific, as different macromolecules can be labelled. Incorporation of a larger number of unnnatural residues can also compromise the structure and function of the macromolecule in question. A more specific way of labelling will need to be carried out by interference with the biochemical machinery.

This is most easily realised with peptides where sequences can be added by genetic modification. By modifying the tRNA and the aminoacyl-tRNA synthtase, the above described methodology can be used for specific labelling of protein of choice by an unnatural amino acid (**Figure 1.81**).[91, 92] A most general approach, however, is to incorporate a small oligopeptide chain at the end of the protein of interest, which can then be recognised and used for labelling.

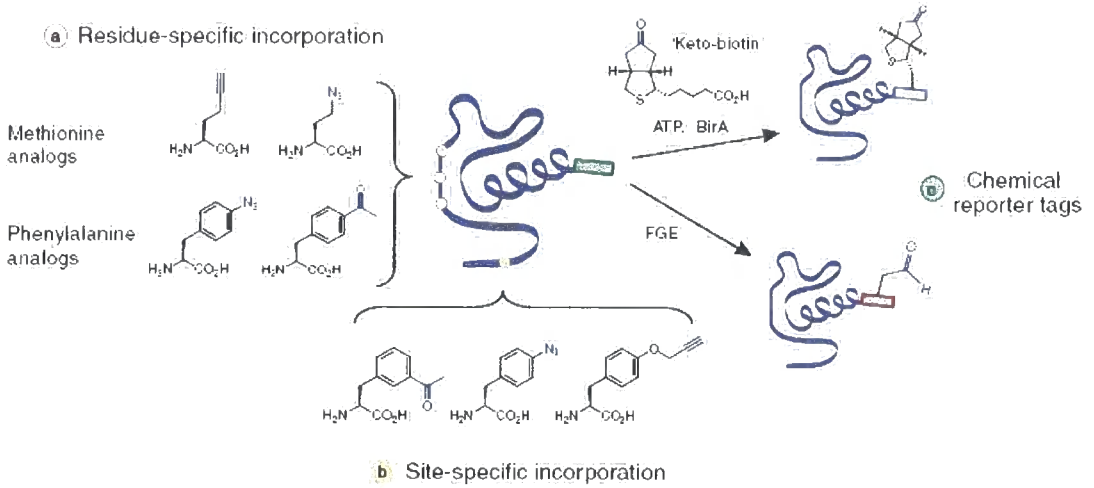

Figure 1. 81 – Some ideas of selective peptide labelling[88]

Such an oligopeptide could be the tetra-cysteine motif used in the formation of FlAsH and ReAsH fluorescent tags.[93] Oligohistidine sequences have also been used for targeting fluorescent probes to a specific protein.[94] Other short peptides can undergo changes during post translational modifications, which can either modify the amino acid residues so that they can be labelled by bioorthogonal reactions (**Figure 1.80**).[95,96] Alternatively, the oligopeptide tag can be labelled directly by an enzymatic reaction such as the reaction of CoA conjugates with the phosphopantetheinyl transferase.[97] Also, an entire enzyme can be tagged to the protein of interest, even though the same problems as for fluorescent proteins will apply, and cause labelling by its action, as in the case of O^6-alkylguanine-DNA alkyltransferase. This enzyme irreversibly transfers an alkyl group from O^6-alkylguanine onto its cysteine residue. Thus, a fluorescent label can be introduced to a protein of interest co-expressed with this enzyme.[98]

All of these techniques still need to be developed for practicable use in targeted fluorescent labelling, but they are a promising starting point for further development.

1.5 Introduction to lanthanide lumniescence

The aim of the work presented in this thesis was the synthesis of luminescent lanthanide complexes as cellular probes. Hence, it is fitting to describe the principles governing lanthanide luminescence at this point.

1.5.1.1 The forbidden nature of *ff* transitions [99, 100, 101, 102, 103]

The predominant oxidation state of lanthanides in solution is +3 and the corresponding $4f^n$ electron configurations apply. The 4*f* electrons are strongly shielded from surroundings by 5*s* and 5*p* outer shells resulting in a weak splitting of the *ff* transitions (~100 cm^{-1}). This results in very sharp absorption and emission bands of lanthanides, in comparison with *dd* bands of transition metals, which are strongly split by ligand fields. Despite this general rule the relative intensities and fine structure of the bands can carry a substantial amount of information (especially for Eu^{3+}).

The *ff* transitions in Ln^{3+} ions are Laporte forbidden with increased intensities for systems without a centre of symmetry or those where the centre of symmetry is removed by coupling the electronic transition with a vibrational state. Low molar extinction coefficients (<10 M^{-1} cm^{-1}) are one practical result of the *ff* transition being forbidden. Long luminescence liftetimes is the second outcome. Whereas the first implication of the forbidden nature of *ff* transition creates an obstacle in the design of lanthanide luminescent complexes, the second is highly favourable, since long luminescence lifetimes are beneficial for cellular imaging purposes.

Lanthanide ions can emit both in the visible range (Tb^{3+}, Eu^{3+}) as well as in the near infrared region (Nd^{3+}, Er^{3+} and Yb^{3+}) part of the spectrum. Only complexes of Tb^{3+} and Eu^{3+} have been synthesised in the presented work.

1.5.2 Sensitised emission

Sensitised excitation of the lanthanide ions is used to bypass the problem of their low extinction coefficients. A suitable organic chromophore is used to absorb the light. Thus, the chromophore is excited to one of its singlet excited states S_1. An intersystem crossing to its triplet excited state T_1 follows after vibrational relaxation to the lowest S_1 level. Chromophore fluorescence is a competition process, hence fast intersystem crossing is necessary for efficient sensitisation. The lanthanide ion is excited by energy transfer from the chromophore T_1 state (**Figure 1.83**). Sufficient separation of the T_1 and lanthanide emissive states is necessary (>1700 cm^{-1}) to prevent thermally activated back energy transfer, which would lead to the reduction of the emission intensity and lifetime. The emissive energy levels lie at 17 240 cm^{-1} ($^5D_0$, Eu^{3+}) and 20 400 cm^{-1} ($^5D_4$, Tb^{3+}), and intramolecular energy transfer to these levels therefore requires that the sensitising triplet possesses an energy in excess of 22 500 cm^{1}.

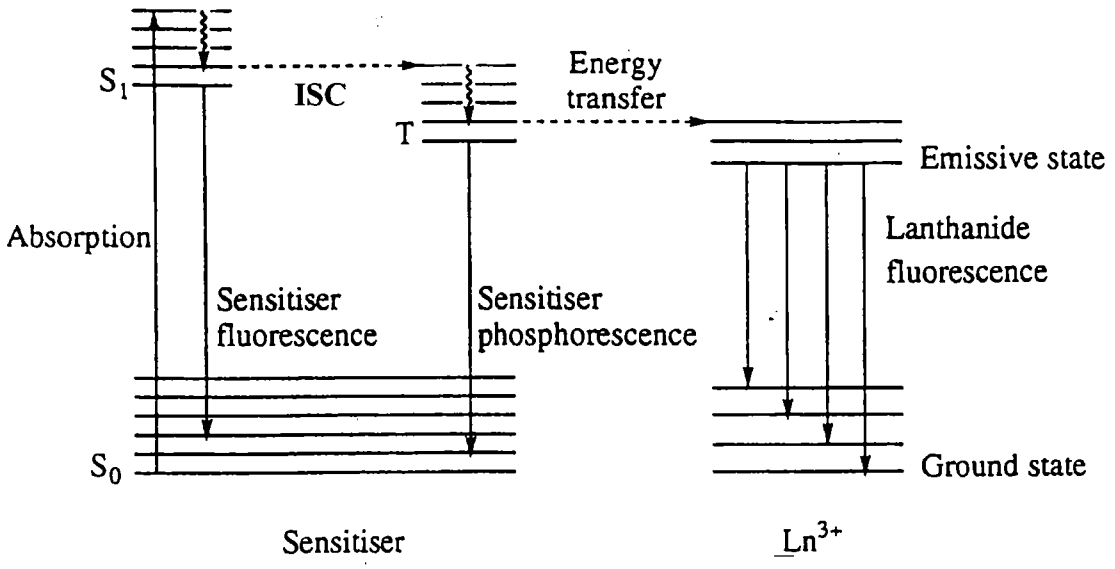

Figure 1.82 – Simplified Jablonski diagram for sensitised emission of lanthanide (III) ions[8, 99]

This involvement of several excited states leads also to large Stokes' shifts for lanthanide emission, which is a further advantage for their use as cellular probes.

1.5.3 Basic features of europium and terbium (III) emission spectra

Emission spectra of lanthanide ions consist of several well defined bands. The ratio of intensities and fine structure of these bands can provide information about the coordination sphere of the lanthanide, especially in the case of europium.

The emissive state of Eu(III) complexes is $^5D_0$ and the strongest emission comes from the transitions to the $^7F_1$ and $^7F_2$ states at 590 and 612 nm respectively (**Figure 1.83**). The transition to the $^7F_1$ state ($\Delta J = 1$) has magnetic dipole character and is not very sensitive to the structure of the coordination sphere. However, the transition to $^7F_2$ ($\Delta J = 2$) state is electric dipole in character with high sensitivity to the nature and symmetry of the coordination sphere. Symmetry determines the number of bands in the $\Delta J = 1$ region giving two bands for complexes with C_4 symmetry and at least three bands for less symmetric ones. The last relatively intense transition is to the $^7F_4$ state, which is predominantly electric dipole in character and thus sensitive to the ligand field. There are more small intensity transitions in the Eu spectrum. The transition to $^7F_0$ at 580 nm is one of them. Its energy is sensitive to ligand environment and it may therefore be used to probe the homogeneity of the europium speciation. Thus, the number of bands in this transition depends on the number of chemically distinct environments of Eu(III) ion.

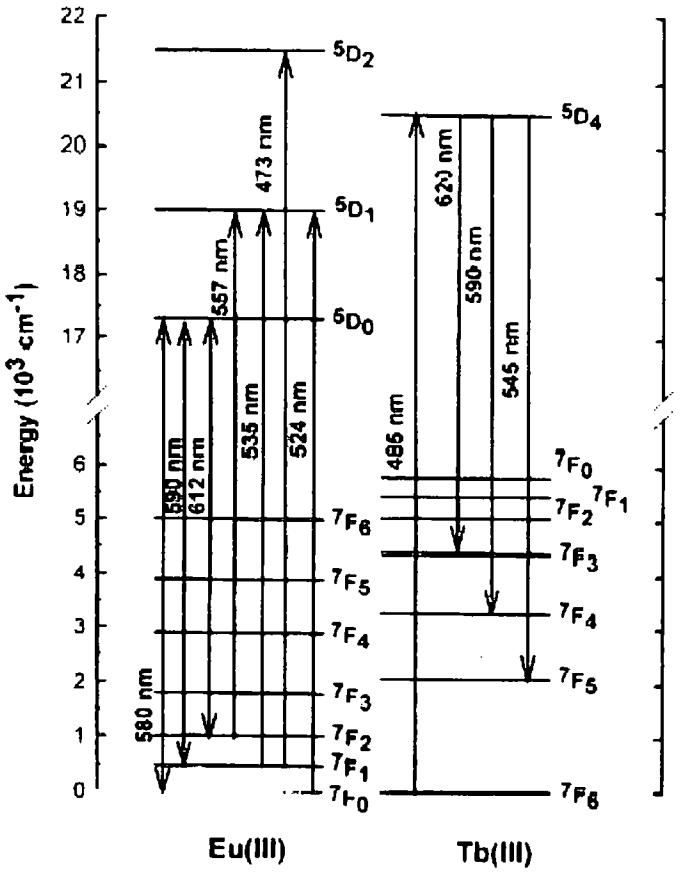

Figure 1.83 – Schematic diagram showing transitions corresponding to different bands in emission spectra of Eu^{3+} and Tb^{3+} [8, 99]

The Tb(III) emission spectrum offers less structural information. Its emissive level is $^5D_4$ and the major band comes from the transition to the $^7F_5$ state ($\Delta J = 1$) at 545 nm (**Figure 1.83**). It is hypersensitive, but not as sensitive as the transition to $^7F_2$ state in Eu(III). Even analysis of the fine structure of the spectrum does not give much information on the coordination sphere of the ion because of the large number of unresolved transitions in the bands.

1.5.4 Energy dissipation pathways[104, 105]

The pathway of sensitised emission of lanthanide ions contains three excited states (**Figure 1.84**). These are: (i) the chromophore singlet excited state (S_1), (ii) the chromophore triplet excited state (T_1) and (iii) the lanthanide excitated state. Energy can either be passed on through the system from S_1 state to the light emission from lanthanide centre or it can be dissipated by a number of competing processes.

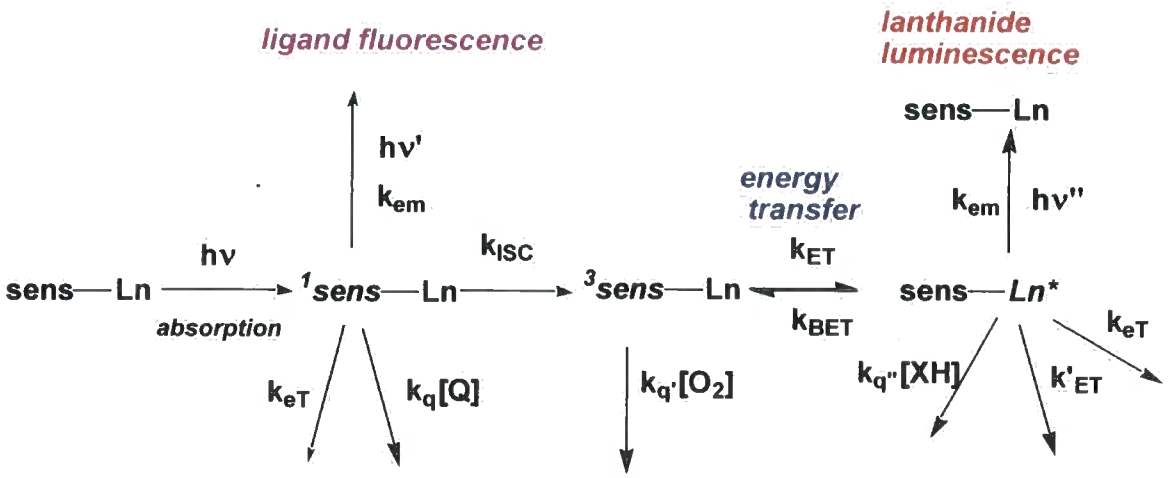

Figure 1.84 – A kinetic scheme of energy transfer processes in the lanthanide ion sensitisation pathway[8, 99]

The singlet state of the chromophore can release its energy by the desired inter system crossing to the triplet state, fluorescence or be quenched by energy or electron transfer. Fast intersystem crossing therefore increases the overall efficiency of the sensitisation pathway.

Molecular oxygen is a classical quencher of triplet states, which yields singlet oxygen and the ground state of the chromophore. Chromophore phosphorescence and back intersystem crossing are the other common competing pathways to the desired energy transfer to the lanthanide ion.

Lanthanide excited state deactivation, apart from the desired emission of a photon, can proceed by several pathways. It was previously mentioned that a small enough energy gap between the lanthanide excited state and chromophore triplet state can result in back energy transfer. Energy then can be dissipated by competing procesess at the triplet state.

It has been experimentally established that OH, NH and CH oscillators can deactivate the lanthanide emissive state. This takes place by vibrational energy transfer to bound solvent molecules or the ligand (**Figure 1.85**). Both emission intensity and lifetime decrease in this case.

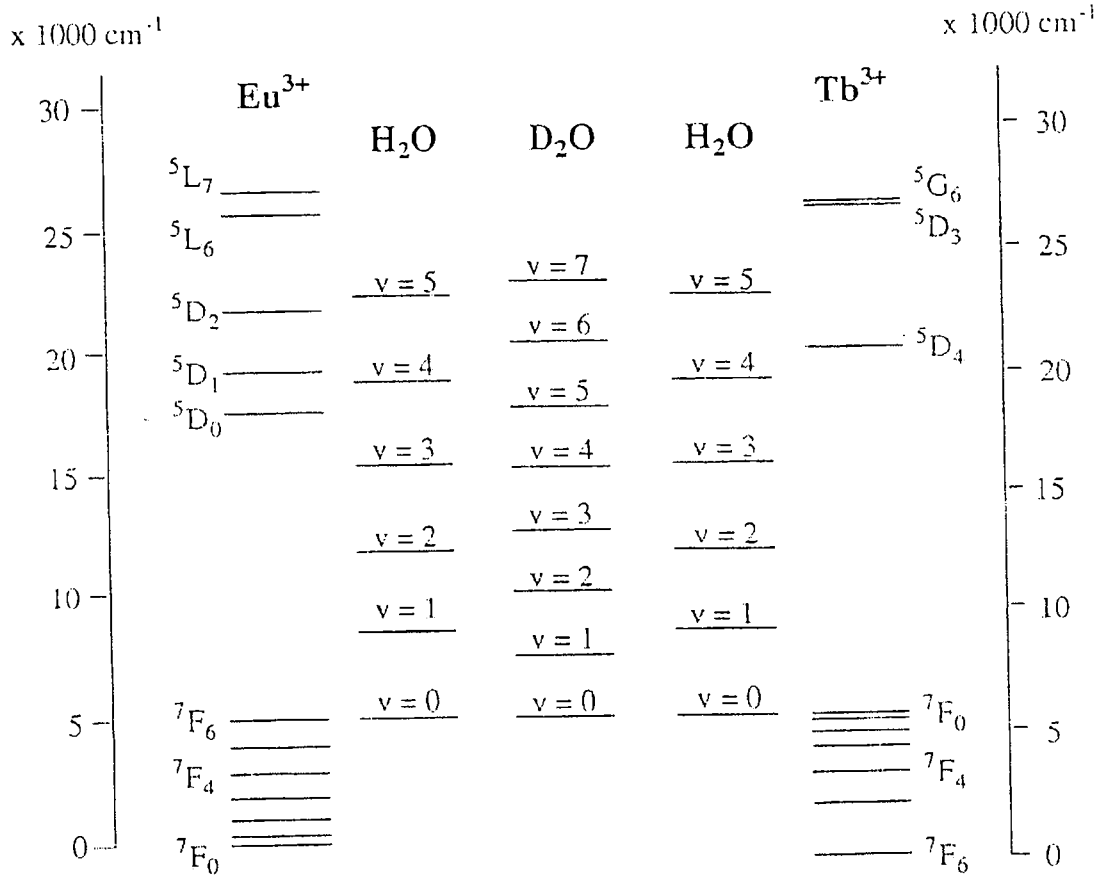

Figure 1.85 – Lanthanide excited state deactivation by vibrational relaxation[8, 99]

It is amine NH groups of the ligand and the OH oscillators in bound water molecules that are the most efficient quenchers. The energy gap of 12 000 cm^{-1} for Eu^{3+} as opposed to 15 000^{-1} for Tb^{3+} makes Eu(III) more sensitive to this type of quenching. This is because in the case of Eu^{3+} the energy is best matched with the third vibrational overtone of OH vibration compared to the fourth overtone in the case Tb^{3+}. The Franck-Condon overlap factor is less favourable for Tb^{3+}. The OD oscillators have a lower frequency and matching is therefore possible only with higher vibrational states, which leads to significantly lower levels of quenching in D_2O. Significant quenching by amide NH and CH vibrations is observed for Eu^{3+} but is much less pronounced for Tb^{3+}.

A further quenching mechanism of the lanthanide excited states by electron transfer from electron rich species will discussed in detail in Chapter 3 of this thesis.

The presence of the deactivation pathways described above implies that the structures of the ligands for the luminescent lanthanide complexes need to be designed carefully to obtain highly emissive complexes. Some of the complexes suitable for cellular imaging were mentioned in earlier sections of this chapter and the knowledge gained in their synthesis and administration in cellular imaging experiments was used as the basis for the work presented herein.

Literature

[1]) D. Evanko, *Nature Methods*, 2005, **2**, 901.
[2]) J. R. Lakovicz, *Principles of Fluorescence Spectroscopy Second Edittion*, Kluwer Academic/Plenum Publishers, New York, Boston, Dordrecht, London, Moscow, 1999.
[3]) J. Zhang, R. E. Campbell, A. Y. Ting, R. Y. Tsien, *Nature Reviews Molecular Cell Biology*, 2002, **3**, 906.
[4]) M. Gumbleton, D. J. Stephens, *Advanced Drug Delivery Review*, 2005, **57**, 5.
[5]) R. P. Haughland, *The Handbook: A Guide to Fluorescent Probes and Labeling Technologies 10th Edition*, Molecular Probes® Invitrogen detection technologies, USA, 2005.
[6]) M. Zimmer, *Chemical Reviews*, 2002, **102**, 759.
[7]) X. Michalet, F. F. Pinaud, L. A. Bentolila, J. M. Tsay, S. Doose, J. J. Li, G. Sundarsesan, A. M. Wu, S. S. Gambhir, S. Weiss, *Science*, 2005, **307**, 538.
[8]) S. Pandya, J. Yu, D. Parker, *Dalton Transactions*, 2006, 2757.
[9]) V. Ntziachristos, *Annual Rivew of Biomedical Engineering*, 2006, **8**, 1.
[10]) J. Rao, A. Dragulescu-Andrasi, H. Yao, *Current Opinion in Biotechnology*, 2007, **18**, 17.
[11]) N. J. Emptage, *Current Opinion in Phamrmacology*, 2001, **1**, 521.
[12]) J. K. Jaiswal, S. M. Simon, *Nature Chemical Biology*, 2007, **3**, 92.
[13]) J. Bewersdorf, R. Schmidt, S. W. Hell, *Journal of Microscopy*, 2006, **222**, 105.
[14]) S. Jakobs, *Biochimica et Biophysica Acta*, 2006, 561.
[15]) K. Kikuchi, H. Takakusa, T. Nagano, *Trends in Analytical Chemistry*, 2004, **23**, 407.
[16]) E. A. Jares-Erijman, T. M. Jovin, *Nature Biotechnology*, 2003, **21**, 1387.
[17]) R. B. Sekar, A. Periasamy, *Journal of Cell Biology*, 2003, **160**, 629.
[18]) B. N. G. Giepmans, S. R. Adams, M. H. Ellisman, R. Y. Tsien, *Science*, 2006, **312**, 217.
[19]) D. Maurel, J. Kniazeff, G. Mathis, E. Trinquet, J. Pin, H. Ansanay, *Analytical Biochemistry*, 2004, **329**, 253.
[20]) P. I. H. Bastiaens, A. Squire, *Trends in Cell Biology*, 1999, **9**, 48.
[21]) F. Festy, S. M. Ameer-Beg, T. Ng, K. Suhling, *Molecular BioSystems*, 2007, **3**, 381.
[22]) J. S. Goodwin, A. K. Kenworthy, *Methods*, 2005, **37**, 154.
[23]) E. Rittweger, B. R. Rankin, V. Westphal, S. W. Hell, *Chemical Physics Letters*, 2007, **442**, 483.
[24]) G. Danuser, C. M. Waterman-Storer, *Annual Review of Biophysics and Biomolecular Structure*, 2006, **35**, 361.
[25]) G. Danuser, C. M. Waterman-Storer, *Journal of Microscopy*, 2003, **211**, 191.
[26]) N. Panchuk-Voloshina, Ro. P. Haugland, J. Bishop-Stewart, M. K. Bhalgat, P. J. Millard, F. Mao, W. Leung, Ri. P. Haugland, *Journal of Histochemistry and Cytochemistry*, 1999, **47**, 1179.
[27]) J. E. Berlier, A. Rothe, G. Buller, J. Bradford, D. R. Gray, B. J. Filanoski, W. G. Telford, S. Yue, J. Liu, C. Cheung, W. Chang, J. D. Hirsch, J. M. Beechem, Ro. P. Haugland, Ri. P. Haugland, *Journal of Histochemistry and Cytochemistry*, 2003, **51**, 1699.
[28]) Y. Urano, M. Kamiya, K. Kanda, T. Ueno, K. Hirose, T. Nagano, *Journal of the American Chemical Society*, 2005, **127**, 4888.
[29]) J. R. Carreon, K. M. Stewart, K. P. Mahon Jr., S. Shin, S. O. Kelley, *Bioorganic &Medicinal Letters*, 2007, **17**, 5182.
[30]) N. C. Shaner, P. A. Steinbach, R. Y. Tsien, *Nature Methods*, 2005, **2**, 905.
[31]) O. Griesbeck, *Current Opinion in Neurobiology*, 2004, **14**, 636.
[32]) F. S. Wouters, P. J. Verveer, P. I. H Basteiaens, *Trends in Cell Biology*, 2001, **11**, 203.
[33]) M. Zaccolo, *Circulation Research*, 2004, 866.
[34]) V. V. Verkhusha, K. A. Lukyanov, *Nature Biotechnology*, 2004, **22**, 289.
[35]) The R. Y. Tsien group website: http://www.tsienlab.ucsd.edu/Documents.htm
[36]) N. Kaji, M. Tokeshi, Y. Baba, *Analytical Sciences*, 2007, **23**, 21.
[37]) A. J. Amoroso, M. P. Coogan, J. E. Dunne, V. Fernández-Moreira, J. B. Hess, A. J. Hayes, D. Lloyd, C. Millet, S. J. A. Pope, C. Williams, *Chemical Communications*, 2007, 3066.
[38]) G. L. Zubay, W. W. Parson, D. E. Vance, *Principles of Biochemistry*, Wm. C. Brown Publishers, USA, 1995.
[39]) C. J. Avers, *Molecular Cell Biology*, Addison-Wesley Publishing company, USA, 1986.
[40]) S. Perticarari, G. Presani, E. Banfi, *Journal of Immunological Methods*, 1994, **170**, 117.
[41]) M. Kubista, B. Akerman, B. Norden, *Biochemistry*, 1987, **26**, 4545.
[42]) L. W. Trestappen, H. Meiners, M. R. Loken, *Journal of Immunological Methods*, 1989, **123**, 103.

[43]) R. B. Knowles, K. S. Kosik, *Proceedings of the National Academy of Sciences USA*, 1997, **94**, 14804.
[44]) Q. Li, Y. Kim, J. Namm, A. Kulkarni, G. R. Rosania, Y. Ahn, Y. Chang, *Chemistry &Biology*, 2006, **13**, 615.
[45]) T. Kanda, K. F. Sullivan, G. M. Wahl, *Current Biology*, 1998, **8**, 377.
[46]) L. Trinkle-Mulcahy, A. I. Lamond, *Science*, 2007, **318**, 1402.
[47]) R. A. Poole, G. Bobba, M. J. Cann, J. C. Frias, D. Parker, R. D. Peacok, *Organic and Biomolecular Chemistry*, 2005, **3**, 1013.
[48]) J. Yu, D. Parker, R. Pal, R. A. Poole, M. J. Cann, *Journal of the American Chemical Society*, 2006, **128**, 2294.
[49]) M. Yasuda, P. Theodorakis, T. Subramanian, G. Chinnadurai, The *Journal of Biological Chemistry*, 1998, **273**, 12415.
[50]) T. Minamikawa, A. Sriratana, D. A. Williams, D. N. Bowser, J. S. Hill, P. Nagley, *Journal of Cell Science*, 1999, **112**, 2419.
[51]) J. F. Keij, C. Bell-Prince, J. A. Steinkamp, *Cytometry*, 2000, **39**, 203.
[52]) C. S. Chen, K. R. Gee, *Free Radical Biology & Medicine*, 2000, **28**, 1266.
[53]) K. M. Robinson, M. S. Janes, M. Pehar, J. S. Monette, M. F. Ross, T. M. Hagen, M.P. Murphy, J. S. Beckman, *Proceedings of the Natural Academy of Sciences USA*, 2006, **103**, 15038.
[54]) P. Mukhopadhyay, M. Rajesh, K. Yoshihiro, G. Haskó, P. Pacher, *Biochemical and Biophysical Research Communications*, 2007, 203.
[55]) S. Taliani, F. Simorini, V. Sergianni, C. La Motta, F Da Settimo, B. Cosimelli, E. Abignente, G. Greco, E. Novellino, L. Rossi, V. Gremigni, F. Spinetti, B. Chelli, C. Martini, *Journal of Medicinal Chemistry*, 2007, **50**, 404.
[56]) Y. Koide, Y. Urano, S. Kenmoku, H. Kojima, T. Nagano, *Journal of American Chemical Society*, 2007, **129**, 10324.
[57]) J. Fernádez-Carneado, M. Van Gool, V. Martos, S. Castel, P. Prados, J. De Mendoza, E. Giralt, *Journal of the American Chemical Society*, 2005, **127**, 869.
[58]) K. K. Maiti, W. S. Lee, T. Takeuchi, C. Watkins, M. Fretz, D. C. Kim, S. Futaki, A. Jones, K. T. Kim, S. E. Chung, *Angewandte Chemie International Edition*, 2007, **46**, 5880.
[59]) G. T. Hanson, R. Aggeleri, D. Oglesbee, M. Cannon, R. A. Capaldi, R. Y. Tsien, S. J. Remington, *The Journal of Biological Chemistry*, 2004, **279**, 13044.
[60]) L. Cole, D. Davies, G. J. Hyde, A. E. Ashford, *Journal of Microscopy*, 2000, **197**, 239.
[61]) K. E. Fogarty, J. F. Kidd, A. Turner, J. N. Skepper, J. Carmichael, P. Thorn, *The Journal of Biological Chemistry*, 2000, **275**, 22487.
[62]) N. J. Dolman, J. V. Gerasimenko, O. V. Gerasimenko, S. G. Voronina, O. H. Petersen, A. V. Tepikin, *The Journal of Biological Chemistry*, 2005, **280**, 15794.
[63]) A. M. Villa, E. Caporizzo, A. Papagni, L. Miozzo, P. Del Buttero, M. D. Grilli, N. Amboldi, F. Fazio, S. M. Doglia, B. Giglioni, *European Journal of Cancer*, 2005, **41**, 1453.
[64]) J. R. Johnson, N. Fu, E. Arunkumar, W. M. Leewy, S. T. Gammon, D. Piwnica-Worms, B. D. Smith, *Angewandte Chemie International Edition*, 2007, **46**, 5528.
[65]) Y. Bretonniere, M. J. Cann, D. Parker, R. Slater, *Organic and Biomolecular Chemistry*, 2004, **2**, 1624.
[66]) D. Brough, M. J. Schell, R. F. Irvine, *Biochemical Journal*, 2005, **392**, 291.
[67]) M. Garstka, B. Borchert, M. Al-Balushi, P. Praveen, N. Kühl, I. Majoul, R. Duden, S. Springer, *Journal of Biological Chemistry*, 2007, **282**, 30680.
[68]) T. Haller, J. Ortmayr, F. Friedrich, H. Völkl, P. Dietl, *Proceedings of the Natural Academy of Sciences*, 1998, **95**, 1579.
[69]) Z. Diwu, Y. Lu, C. Zhang, D. H. Klaubert, R. P. Haugland, *Photochemistry and Photobiology*, 1997, **66**, 424.
[70]) W. C. Black, M. D. Percival, *ChemBioChem*, 2006, **7**, 1525.
[71]) C. P. Montgomery, L. Lamarque, D. Parker, *Chemical Communications*, 2007, 3841.
[72]) R. A. Poole, C. P. Montgomery, E. J. New, A. Congreve, M. Botta, D. Parker, *Organic and Biomolecular Chemistry*, 2007, **5**, 2055.
[73]) L. A. Bagatolli, *Biochimica et Biophysica Acta*, 2006, 1541.
[74]) S. Ozaki, D. B. DeWald, J. C. Shope, J. Chen, G. D. Prestwich, *Proceedings of the National Academy of Sciences USA*, 2000, **97**, 11286.
[75]) P. S. Upster, R. E. Pagano, *Methods of Enzymology*, 1989, **171**, 850.
[76]) D. Wüstner, *Chemistry and Physics of Lipids*, 2007, **146**, 1.

[77]) L. A. Munishkina, A. L. Fink, *Biochimica et Biophysica Acta*, 2007, 1862.
[78]) A. E. Johnson, *Traffic*, 2005, **6**, 1078.
[79]) R. E. Pagano, R. Watanabe, C. Wheatley, C. Chen, *Chemistry and Physics of Lipids*, 1999, **102**, 55.
[80]) C. T. Hauser, R. Y. Tsien, *Proceedings of the National Academy of Sciecnes USA*, 2007, **104**, 3693.
[81]) J. F. Díaz, I. Barasoain, J. M. Andreu, *The Journal of Biological Chemistry*, 2003, **278**, 8407.
[82]) E. Alli, J. Bash-Babulla, J. M. Yang, W. N. Hait, *Cancer Research*, 2002, **62**, 6864.
[83]) V. P. Trochilin, *Annual Reviews of Biomedical Engineering*, 2006, **8**, 343.
[84]) J. Temsamani, P. Vidal, *Drug Discovery Today*, 2004, **9**, 1012.
[85]) C. Rudolph, C. Plank, J. Lausier, U. Shillinger, R. H. Müller, J. Rosenecker, *The Journal of Biological Chemistry*, 2003, **278**, 11411.
[86]) K. Licha, C. Hessenius, A. Becker, P. Henklein, M. Bauer, S. Wisniewski, B. Wiedenmann, W. Semmler, *Bioconjugate Chemistry*, 2001, **12**, 44.
[87]) J. Farinas, A. S. Verkman, *The Journal of Biological Chemistry*, 1999, **274**, 7603.
[88]) J. A. Prescher, C. R. Bertozzi, *Nature Chemical Biology*, 2005, **1**, 13.
[89]) N. J. Agard, J. M. Baskin, J. A. Prescher, A. Lo, C. R. Bertozzi, *Chemical Biology*, 2006, **1**, 644.
[90]) J. C. M. van Hest, K. L. Kiick, D. A. Tirrell, *Journal of the American Chemical Society*, 2000, **122**, 1282.
[91]) L. Wang, P. G. Schultz, *Angewandte Chemie International Edition*, 2005, **44**, 34.
[92]) I. Chen, A. Y. Ting, *Current Opinion in Biochechnology*, 2005, **16**, 35.
[93]) T. Gronemeyer, G. Godin, K. Johnson, *Current Opinion in Biotechnology*, 2005, **16**, 453.
[94]) E. G. Guignet, J. M. Segura, R. Hovius, H. Vogel, *Chemical Physics and Physical Chemistry*, 2007, **8**, 1221.
[95]) P. J. Hudson, C. Souriau, *Nature Methods*, 2003, **9**, 129.
[96]) T. Dierks, B. Schmidt, L. V. Borrisenko, J. Peng, A. Preusser, M. Mariappan, K. von Figura, *Cell*, 2003, **113**, 435.
[97]) J. Yin, P. D. Straight, S. M. McLoughlin, Z. Zhou, A. J. Lin, D. E. Golan, N. L. Kelleher, R. Kolter, C. T. Walsh, *Proceedings of the National Academy of Sciences USA*, 2005, **102**, 15815.
[98]) A. Keppler, S. Gendreizig, T. Gronemeyer, H. Pick, H. Vogel, K. Johnson, *Nature Biotechnology*, 2003, **21**, 86.
[99]) R. Poole, *Highly Emissive Tetraazatriphenylene Complexes*, PhD. Thesis, University of Durham, 2006.
[100]) D. Parker, J. A. G. Williams, *Metal Ions in Biological Systems*, Marcel Dekker, Inc., New York, Volume 40, 233.
[101]) A. Døssing, European Journal of Inorganic Chemistry, 2005, 1425.
[102]) F. A. Cotton, G. Wilkinson, C. A. Murillo, M. Bochman, R. Grimes *Advanced Inorganic Chemistry, 6th Edition*, J. Wiley & Sons Inc, New York, 2000.
[103]) D. Parker, J. A. G. Williams, *Journal of Chemical Society Dalton Transactions.*, 1996, 3613.
[104]) R. S. Dickins, D. Parker, A. S. de Sousa, J. A. G. Williams, *Chemical Communications*, 1996, 697.
[105]) A. Beeby, I. M. Clarkson, R. S. Dickins, S. Faulkner, D. Parker, L. Royle, A. S. de Sousa, J. A. G. Williams, M. Woods, *Journal of Chemical Society Perkin Transactions 2*, 1999, 493.

CHAPTER 2

New Chromophores and their Integration into Lanthanide (III) Complexes

2 New Chromophores and their Integration into Lanthanide (III) Complexes

Luminescent complexes of Tb^{3+} and Eu^{3+}, based on the cyclen (1,4,7,10-tetraazacyclododecane) macrocycle, containing suitable sensitizing chromophores and various pendant arms have been synthesized. The ability to stain live and fixed cells with these complexes has been observed.[1] Issues with the ease of crossing the cell membrane and sensitivity to quenching of the Ln^{3+} excited states have been identified and tentatively related to certain structural features of these complexes. The synthesis and photophysical investigation of two new chromophores incorporating carboxylic acid groups to allow conjugation, and the synthesis and characterisation of their DO3A complexes are discussed in this chapter.

2.1 Sensitizer structures

The core structures of the new chromophores are based on sensitizers previously used in luminescent complexes to stain cells for fluorescence microscopy experiments; namely 7-methyl-dipyrido[3,2-f:2',3'-h]quinoxaline, **1**, and 2-methylazathioxanthone, **2** (**Figure 2.1**).

1 2

Figure 2.1 – Parent structures of desired chromophores

These sensitisers have previously been integrated into emissive systems, such as $[TbL^1]^{3+}$ and $[EuL^2]^{3+}$ (**Figure 2.2**).[2, 3]

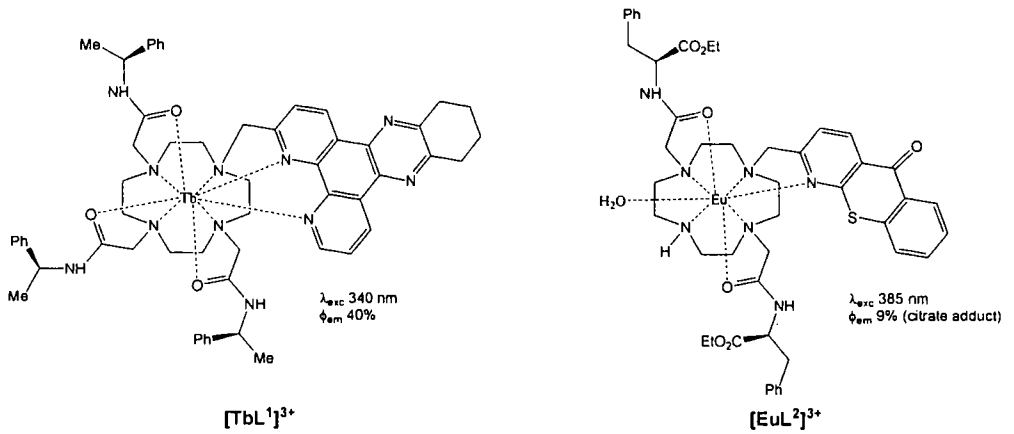

Figure 2.2 – Emissive complexes incorporating tetraazatriphenylene and azathioxanthone chromophores

The structures (**1**, **2**) were amended by incorporating carboxylic acid groups into the ring structure. Two carboxylic groups were attached to the tetraazatriphenylene chromophore into positions 2 and 3. One carboxylic group, in position 7, was attached to the azathioxanthone structure. Thus, the following chromophore core structures were obtained; dipyrido[3,2-f:2',3'-h]quinoxaline-2,3-dicarboxylic acid, **3**, and 7-carboxyazathioxanthone, **4** (**Figure 2.3**).

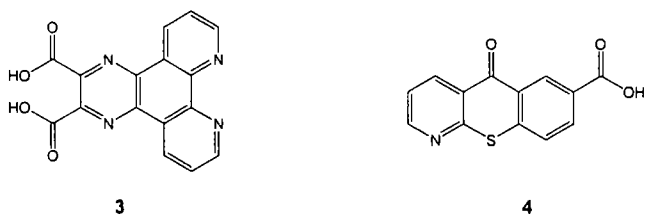

3 **4**

Figure 2.3 – Target sensitizer structures containing carboxylic acid groups

The carboxylate functional group was introduced into the chromophore structure to serve as a possible linking group for conjugation of the desired lanthanide (III) complexes. An additional aspect was to study their effect on the sensitivity of the complexes to quenching by electron rich species such as iodide, ascorbate or urate. It was postulated that the negative charge of the deprotonated carboxylic acid group (as the quenching experiments are to be performed at physiological pH) would render

the complexes less sensitive to this type of quenching, by virtue of Coulombic repulsion to encounter.

2.2 Chomophore Synthesis

2.2.1 Synthesis of the Tetraazatriphenylene Chromophore

Being derived from the dipyrido[3,2-f:2',3'-h]quinoxaline (dpq) chromophore, the new carboxylic acid functionalised tetraazatriphenylene chromophore, **3**, was expected to retain its attractive properties for sensitisation of lanthanide luminescence. These may be listed as follows: high molar extinction coefficient at wavelengths above 340 nm; an absence of chromophore fluorescence; fast intersystem crossing to the triplet energy state that is sufficiently high in energy to avoid back energy transfer from the Tb^{3+}excited state.[4]

The synthetic steps were expected to follow established methodology, used for the synthesis of related 'dpq' and 'dpqc' chromophores, changing only the diamine reactant to introduce the carboxylate functionality.

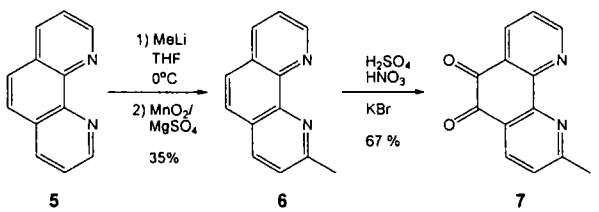

Scheme 2.1 – Synthesis of 2-methyl-1,10-phenanthroline-5,6-dione

The synthesis starts by methylation of 1,10-phenanthroline, **5**, in position 2, creating a site for attachment into the ligand structure. The methylation is achieved by reaction with MeLi in dry THF, which leads to the formation of a dihydro species that is subsequently re-aromatised by reaction with MnO_2, to yield the desired 2-methyl-1,10-phenanthroline, **6** (**Scheme 2.1**). This was then oxidised to the corresponding 5,6-quinone, **7**, using KBr, H_2SO_4 and HNO_3. This reaction involves generation of molecular bromine *in situ*. The quinone can then be used in a

cyclisation reaction, with a chosen diamine, to form the extended heteroaromatic structure with appropriate functionality.

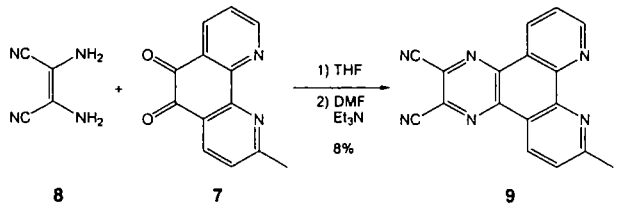

8 7 9

Scheme 2.2 – Attempts to obtain the desired heterocyclic structure by cyclisation with 2,3-diamino-maleinonitrile

Initial attempts at the synthesis of dipyrido[3,2-f:2',3'-h]quinoxaline, with the desired functionality were carried out according to a published procedure, based on the reaction of 2,3-diamino-maleinonitrile, **8**, with the dione, **7** (**Scheme 2.2**). The reaction, however, yielded an insoluble black, tar-like, material, from which only very small amounts of the desired product, **9**, could be recovered. Hence, a different diamine precursor had to be identified. 2,3-Diamino-succinic acid, **10**, was chosen as a suitable candidate. It was esterified to give the diethyl ester, **11**, using dry HCl gas in dry EtOH (**Scheme 2.3**).

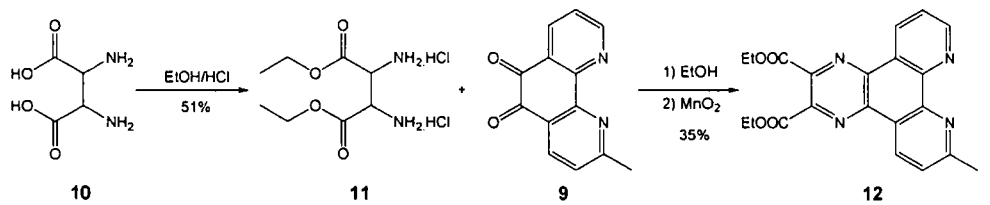

10 11 9 12

Scheme 2.3 – Synthesis of the desired tetraazatriphenylene chromophore as its diethyl ester

The cyclisation reaction between **11** and **9** was, however, not followed by a spontaneous air-promoted aromatisation to the desired product, **12**, as was the case for other diamines. The diethyl-7-methyl-dipyrido[3,2-f:2',3'-h]quinoxaline-2,3-dicarboxylate, **12**, was obtained from the dihydro precursor by the action of MnO_2 (**Scheme 2.3**). An aqueous EDTA extraction had to be used during the work-up procedure, to remove traces of manganese (II) salts from the product.

Having obtained the desired chromophore structure, containing the carboxylate functionality, the methyl group needed to be transformed into a haloalkyl group, so that it could be used in an S_N2 alkylation reaction with a cyclen ring nitrogen. Previous experience showed that direct bromination using N-bromosuccinimide was not possible, and an alternative reaction sequence had to be adopted (**Scheme 2.4**).

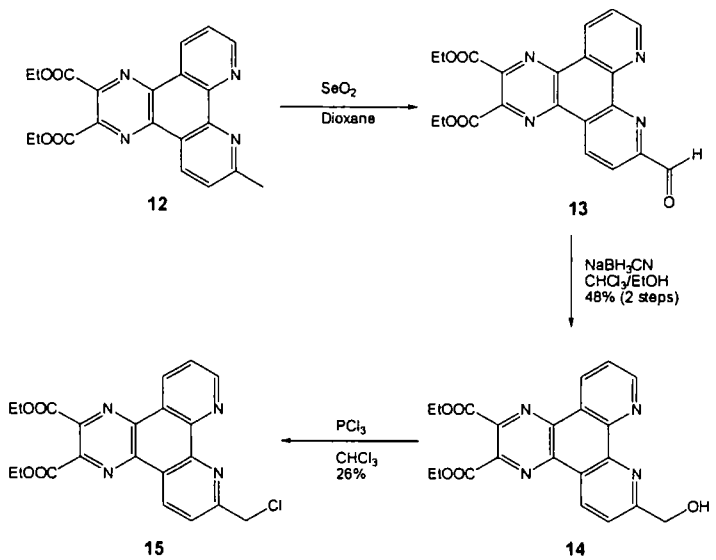

Scheme 2.4 – Functionalisation of the chromophore methyl group for cyclen alkylation

The methyl group was first transformed into the corresponding carboxaldehyde **13** using selenium dioxide in dioxane. The aldehyde was reduced to the alcohol, **14**, by sodium cyanoborohydride. This reagent gave better results than sodium borohydride, used in the synthesis of analogues of this chromophore. Finally, the alcohol **14** was converted to the desired chloromethyl compound **15** using PCl_3. The overall yield of the reaction sequence was rather low, but sufficient material was obtained for the further steps of the ligand synthesis.

2.2.2 Synthesis of the azathioxanthone chromophore

The synthesis of azaxanthones and azathioxanthones is carried out in two key steps. The first involves the coupling of a phenol or thiophenol of choice with a suitably functionalised 2-chloronicotinic acid. The heteroaromatic ring system is subsequently formed by an electrophilic cyclisation reaction in hot polyphosphoric acid (PPA).[5]

2-Chloro-6-methylnicotinic acid, **26**, and methyl-4-thiobenzoate, **25**, were considered the reactants of choice for the coupling reaction. The latter was not commercially available and had to be prepared from a suitable precursor.

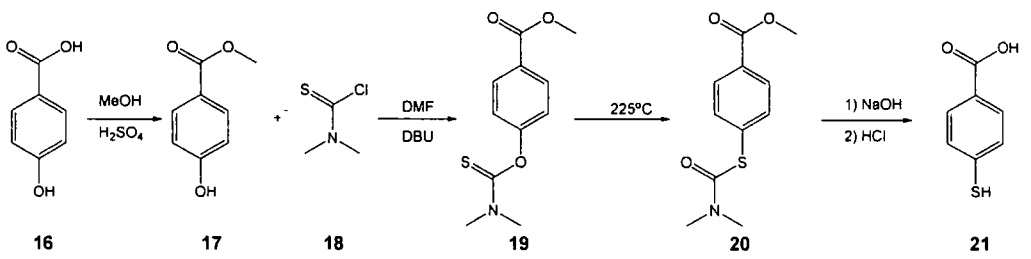

Scheme 2.5 – Synthetic route to 4-thio-benzoic acid

In preliminary work, the synthesis was based on 4-hydroxybenzoic acid, **16**. This was esterified in methanol catalysed in the presence of concentrated H_2SO_4. The esterification was followed by reaction with dimethyl thiocarbamoyl chloride to yield the thiocarbamate **19**. A high temperature (225°C) rearrangement led to the formation of the precursor **20** with sulphur attached to the aromatic ring. The final step in the sequence involved aqueous base hydrolysis to yield the 4-thio-benzoic acid, **21**. The length and modest yields of this reaction sequence led to consideration of an alternative sequence, starting from *p*-anthranilic acid, **22**. (**Scheme 2.6**)

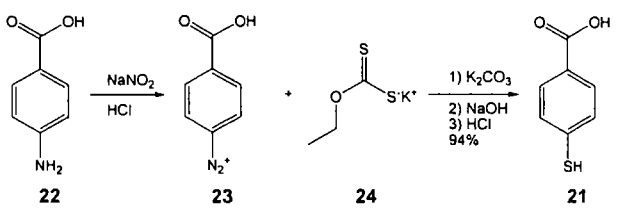

Scheme 2.6 – Alternative synthetic route to 4-thio-benzoic acid

In this alternative reaction sequence, the amino group was converted into the corresponding diazonium salt **23**, which was reacted with potassium ethyl xanthate, **24**. The desired 4-thiobenzoic, **21**, acid was obtained after base hydrolysis.

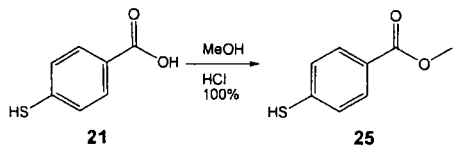

Scheme 2.7 – Synthesis of methyl-4-thio-benzoate

Esterification of the carboxylic acid **21** in methanol catalysed by dry HCl, yielded the desired methyl-4-thiobenzoate, **25**, quantitatively (**Scheme 2.7**).

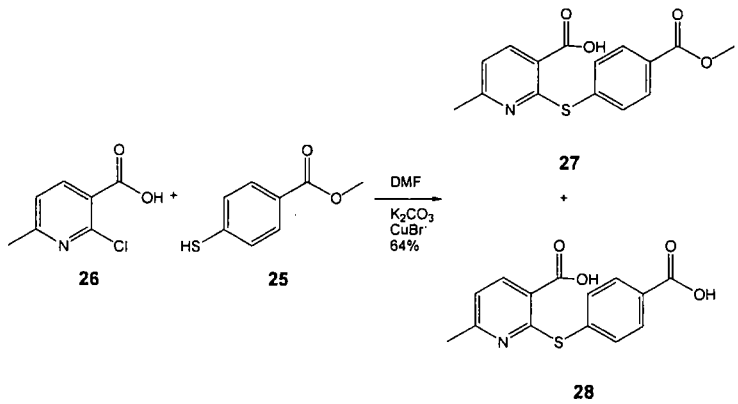

Scheme 2.8 – Nucleophilic aromatic coupling reaction

The methyl-4-thiobenzoate, **25**, was subsequently used in the coupling reaction with 2-chloro-6-methyl nicotinic acid, **26**. The reaction was carried out in DMF using K_2CO_3 as base and CuBr as a catalyst. This procedure is different to the one used in the synthesis of azaxanthones, where the reaction is carried in molten phenol using sodium methoxide deprotonation prior to the reaction. Partial hydrolysis of the methyl ester was observed (^{1}H NMR analysis) in the isolated product. The mixture of the ester **27** and the acid **28** was carried forward for the cyclisation reaction (**Scheme 2.9**)

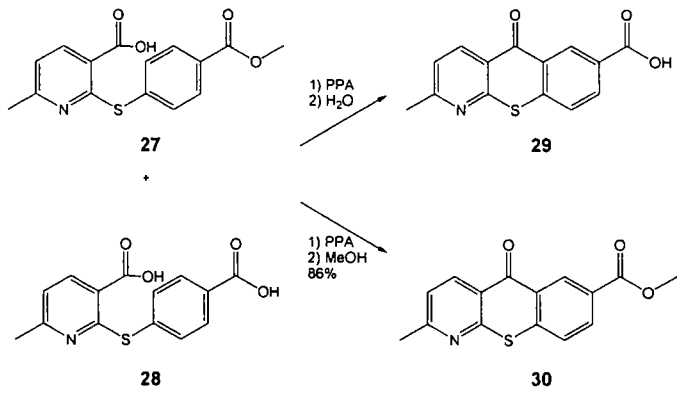

27 + 28 → 29 + 30

Scheme 2.9 – Chromophore cyclisation

The cyclisation reaction was carried out by heating the starting material in polyphosphoric acid (PPA) for 20 hours (**Scheme 2.9**). Performing the reaction work up in water, as was the case of other azaxanthones and azathioxanthones, led to the hydrolysis of the ester. The isolation of the acid product proved to be cumbersome and isolated yields were mediocre. Much better results were achieved by working the reaction up using methanol. The desired azathioxanthone, **30**, was thus obtained in good yield.

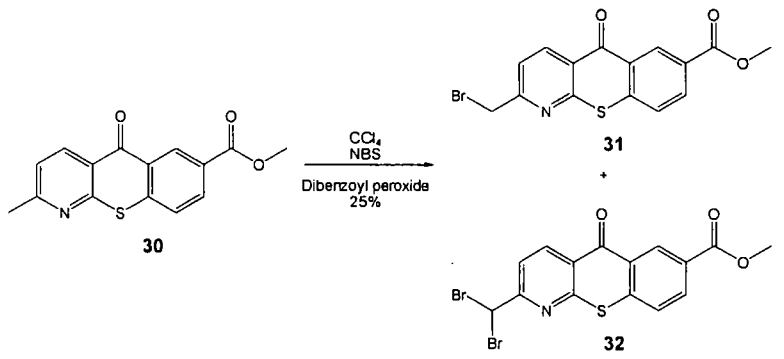

30 → 31 + 32

Scheme 2.10 – Chromophore methyl group bromination

The functionalisation of the methyl group was performed by benzylic bromination with N-bromosuccinimide (NBS) (**Scheme 2.10**), using dibenzoyl peroxide as the radical initiator. The bromination does not, however, stop after the formation of the desired product **31** and proceeded to the dibrominated compound **32**. Hence, the reaction needed to be monitored by ^1H NMR to determine the optimal conversion, at which point the reaction mixture contained the highest proportion of the desired

product. The starting material and both products were isolated in the chromatographic separation of the reaction mixture. The dibrominated product **32** was converted into the monobromo species **31** in a reductive reaction using diethyl phosphite (**Scheme 2.11**).

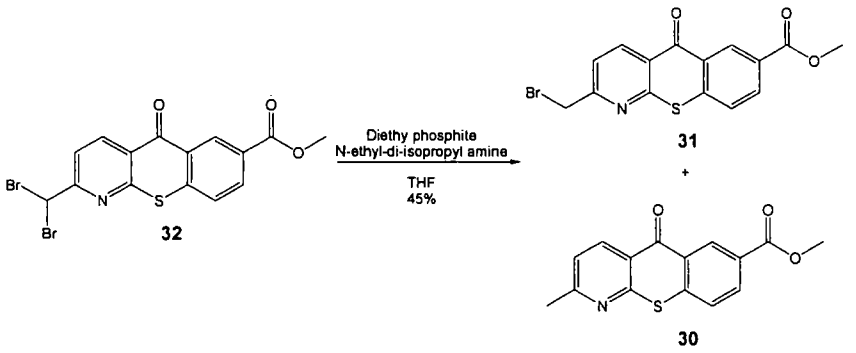

Scheme 2.11 – Debromination reaction

This reaction proceeds to the completely debrominated azathoxanthone **30** as well as the desired monoboromo compound **31**. The parent azathioxanthone can thus be recycled to increase the overall efficiency of this sequence.

2.3 Complex Synthesis

2.3.1 DO_3A Alkylation

1,4,7,10-Tetraazacyclododecane-1,4,7-triacetic acid was chosen as the core ligand structure for the first series of complexes incorporating the new chromophores. The functionalisation of the cyclen ring was carried out on the tris *t*-butyl ester of DO3A (**Scheme 2.12**).

Alkylation reactions were carried out in acetonitrile in each case, using K_2CO_3 and Cs_2CO_3 as bases for the tetraazatriphenylene and azathiaxanthone examples, respectively. In each case, the *N*-alkylated product was purified by column chromatography on neutral alumina.

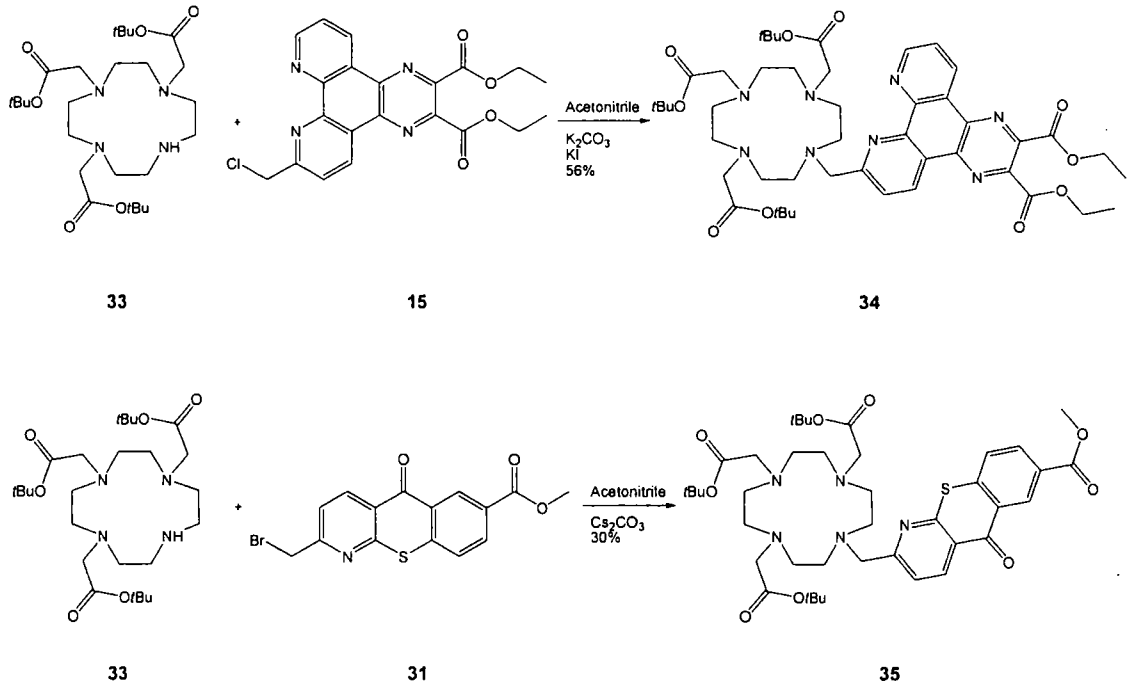

33 **15** **34**

33 **31** **35**

Scheme 2.12 – DO3A alkylation with chromophores

2.3.2 Ligand Deprotection and Complexation

The tetraazatriphenylene containing ligand was deprotected by acid hydrolysis of each ester group in hot 6M HCl (**Scheme 2.13**).

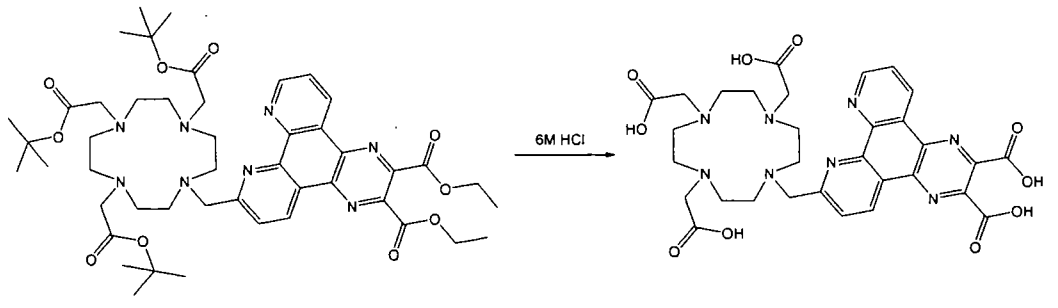

34 **36**

Scheme 2.13 – Ligand deprotecion

Thus, the desired ligand containg free carboxylic acid groups, **36**, was obtained. Direct complexation with a Ln (III) salt was expected to yield the desired complex.

Two different deprotection approaches had to be used in the azathioxanthone system, as a result of difficulties in subsequent synthetic steps (**Scheme 2.14**).

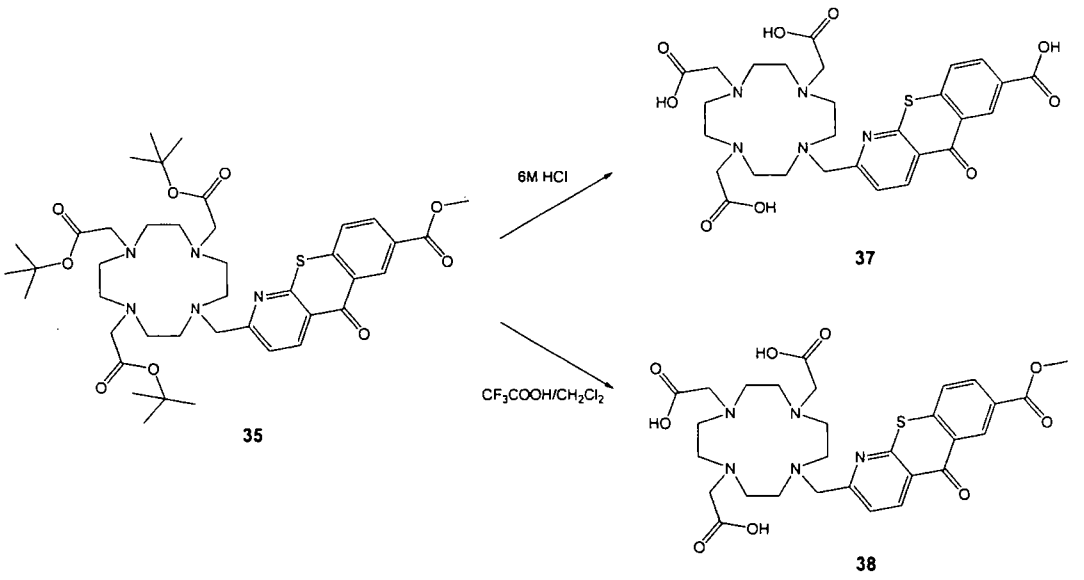

Scheme 2.14 – Ligand deprotection

Aqueous acid hydrolysis of the protected ligand, removing all of the ester groups to yield compound, **37**, was carried out as well as selective removal of the *t*-butyl ester groups by TFA in CH_2Cl_2, leading to ligand **38**.

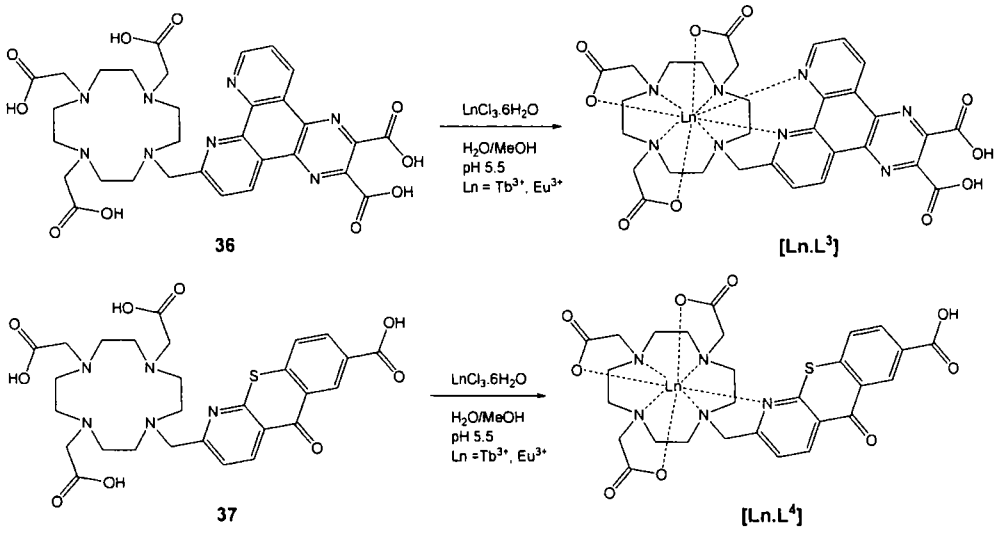

Scheme 2.15 – Complexation reaction with Ln (III) salts

The tetraazatriphenylene containing ligand **36** was complexed with terbium or europium chloride in a water/methanol mixture (**Scheme 2.15**). The pH of the complexation reaction mixture was maintained at 5.5 by addition of dilute aqueous KOH solution. The crude reaction mixtures were purified by reverse phase HPLC chromatography to yield the desired complexes **[Tb.L^3]** and **[Eu.L^3]**.

Attempts to perform the complexation reaction of the azathioxanthone containing ligand **37** in a similar manner to obtain complexes **[Ln.L^4]** were unsuccessful (**Scheme 2.15**). Formation of a precipitate was observed shortly after the addition of the lanthanide salt. Tb^{3+} and Eu^{3+} emission profiles were observed from the reaction mixtures, but the luminescence lifetimes measured were significantly shorter than anticipated from results in similar systems. Furthermore, no Ln emission signal was observed after the treatment of the samples at pH 10 (a treatment used for the removal of excess Ln salt). This led to the conclusion that the desired complexes **[Ln.L^4]** had not been formed.

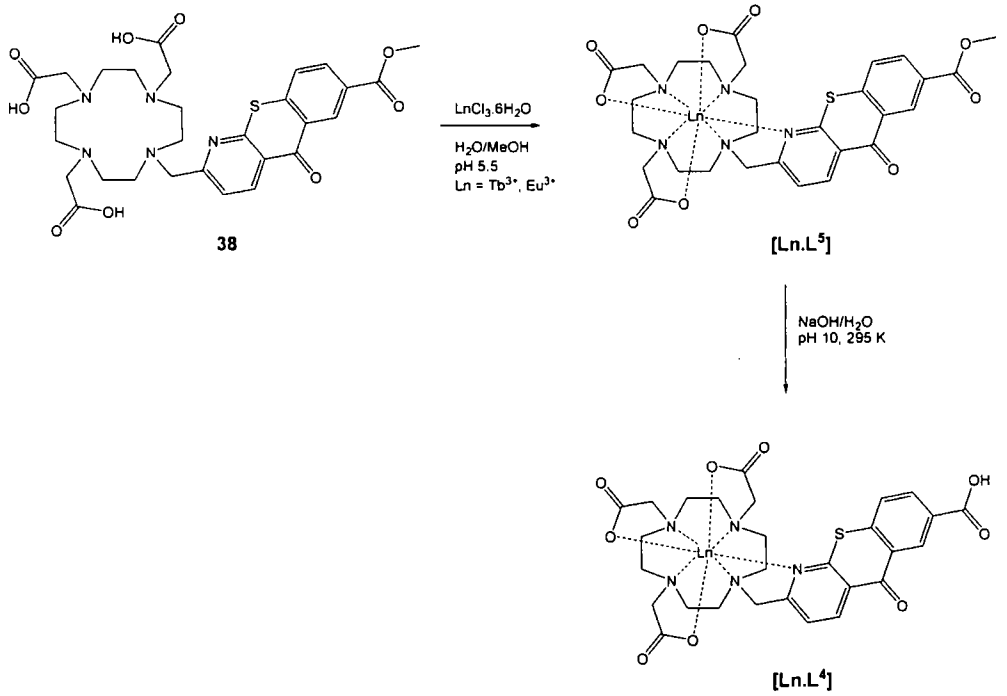

Scheme 2.16 –Complexation and ester hydrolysis

The proposed explanation of this observation was that the Ln^{3+} ion was loosely complexed by the chromophore carboxylate groups, preventing it from being properly installed into the ligand cage. This complex would be expected to have a reduced luminescence lifetime due to a higher number of coordinated waters, and would also be expected to be easily hydrolysed into $Ln(OH)_3$ under basic conditions. To avoid this problem, the partially deprotected ligand **38** was prepared (**Scheme 2.14**) and the lanthanide (III) complexes **[Ln.L^5]** were synthesised (**Scheme 2.16**).

The complexes **[Ln.L^5]** were purified by reverse phase HPLC chromatography. The subsequent hydrolysis of the methyl ester was attempted using mild base conditions (NaOH, pH 10; **Scheme 2.16**). The reaction was slow and a significant degree of decomplexation was observed. Small quantities of the desired complexes **[Ln.L^4]** were however obtained, after HPLC purification.

2.4 Azaxanthone chromophore

In a parallel project, the DO3A complexes incorporating azaxanthone chromophore analogous to the 7-carboxyazathioxanthone, **4**, were synthesised. The chromophore core structure was 7-carboxyazaxanthone, **39** (**Figure 2.4**).

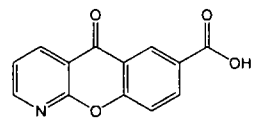

39

Figure 2.4 – Azaxanthone chromophore containing a carboxylic acid group

2.4.1 Chromophore synthesis

The synthesis of the azaxanthone chromophore **41** and its bromomethyl derivative **42** was carried out in a similar fashion as for the azathioxanthone chromophore (**Scheme 2.17**).

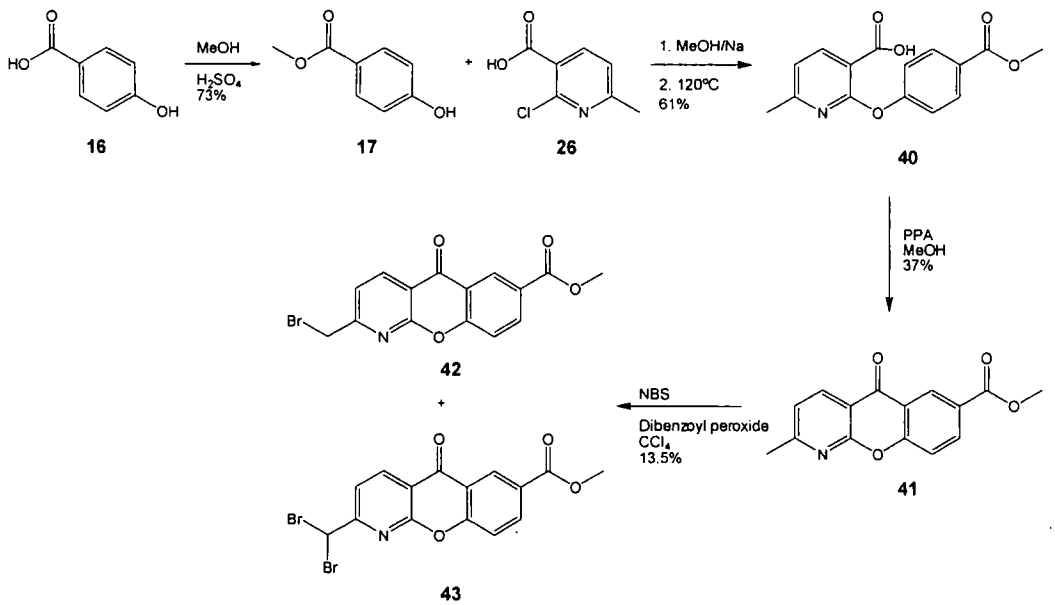

Scheme 2.17 – Synthesis of the bromomethyl derivative of the desired azaxanthone chromophore

In this sequence, methyl-4-hydroxybenzoate, **17**, was coupled to the 2-chloro-6-methylnicotinic acid in this reaction sequence. The coupling reaction was carried out in a different manner, compared to the azathioxanthone synthesis. Excess of the phenol, which melted at the reaction temperature, was used as the solvent and the deprotonation was carried out with sodium methoxide in methanol, generated *in situ*. The cyclisation and bromination reaction followed the scheme described above. Once again, both the desired bromomethyl derivative **42** and the undesired dibromo compound **43** were isolated. The reductive debromination, described above (**Scheme 2.8**), was employed to improve the overall yield of the desired bromomethyl derivative **42**.

2.4.2 DO3A complex synthesis

For initial investigation of this chromophore, the Ln (III) complexes based on 1,4,7,10-tetraazacyclododecane-1,4,7-triacetic acid (DO3A) were synthesised. The synthesis was carried out following the previously described route starting from the *t*-butyl ester of DO3A.

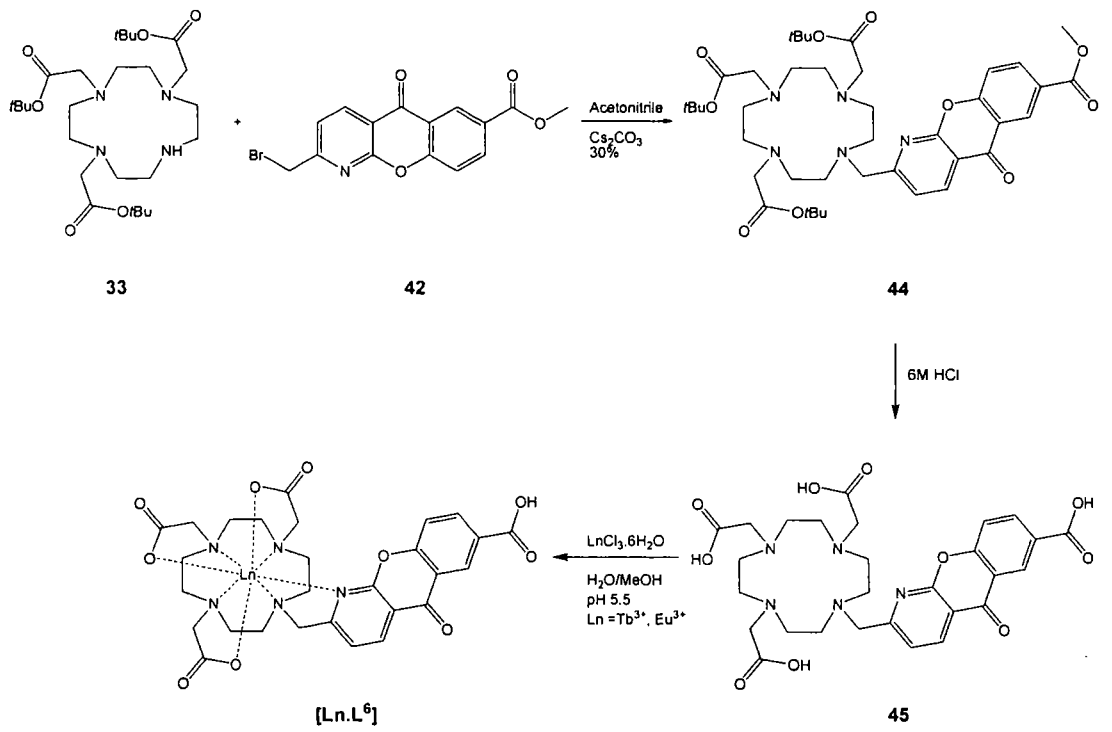

33 42 44

[Ln.L^6] 45

Scheme 2.18 – Synthesis of the DO3A complexes incorporating the azaxanthone chromophore

2.5 Synthesis of complexes incorporating amide arms

The DO3A complexes are suitable for assessing the ability of the chromophores to sensitise the luminescence of Ln(III) ions, as well as for further solution experiments. Our previous work has, however, shown that they are not particularly suitable for cellular experiments because of their intrinsic sensitivity to quenching by endogenous reductants such as ascorbate and urate (see Chapter 3). It was the more lipophilic 3+ charged complexes such as $[\mathbf{TbL^1}]^{3+}$ and $[\mathbf{EuL^2}]^{3+}$ that were considered more appropriate for preliminary cellular imaging experiments. Hence, the new chromophores were incorporated into complexes bearing the (*S*)-1-phenylethylacetamide arm, for these cellular imaging experiments (discussed in detail in Chapter 4).

Protective groups need to be employed to achieve selective alkylation of the cyclen nitrogens.

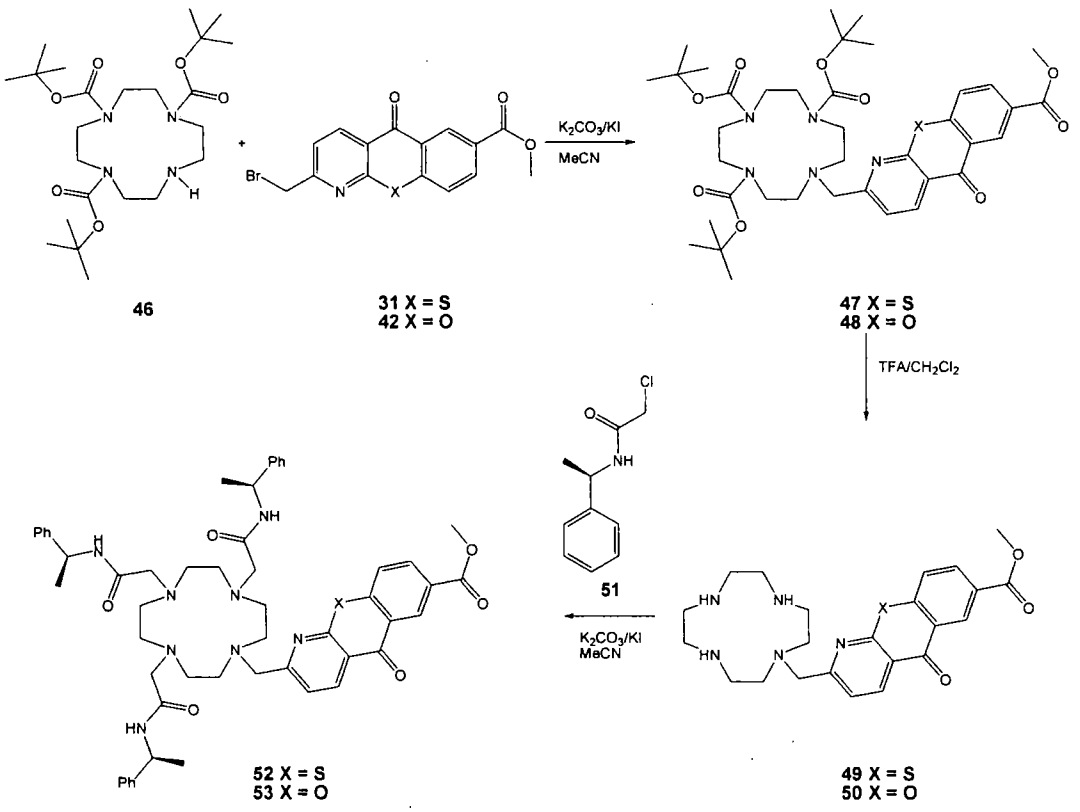

Scheme 2.19 – Ligand synthesis for the amide arm series of complexes

The synthesis of the ligands containing amide arms began with the alkylation of the unprotected nitrogen of *tris Boc*-cyclen, **46**, using the bromomethyl derivative of the azathioxanthone, **31**, or azaxanthone, **42**. The protecting Boc groups were then removed in a reaction with dry TFA in DCM to give the ligand precursors **49** and **50**. The ligand synthesis was then accomplished by alkylating the free amino groups of the cyclen with (*S*)-1-phenylethylchloroacetamide, **51**..

The prepared ligands **52** and **53** were then used in complexation reactions with the Ln(III) salts. The standard procedure of such a reaction, using an appropriate Ln(III) triflate salt in dry acetonitrile was used.

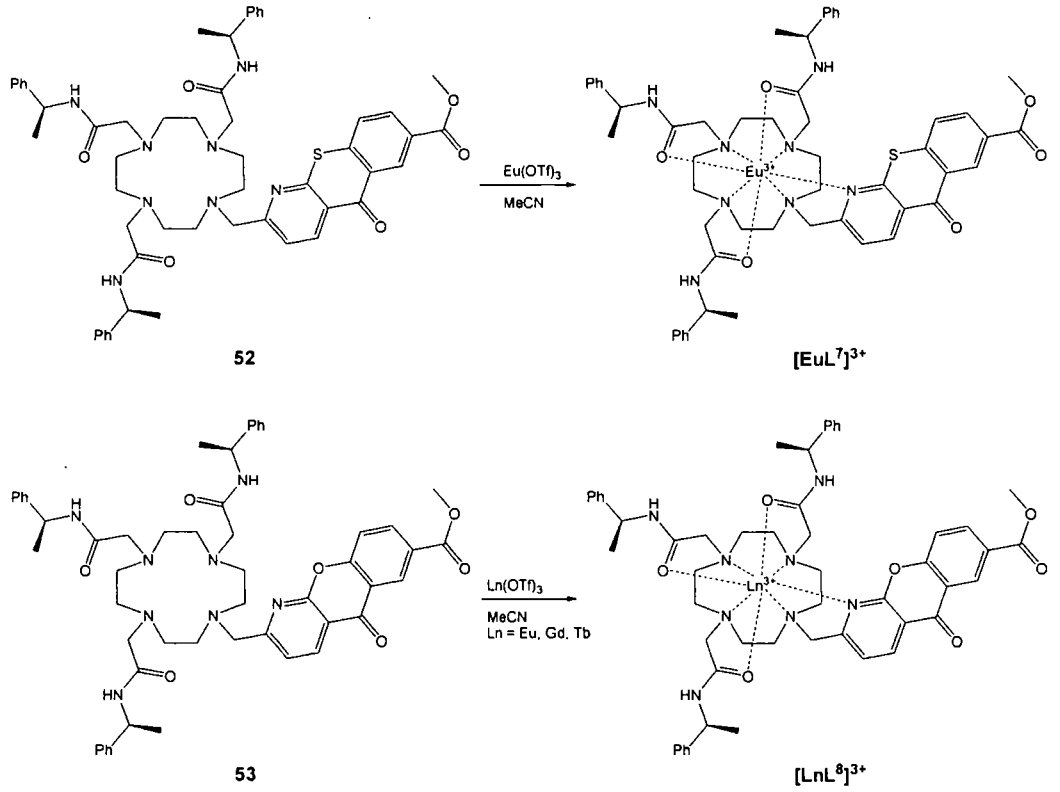

52 $[EuL^7]^{3+}$

53 $[LnL^8]^{3+}$

Scheme 2.20 – Complexation reactions forming the phenyl amide series of complexes

The complexes were purified by precipitation onto dry Et_2O, which was followed by an anion exchange reaction to replace the triflate anion with a more water soluble chloride counterion.

2.6 Photophysical Charcterisation of the Chromophores

An organic chromophore needs to fulfil several characteristics to be considered suitable as a senzitizing moiety for lanthanide luminescence. The most important are: high molar extinction coefficient, fast intersystem crossing and suitable energy of the triplet excited state. Furthermore, for practical considerations in fluorescence microscopy, absorption above 340 nm is important for the complexes considered for cellular imaging.

2.6.1 Azaxanthone and Azathiaxanthone Chromophores

Aromatic ketones are known to populate effectively their triplet state, hence benzophenones and acridones have been used in previous work to sensitize lanthanide luminescence.[6] Several photophysical studies have suggested that hetero-atom derivatives of acridones such 1-azaxanthone and 1-azathioxanthone should possess suitable properties as sensitizers of lanthanide luminescence.[7, 8, 9] Furthermore, the replacement of a phenyl group with a pyridyl moiety in the chromophore structure, introduces another possible binding atom into the ligand. This should decrease the distance between the chomophore and the metal, thus increasing the efficiency of energy transfer to the metal centre.

The carboxymethyl substituted azaxanthone **41** and azathioxanthone **30**, were synthesised as a part of a small library of chromophores, with the aim of studying the effect of substitution of the core structures on their photophysical properties.[10]

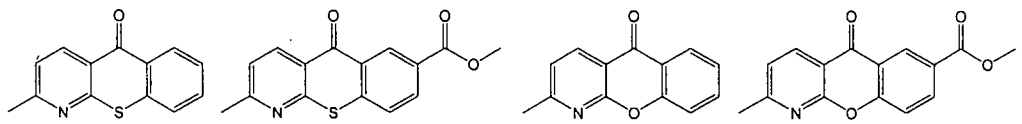

54 **30** **55** **41**

Figure 2.5 – Structures of α-methyl azathioxanthone and azaxanthone chromophores

Structure	λ_{max}/nm (ε, $M^{-1}cm^{-1}$)[a]	λ_{em}/nm[a]	E_T/cm^{-1} [b]
54	371 (6,770)	425	23,700
30	369 (5,360)	433	23,800
55	330 (6,900)	405	24,800
41	328 (5,720)	392	24,900

Table 2.1 – Photophysical properties of selected azaxanthone and azathioxanthone chromophores a: (MeOH, 295 K); b: (Et_2O-isopentane-ethanol glass, 77 K)

The small energy gap of the $n\pi^*$ and $\pi\pi^*$ excited states led to the expectation that the photophysical properties would be sensitive to substitution, as well as to solvent effects.

The data in **Table 2.1** show that the introduction of the carboxymethyl group into the chromophore structure does lead to small changes in the singlet and triplet excited state energies. It needs to be mentioned that a significantly higher amount of fluorescence was observed for the 1-azathioxanthone chromophores in comparison to the 1-azaxanthone ones. A similar trend was observed with the introduction of an alkyl substitutuent, such as a *t*-butyl group in position 7, **56**.

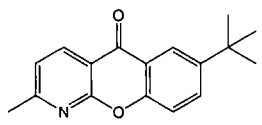

56

Figure 2.6 – 7-*t*Butyl-1-azaxanthone

More dramatic substituent effects were observed with the introduction of amino or methoxy groups, **Figure 2.7**, in which lone pair conjugation can occur.

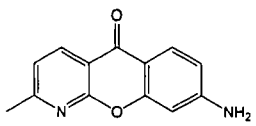

57

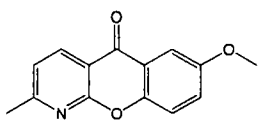

58

Figure 2.7 – Amino and methoxy derivatives of the azaxanthone chromophore

Structure	λ_{max}/nm (ε, $M^{-1}cm^{-1}$)[a]	λ_{em}/nm[a]	E_T/cm^{-1}[b]
57	356 (18,000)	458	21,600
58	355 (4,845)	453	21,500

Table 2.2 – Photophysical properties for azaxanthone chromophores with strongly electron donating substituents a: (MeOH, 295 K); b: (Et_2O-isopentane-ethanol glass, 77 K)

These changes are also demonstrated in the following absorption and phosphorescence spectra, **Figure 2.8**, showing the difference between 1-azaxanthone, **55**, and 8-amino-1-azaxanthone, **57**.

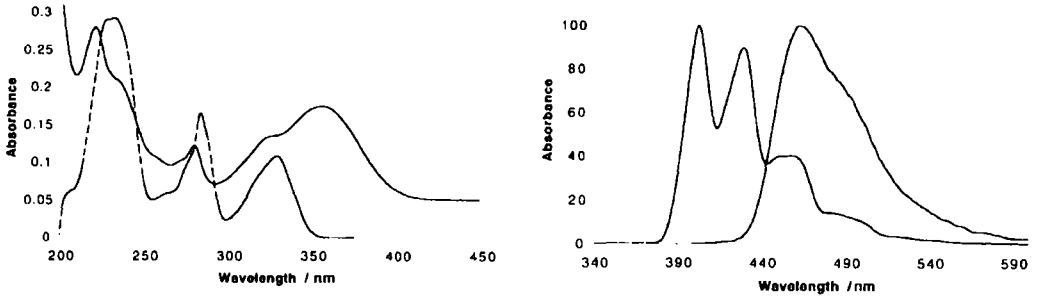

Figure 2.8 – Absorption and phosphorescence spectra for 1-azaxanthone and 8-amino-1-azaxanthone

These results show that structures **57** and **58** are not suitable for sensitisation of lanthanide luminescence. The energy of their triplet state (21,600 cm^{-1}) is too low for efficient Tb^{3+} sensitization and they possess several hundred fold higher fluorescence, which would be expected to significantly decrease the overall Ln^{3+} emission quantum yield.

Small changes in absorption maximum for the parent 1-azaxanthone, **55**, were observed in different solvents. The absorption band at lowest energy shifted from 329 nm in EPA to 330 nm in MeOH and 334 nm in water. This can be explained by an increased $\pi\pi^*$ contribution to the predominantly $n\pi^*$ character of the singlet excited state. The extinction coefficient of this peak also shows solvent dependence, going from 6,900 $M^{-1}cm^{-1}$ in MeOH to 4,500 $M^{-1}cm^{-1}$ in 33% water-MeOH. A blue shift and a decrease in fluorescence intensity was observed for the azaxanthones with decreasing solvent polarity, with no observable fluorescence in CH_2Cl_2, EtOAc, THF and toluene. The effect of solvent on the chromophore fluorescence was even more significant for the thioxanthones, where the amount of fluorescence observed varied to a greater extent. The variation of the fluorescence emission maxima with solvent polarity are shown in **Figure 2.9**, showing a reasonable correlation with Reichardt's classical solvent polarity parameter, E_T30.

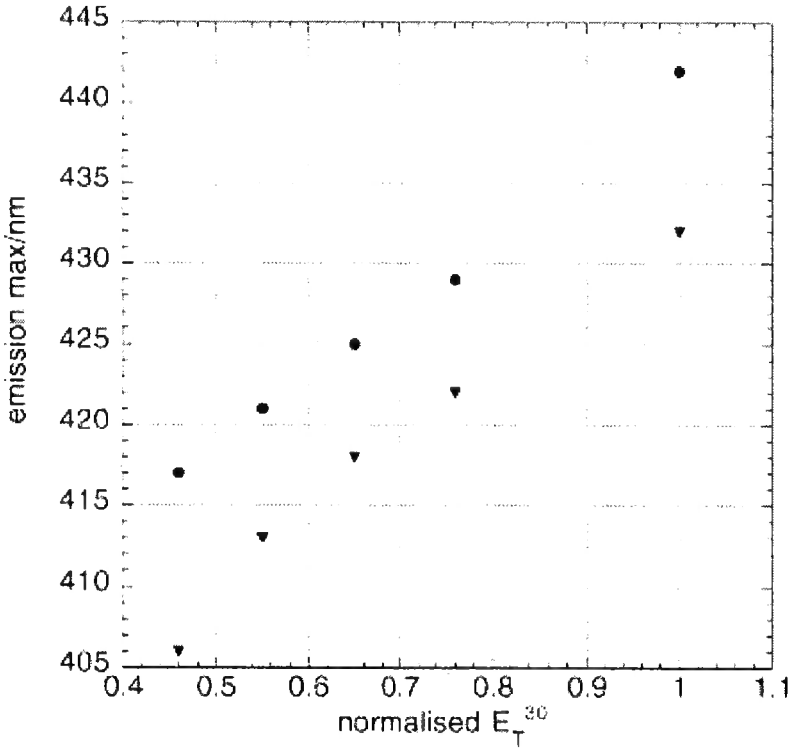

Figure 2.9 – Solvatochromic effects on azathioxanthone chromophore fluorescence

2.6.2 Tetraazatriphenylene chromophores

It has been shown that the tetraazatriphenylene chromophore is a very good sensitizer of lanthanide luminescence. Several tetraazatriphenylene derivatives have been assessed for this purpose in recent publications and some (**59**, **60**) have been incorporated into well-defined Ln^{3+} complexes used in cellular imaging.

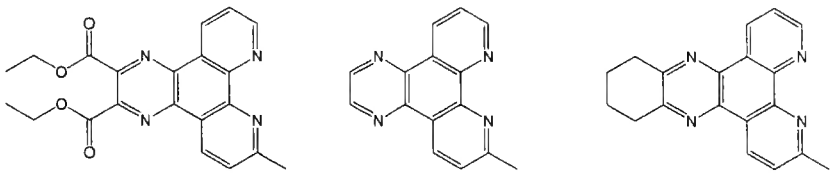

Figure 2.10 – Tetraazatriphenylene chromophore structures

Structure	λ_{max}/nm (ε, $M^{-1}cm^{-1}$)[a]	λ_{em}/nm[a]	E_T/cm^{-1}[b]
12	355 (5,430)	Not observed	22,800
59	340 (3,800)	Not observed	23,800
60	347 (6,400)	Not observed	23,400

Table 2.3 – Photophysical properties of tetraazatriphenylene chromophores; a: (295 K, MeOH), b: (Et_2O-isopentane-ethanol glass, 77 K)

The results show that the new tetraazatriphenylene bearing a di-carboxyethyl substitution has maintained the adequate properties for practicable lanthanide sensitization. Efficient absorption at wavelengths exceeding 350 nm is still present. The lack of chromophore fluorescence is consistent with fast intersystem crossing. Also, the triplet energy is sufficient for both Tb^{3+} and Eu^{3+} sensitization.

2.7 Characterisation of complexes

2.7.1 HPLC separation and analysis

The purity of the prepared complexes was assessed by reversed phase HPLC. The complexes $[\mathbf{LnL^3}]^{2-}$ and $[\mathbf{LnL^5}]$ both showed one major peak in the chromatograms of the crude complexation mixtures. This was purified by semi preparative HPLC, also with the aim of removing the salts contained in the crude samples. The purification and analysis of complexes $[\mathbf{LnL^8}]^{3+}$ is discussed in Chapter 4.

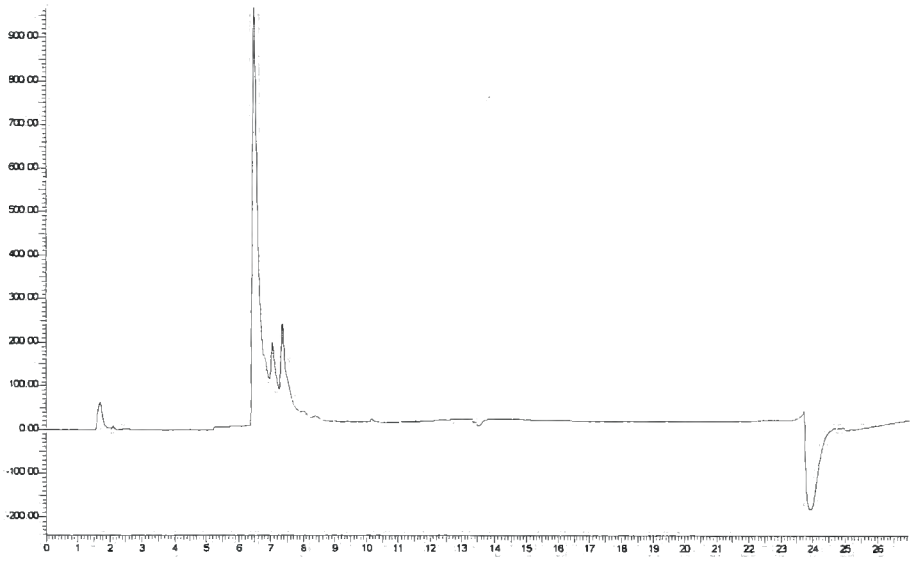

Figure 2.11 – Chromatogram of the crude complexation mixture for $[LnL^3]^{2-}$ (Method A with TFA, Appendix)

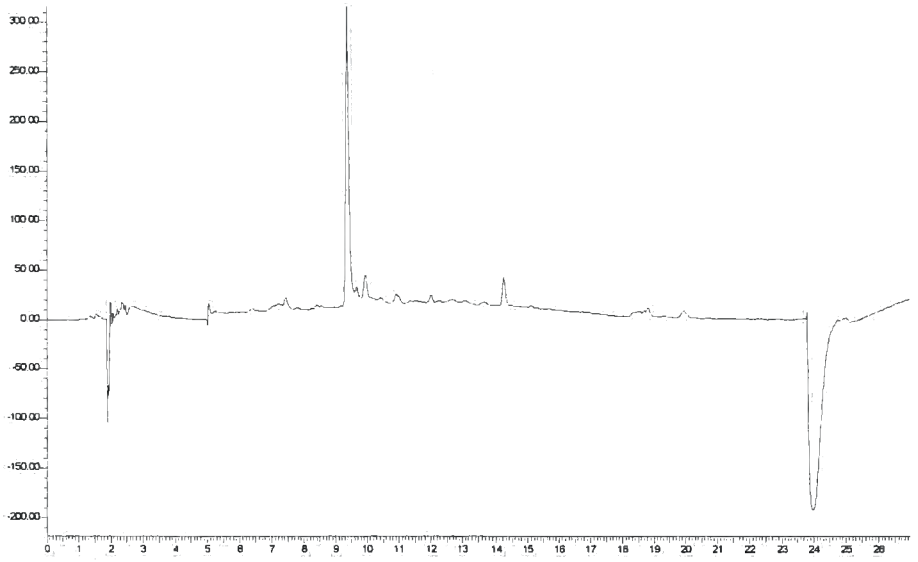

Figure 2.12 – Chromatogram of the crude complexation mixture for $[LnL^5]$ (Method A no acid, Appendix)

2.7.2 ^{1}H NMR analysis

The paramagnetism of lanthanide (III) ions, which makes them useful for applications such as MRI relaxation and MRS shift agents, has complicating implications in the ^{1}H analysis of their complexes. Both shifting and broadening of signals is frequently observed, the extent of which is dependent on the lanthanide (III)

ion, the distance between the atom and the metal and its orientation in relation to the principal axis of the complex. It is the macrocycle ring protons that are the most shifted in the cyclen based complexes prepared in this work. Eu^{3+} and Yb^{3+} are the lanthanide ions of choice for ^1H NMR analysis of lanthanide complexes.[11]

It has been observed that DO3A based complexes exist as a mixture of stereoisomers in solution at room temperature, which leads to the broadening of the ^1H NMR signals, decreasing spectral resolution and precluding detailed analysis. Similar behaviour was observed for the newly synthesised Eu^{3+} complexes **[Eu.L^3]** and **[EuL^5]**. A well defined ^1H NMR spectrum was observed for the triamide complex **[Eu.L^8]$^{3+}$ (Figure 2.13)**.

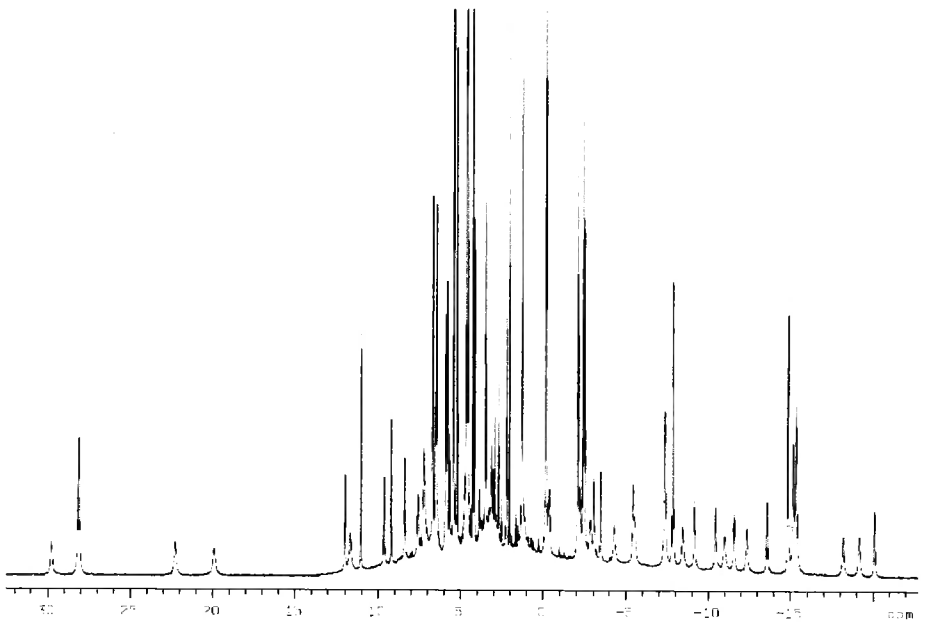

Figure 2.13 – ^1H NMR spectrum of [EuL^8]$^{3+}$ (D_2O, 295 K, pD 6)

2.7.3 Photophysical characterisation of complexes

2.7.3.1 Absorption and emission spectra

The absorption spectra of the complexes were recorded in water at 295 K. Their spectral form did not vary with the lanthanide ion and they closely resembled the absorption spectra of the chromophores used.

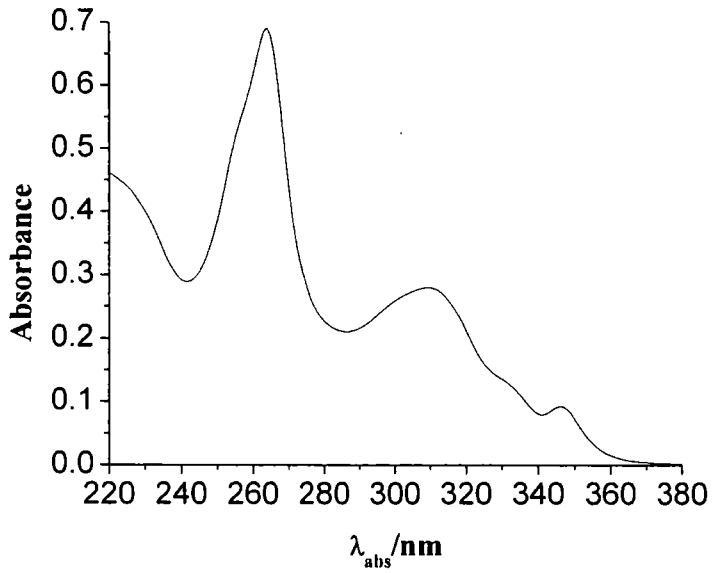

Figure 2.14 – Absorption spectrum for the anionic dpq complex, $[LnL^3]^{2-}$, (H_2O, 295 K)

Complexes with the tetraazatriphenylene chromophore possessed the longest wavelength absorption at 347 nm (**Figure 2.14**).

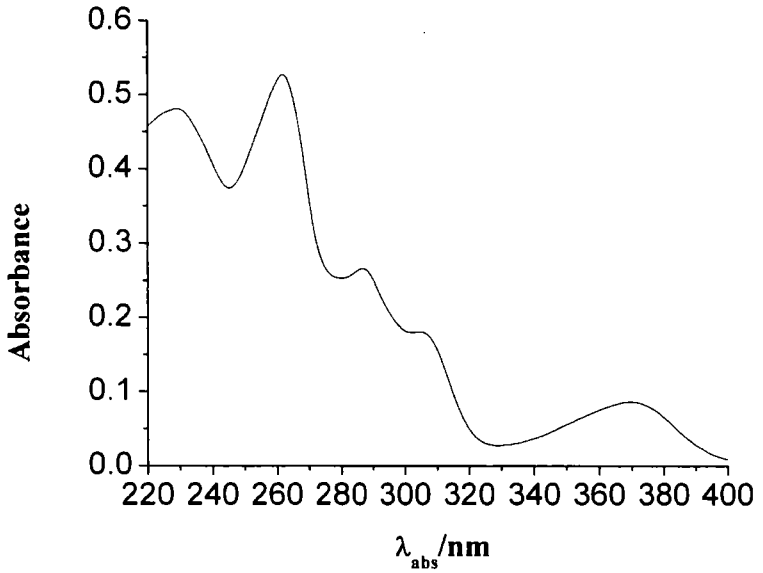

Figure 2.15 - Absorption spectrum for the azathioxanthone complex, $[LnL^5]$, (H_2O, 295 K)

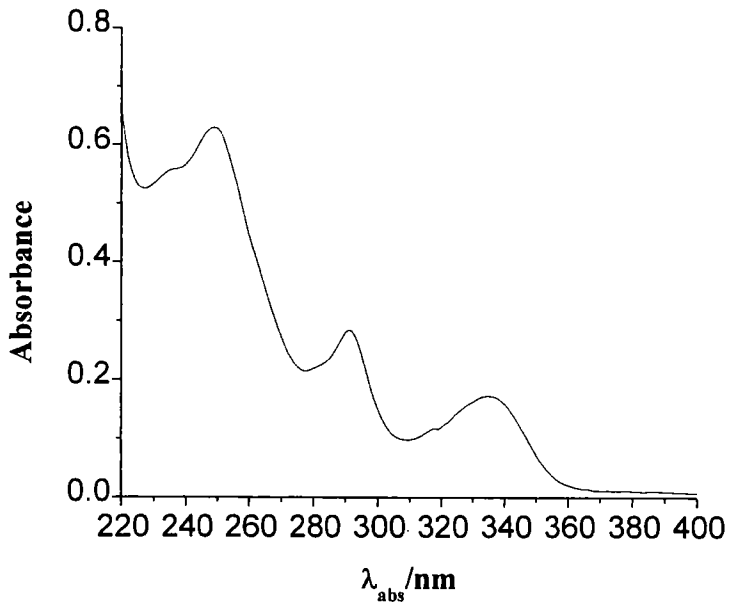

Figure 2.16 – Absorption spectrum for the azaxanthone complex, $[LnL^8]^{3+}$, (H_2O, 298 K)

Figures 2.15 and **2.16** demonstrate the spectral differences between the azathioxanthone and azaxanthone chromophores, with the latter absorbing at higher energy.

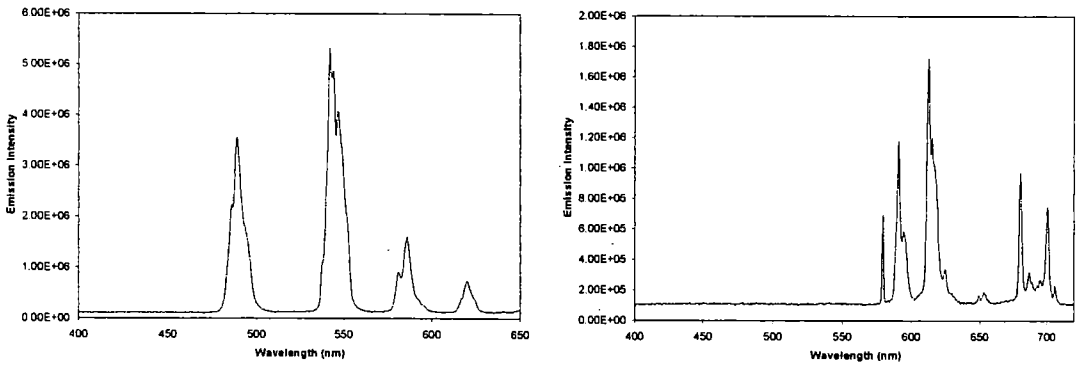

Figure 2.17 – Emission spectra for the anionic tetraazatriphenylene complex, $[LnL^3]^{2-}$, Ln = Tb (left), Ln = Eu (right), (H_2O, 298 K)

The emission spectra were recorded in water at 298 K. Emission spectra of DO3A complexes **[Ln.L^3]** containing the tetraazatriphenylene chromophore, showed strong lanthanide emission and an absence of chromophore fluorescence.

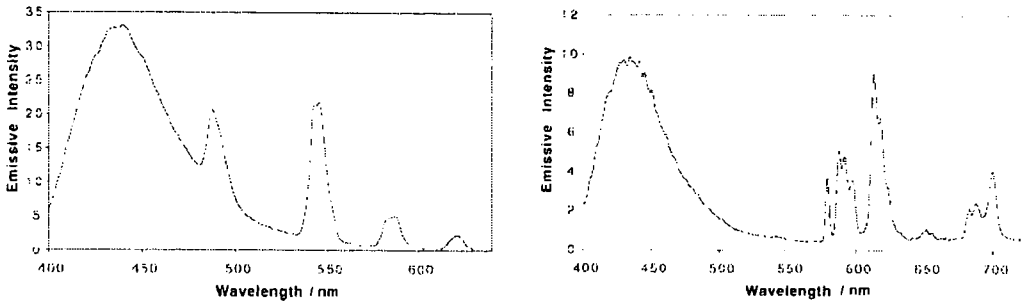

Figure 2.18 – Emission spectra for the azathioxanthone complex,[LnL^5], (H_2O, 298 K)

The emission spectra of the azathioxanthone complex, **[Ln.L^5]**, showed a significant amount of chromophore fluorescence, with a rather weak lanthanide emission.

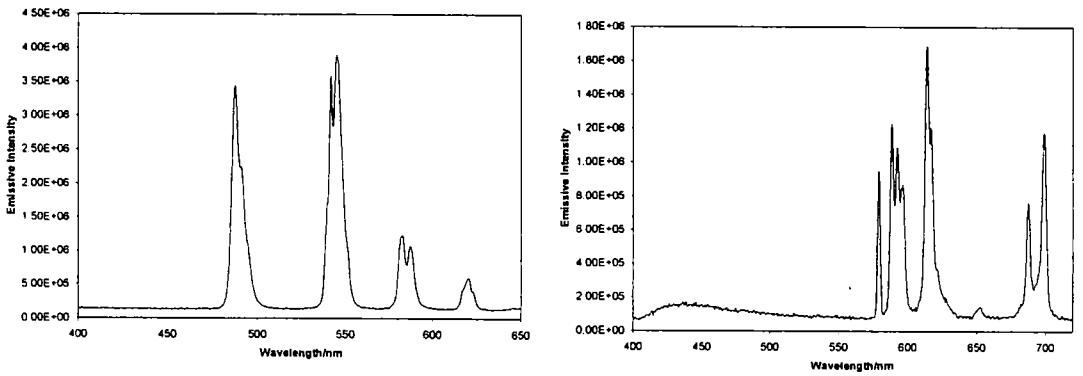

Figure 2.19 – Emission spectra for the azaxanthone complex, [LnL^8]$^{3+}$, (H_2O, 298K)

The emission spectra of the cationic triphenylamide complexes **[Ln.L^8]$^{3+}$** exhibited strong lanthanide emission and a very weak chromophore fluorescence could be discerned in the case of the europium complex, **[Eu.L^8]$^{3+}$**.

2.7.3.2 Luminescence lifetime measurements and hydration state analysis

Luminescence quantum yields and luminescence lifetimes are highly informative about the photophysical properties of the emissive complexes.

The lanthanide emission quantum yield is indicative of the overall efficiency of the process that populates the lanthanide excited state and its emissive relaxation.

Complex	*Lifetime in H_2O (ms)*	*Lifetime in D_2O (ms)*	*q*	*Quantum yield (%)*
$[Tb.L^3]^{2-}$	2.26	2.41	0	55
$[Eu.L^3]^{2-}$	1.07	1.61	0	17
$[Tb.L^9]$	1.46	N.d.	N.d.	33
$[Eu.L^9]$	1.08	N.d.	N.d.	18
$[Tb.L^5]$	0.53	0.62	1.1	2.2
$[Eu.L^5]$	0.51	1.62	1.3	2.1
$[Tb.L^{10}]$	1.89	2.88	0.64	12
$[Eu.L^{10}]$	0.60	2.08	1.1	8
$[Tb.L^8]^{3+}$	1.60	N.d.	N.d.	19
$[Eu.L^8]^{3+}$	0.58	N.d.	N.d.	N.d
$[Tb.L^{11}]^{3+}$	1.65	2.89	1.00	37
$[Eu.L^{11}]^{3+}$	0.54	1.73	0.97	8

Table 2.4 – Emission lifetimes and quantum yields of selected lanthanide complexes

The emission lifetime, in turn, gives information about the coordination sphere of the metal defined by the corresponding ligand, and the extent to which it protects the lanthanide excited state from non-radiative deactivation processes.

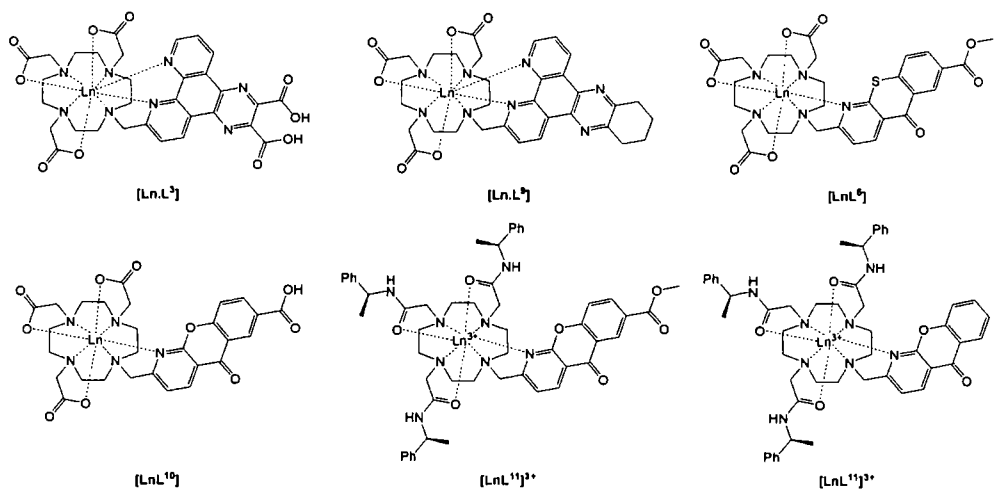

Figure 2.20 – Structures of the complexes used for comparison of emission data

Thus, it can be seen that the complexes incorporating the new tetraazatriphenylene chromophore, $[LnL^5]^{2-}$, have maintained the favourable photophysical properties of

previous complexes bearing analogous chromophores, such as **[LnL^9]**. Indeed, both the luminescence lifetime and the quantum yield are actually increased.

In the case of the azathioxanthone complexes **[LnL^3]**, the photophysical characteristics are not so favourable, with both quantum yields and luminescence lifetimes decreased in comparison to analogous azaxanthone complexes **[LnL^{10}]**.

Measurement of the luminescence lifetimes in H_2O and D_2O for the newly synthesised complexes allowed an estimation of the hydration state of each complex. The tetraaztriphenylene complexes, based on a nonadentate ligand, did not have a bound water molecule. The thiaazaxanthone complexes, derived from an octadentate ligand, bind one water molecule at the metal centre. The number of bound water molecules was calculated according to the following equations[12]:

$$q_{Eu} = 1.2 \cdot \left(k_{H2O} - k_{D2O} - 0.25 - x \cdot (0.075)\right) \quad (1)$$

$$q_{Tb} = 5 \cdot \left(k_{H2O} - k_{D2O} - 0.06\right) \quad (2)$$

In these equations, k_{H2O} and k_{D2O} are the radiative decay rate constants in water and deuterium oxide respectively; the term 0.25 for Eu (0.06 for Tb) refers to quenching due to second sphere water molecules and the 0.075 term refers to amide NH quenching for Eu complexes.

2.7.3.3 CPL measurements for triamide complexes

Since the triamide complexes **[LnL^8]$^{3+}$** are chiral, their photophysical properties can be further investigated by chiroptical methods. Circular dichroism measurements, which assess the difference in absorption of right and left circularly polarised light (ground state investigation), are not easily used for these complexes. This is because the measurement of the lanthanide absorption spectrum is necessary and requires relatively concentrated solutions, due to the forbidden nature of the f-f transitions. Circularly polarised luminescence (excited state investigation), on the other hand,

can be used as it measures the differential amounts of right and left circularly polarised light emitted by lanthanide (III) centre. Thus, CPL can provide information about the helicity and structure of the complex as well as reporting on the electronic and magnetic environment of the lanthanide (III) ion.[13, 14]

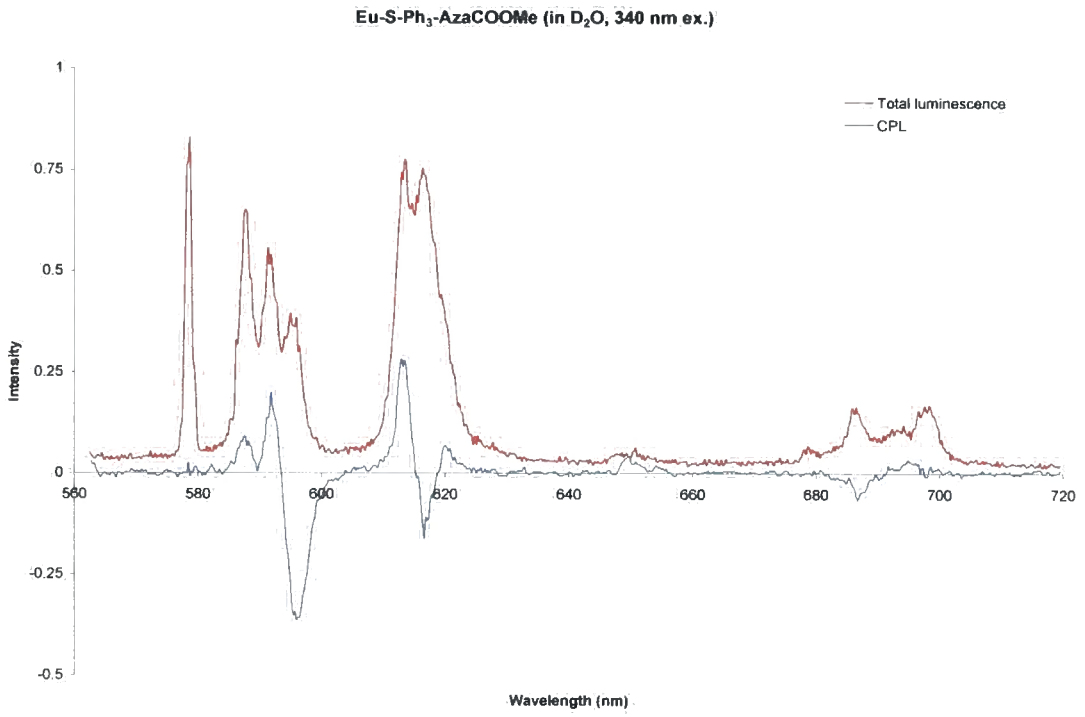

Figure 2.21 – Emission and CPL spectra of $[EuL^8]^{3+}$

A description of the "degree of chirality" sensed by the electronic transition is obtained using the dissymmetry factors, g_{em}, equation (3), where $I_{L\,(R)}$ is the intensity of the left (right) circularly polarised component.

$$g_{em} = \frac{2 \cdot (I_L - I_R)}{(I_L + I_R)} \qquad (3)$$

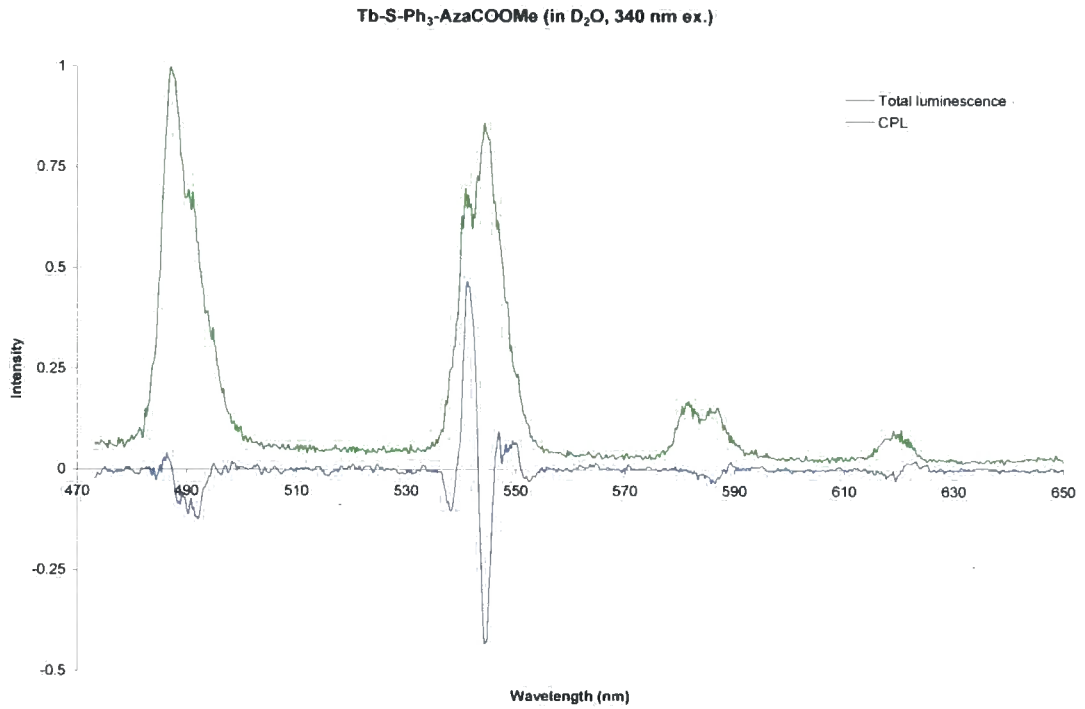

Figure 2.22 – Emission and CPL spectra of $[TbL^8]^{3+}$

The g_{em} factors were calculated for the $[LnL^8]^{3+}$ complexes and are compared to values for the related tetraphenyl amide complexes (*S*)-Δ-$[LnL^{12}]^{3+}$ for which the absolute configuration has been verified by X-ray crystallography.[15]

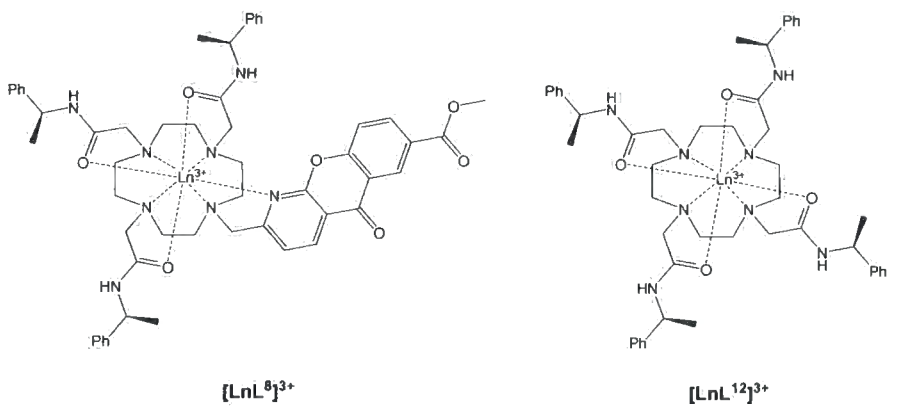

Figure 2.23 – Comparison of complex (*SSS*)-$[LnL^8]^{3+}$ and the parent tetraamide complex (*SSSS*)-Δ(λλλλ)-$[LnL^{12}]^{3+}$

Complex	g_{em}^{589}	g_{em}^{595}	g_{em}^{615}
(*SSS*)-$[EuL^8]^{3+}$	+0.009	-0.077	+0.011
(*S*)-Δ-$[EuL^{12}]^{3+}$	+0.09	-0.09	+0.08

Complex	g_{em}^{541}	g_{em}^{544}	g_{em}^{547}
(*SSS*)-$[TbL^8]^{3+}$	+0.080	-0.050	+0.018
(*S*)-Δ-$[TbL^{12}]^{3+}$	+0.14	-0.1	+0.17

Table 2.5 – Comparison of g_{em} values for the (*SSS*)-enantiomers of $[LnL^8]^{3+}$ and (*S*)-Δ-$[LnL^{12}]^{3+}$

The sign and sequence of the transitions for the Eu and Tb complexes $\mathbf{[LnL^8]^{3+}}$ was the same as for the $\mathbf{(S)\text{-}\Delta\text{-}[LnL^{12}]^{3+}}$. Hence, a Δ-helicity can be assigned to these complexes.

2.7.3.4 Two photon excitation

As has been discussed in the introduction (Section 1.1.2), two photon excitation is currently being pursued for certain fluorescent probes in biological imaging, as it offers higher resolution and deeper tissue penetration and may cause less photodamage. Only a limited number of reports have been published so far dealing with two photon excited luminescence of lanthanides. [16, 17]

Recently, two photon emission spectra were recorded for two europium complexes synthesised in Durham, $\mathbf{[EuL^{13}]^{3+}}$ and $\mathbf{[EuL^{14}]^{3+}}$.[18]

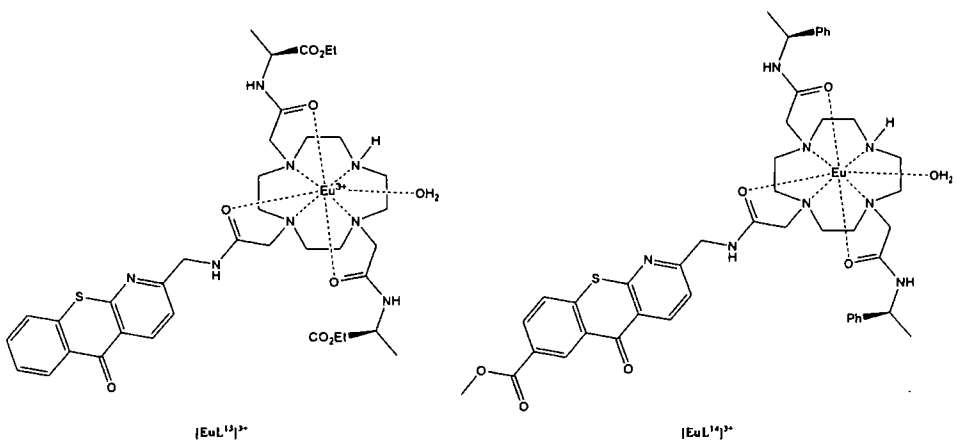

Figure 2.24 – Complexes used in initial two photon excitation experiments

The two photon excitation was achieved at 758 nm using a cavity dumped mode locked Ti-sapphire laser. The experimental set-up did not allow recording of the $\Delta J=4$ manifold above 680 nm.

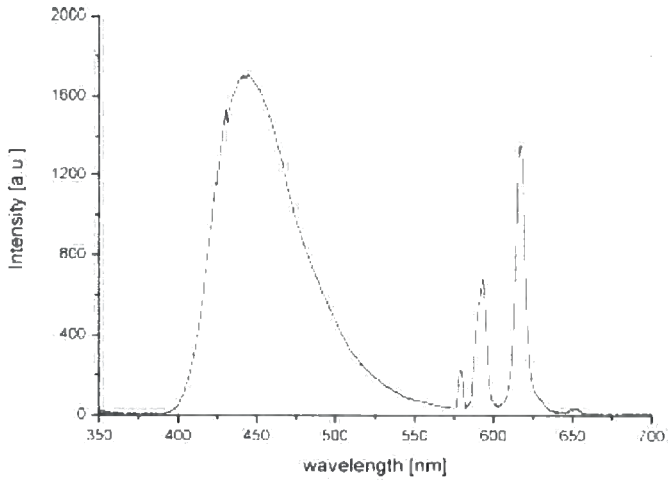

Figure 2.25 – Emission spectrum of $[EuL^{13}]^{3+}$ recorded in D_2O using two photon excitation at 758 nm

Similarly two photon excitation was achieved for $[EuL^{7}]^{3+}$, with excitation at 770 nm.

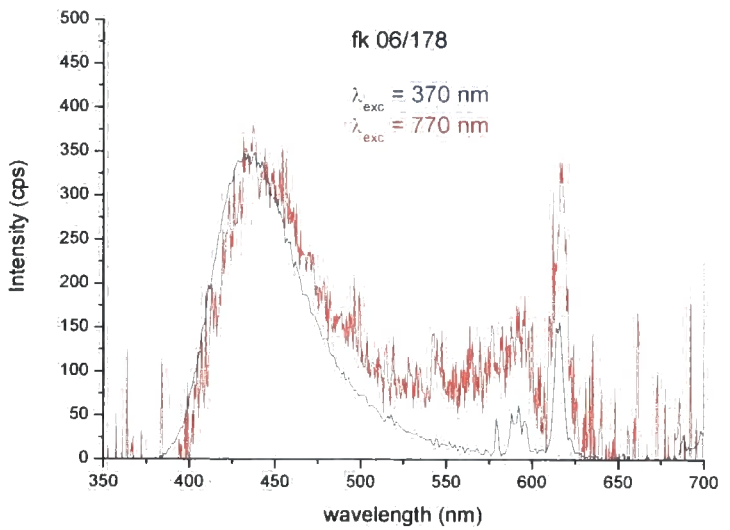

Figure 2.26 – Emission spectra for $[EuL^{8}]^{3+}$ acquired using single photon (blue) and two photon (red) excitation (H_2O, 298 K)

The lower signal to noise ratio for the Eu^{3+} emission is due to the fact that the emission spectrum for $[\mathbf{EuL^7}]^{3+}$ was measured in H_2O, as opposed to D_2O for $[\mathbf{EuL^{13}}]^{3+}$.

The possibility for two photon excitation of the azaxanthone complexes was demonstrated with $[\mathbf{TbL^8}]^{3+}$ using excitation at 670 nm from a Ti-Sapphire laser. The slope of the plot of $\log(I_{obs})$ versus log (power) was 2.03, consistent with a two photon excitation process.

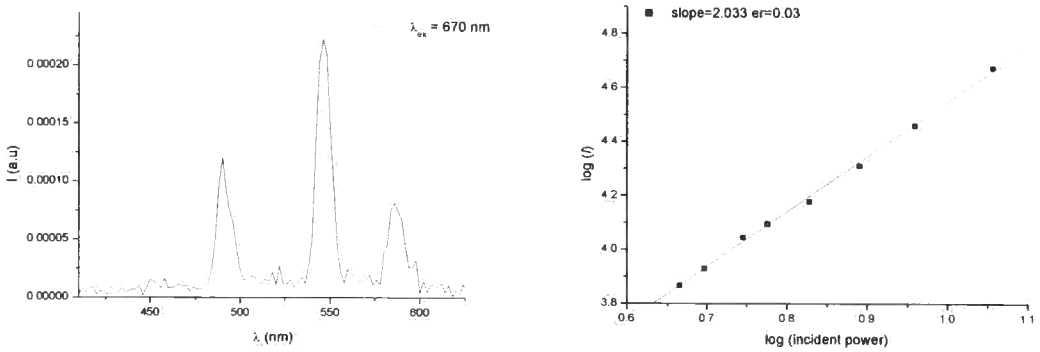

Figure 2.27 – Two photon emission spectrum of $[\mathbf{TbL^8}]^{3+}$ and the power dependence of the emission intensity; 670 nm excitation

These experiments have demonstrated the possibility of using two photon excitation in fluorescence microscopy experiments involving complexes prepared in Durham.

2.7.4 Further experiments assessing potential for use in high throughput assays

The tetraazatriphenylene complexes $[\mathbf{LnL^5}]^{2-}$ were tested, by our collaborators in CisBio international, for stability in media containing different metal ion salts. HPLC and MS analysis was also carried out on the samples submitted for the tests. It should be noted that these samples had been kept in solution for over two years under ambient laboratory conditions, prior to this analysis.

Two major peaks were observed by analytical HPLC and were isolated by HPLC, for both the Tb^{3+} and Eu^{3+} complexes.

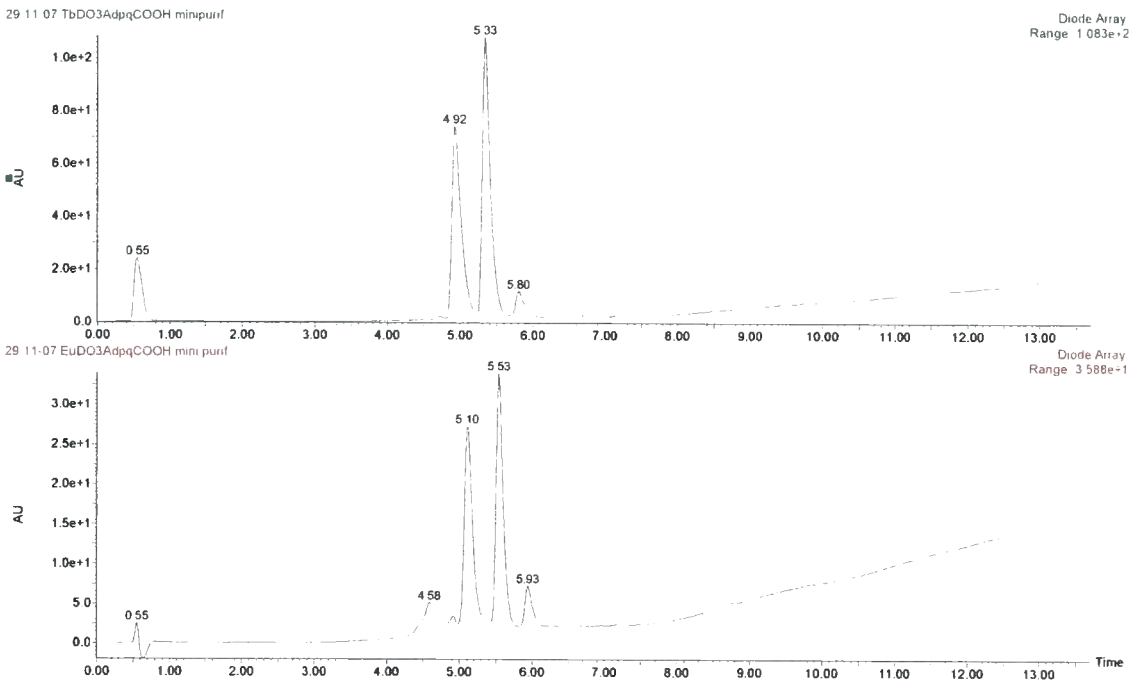

Figure 2.28 – HPLC analysis of samples submitted for stability testing to CisBio, performed in CisBio by Dr. R. A. Poole

The MS analysis showed both major peaks (4.92 and 5.33 min) to have the same mass, corresponding to the loss of one carboxylate group from the complex (complexes **[LnL^{15}]** and **[LnL^{16}]**). The minor peak with retention time of 5.80 min was shown to correspond to the dpq complex **[LnL^{17}]** without any carboxylic groups. This observation was further supported by the UV-Vis absorption spectra where the longest wavelength absorption for this peak was 340 nm, corresponding to previous results with the dpq chromophore.[19]

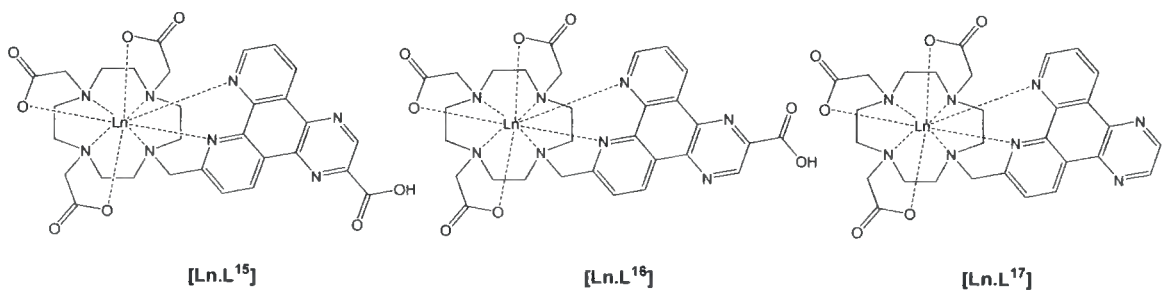

Figure 2.29 – Structures of the partially and fully decarboxylated complexes

T = 0

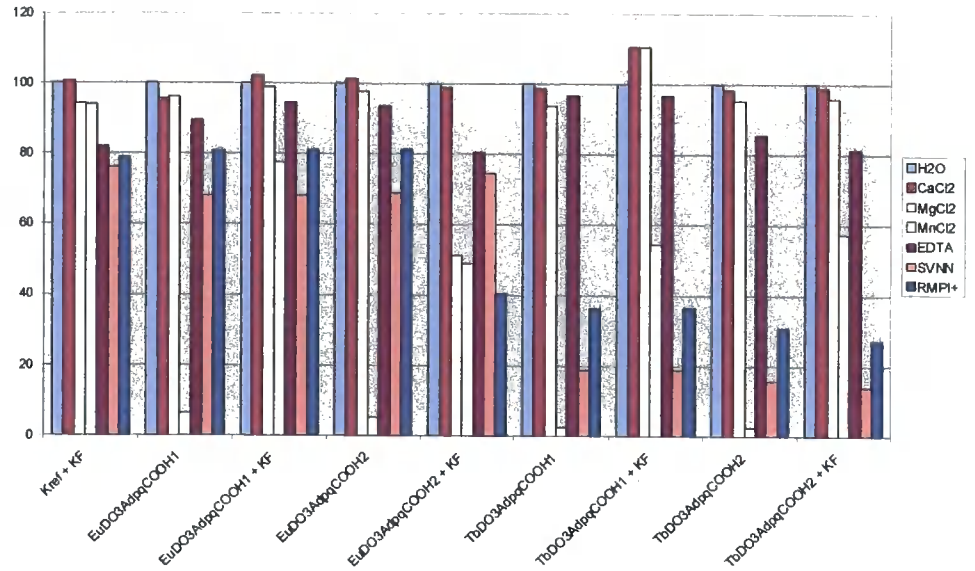

T = overnight

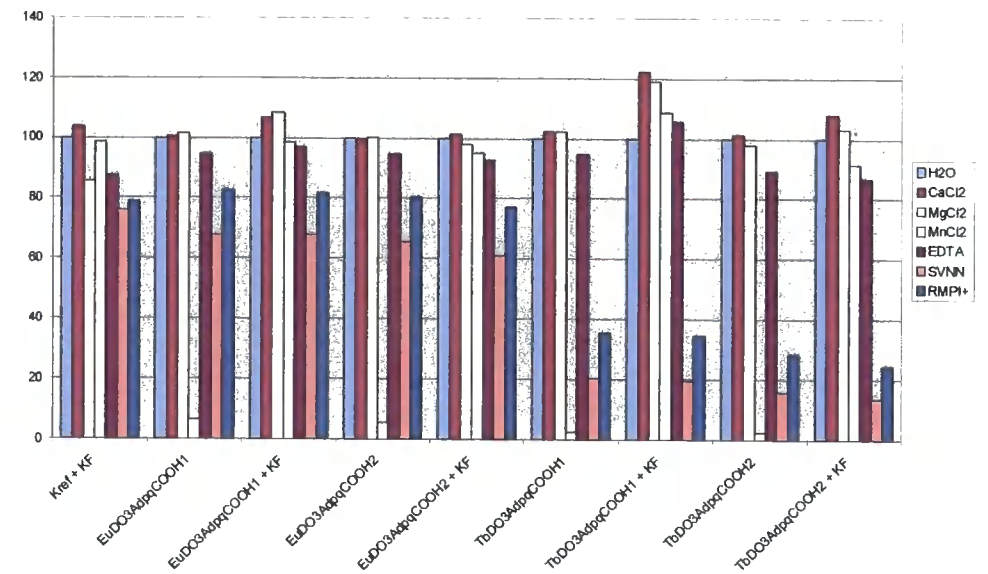

Figure 2.30 – Stability test in presence of $CaCl_2$ (20 mMf), $MgCl_2$ (20mMf), $MnCl_2$ (20 mMf), EDTA (20mMf), SVNN (New Born Calf Serum, 50 %), RPMI++ (Roswell Park Memorial Institute cell medium, 50 %). (Measured for purified samples of the 1st and 2nd major peaks by HPLC of the Eu and Tb complexes in HEPES buffer pH 7, 50 mM + 0.1 % BSA with and without KF at 0.4 M. Complex concentration was 1 uM).

The samples were however highly emissive and so were examined in the stability test (**Figure 2.30**), where the emission intensity was measured in the presence of several

salts and in biological media. These conditions correspond to assay conditions used in different protocols commercially.

The results are consistent with a high stability of the complexes with time, with the exception of the observed sensitivity to Mn^{2+} ions.

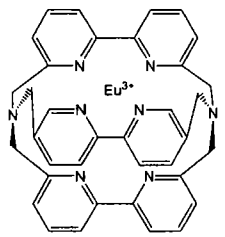

Figure 2.31 – Structure of the reference Eu^{3+} cryptate K_{ref} used in the stability experiment

The observation of stepwise decarboxylation for the aged samples is not surprising. Decarboxylation of carboxylic acids in the α-position to pyridine, quinoline or pyrazine groups is well established in the literatue and is usually associated with a thermally activated process for the protonated ligand.

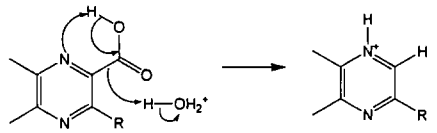

Scheme 2.21 – Possible mechanism of decarboxylation of tetrazatryphenylene complexes [LnL^5]

2.8 Chromophore modification by N-oxide formation

The longest wavelength absorption maximum in the azaxanthone spectrum, lying just below 340 nm, is on the borderline for practicable use in fluorescence microscopy. Previous work in Durham has shown that the formation of the *N*-oxide on the pyridine ring of the azaxanthone chromophore shifts the absorption maximum more than 10 nm to the red.[20] The DO3A complexes containing this modified azaxanthone chomophore were prepared to assess their utility in sensitising lanthanide luminescence.

2.8.1 Complex synthesis

The synthesis was carried out along the established route for azaxanthone synthesis, preparing the bromomethyl derivative **64** in three steps. This was then used to alkylate the *tris-tert*butyl ester of DO3A, **33**.

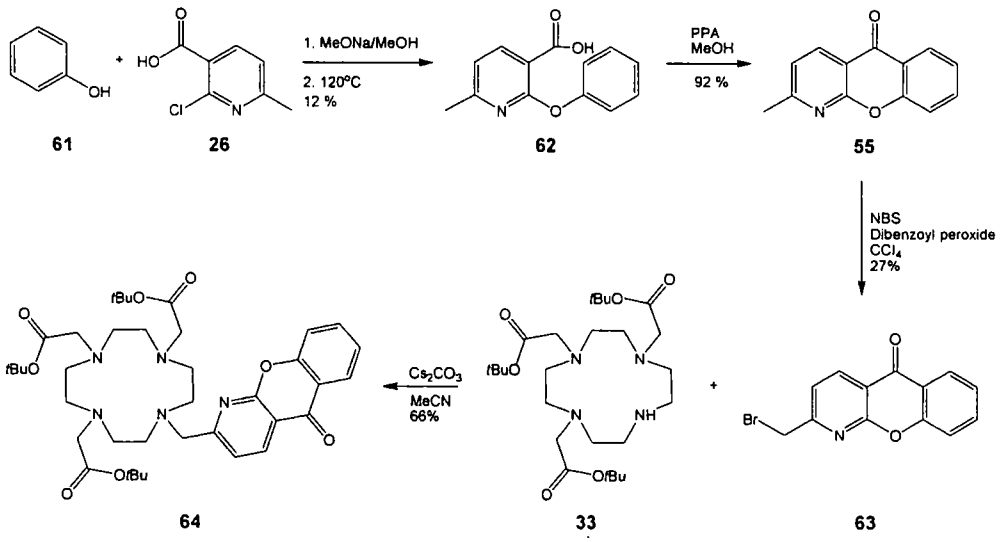

Scheme 2.22 – Synthesis of an azaxanthone substituted DO3A derivative

The protected ligand was obtained following alkylation in acetonitrile. The *t*-butyl esters were removed by TFA/DCM at room temperature followed by boiling of the crude reaction mixture in H_2O_2/TFA, to allow the formation of the desired N-oxide.

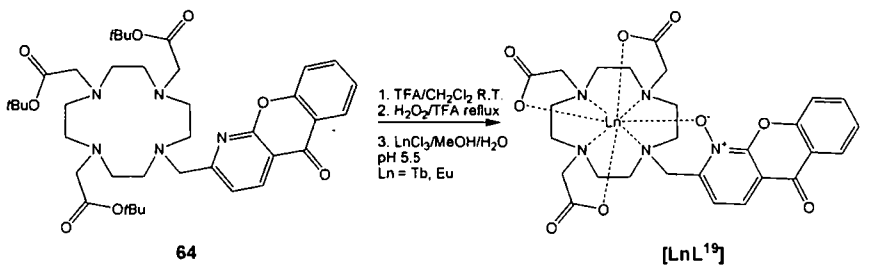

Scheme 2.23 – Synthesis of N-oxide complexes

The complexes were then formed by reacting with appropriate lanthanide chlorides in aqueous methanol mixtures, with the pH kept at 5.5.

2.8.2 Photophysical properties of the N-oxide complexes

The absoption spectrum of **[TbL^{19}]** recorded in H_2O showed that a shift of 10 nm for the longest wavelength absorption was achieved, by transforming the pyridine of the azaxanthone to its N-oxide.

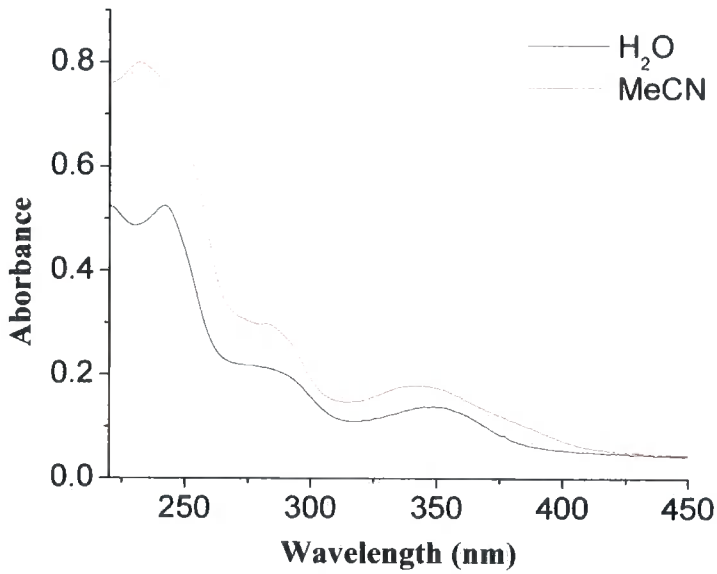

Figure 2.32 – Absorption spectra for the N-oxide complex [TbL^{19}] recorded in H_2O and MeCN (298 K)

The emission spectrum recorded in water, however, showed no lanthanide emission. Only a broad fluorescence at 500 was observed. Lanthanide emission was only observable in a dry aprotic solvent (e.g. MeCN).

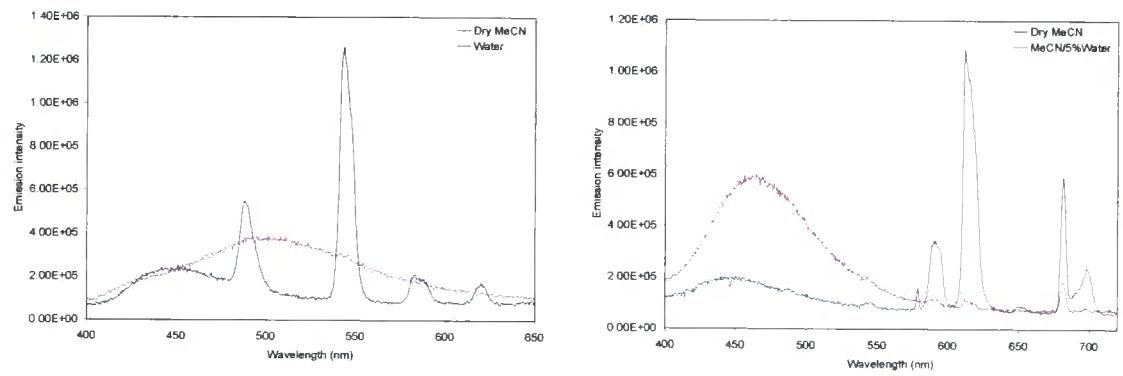

Figure 2.33 – Emission spectra of complexes [LnL^{19}] recorded in dry MeCN and water (MeCN/H_2O)

Even a small amount (5% v/v) of water added to the dry acetonitrile solution of the N-oxide complex led to nearly complete removal of the lanthanide luminescence. This could be the result of weak binding of the chromophore N-oxide to the metal ion as a result of strain in the bite angle. Thus, the chromophore is easily displaced by competitive coordination of water molecules. These results showed that the N-oxide complexes were not suitable for cellular imaging by fluorescence microscopy and were not developed further.

2.9 Phosphinate complexes

Previous work in Durham has shown that tetrakis phosphinate complexes, $[LnL^{20}]^-$, possess long luminescence lifetimes (nearly 4 ms of Tb^{3+} complex), and high overall emission quantum yields, up to 44% in H_2O.[21]

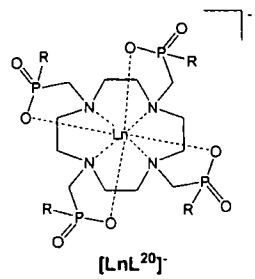

Figure 2.34 – Tetrakis phospinate comlexes

This observation, together with the possibility to vary the lipophilicity of the complex by variation of the alkyl group R, made complexes incorporating three phophinate pendant arms and a chromophore an interesting target. Complexes with two different alkyl groups (methyl, benzyl) were selected as goals for initial work.

2.9.1 Complex synthesis

Two different strategies were used in the synthesis of the two analogous ligands. Each route involved protection and deprotection steps to achieve the selective substitution of the cyclen ring nitrogens.

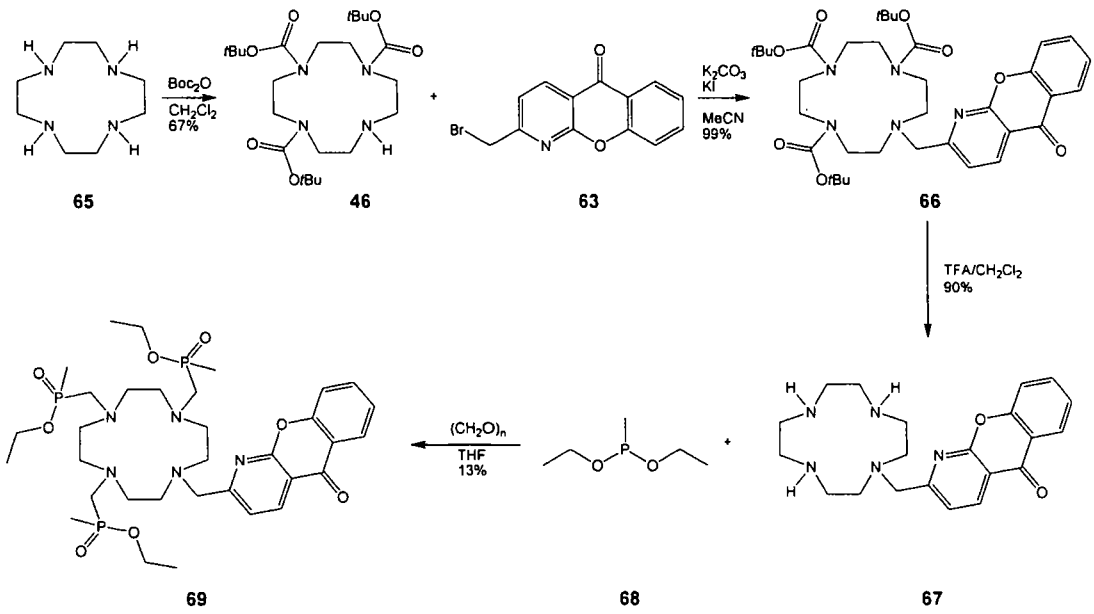

Scheme 2.24 – Synthesis of the methyl phosphinate ligand, L^{21}

The synthesis of the protected methyl phosphinate ligand, **69**, commenced with protection of three cyclen ring nitrogens by Boc groups. The remaining nitrogen was alkylated with the bromomethyl derivative of 1-azaxanthone, **63**, in a subsequent reaction. The protecting Boc groups were removed by TFA in dry CH_2Cl_2 and the monosubstituted cyclen derivative **67** was reacted with diethoxymethylphosphine and *para*-formaldehyde, to yield the protected ligand **69**.

The synthesis of the benzyl phosphinate ligand, **74**, began with a series of protecting and deprotecting reactions aimed at obtaining the mono-Boc protected cyclen derivative **70**. The cyclen was first acylated at three ring nitrogens by ethyl trifluoroacetate, and the remaining position was protected by a Boc group. The derivative **70** was then obtained following mild base hydrolysis. The phosphinate pendant arms were introduced in an Arbusov reaction with diethoxybenzylphosphine, **71**, and paraformaldehyde in dry THF. This was followed by the removal of the Boc protection with TFA in DCM and alkylation of the free cyclen nitrogen to give the desired protected ligand **74**.

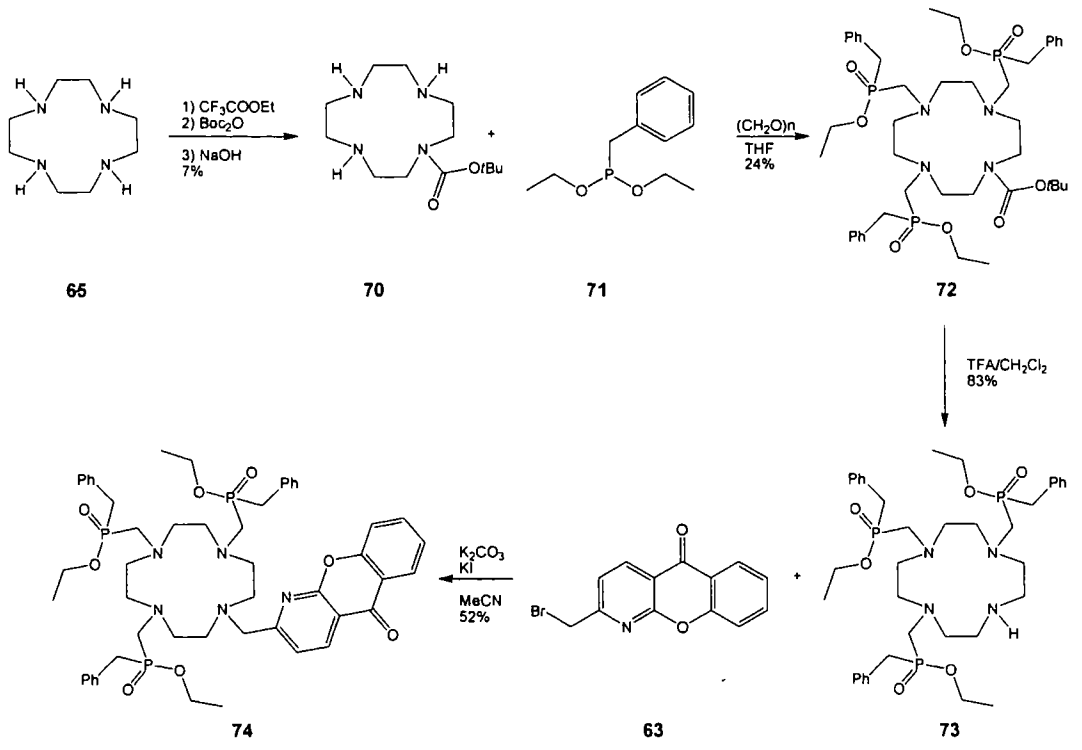

Scheme 2.25 – Synthesis of the benzyl phosphinate ligand, L^{22}

The synthesis was completed by acid hydrolysis of the phosphinate ethyl groups and complexation with an appropriate lanthanide (III) salt in aqueous methanol adjusting the pH to 6. The neutral complexes, **[LnL^{21}]** and **[LnL^{22}]**, were purified by column chromatography on alumina.

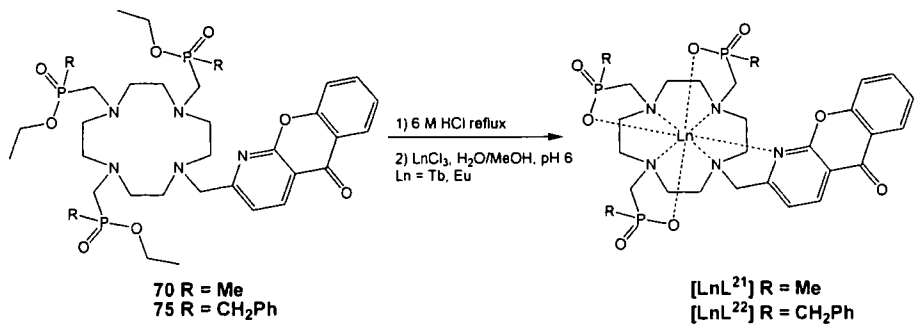

Scheme 2.26 – Synthesis of the phosphinate complexes, [LnL^{18}] and [LnL^{19}]

2.9.2 Complex properties

The phosphinate complexes containing the azaxanthone chromophore had the favourable luminescence properties that were expected. The luminescence lifefitimes are summarised in **Table 2.6**.

Ligand	*Tb*	*Eu*
$\mathbf{L^{18}}$	3.57 ms	1.16 ms
$\mathbf{L^{19}}$	3.63 ms	1.25 ms

Table 2.6 – Luminescence lifetimes for the phosphinate complexes (H_2O, 295 K)

The luminescence lifetime in D_2O was measured for the benzyl phosphinate complex **[TbL^{22}]** and was found to be 3.58 ms. This indicates that there are no water molecules directly bound to the metal centre, even though the ligand is only octadentate. This behaviour was observed with other complexes bearing the benzyl phosphinate pendant arms and is probably due to the steric hindrance of the metal centre by the benzyl groups and the overall lipophilic character of the complex.[22] The luminescence quantum yield for the benzyl phosphinate complex **[TbL^{22}]** was 44%.

These results were not further developed, apart from quenching studies (Chapter 3), in this thesis but were taken as an encouragement to use phosphinate arms in further work with luminescent complexes.

2.10 Conclusions

Two new chromophores incorporating carboxylic acid functionality and their DO3A complexes have been synthesised. Their photophysical properties were investigated. The tetraazatriphenylene chromophore, **12**, gives rise to highly emissive complexes. The only drawback in the case of this chromophore is its tendency over time to lose one or even both of its carboxylic acids. The monocarboxylate complexes have, however, been shown to be highly emissive and stable with time in media used for commercial assays. The monoacid complexes also retain one possible conjugation

point. Complexes of the azathioxanthone chromophore exhibit only weak lanthanide emission. This is in part due to strong chromophore fluorescence in aqueous media.

An analogous azaxanthone chromophore, containing a carboxylic acid ester, has been incorporated into cationic amide arm complexes, which have been shown to be highly emissive. Further work with these complexes is presented in Chapter 4.

Further work was aimed at amending properties of the azaxanthone chromophore by making its N-oxide. The N-oxide complexes are not emissive in aqueous media and cannot be used for cellular imaging purposes. Phosphinate pendant arm complexes have been synthesised as well, and have been shown to have good photophysical properties.

Literature

[1]) S. Pandya, J. Yu, D. Parker, *Dalton Transactions*, 2006, 2757.
[2]) R. A. Poole, G. Bobba, M. J. Cann, J. C. Frias, D. Parker, R. D. Peacock, *Organic and Biomolecular Chemistry*, 2005, **3**, 1013.
[3]) J. Yu, D. Parker, R. Pal, R. A. Poole, M. J. Cann, *Journal of the American Chemical Society*, 2006, **128**, 2294.
[4]) E. B. van der Tol, H. J. Van Ramesdonk, J. W. Verhoeven, F. J. Steemers, E. G. Kerver, W. Verboom, D. N. Reinhoudt, *Chemistry an Europena Journal*, 1998, **4**, 2315.
[5]) F. J. Villani, T. A. Mann, E. A. Wefer, J. Hannon, L. L. Larca, M. J. Landon, W. Spivak, D. Vashi, *Journal of Medicinal Chemistry*, 1975, **18**, 1.
[6]) P. Atkinson, Y. Bretonniere, D. Parker, *Chemical Communications*, 2004, 438.
[7]) H. J. Pownall, J. R. Huber, *Journal of the American Chemical Society*, 1971, **93**, 6429.
[8]) L. J. Martínez, J. C. Scaiano, *Journal of Physical Chemistry A*, 1999, **103**, 203.
[8]) M. G. Neumann, M. H. Gehlen, M. V. Encinas, N. S. Allen, T. Corrales, C. Peinado, F. Catalina, *Journal of Chemical Society, Faraday Transactions*, 1997, **93**, 1517.
[10]) P. Atkinson, K. S. Findlay, F. Kielar, R. Pal, D. Parker, R. A. Poole, H. Puschmann, S. L. Richardson, P. A. Stenson, A. L. Thomson, J. Yu, *Organic and Biomolecular Chemistry*, 2006, **4**, 1707.
[11]) D. Parker, R. S. Dickins, H.Puschman, C. Crossland, J. A. K. Howard, *Chemical Reviews*, 2002, **102**, 1977.
[12]) A. Beeby, I. M. Clarkson, R. S. Dickins, S. Faulkner, D. Parker, L. Royle, A. S. de Sousa, J. A. G. Williams, M. Woods, *Journal of Chemical Society, Perkin Transactions 2*, 1999, 493.
[13]) J. P. Riehl, F. S. Richardson, *Chemical Reviews*, 1986, **86**, 1.
[14]) J. I. Bruce, D. Parker, S. Lopinski, R. D. Peacock, *Chirality*, 2002, **14**, 562.
[15]) R. S. Dickins, J. A. K. Howard, C. L. Maupin, J. M. Moloney, J. P. Riehl, G. Siligardi, J. A. G. Williams, *Chemistry an Europena Journal*, 1995, **5**, 1095.
[16]) L. M. Fu, X. F. Wen, X. C. Ai, Y. Sun, Y. S. Wu, J. P. Zhang, Y. Wang, *Angewandte Chemie International Edition*, 2004, **43**, 2.
[17]) A. Picot, F. Malvolti, B. Le Guennic, P. L. Baldeck, J. A. G. Williams, C. Andraud, O. Maury, *Inorganic Chemistry*, 2007, **46**, 2659.
[18]) L. O. Pålsson, R. Pal, B. S. Murray, D. Parker, A. Beeby, *Dalton Transactions*, 2007, 5726.
[19]) G. Bobba, Y. Bretonnière, J. C. Frias, D. Parker, *Organic and Biomolecular Chemistry*, 2003, **1**, 1870.
[20]) P. Atkinson, *Chemoselective Phospho-Anion Binding Studies*, PhD. Thesis, 2005, Durham.
[21]) C. J. Broan, E. Cole, K. J. Jankowski, D. Parker, K. Pulukkody, B. A. Boyce, N. R. A. Beeley, K. Millar, A. T. Millican, *Synthesis*, 1992, 63.
[22]) K. Senanayake, A. L. Thomson, J. A. K. Howard, M. Botta, D. Parker, *Dalton Transactions*, 2006, 5423.

CHAPTER 3

Quenching studies

3 Quenching studies

A large number of factors needs to be taken into consideration during the design of luminescent lanthanide complexes for cellular imaging purposes.[1,2] Some of these, such as the prerequisites for sensitizing chromophores, have been discussed in previous chapters. Further understanding can be obtained from a mechanistic analysis of the pathway leading to lanthanide emission, **Scheme 3.1**

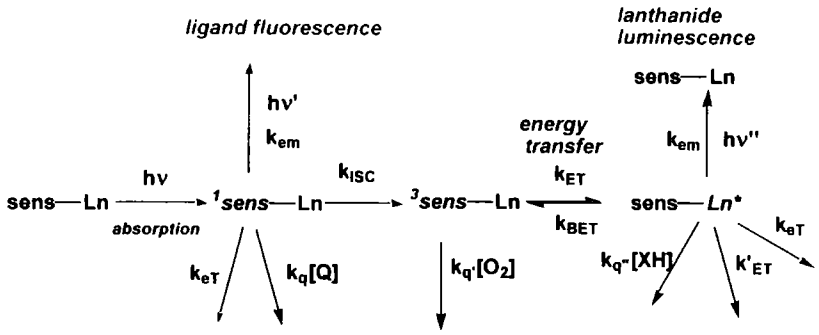

Scheme 3.1 – Photophysical kinetic scheme for sensitised lanthanide luminescence

This scheme shows that there are three excited states in the overall excitation pathway. The first two are the singlet and triplet excited states of the chromophore and the third one is the excited state of the lanthanide ion. The chromophore excited states can undergo several other energy-, electron- or vibrational- relaxation processes, which can lead to a decreased quantum yield for lanthanide emission. Thus, the sensitizing chromophores need to be chosen with care. The deliberate controlled perturbation of these excited states can also be used in the design of sensitive probes.[3,4]

The lanthanide excited state can be quenched by a variety of processes. Vibrational deactivation by energy matched X-H (X = O, C or N) oscillators is well known. The sensitivity of Tb^{3+} and Eu^{3+}excited states to vibrational quenching by OH and amine NH groups needs to be considered in ligand design.[5,6] Energy transfer to chromophores with appropriate absorption spectra can also occur and has found application in many time resolved assays.[7,8]

Furthermore, another quenching pathway, involving an electron/charge transfer process, can be anticipated. The terbium $^5D_4$ and europium $^5D_0$ excited states lie high above their ground states at 244 and 206 kJ mol^{-1} respectively. In addition, these excited states have lifetimes of the order of milliseconds. This energy can be utilised as a driving force for an electron-transfer process.[9] It has been observed that this process occurs in the presence of electron rich species, which can, in the limiting case, be oxidised with the concomitant reduction of the complex. The facility of such a process can be assessed using the Weller equation (1).[10]

$$\Delta G_{ET} = nF\left[(E_{ox} - E_{red}) - E_{Ln^*} - e^2/\varepsilon r\right] J\,mol^{-1} \qquad (1)$$

Here, E_{ox} is the oxidation potential of the electron donor (quencher), E_{red} is the reduction potential of the complex, E_{Ln^*} is the energy of the lanthanide excited state (2.52 and 2.13 eV for terbium and europium respectively) and $e^2/\varepsilon r$ is a Coulombic attraction factor correcting for the transient formation of a charge separated species, which is usually small (< 0.2 eV).[4]

The first implication, obvious from equation (1) is that terbium complexes should be quenched more readily by this mechanism than europium complexes of the corresponding ligands, due to the higher energy of the terbium excited state (difference of 38 kJ mol^{-1}). This in turn implies, at least in the case of terbium complexes, that the electron is accepted by the heterocyclic chromophore, rather than the metal.[9]

Thus, knowing the reduction potential of the chromophores, and using equation (1), an estimate can be obtained as to which electron rich species should be expected to exhibit this kind of quenching. For the tetraazatriphenylene complexes, with the chromophore reduction potential of -1.1 V, and halide anions it is only iodide (E_{ox} = + 0.54 V)[11] that should effectively quench the lanthanide luminescence. The oxidation potentials of + 1.07 V and + 1.36 V for bromide and chloride respectively should rule them out as possible quenchers.[4,9]

As these lanthanide complexes were developed for cellular imaging, other electron rich species needed to be investigated as possible quenchers of lanthanide emission. The two most obvious ones are urate (E_{ox} = +0.59 V) and ascorbate (E_{ox} = +0.30 V).[12] These two compounds are present in most eukaryotic cells with concentrations ranging from 0.1 to 1 mM and probably act in synergy, as part of the cell's antioxidation mechanisms.

In addition, initial observations of this type of quenching have shown that it is both the emission intensity and its lifetime that are reduced. This indicates that a dynamic/collisional quenching process is taking place.[4, 9]

3.1 Investigation of dynamic quenching

The Stern-Volmer equation (2) is commonly used to quantify the extent of quenching by a given quencher[13]:

$$I_0/I = 1 + k_q \tau_0 [Q] = 1 + K_{SV}[Q] \qquad (2)$$

I_0 and I in equation (2) are luminescence intensities in the absence and presence of the quencher respectively, k_q is the rate constant for the bimolecular quenching process, τ_0 is the luminescence lifetime in the absence of quencher and [Q] is the quencher concentration. The product of k_q and τ (K_{SV}) is the Stern-Volmer quenching constant, which has units M^{-1}. The quenching susceptibility is usually quoted as the inverse value of the Stern-Volmer K_{SV} (M), which indicates the concentration at which the luminescence is quenched to 50% of its initial value.[13]

A similar equation relating luminescence lifetimes can be used for dynamic quenching, equation (3).

$$\tau_0/\tau = 1 + K_{SV}[Q] \qquad (3)$$

A linear relationship is thus obtained. An example of the experimental approach is given below (**Fig 3.1**) for the quenching of the lanthanide excited state by iodide and ascorbate in the dianionic complex $[LnL^3]^{2-}$.

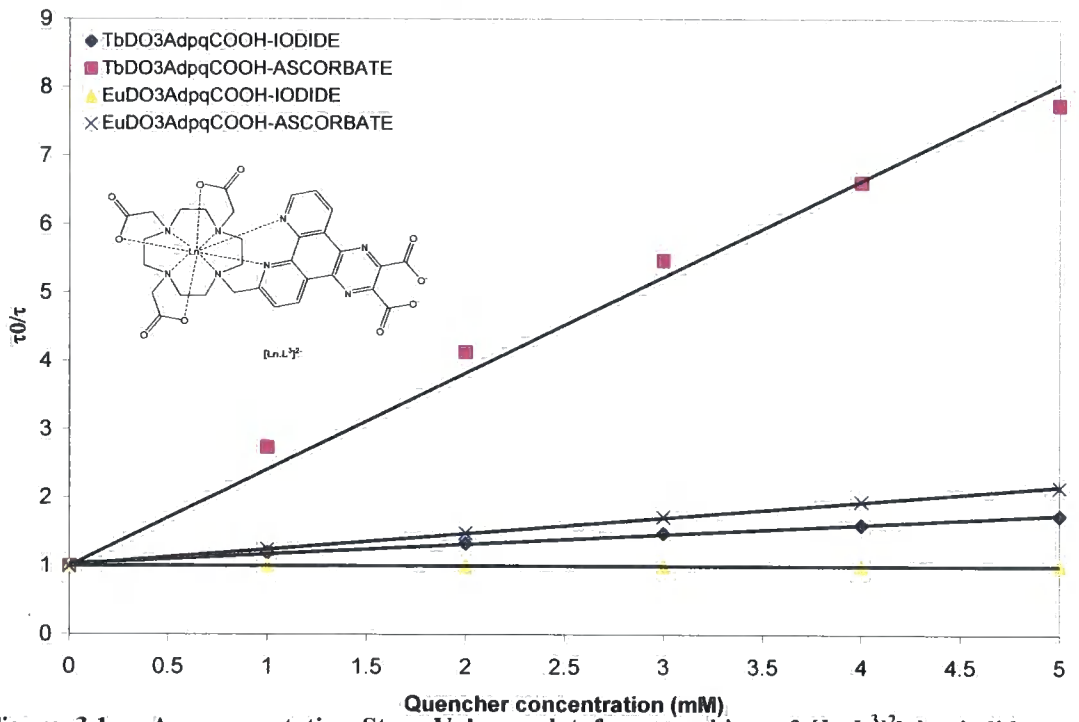

Figure 3.1 – A representative Stern-Volmer plot for quenching of $[LnL^3]^{2-}$ by iodide and ascorbate (298 K, pH 7.4, 100 mM HEPES, 10 mM NaCl)

A range of complexes, including those prepared as a part of this thesis, were studied in terms of their susceptibility to this type of dynamic quenching, with the aim to enhance the understanding of the underlying mechanisms. The need for such a study was evident, especially as initial experiments showed deviations from predictions based on the idealised relationships implicit in equations (1), (2) and (3).[9]

3.2 Dynamic quenching studies with a series of lanthanide complexes

The usual experimental set up for quenching studies involved a solution of a given complex at ~10 μM buffered to pH 7.4 with 100 mM HEPES buffer and containing 10 mM NaCl. The measurements were carried out at 298 K.

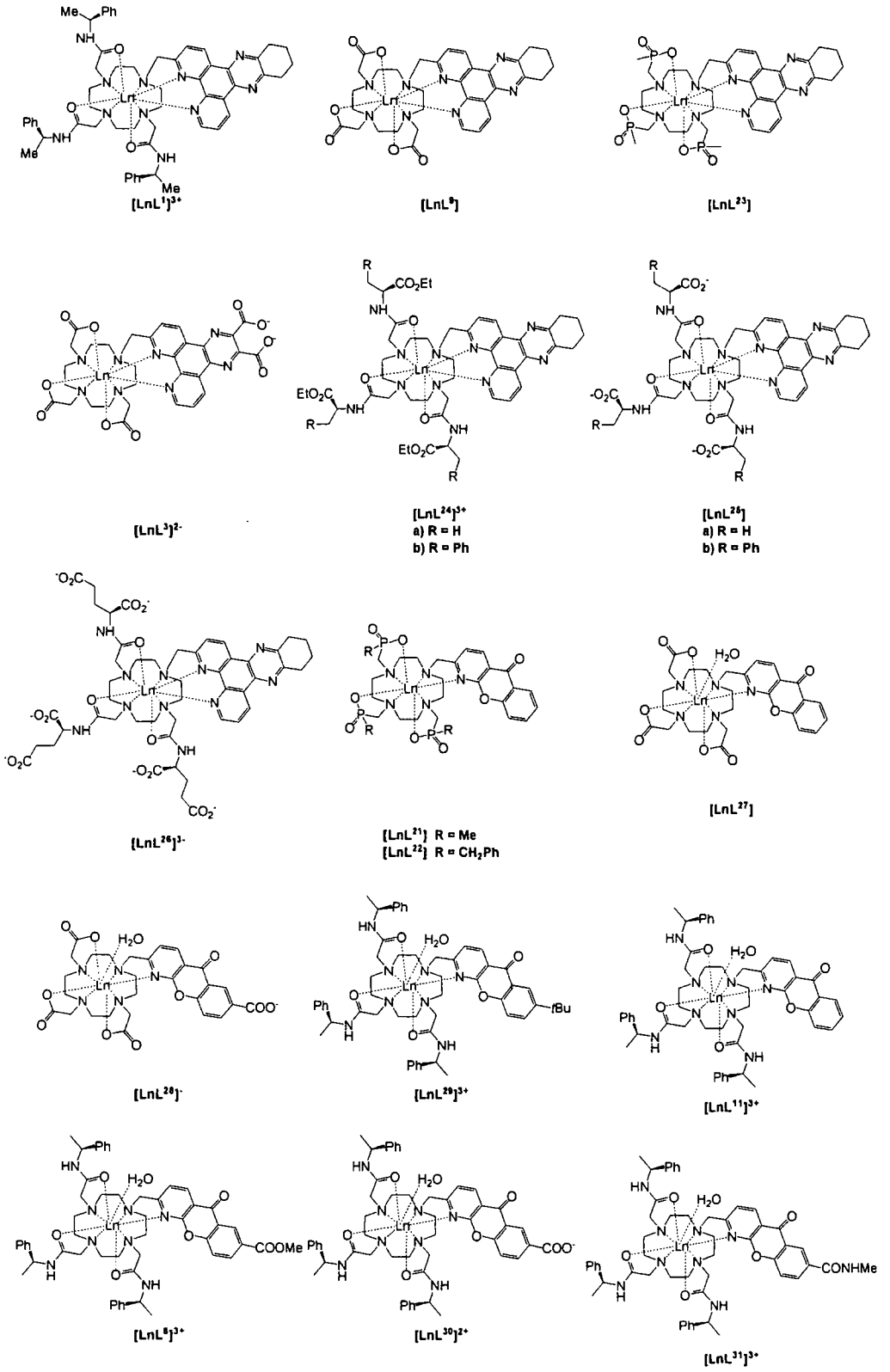

Scheme 3.2 – List of complexes used in the quenching study

3.2.1 Quenching with potassium iodide

The data obtained with solutions containing varied concentrations of potassium iodide followed the relationship implicit in equation (3) and gave linear Stern-Volmer plots. The results are summarised in Table 1.

Entry	*Complex*	*Terbium*	*Europium*
1	$[LnL^{1}]^{3+}$	0.92	27
2	$[LnL^{9}]$	2.10	>1000
3	$[LnL^{3}]^{2-}$	6.90	>1000
4	$[LnL^{24a}]^{3+}$	1.64	85.5
5	$[LnL^{24b}]^{3+}$	2.35	10.8
6	$[LnL^{25a}]$	2.25	>1000
7	$[LnL^{22b}]$	3.21	>1000
8	$[LnL^{26}]^{3-}$	2.50	>1000
9	$[LnL^{21}]$	36.6	120
10	$[LnL^{22}]$	26.2	139
11	$[LnL^{27}]$	53.5	125
12	$[LnL^{28}]^{-}$	35.2	N.d.
13	$[LnL^{29}]^{3+}$	10.9	250
14	$[LnL^{11}]^{3+}$	9.20	278
15	$[LnL^{8}]^{3+}$	5.60	N.d.
16	$[LnL^{30}]^{2+}$	>1000	N.d.

Table 3.1 – Inverse Stern-Volmer quenching constants K_{SV}^{-1} (mM) for quenching of the lanthanide luminescence by iodide (298 K, 10 μM complex, pH 7.4, 10 mM NaCl, 0.1 M HEPES buffer)

The expected higher sensitivity of terbium complexes to quenching is maintained in every case. The following order of susceptibility to quenching was observed for charged complexes positive > neutral > negative. This trend can be explained by simple electrostatic attraction/repulsion ideas and is evident especially for entries 1-3 and to a lesser extent, for entries 4, 6 and 8.

The susceptibility to quenching is also a function of the reduction potential of the chromophore. This trend is observed for a set of complexes with different chromophores but identical pendant arms, such as entry 1 and 11. The azaxanthone complexes are quenched to a lesser extent than the tetraazatriphenylene ones, as their standard reduction potentials are -1.6 and -1.1 V.

3.2.2 Quenching with Urate and Ascorbate

A similar study was carried out using uric and ascorbic acid as the quenching agents.

Entry	*Complex*	*Urate*		*Ascorbate*	
		Terbium	Europium	Terbium	Europium
17	$[LnL^{1}]^{3+}$	0.025	0.07	0.18	0.39
18	$[LnL^{9}]$	0.005	0.11	0.35	2.92
19	$[LnL^{3}]^{2-}$	0.01	0.16	0.75	4.13
20	$[LnL^{24a}]^{3+}$	0.009	0.49	0.24	0.51
21	$[LnL^{24b}]^{3+}$	0.018	0.028	0.47	0.47
22	$[LnL^{25a}]$	0.05	0.05	0.55	1.13
23	$[LnL^{25b}]$	0.03	0.08	0.99	7.50
24	$[LnL^{26}]^{3-}$	0.012	0.084	0.38	2.55
25	$[LnL^{21}]$	0.02	N.d.	0.48	N.d.
26	$[LnL^{22}]$	0.06	0.36	0.93	11.3
27	$[LnL^{27}]$	0.012	0.28	0.57	8.90
28	$[LnL^{28}]^{-}$	0.01	N.d.	0.61	N.d.
29	$[LnL^{29}]^{3+}$	0.02	0.27	0.30	1.52
30	$[LnL^{11}]^{3+}$	0.04	0.60	0.37	1.50
31	$[LnL^{8}]^{3+}$	0.018	N.d.	0.19	N.d.
32	$[LnL^{30}]^{2+}$	>1000	N.d.	>1000	N.d.

Table 3.2 – Inverse Stern-Volmer quenching constants K_{SV}^{-1} (mM) for quenching of the lanthanide luminescence by urate and ascorbate (298 K, 10 μM complex, pH 7.4, 10 mM NaCl, 0.1 M HEPES buffer)

The higher susceptibility of terbium complexes to quenching was also observed with these quenchers. Other results obtained from this study, did not adhere to the predictions based on equations 1-3.

Most importantly, each complex showed a much higher sensitivity (up to an order of magnitude) to quenching by urate compared to ascorbate. This behaviour does not match the expectation based on their oxidation potentials of +0.59 and +0.30 V, respectively. The sensitivity to quenching by urate/ascorbate mirrored the ease of reduction of the chromophore, for complexes based on the same ligand parent structure (e.g. DO3A). No overall trend was evident, however, based on overall charge i.e. coulombic effects, as was the case for iodide. The steric shielding of the metal centre seems to play a more important role. Comparing, for example, the azaxanthone DO3A complex (Entry 27) to its benzyl phosphinate analogue (Entry 26), it is evident that the more sterically hindered benzyl phospinate complex is less sensitive to quenching.

The data presented in Table 3.2 were obtained with concentrations of urate in the range from 5 to 50 μM and ascorbate 50 to 500 μM. This concentration range had to be used as the Stern-Volmer plots of τ_0/τ versus quencher concentration showed deviation from linearity predicted by equation 3, consistent with saturation behaviour.

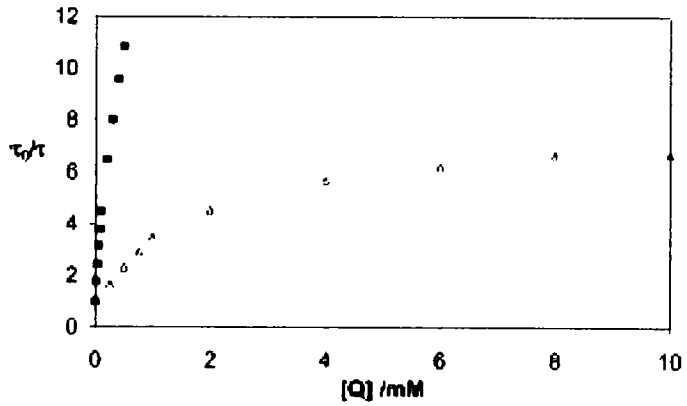

Figure 3.2 – Nonlinear behaviour of τ_0/τ plots for urate (squares) and ascorbate (open triangles) with complex $[TbL^{11}]^{3+}$ (pH 7.4, 0.1 M HEPES, 10 mM NaCl, 10 μM complex, 295 K)[9]

This effect is especially marked for terbium complexes in quenching experiments with urate. Non-linear behaviour and the tendency to reach a limiting τ_0/τ value was also observed with high concentrations of ascorbate as well. This nonlinear behaviour was most evident with cationic complexes, such as $[\mathbf{LnL^1}]^{3+}$, where deviations from linearity were observed at 50-200 μM urate concentration. Urate concentrations 3-4 times higher were required for such an effect with the corresponding neutral and anionic complexes.

Thus, another parameter was needed to be defined in order to describe the quenching behaviour exhibited by urate and ascorbate. The τ_0/τ value, at a fixed quencher concentration was considered. Analysing these values for example for complexes $[\mathbf{LnL^1}]^{3+}$, $[\mathbf{LnL^9}]$ and $[\mathbf{LnL^{23}}]^{3-}$ with 50μM urate, τ_0/τ values are 5.1, 11.5 and 5.6 respectively. It can be clearly seen that the charge effects that dominated iodide quenching are not important in this case. Indeed, the cationic complex is the least sensitive. This behaviour is further emphasised by examining the limiting τ_0/τ values, which are 8 for the cationic complex and >20 for the other two.

3.2.3 Amide arm complexes of functionalised azaxanthone complexes

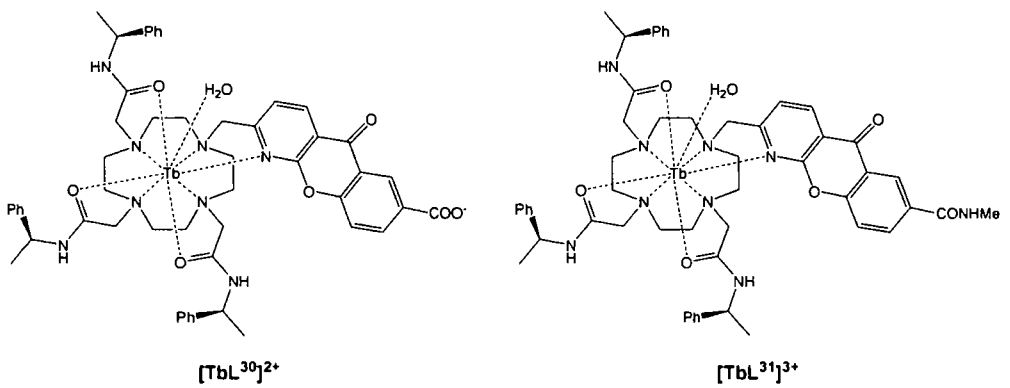

Figure 3.3 – Structures of complexes showing limited sensitivity to quenching by electron rich species

A surprising result was observed for the 'phenyl amide' arm azaxanthone complexes with carboxylate $[TbL^{30}]^{2+}$ and methylamide $[TbL^{31}]^{3+}$ groups in the chromophore structure. The carboxylate complex was virtually unquenched. (**Figure 3.4**).

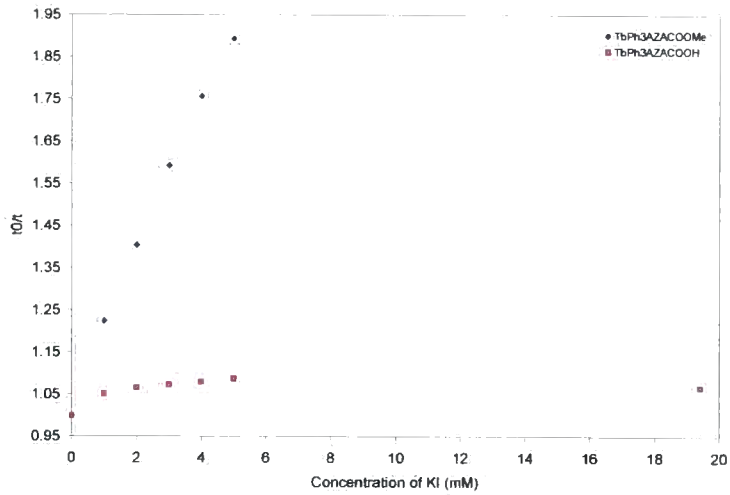

Figure 3.4 – Stern-Volmer plot comparing quenching by iodide of the methyl ester $[TbL^{8}]^{3+}$ and carboxylate acid $[TbL^{30}]^{2+}$ complexes (pH 7.4, 0.1 M HEPES, 10 mM NaCl, 10 µM complex, 295 K)

Furthermore, the methylamide complex, $[TbL^{31}]^{3+}$, shows high resistance to being quenched as well, with a τ_0/τ value of only 1.03 in the presence of 19.7 mM iodide.

Similarly in the case of ascorbate and urate quenching nearly no sensitivity was observed for the carboxylate complex, $[TbL^{30}]^{2+}$.

The methylamide was also resistant to quenching, with τ_0/τ values of 2.09 and 1.06, for ascorbate (19.7 mM) and urate (0.2 mM) respectively.

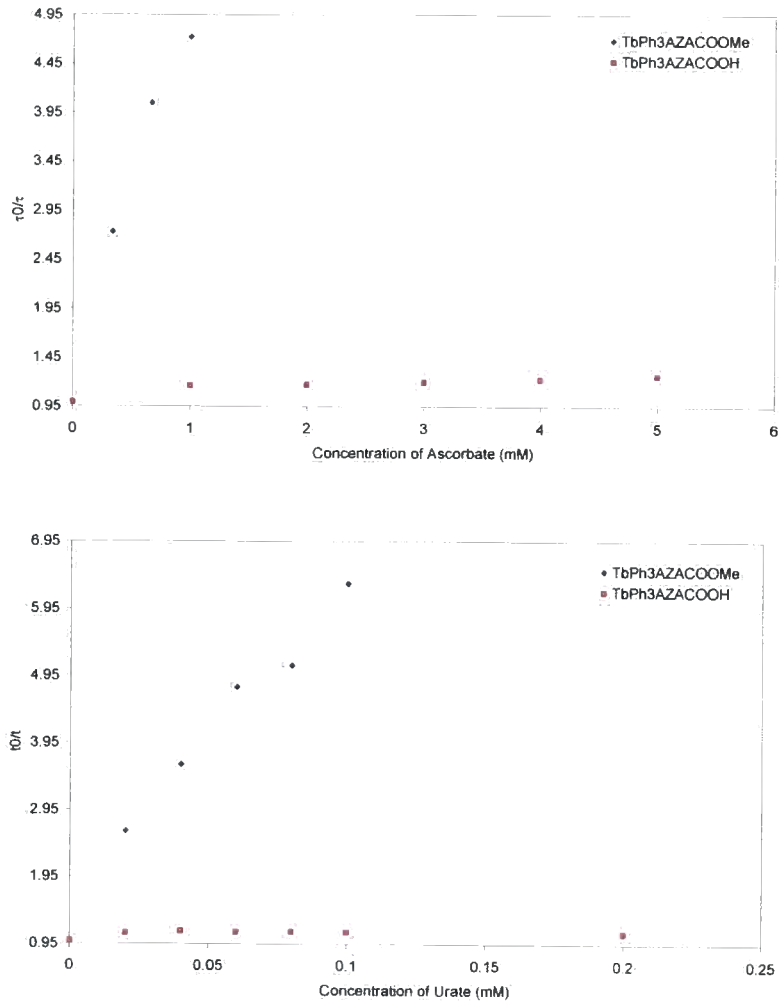

Figure 3.5 – Stern-Volmer plots comparing quenching by ascorbate and urate of the methyl ester $[TbL^{8}]^{3+}$ and carboxylic acid $[TbL^{30}]^{2+}$ complexes (pH 7.4, 0.1 M HEPES, 10 mM NaCl, 10 μM complex, 295 K)

These results can be rationalised in terms of simple Coulombic repulsion for the carboxylate complex $[TbL^{30}]^{2+}$, as the acid group is deprotonated under the conditions of the experiment giving the chromophore a local negative charge. This effect, however, was not so dramatic for the tetraazatriphenylene complexes $[LnL^{3}]^{2-}$. Furthermore, it cannot explain the relatively high insensitivity to quenching of the methylamide $[LnL^{31}]^{3+}$ complex. Another possibility is a change of the reduction potential of the chromophore. But, the introduction of an electron withdrawing carbonyl group should increase the susceptibility of the chromophore to reduction

and thus increase the sensitivity to quenching, as was the case for the methyl ester. Thus, further investigation is needed for a greater understanding.

3.2.4 Investigation of the Quenching Mechanism

The observation of non-linear behaviour in the quenching of lanthanide emission by urate and ascorbate, as well as the unexpected sensitivity to quenching by urate, led to the need to explore further the underlying quenching mechanism.

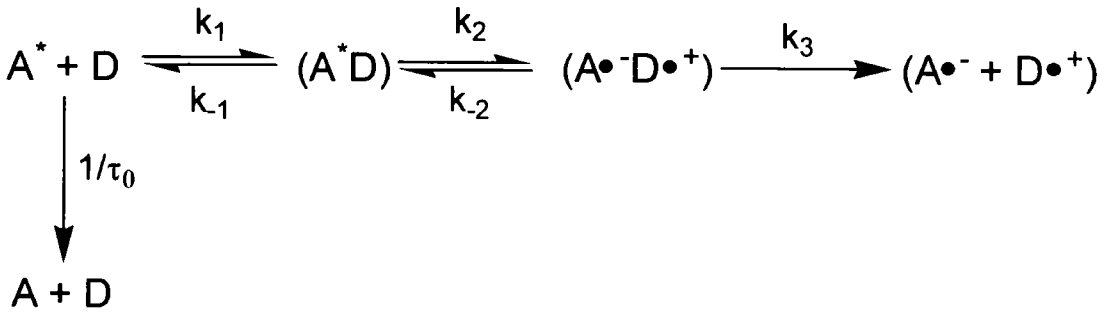

Scheme 3.4 – Kinetic scheme for collisional quenching proposed by Weller and Rehm[14]

The Stern-Volmer model used to interpret the quenching data is based on the kinetic scheme proposed by Weller and Rehm (**Sheme 3.4**).[15] This model assumes the formation of an encounter complex (A*D), with overall kinetics being controlled by diffusion, followed by electron transfer from the donor to the acceptor.

An alternative scheme has been proposed, during the analysis of quenching data for certain systems, especially pairs of aromatic donors and acceptors. In this case, a relatively long lived exciplex is postulated as an intermediate in the mechanism (**Scheme 3.5**).[16, 17]

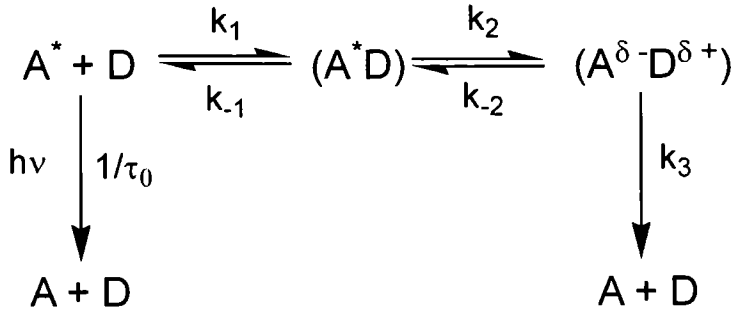

Scheme 3.5 – Kinetic scheme for quenching involving an associative step, forming a long lived exciplex

In this case, provided that $k_{-2}>>k_3$, an equilibrium constant K_{ex} for the formation of the exciplex can be defined:

$$K_{ex}=\frac{k_1 k_2}{k_{-1}k_{-2}} \tag{4}$$

The exciplex lifetime is then dependent on $(k_3)^{-1}$. The 'Stern-Volmer' quenching constants obtained in measurements where such a mechanism is in operation, have limited validity, and have a different meaning than defined earlier. A new, nonlinear, relationship for the dependence of lanthanide luminescence on quencher concentration can then be defined:

$$\frac{\tau_0}{\tau}=\frac{(1+k_3\tau_0 K_{ex}[Q])}{(1+K_{ex}[Q])} \tag{5}$$

This relationship also includes the possibility of a limiting value of τ_0/τ being equal to $k_3\tau_0$ at high quencher concentrations. The formation of the long lived exciplex can be enhanced by weak forces such as charge transfer, hydrogen bonding or π-π interactions. In particular, charge transfer between the π systems is likely, especially in the case of the electron rich urate anion and the electron poor chromophores.

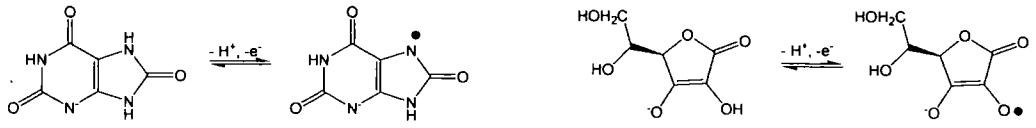

Scheme 3.6 – Urate and ascorbate one electron oxidation[9]

As an association step is involved in the mechanism according to **Scheme 3.5** it should be expected that this process would occur to a lesser extent with increasing temperature. This is contrary to processes that conform to **Scheme 3.4**, which are purely collisional and should be activated with increasing temperature.

Therefore, the temperature dependence of emission lifetime of $[TbL^{11}]^{3+}$ was measured for a fixed quencher concentration. The conditions were the same as for other quenching experiments (10 μM complex, pH 7.4, 10 mM NaCl, 100 mM HEPES). The quencher concentration was half the value of K_{SV}^{-1} for iodide and ascorbate and 50 μM for urate. The results are summarised in the Arrhenius plot (**Figure 3.6**), where ln(k) is plotted against 1/T.

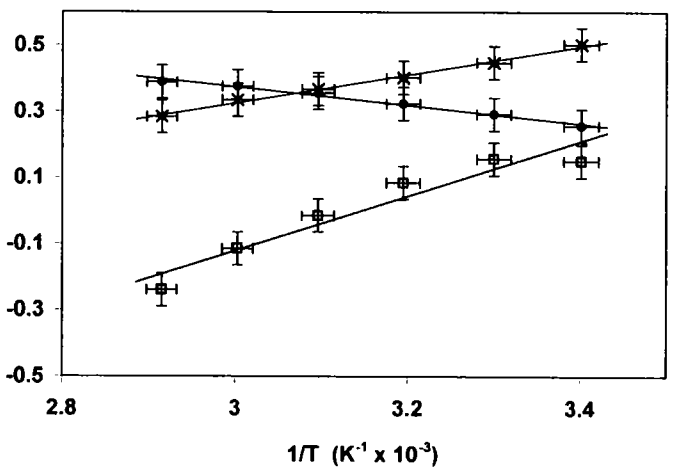

Figure 3.6 – Arrhenius plot for quenching of $[TbL^{11}]^{3+}$ with iodide (circles), urate (crosses) and ascorbate (squares)[9]

The different behaviour observed for urate and ascorbate, as compared to iodide, supports the suggestion that different processes might be involved. Further analysis of this data shows a small positive activation enrgy E_a = + 1.5 (±0.3) kJ mol^{-1} for iodide and negative values of - 6 and – 3.6 kJ mol^{-1} were found for ascorbate and

urate, respectively. The activation entropies for urate and ascorbate could then be estimated using Eyring's transition state analysis, and a negative value for $\Delta S^{\ddagger}$ = -260 (± 20) J mol^{-1} K^{-1} was found, in accord with the proposed associative process.

An experiment testing the effect of ionic strength was carried out to further test this hypothesis. It was again carried out with $[\mathbf{TbL^{11}}]^{3+}$ under the conditions of previous experiments (10 μM complex, pH 7.4, 100 mM HEPES, 298 K and with 40 μM urate or 10 mM iodide), and with NaCl concentration varied from 10 to 800 mM. The lifetime dropped from 1.50 to 1.25 ms in a control experiment, without added quencher, in the concentration range of added NaCl. The lifetime change in the case of urate was rather small going from 0.6 to 0.8 ms at 0.8 M NaCl. A more dramatic increase in lifetime was observed for iodide, where the change was from 0.7 to 1.25 ms, reaching this limit at only 0.2 M NaCl concentration. This is in line with expectations based on the sensitivity of collisional encounters of charged species to ionic strength.

The data obtained for the temperature and ionic strength dependence of the luminescence lifetime support the idea that iodide quenching happens by purely collisional process. In contrast, an associative process, likely to involve an exciplex is more plausible for ascorbate and urate. This hypothesis has subsequently been supported by quenching experiments with selected catechols, which showed similar behaviour to urate, as expected from their structure.[9]

3.3 Urate sensing

The high sensitivity of lanthanide emission to quenching by urate, which can be an issue in the cellular imaging use of these complexes, can however be useful. The fact that the K_{SV}^{-1} values for urate are an order of magnitude lower than for ascorbate and several orders of magnitude lower than for iodide, indicate the possibility to use this quenching potency for determination of urate concentration, even in the presence of these species.[18]

Measuring urate concentration is an interesting goal as it is an important marker measured in clinical conditions. Uric acid is the final metabolic product for purines, such as nucleobases adenine and guanine. Their metabolites are converted to uric acid in the liver, with its equilibrium concentration in the body being controlled by its relative rate of synthesis and renal excretion.

Elevated uric acid levels (hyperuriceamia) are most commonly associated with gout, increased breakdown of cell nuclei and renal disease. Increased uric acid levels are observed often also for leukemia, lymphoma or myeloma, where uric acid levels need to be monitored to avoid kidney damage.[19] Gout patients suffer from pains and inflammations caused by uric acid precipitation in joints. Kidney stone formation is also more likely due to elevated uric acid concentrations (above 0.60 mg/ml in serum and between 1.5 and 4.5 mmol/ml in urine). Elevated uric acid levels can also be linked to inappropriate diet and intoxications such as overconsumption of alcohol. Defects leading to decreased uric acid levels (hypouriceamia) are less common and are usually linked to AIDS, diabetes, mellitus and some malignant diseases. Thus, the need for quick and accurate measurement of uric acid concentration in biological liquids is obvious, so that appropriate treatment can be used.[20, 21]

3.3.1 Current assays for uric acid

Uric acid assays used currently for *in vitro* analysis of uric acid concentrations in samples of biological liquids are based on the action of the uricase enzyme. This enzyme transforms uric acid into a more water soluble product (allantoin) and produces hydrogen peroxide as a side product.[22, 23] Hydrogen peroxide is then the detected analyte. The detection can be done in several ways; oxidation of a phenolic dye to a strongly coloured compound or by the action of peroxidise enzyme, leading to the production of an intensively coloured chromogen or a strongly emissive fluorophore. These methods have, however, several drawbacks. Firstly, they suffer from ascorbate interference (leading to the need of co-administration of ascorbate oxidase) and bilirubin. A linear response for the clinically used kits is obtained for the concentration range from 0.12 to 6 mmol l^{-1} in urine and 0.09 to 1.8 mmol l^{-1} in

plasma and serum. Furthermore, the analysis requires at least 30 minutes of incubation and careful pH control.[24] Careful storage to avoid contamination, damage or denaturation is also needed, both for the enzymes and the dyes involved.

3.3.2 Ratiometric measurement using a Tb/Eu mixture

The fact that a europium complex of a given ligand is quenched to a lesser extent than its terbium analogue allows the use of quenching of lanthanide emission to measure urate concentration. In a mixture where both europium and terbium complexes of a common ligand are present, the urate concentration can be related to the ratio of the terbium and europium emission intensity, at selected wavelengths (e.g. 546/616 or 546/700). Thus, a ratiometric measurement of the desired variable is obtained.

Such a ratiometric measurement is very desirable, as the measured signal is solely a function of one variable; uric acid concentration in this case. Since in this system the two ligands are the same, differing only in the metal ion, all interferences will happen to both ligands to the same extent and will be eliminated, as the intensity ratio is measured. Such interferences include sample to sample variation of protein content, light scattering by particulates or differing surface adhesion. Interferences more specific for the given system, such as static quenching of the chromophore singlet excited state (e.g. by halides)[25], will be also eliminated, as they will happen to the same extent for each component.

3.3.3 Proof of concept experiments

Initial experiments have been carried out with complexes $\mathbf{[LnL^{26}]^{3-}}$. A 1:1 mixture of the corresponding terbium and europium complexes was prepared at pH 7.4 in 100 mM HEPES buffer. The absorbance was 0.1 at both 313 and 348 nm (approximately corresponds to 5 μM solution of each complex).

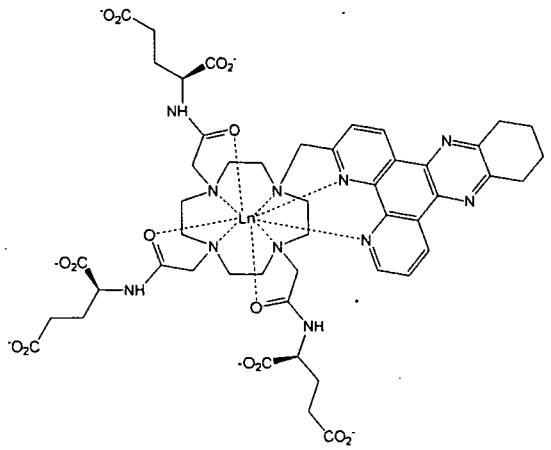

$[LnL^{26}]^{3-}$

Figure 3.7 – Structure of complex $[LnL^{26}]^{3-}$ used in proof of concept experiments for urate concentration determination

A 1 mM solution of uric acid was prepared (standardised with absorbance at 290 nm; $\varepsilon = 1.22*10^4\ M^{-1}\ cm^{-1}$) in 100 mM HEPES (pH 7.4). Triplicate measurements were carried out with uric acid concentrations ranging from 0 to 50 μM, to obtain a calibration curve. Urine samples from healthy volunteers were prepared as well in 100, 300 and 500 fold dilution and triplicate measurements were taken as well. Measurements were carried out using an Analytik Flash Scan plate reader, using 96 well plates. Ten spectra were recorded and averaged and 546/616 and 546/700 ratios were calculated and plotted against uric acid concentrations to obtain the calibration curve, which was tentatively fitted with biexponential decay. A high precision of this measurement was demonstrated by less than a 1% variation in the ratios measured for any given uric acid concentration. This high accuracy is inherent to ratiometric measurements.

Uric acid concentrations in the urine samples were easily calculated using the calibration curve. Parallel measurements were carried out using a commercial uric acid assay (Invitrogen, Amplex Red Uric Acid kit), which uses horseradish peroxidise, on these samples as well. The two methods gave uric acid concentrations, which were within 10% from each other. It should be noted that the enzyme kit precision is estimated to be no better than 10%.

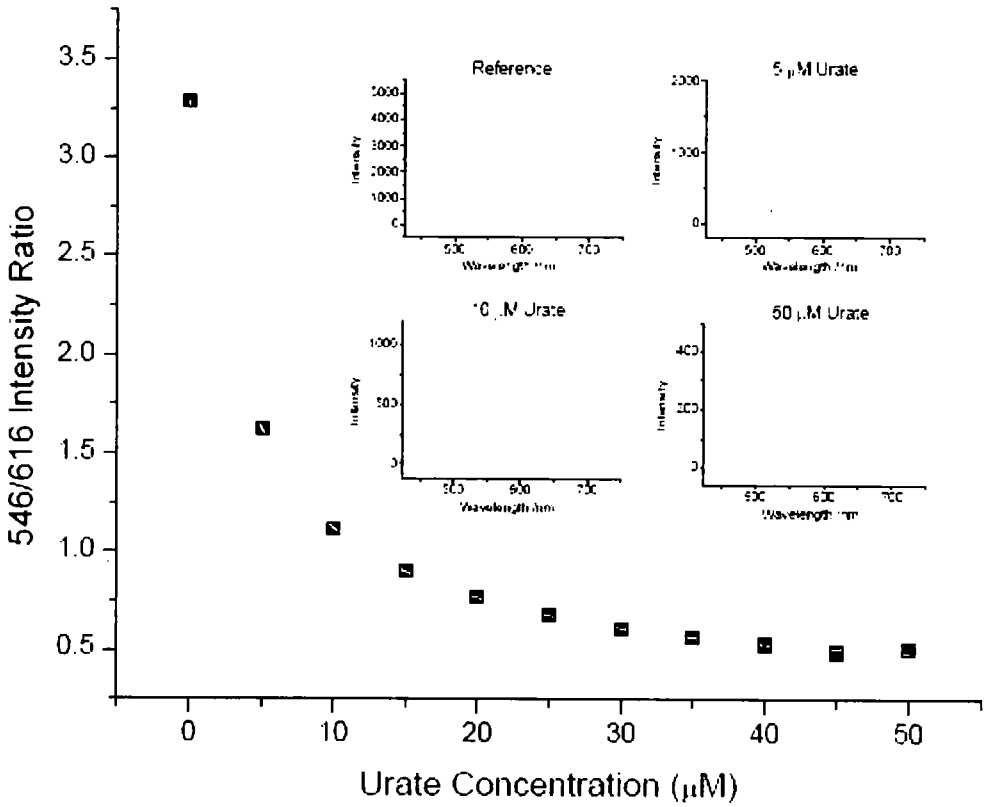

Figure 3.8 – Plot of varitation of the Tb (546 nm) and Eu (616 nm) emission intensity ration as a function of added urate (pH 7.4, 0.1 HEPES, 298 K)[18]

Thus, a ratiometric, nonezymatic assay for uric acid in urine and possibly other biological fluids, with accuracy at least comparable to current commercial assays, can be envisaged on the basis of these results.

3.4 Protein Effect

All of the complexes presented in the study contain a heterocyclic chromophore consisting of at least three fused aromatic rings. Such a structure can exhibit reversible binding with proteins, as has been recently observed by modulation of emission and relaxivity (Gd^{3+}) in protein titration measurements.[26] Serum albumins are one of the most abundant proteins in mammalian cells, and well known for binding aromatic guests. It was therefore considered fitting to study their effect on quenching susceptibility for selected luminescent complexes ($[TbL^{1}]^{3+}$, $[TbL^{24a}]^{3+}$, $[TbL^{24b}]^{3+}$ and $[TbL^{9}]$).

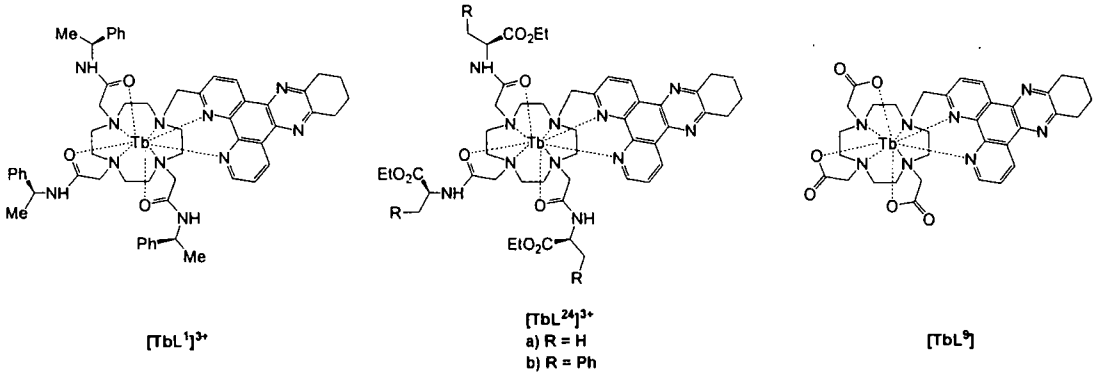

Figure 3.9 – Complexes used in the protein binding study

The addition of bovine serum albumin to each of the mentioned complexes led to a decrease in their emission intensities and lifetimes.

The lifetimes were also measured in a solution containing 0.4 mM of serum albumin and 0.1 mM of uric acid. The luminescence lifetimes obtained were 0.57, 0.38, 0.28 and 0.06 ms for $[TbL^{1}]^{3+}$, $[TbL^{24a}]^{3+}$, $[TbL^{24b}]^{3+}$ and $[TbL^{9}]$ respectively. This demonstrates that the DO3A complex $[TbL^{9}]$ is sensitive to quenching by urate in the presence of protein to a much higher degree than the other complexes. These results offer an explanation to the difficulties experienced in fluorescence microscopy experiments using this complex.

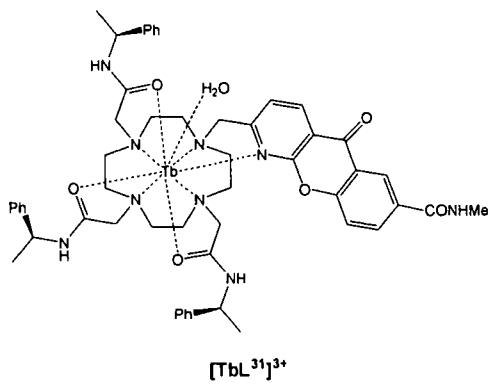

Figure 3.10 – Structure of methylamide complex $[TbL^{31}]^{3+}$

For azaxanthone complexes, such as $[TbL^{31}]^{3+}$, the luminescence lifetime was reduced only from 1.52 to 1.40 upon addition of protein, and the lack of sensitivity of the amide complexes to quenching by urate was mentioned earlier.

3.5 Conclusions

A large number of complexes have been studied in terms of their susceptibility to quenching by electron rich species such as iodide, ascorbate and urate. Empirical rules relating structure and this quenching sensitivity could, thus, be established. Further work has demonstrated a fundamental difference in the quenching by iodide, which proceeds by a purely collisional mechanism, and ascorbate and urate, which are postulated to involve formation of a relatively long lived exciplex.

It has been demonstrated that the difference in sensitivity to quenching displayed by analogous terbium and europium complexes can be used to measure concentrations of the quenching species (e.g. urate) even in biological samples (e.g. urine, plasma).

Literature

[1]) S. Pandya, J. Yu, D. Parker, *Dalton Transactions*, 2006, 2757.
[2]) J. C. G. Bünzli, C. Piguet, *Chemical Society Reviews*, 2005, **34**, 1048.
[3]) D. Parker, R. S. Dickins, H.Puschman, C. Crossland, J. A. K. Howard, *Chemical Reviews*, 2002, **102**, 1977.
[4]) R. A. Poole, G. Bobba, M. J. Cann, J. C. Frias, D. Parker, R. D. Peacock, *Organic and Biomolecular Chemistry*, 2005, **3**, 1013.
[5]) R. S. Dickins, D. Parker, A. S. de Sousa, J. A. G. Williams, *Chemical Communications*, 1996, 697
[6]) A. Beeby, I. M. Clarkson, R. S. Dickins, S. Faulkner, D. Parker, L. Royle, A. S. de Sousa, J. A. G. Williams, M. Woods, *Journal of the Chemical Society, Perkin Transactions 2*, 1999, 493.
[7]) K. Blomberg, P. Hurskainen, I. Hemmilä, *Clinical Chemistriy*, 1999, **45**, 855.
[8]) J. Yuan, G. Wang, *Trends in Analytical Chemistry*, 2006, **25**, 490.
[9]) F. Kielar, C. P. Montgomery, E. J. New, D. Parker, R. A. Poole, S. L. Richardson, P. A. Stenson, *Organic and Biomolecular Chemistry*, 2007, **5**, 2975.
[10]) A. Weller, *Pure and Applied Chemistry*, 1968, **16**, 115.
[11]) S. Steenken, P. Netta, *Journal of Physical Chemstry*, 1982, **86**, 3661.
[12]) M. G. Simic and S. V. Jovanovic, *Journal of the American Chemical Society*, 1989, **111**, 5778.
[13]) J. R. Lakovicz, *Principles of Fluorescence Spectroscopy Second Edittion*, Kluwer Academic/Plenum Publishers, New York, Boston, Dordrecht, London, Moscow, 1999.
[14]) D. Rehm, A. Weller, *Ber. Bunsen-Ges. Phys. Chem.*, 1969, **73**, 834.
[15]) D. Rehm, A. Weller, *Israel Journal of Chemistry*, 1970, **8**, 259.
[16]) M. G. Kuzim, *Pure and Applied Chemistry*, 1993, **65**, 1653.
[17]) M. Dossot, D. Brurget, X. Allonas, P. Jacques, *New Journal of Chemistry*, 2001, **25**, 194.
[18]) R. A. Poole, F. Kielar, S. L. Richardson. P. A. Stenson, D. Parker, *Chemical Communications*, 2006, 4084.
[19]) M. L. Bishop, J. L. Duben-Engelkirk, E. P. Fody, *Clinical Chemistry 2nd Edition*, 1992, J.B. Lippincott, Philadelphia.
[20]) B. N. Ames, *Science*, 1983, **221**, 1256.
[21]) N.Gochman, J. M. Schmitz, *Clinical Chemistry*, 1971, **17**, 1154.
[22]) P. Kabasakalian, S. Kalliney, A. Wescott, *Clinical Chemistry*, 1993, **19**, 522.
[23]) P. H. Duncan, N. Grochman, T. Cooper. E. Smith, D. Bayse, *Clinical Chemistry*, 1982, **28**, 284.
[24]) V. Towne, M. Will, B. Oswald, Q Zhao, *Analytical Biochemistry*, 2004, **334**, 290.
[25]) D. Parker, P. K. Senanayake, J. A. G. Williams, *Journal of the Chemical Society, Perkin Transactions 2.*, 1998, 2129.
[26]) J. Yu, D. Parker, R. Pal, R. A. Poole, M. J. Cann, *Journal of the American Chemical Society*, 2006, **128**, 2294.

CHAPTER 4

Conjugation Experiments and Cellular uptake studies

4 Conjugation Experiments and Cellular uptake studies

Considerable progress has been made in the field of highly emissive and well defined lanthanide (III) complexes over the past decade. These complexes have found use in several assays and sensors, often employing time resolved methods. They can provide information in their spectral profile, luminescence lifetime or circular polarisation. In particular, their long luminescence lifetimes make them very attractive for applications in cellular imaging, where time gating can significantly reduce the signal to noise ratio. Thus, it comes as no surprise that lanthanide complexes capable of traversing the cellular membrane have been developed and observed in fluorescence microscopy experiments. A mechanistic understanding of the uptake and subsequent fate of these complexes in cells needs to be developed.[1, 2, 3]

Differential localisation profiles within cellular compartments for a range of Eu and Tb complexes have been established. However, the key structural elements that determine the predominant localisation profile have not yet been established unequivocally.

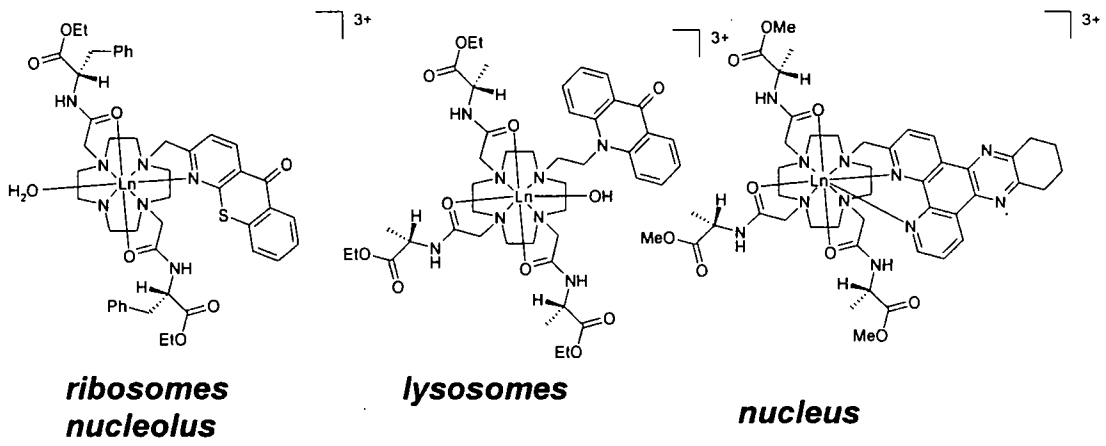

Figure 4.1 – Different cellular localisation profiles for selected emissive lanthanide complexes[4, 5, 6]

A more versatile approach in the development of complexes with defined localisation profiles, could involve an emissive complex, which can be conjugated to different localisation moieties (vectors). Thus, the localisation profile would be determined primarily by the nature of the attached vector.

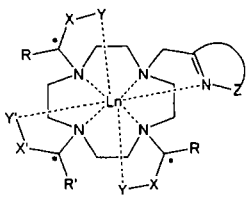

Figure 4.2 – General structure of emissive lanthanide complex based on cyclen, incorporating three pendant arms and a heterocyclic chomophore

Considering cyclen based complexes, represented by the generalised structure in **Figure 4.2**, incorporating three pendant arms and a heterocyclic sensitiser, two general points of attachment can be envisaged. The linking group could either be incorporated into the heterocyclic chromophore structure or via one of the pendant arms. The position *trans* to the chromophore is the most likely one to be chosen for the linking arm, due to synthetic considerations. Such an approach has been employed previously (**Figure 4.3**), and is being further developed as a part of current work in Durham.

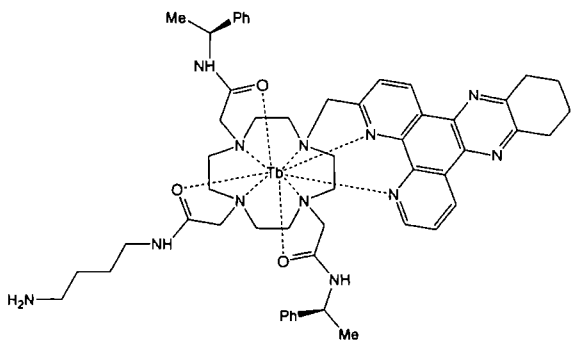

$[TbL^{32}]^{3+}$

Figure 4.3 – Structure of a complex bearing a free amino group in the pendant arm as an attachment point for protein conjugation using isothiocyanate methodology[7]

Incorporating the linking group into the chromophore structure, even if complicating chromophore synthesis, will be advantageous in later synthetic steps, as the N-linked donor groups can be the same, which removes protection and deprotection steps needed for introduction of different pendant arms. Also, in the case where conjugation of a responsive system would be desired, linking through the chromophore could be beneficial. This is due to the fact that the pendant arms defining the coordination sphere of the metal need to be engineered and introduced solely with the aim to tune the properties of the complex for the given responsive function. This is more difficult if one of them is to be used as a linking point.

4.1 Conjugation using a linking group incorporated into the chromophore structure

The synthesis of three chomophores containing a carboxylic acid/ester group, which can be utilised as a linking point in conjugation work, has been described in chapter 2 (**Figure 4.4**).

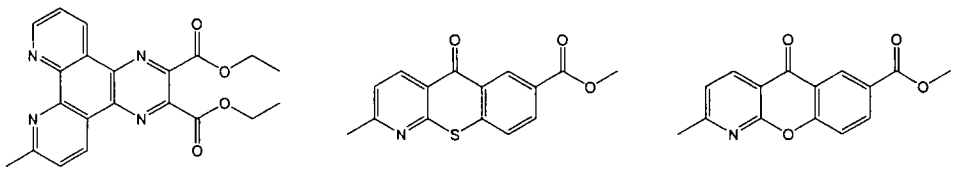

12 30 41

Figure 4.4 – Structures of three chromophores bearing carboxylic ester groups which can be utilised for conjugation via amide bond formation

Each of the chromophores has advantages and disadvantages. The tetraazatriphenylene, **12**, gives rise to highly emissive complexes with excitation at 348 nm, but its synthesis is moderately difficult with rather low overall yields. The azaxanthone, **41**, and azathioxanthone, **30**, chrompohores are obtained more readily. Moreover, complexes bearing the azathioxanthone chromophore, **30**, can be excited at 370 nm. The excitation wavelength for azaxanthone complexes is at 336 nm, but the peak tails well above the 340 nm needed for practicable use in fluorescence imaging. The high amount of chromophore fluorescence (φ_{fl} up to 50% in water),

low quantum yields of lanthanide luminescence and oxygen sensitivity for terbium complexes limit the uses of the azathioxanthone chromophore, **30**. The azaxanthone chromophore gives complexes with quite good quantum yields (φ_{H2O}^{Tb} = 20-40 %) and so was chosen as the chromophore of choice for the conjugation work. It should be noted that first attempts of conjugation experiments were carried out on complexes with the azathioxanthone chromophore.

Several different types of pendant arms have been incorporated into the ligand used in the luminescent lanthanide complexes. The three major types of pendant arms used are the carboxylate arm, the amide pendant arm and the phosphinate pendant arm.

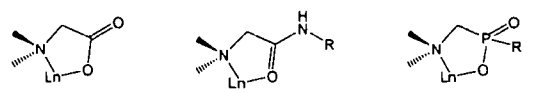

Figure 4.5 – Structures of the most commonly used chelating groups in emissive lanthanide complexes

Some of the lanthanide complexes bearing only carboxylate pendant arms have not been observed in cells in fluorescence microscopy experiments. This is believed to be due to their high susceptibility to quenching by species such as urate or axorbate and their low protein binding affinity (Chapter 3). Complexes incorporating amide arms have been established as being observable in fluorescence microscopy. Their simple and versatile synthesis, allowing the variation of the group R, is also beneficial. Phosphinate pendant arms give rise to very emissive complexes, especially for lipophilic R groups, such as benzyl. Their more difficult synthesis and low water solubility are their drawbacks, even though preliminary experiments indicated that these complexes are observable in fluorescence microscopy experiments. The amide arm using the *S*-1-phenylethyl amine was chosen for intial coupling studies, as complexes of this pendant arm have been well studied in cellular experiments and comparisons to complexes bearing different chromophores could be made.

4.1.1 HPLC methods for monitoring and purification

As has been noted before, lanthanide (III) ions are paramagnetic, which has implications for NMR measurement. Routine use of NMR in the same way as for organic compounds and complexes of other metals is more difficult, even though relatively sharp ^{1}H NMR spectra can be obtained for complexes of certain lanthanides (e.g. Eu^{3+} or Yb^{3+}). Also, reaction monitoring methods used in organic chemistry, such as thin layer chromatography, usually cannot be used due to the charged nature of the complexes. Reversed phase HPLC, however, is ideally suited to monitor the progress of reactions of the complexes that will be described in the following sections. Due to the highly polar nature and the milligram quantities used, reversed phase chromatography was also the method of choice for purification in many instances. The chromatographic gradients used in this work are described in Appendix 1 and a selection of representative chromatograms is presented in Appendix 2.

4.1.2 Development of conjugation methodology

The synthesis of complexes incorporating azaxanthone or azathioxanthone chromophores with (methoxy)carbonyl substitution was described in chapter two ($[\mathbf{LnL^7}]^{3+}$ and $[\mathbf{LnL^8}]^{3+}$).

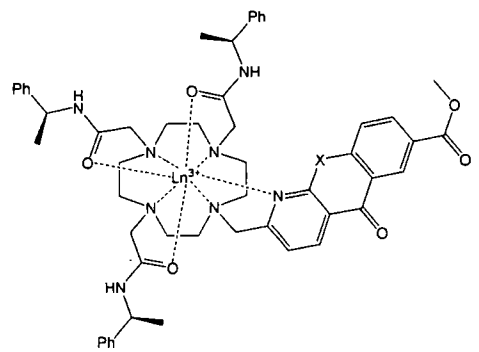

X = S; $[LnL^7]^{3+}$; Ln = Eu
X = O; $[LnL^8]^{3+}$; Ln = Eu, Gd, Tb

Figure 4.6 – Generalised structure of amide arm complexes prepared as a starting point for conjugation experiments

Even though the methyl ester can, in theory, react with primary amines to form an amide bond, such a reaction usually needs rather forcing conditions and a large excess of amine, which can lead to metal decomplexation. A different route needs to be employed, providing a more active derivative of the carboxylic function towards nucleophilic attack. Hence, the methyl ester was converted to the carboxylic acid by mild base hydrolysis (KOH, pH 10, H_2O/MeOH, 298 K).

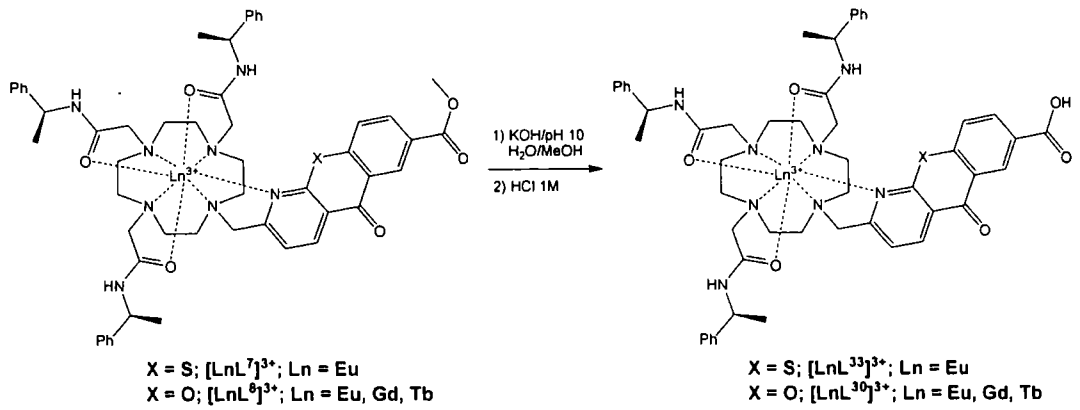

Scheme 4.1 – Mild base hydrolysis of chromophore ester group (Appendix 2, Chromatograms 6.2.1 and 6.2.2)

Amide bond formation is a well studied problem and a wide range of methods for carboxylic acid activation has been developed. Initial attempts to activate the carboxylic acid in the azathioxanthone complex $[\mathbf{EuL^{33}}]^{3+}$, were carried out with PL-IIDQ resin, which activates the carboxylic acid by the formation of a mixed anhydride, in a manner similar to the use of chloroformates.

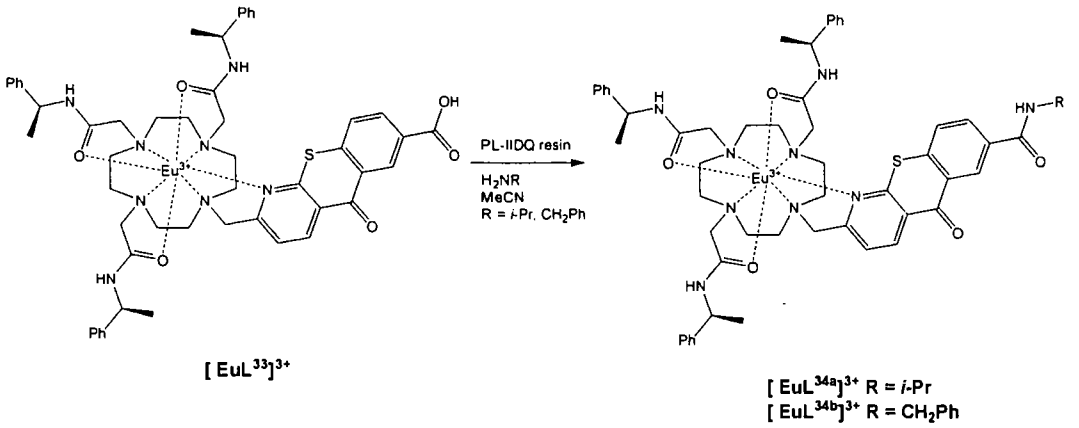

Scheme 4.2 – Attempt of amide bond formation using heterogeneous catalyst (PL-IIDQ resin)

This attempt was, however, unsuccessful. Isobutyl chloroformate was used in the next attempt, carried out in single phase, to determine whether the mixed anhydride methodology is feasible.

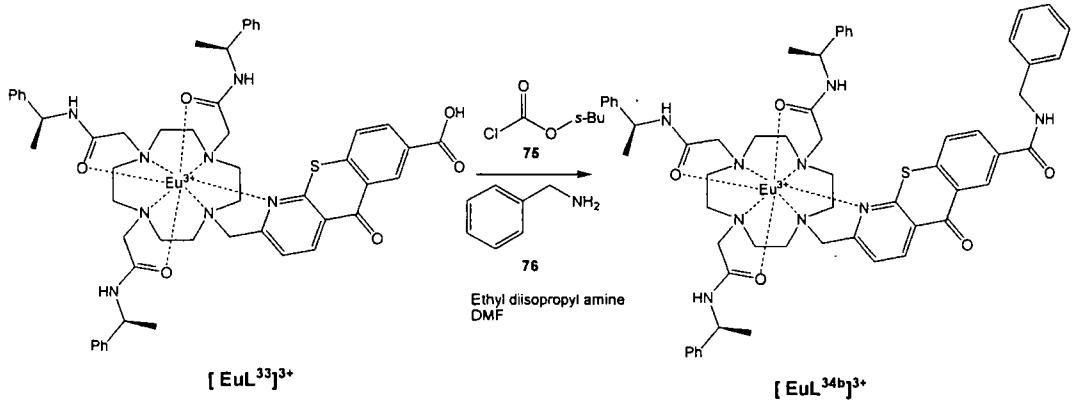

Scheme 4.3 – Attempt of amide bond formation using mixed anhydride activation

Initial positive results were however not reproducible and new methods using more modern activation strategies were employed subsequently. A single step EDC/HOBt catalysed amide forming reaction was tried out in the next attempt.

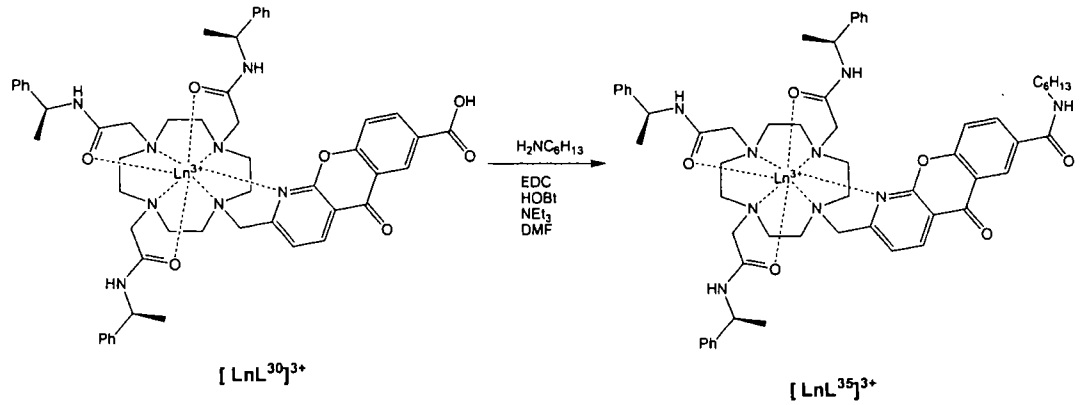

Scheme 4.4 – Amide bond formation using EDC and HOBt catalysis

Reproducible results were obtained using this methodology. Excess EDC and HOBT had to be used to achieve modest conversions (50%) and significant side product formation was observed. Further methods were therefore tested to obtain a more practicable conjugation route. A two step sequence was chosen, involving the formation and isolation of the intermediate N-hydroxysuccinimidyl (NHS) active ester.

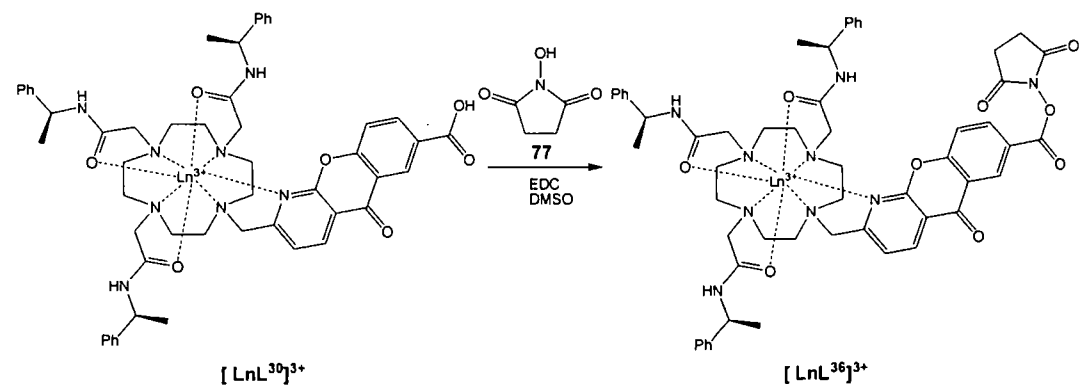

Scheme 4.5 – Formation of the N-hydroxysuccinimdyl activated ester (Appendix 2, chromatogram 6.2.3)

The active ester complex, $[\mathbf{LnL^{36}}]^{3+}$, was isolated, purified and stored in the dark at low temperature (-18°C).

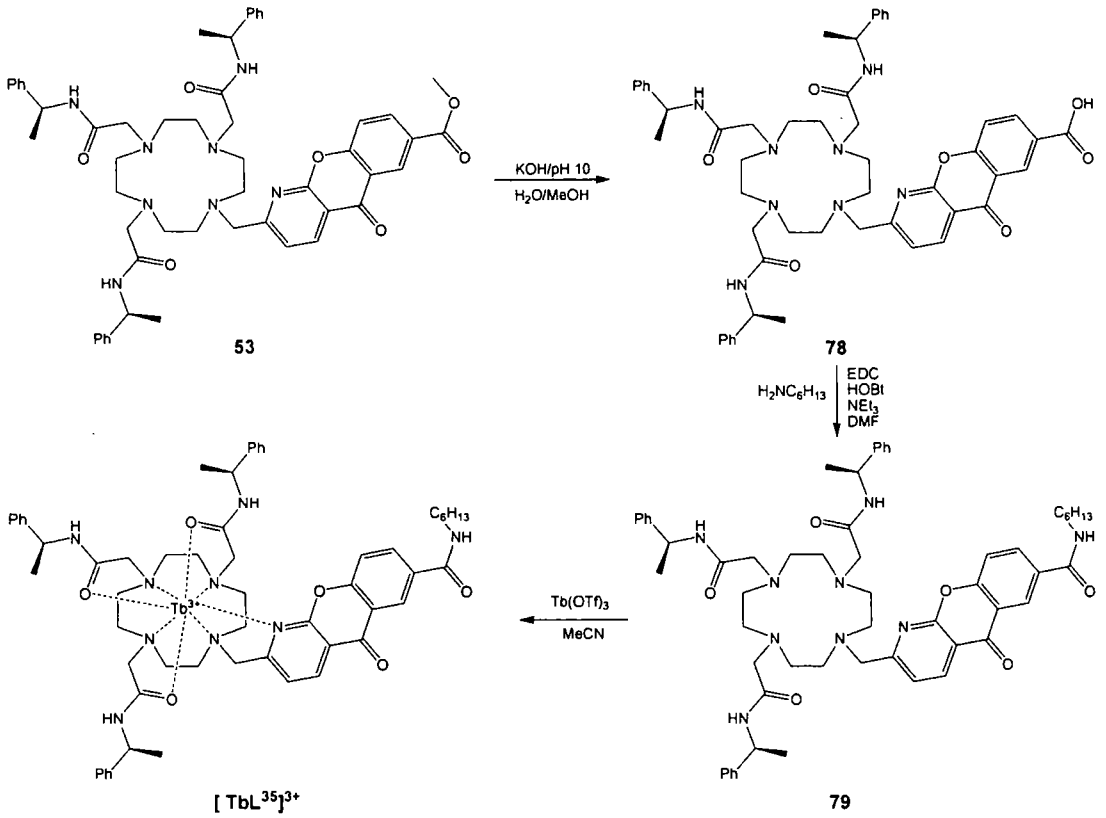

Scheme 4.6 – Alternative reaction scheme with amide bond formation at the ligand stage

An alternative approach, where the coupling was attempted on the ligand, was tried out as well. This route, gave results establishing its feasibility, but was not used as it is more suitable to have the conjugation step after complexation as this leads to a smaller number of reactions. Also, the possibility to store the active ester complexes $[\mathbf{LnL^{36}}]^{3+}$ makes that route very pragmatic.

4.1.3 Synthesis of simple amide derivatives

Having identified the NHS active ester complex, $[\mathbf{LnL^{36}}]^{3+}$, as a key intermediate for the conjugation experiments, its versatility in reactions with different amines needed to be established. Three primary amines of differing alkyl chain length (methyl, hexyl and dodecyl), were chosen for initial 'proof of concept' experiments. The other motive for choosing these amines was the desire to investigate whether this structural change would result in different behaviour in cellular experiments.

The reaction of the active ester complex, $[\mathbf{LnL^{36}}]^{3+}$, with the amines in dry DMF is fast and proceeds cleanly. Complete conversion was observed by reverse phase HPLC for samples of the reaction mixture taken for analysis 30 minutes after reaction initiation.

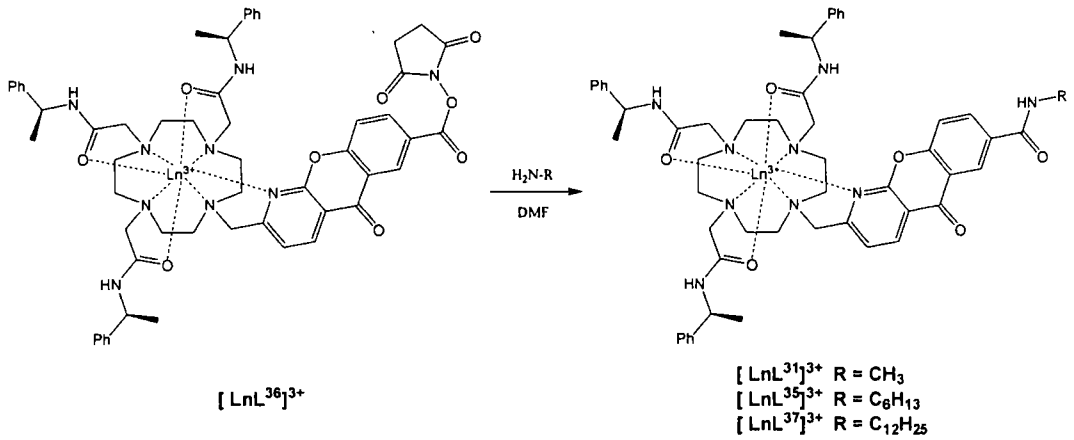

Scheme 4.7 – Reaction of the active ester complex with primary amines (Appendix 2, chromatograms 6.2.4-6.2.6)

The amide complexes were purified by precipitation onto Et_2O, followed by preparative reverse phase HPLC. These experiments were carried out with Tb^{3+} complexes only, with the exception of the hexylamide example.

The amide complexes remained strongly emissive and the luminescence lifetimes in H_2O were in the expected range 1.5 – 1.7 ms.

4.1.4 Conjugation to oligoarginine peptide sequences

It is known that peptide sequences with a high content of positively charged residues such as arginines, aid the translocation of various compounds across the cellular membrane.[8, 9] Two simple peptides were therefore selected for conjugation to the active ester complex, $[\mathbf{LnL^{36}}]^{3+}$, (H-Arg_7-OH and H-LysArg_7-OH). The H-Lys-Arg_7-OH sequence was chosen as its primary amine group was expected to be more reactive in the conjugation reaction than the terminal α-amino group of arginine in the other peptide or, indeed, its own α-amino group.

The peptides were supplied as their hydrochloride salts and therefore a base needed to be used in the coupling reactions to deprotonate the ammonium groups. No reaction was observed in initial experiments using dry DMF as a solvent and diisopropyl-ethylamine or 4-dimethylamino pyridine, even with elevated reaction temperature (40°C). This problem occurred with each peptide.

Formation of product was observed when carrying out the reaction in H_2O buffered with 0.1 M HEPES to pH 7.4. The hydrolysis of the active ester was observed as a competing reaction and an excess of complex $[\mathbf{LnL}^{36}]^{3+}$ had to be used. The conjugates were purified using HPLC separation.

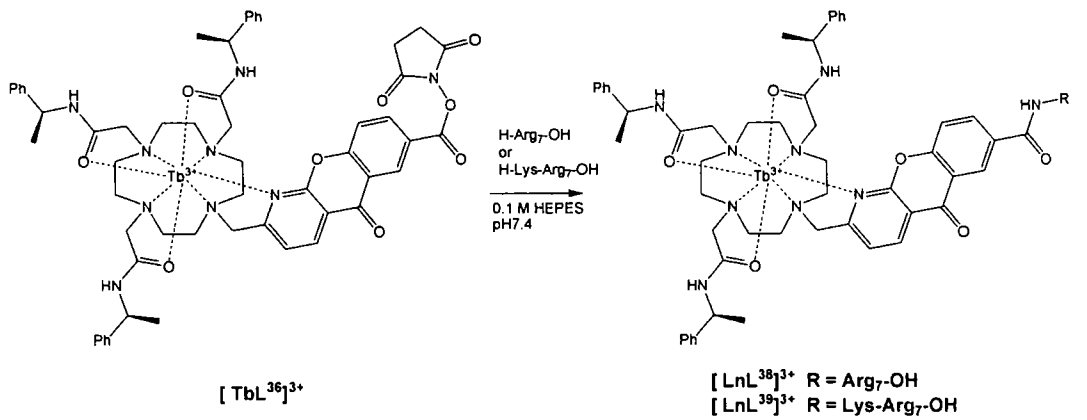

Scheme 4.8 – Conjugation of oligopeptide sequences (Appendix 2, chromatograms 6.2.7 and 6.2.8)

The luminescence properties showed that the lifetime remained virtually unchanged in comparison to other derivatives, but a decrease in the overall luminescence quantum yield was apparent and will be discussed in section 4.

4.1.5 Conjugate with a 'non-peptidic' oligoguanidinium vector

As has been mentioned in the introduction (p. 34), the oligoguanidinium vector, synthetised by de-Mendoza and conjugated to fluorescein, resulted in mitochondrial localisation of the conjugate. The vector was obtained as a kind gift from the group of de-Mendoza as a part of a collaboration. The coupling reaction was carried out in

DMF. The purification was achieved by precipitation of the reaction mixture onto Et_2O and by HPLC separation.

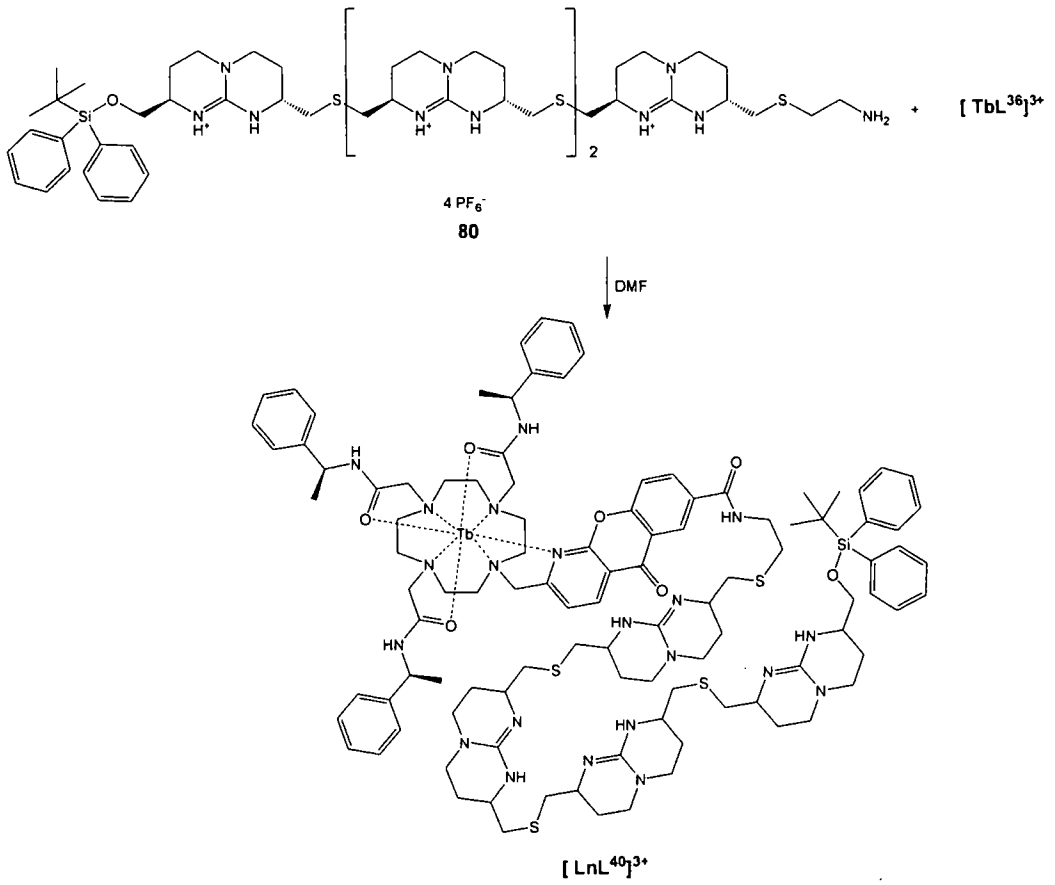

Scheme 4.9 – Synthesis of the oligoguanidinium conjugate (Appendix 2, chromatograms 6.2.9 and 6.2.10)

Reduced luminescence quantum yield, but unchanged luminescence lifetime was observed in this case as was the case for the oligoarginine peptide conjugates.

4.1.6 Conjugation to PAMAM dendrimer

In their earlier work, Lukes *et. al.* have observed enhanced relaxivities for Gd^{3+} complexes conjugated to a PAMAM dendrimer. [10] The functionality of these conjugates can be enhanced by incorporating labels of different types, such as a fluorophore. Thus, a dual imaging (MRI/Optical) probe could be obtained. The

synthesis of a conjugate containing emissive lanthanide complex and Gd^{3+} complex was planned as a joint project between Durham and the Prague goup.

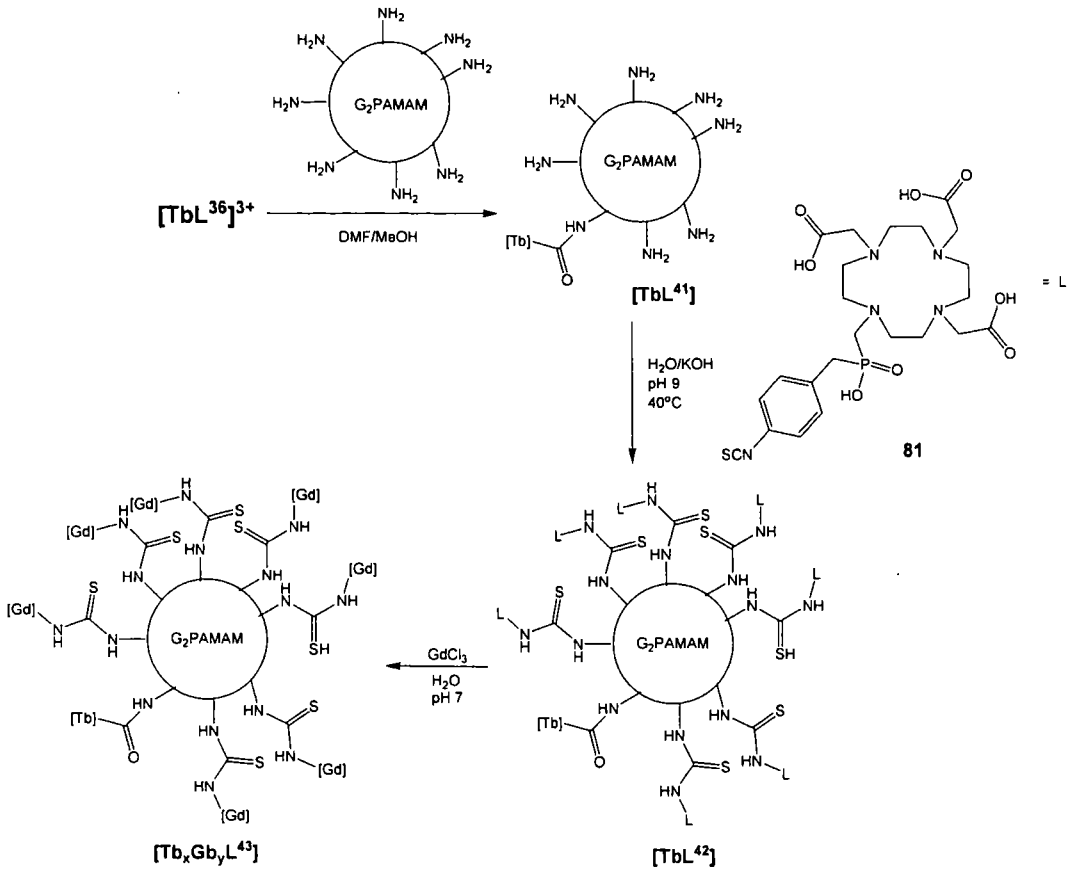

Scheme 4.10 – Synthesis of the Tb/Gd dendrimer conjugate

The coupling of the active ester complex $[\mathbf{TbL^{36}}]^{3+}$ with a G_2-PAMAM dendrimer (16 terminal amino groups) was carried out in DMF/MeOH. The only control used for the number of complexes loaded per dendrimer was the stoichiometry of the two reactants, with the aim of gaining an average loading of 1-2 complexes per dendrimer. The purification of the conjugate was carried out by dialysis using benzoylated cellulose tubing (cut off 1200 g/mol, Appendix 2 chromatograms 6.2.11-6.2.14).

Further steps of the synthesis were carried out in Prague in the group of Professor Lukes. The remaining (14-15) amino groups of the conjugate $[\mathbf{TbL^{42}}]$ were coupled with an excess of the isothiocyanate ligand **81**. The reaction mixture was purified by

ultrafiltration on YM3 membrane with the cut off at 3000 g/mol. The synthesis was accomplished by complexation of the conjugated ligand moieties with $GdCl_3$ and the reaction mixture was again ultrafiltered on the YM3 membrane to obtain the conjugate complex **[$Tb_xGd_yL^{43}$]**.

The emission spectrum of the final conjugate shows Tb emission overlaying significant organic fluorescence. The lifetime of the terbium emission in H_2O is 1.77 ms. This indicates that the Tb^{3+} cation remains in the well defined coordination sphere of the ligand , $\mathbf{L^{36}}$.

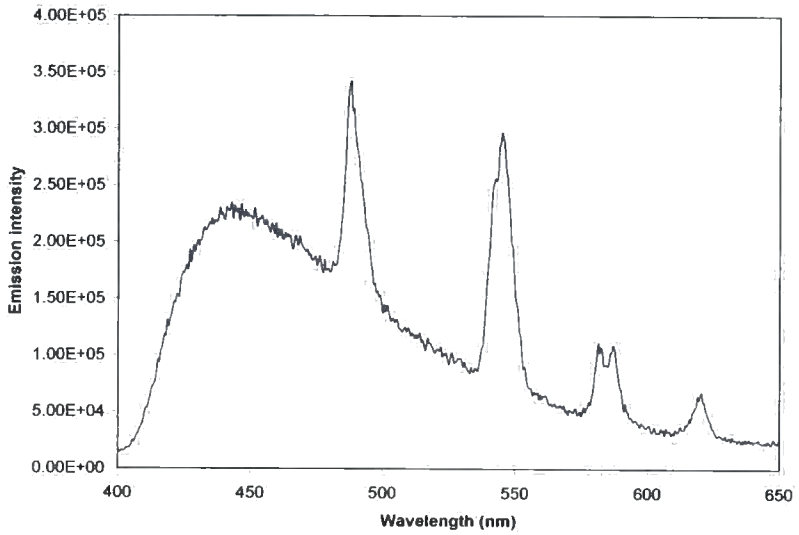

Figure 4.7 – Emission spectrum of [$Tb_xGd_yL^{43}$]

The ICP-MS measurement, however, showed the Tb:Gd ratio to be 1:50 instead of the expected 1:15. This is most likely due to loss of Tb^{3+} during the conjugation and complexation reactions in the steps following conjugation of complex **[TbL^{36}]$^{3+}$**. Even though this shows the need to optimise the synthetic route in any future work, the remaining data prove that the synthesis of a dual imaging probe is possible using this strategy.

4.1.7 Conjugation of a quencher molecule

Catechol molecules are effective quenchers of the lanthanide excited state, as has been mentioned in Chapter 3. The 3,4-methylenedioxy-benzylamine has been used in current project in Durham. The aim of this work is the synthesis of complexes containing covalently linked quenchers, such as complexes $[LnL^{44}]^+$, as potential probes for reactive oxygen species. In this case, the quencher is integrated into the pendant arm.

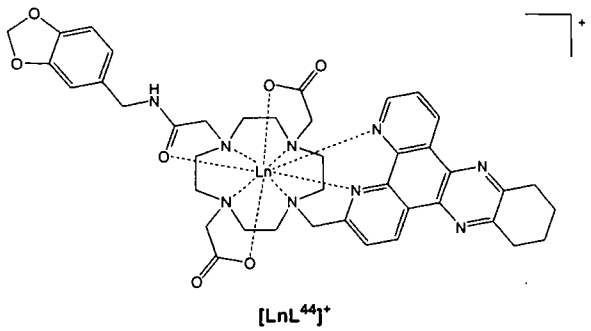

Figure 4.8 – Complex containing a covalently linked quencher molecule

A significantly decreased luminescence lifetime and emission quantum yield was observed for the terbium complex, consistent with intramolecular quenching of the Tb excited state by the electron-rich aromatic moiety.[11]

Thus, it was of interest to prepare the conjugate of complexes $[LnL^{36}]^{3+}$, incorporating a 3,4-methylenedioxy benzylamine moiety, to investigate the effect on lanthanide luminescence.

The coupling reaction was carried out in dry DMF and the reaction mixture was purified by precipitation from diethyl ether followed by HPLC separation.

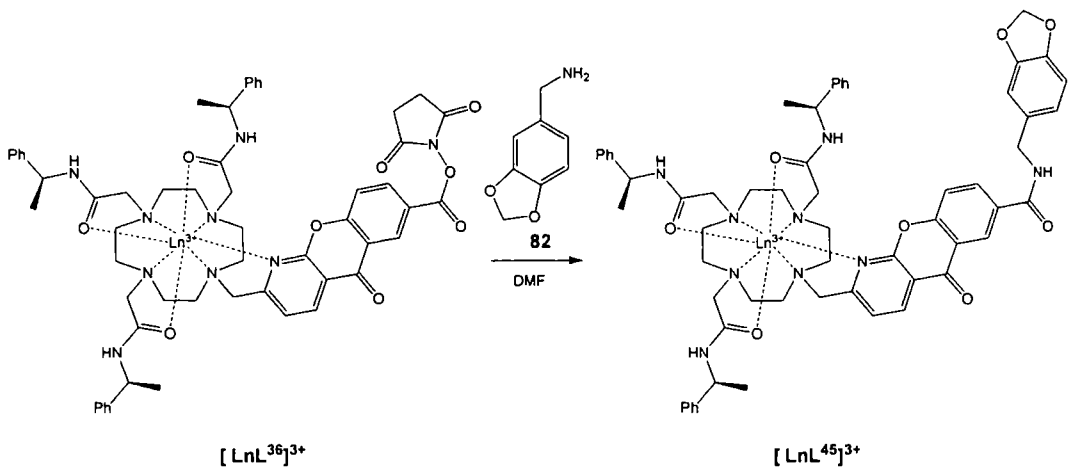

Scheme 4.11 – Conjugation of 3,4-methylenedioxybenzyl amine (Appendix 2, chromatogram 6.2.15; chromatography Method D)

The luminescence lifetime (1.38 ms) was decreased for the Tb^{3+} complex, compared to analogous amide derivatives described (ca. 1.6 ms), but not as significantly as expected. There was no significant change to the lifetime of the Eu^{3+} complex. Both complexes have, however, a significantly reduced overall quantum yield, in a similar way to the conjugates with the peptide and oligoguanidinium vector.

4.1.8 Cholesterol conjugate

Cholesterol is an important component of biological membranes and several fluorescently labelled derivatives have been used to study its partitioning in cellular media.[12] Thus, attempting to synthesise a conjugate with, a suitably derivatised cholesterol moiety was identified as an interesting target.

The only possibility for straightforward conjugation offered by the cholesterol molecule is its hydroxyl group. A direct conjugation to form a cholesteryl ester is possible, but a small spacer (4-aminobutanoic acid) was chosen, as the amino group is more reactive with the NHS ester of $[\mathbf{LnL^{36}}]^{3+}$.

The synthesis was carried out in three steps starting with a coupling of cholesterol, **83**, and Boc protected 4-aminobutanoic acid, **84**. EDC and HOBt were used as the

activating reagents in dry MeCN and $CHCl_3$. The product, **85**, was crystallised from a $CHCl_3$/MeOH mixture.

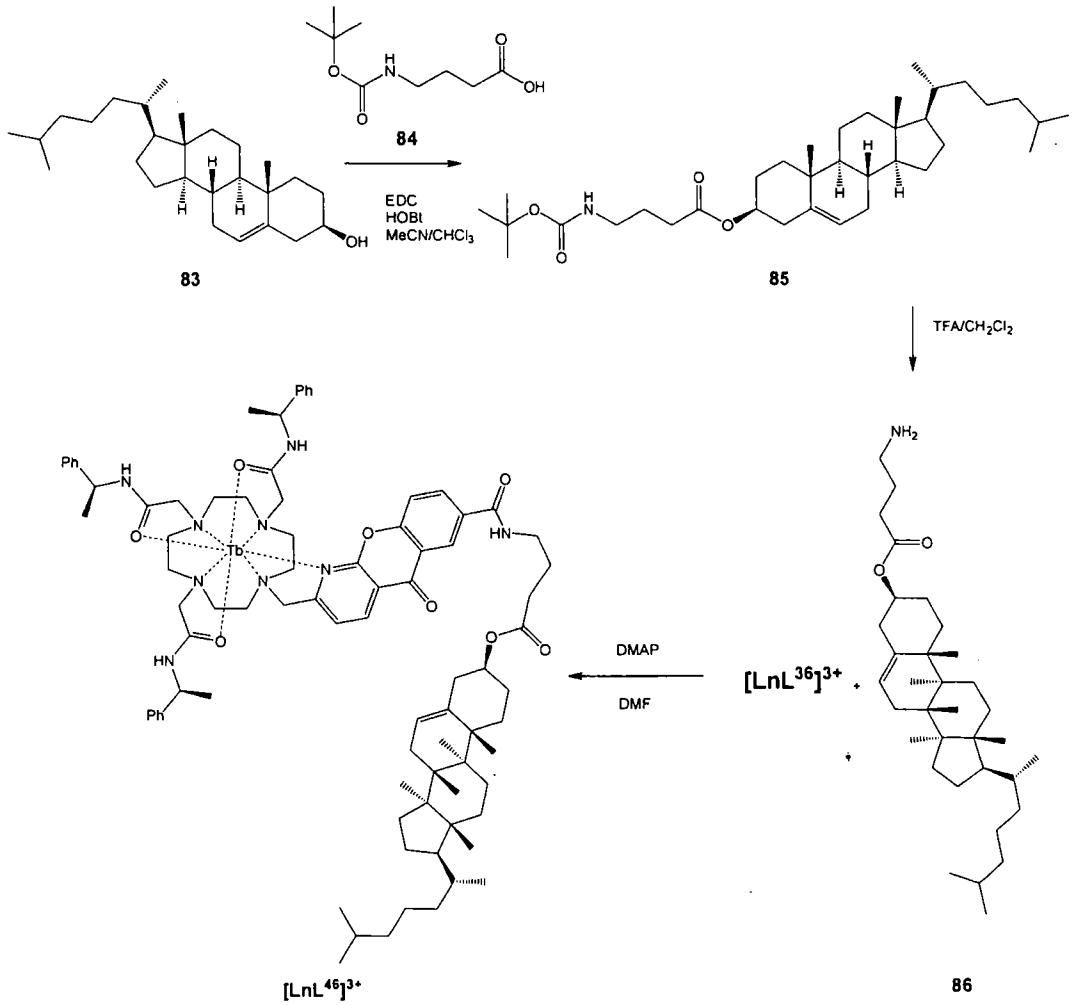

Scheme 4.12 – Synthesis of a cholesterol conjugate (Appendix 2, chromatograms 6.2.16 and 6.2.17)

The structure of the cholesteryl ester **85** was established by partial assignment of its ^1H and ^{13}C NMR spectra, in comparison to that of cholesterol, **87**, itself and using the literature assignments of cholesterol ^1H and ^{13}C NMR spectra.[13] The spectra are displayed in Appendix 3 and a partial assignment is shown in **Figure 4.9**. The most diagnostic change of the shift of the proton in position 3 on the cholesterol structure, which moves from 3.53 ppm in cholesterol, **87**, to 4.62 ppm in the cholesteryl ester **85**. This is the expected change of a ^1H NMR shift for protons on an α-carbon of an aliphatic alcohol, being transformed into the corresponding carboxylic acid ester.

Further evidence for the formation of ester **85** is the 2:1 peak integral ratio of the signal at 3.15 ppm, corresponding to the protons on carbon 4 of the butanoate chain, and the signal at 5.36 ppm, corresponding to the double bond proton of the cholesterol structure. It is expected that the remaining part of the cholesterol structure will not be affected by this transformation; hence, no benefit was seen in completing the assignment of the ^{1}H and ^{13}C NMR spectra.

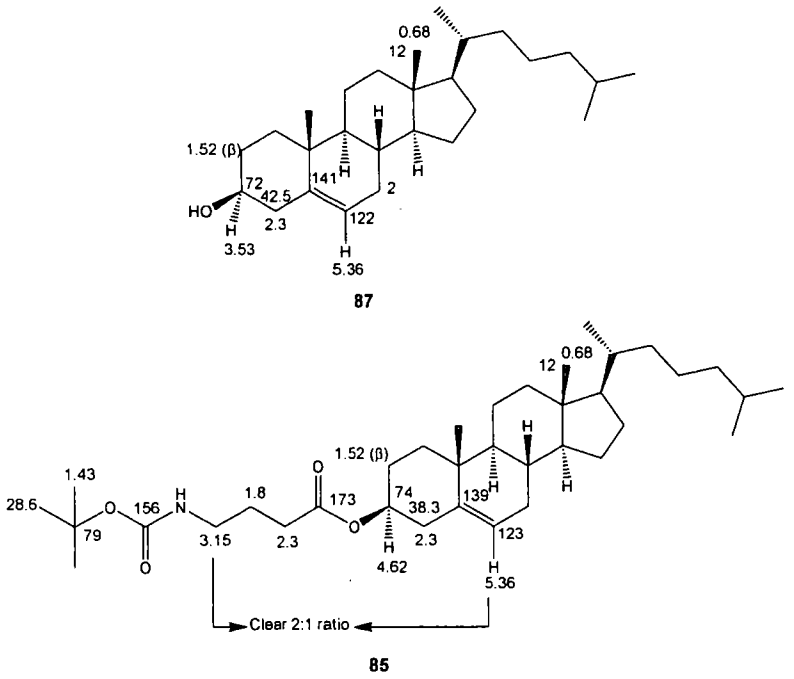

Figure 4.9 – Partial assignment of ^{1}H and ^{13}C resonances for cholesterol, 87, and the cholesteryl ester, 85

The Boc group was removed by TFA in CH_2Cl_2 and the deprotected cholesterol derivative **86** was coupled with the active ester complex $[TbL^{36}]^{3+}$. The reaction was carried out in dry DMF using 4-dimethylaminopyridine as a nucleophilic catalyst for the coupling with cholesterol derivative **86**, which was not neutralised in the work up, as a danger of lactam ring formation was anticipated. The product was purified by precipitation onto diethyl ether and HLPC separation.

The luminescence properties did not change in any significant way, compared to other derivatives, and the emission lifetime, τ_{Tb}, in H_2O was 1.42 ms.

4.1.9 Coupling to Human Serum Albumin

Conjugation of the terbium complex to Human Serum Albumin (HSA) was also carried out. The interest was both in proving the possibility to couple the active ester complexes directly to macromolecules such as proteins, as well as to create a covalently linked HSA conjugate, allowing a comparison of its properties to results obtained in experiments exploring the noncovalent interactions of luminescent lanthanide complexes with HSA.

The reaction was carried out in water over 24 h and the reaction mixture was purified by dialysis on cellulose tubing with a cut off of 8000 g/mol. The isolated conjugate maintained a Tb^{3+} luminescence lifetime of 1.63 ms in water.

4.1.10 Comparison of emission spectra of complexes containing different carboxylic acid derivatives in the chromophore structure

The detailed structure of lanthanide emission spectra, especially for Eu^{3+}, is dependent on the primary coordination sphere of the metal and can be very informative.[14] Differential changes in the intensities and structures of the bands can be used for ratiometric measurements. It was therefore of interest to compare the emission spectra of the methyl ester, $[\mathbf{EuL^{8}}]^{3+}$, carboxylic acid, $[\mathbf{EuL^{30}}]^{3+}$, and the hexylamide, $[\mathbf{EuL^{35}}]^{3+}$ complexes. Significant changes in the spectral form could be utilised in a design of a ratiometric determination of interconversion of these functional derivatives of carboxylic acid (e.g. to track enzymatic kinetics).

As can be seen from **Figure 4.10** there is an overall emission intensity decrease for the amide, $[\mathbf{EuL^{35}}]^{3+}$, and carboxylic acid, $[\mathbf{EuL^{30}}]^{3+}$, complexes when compared to the methyl ester complex, $[\mathbf{EuL^{8}}]^{3+}$.

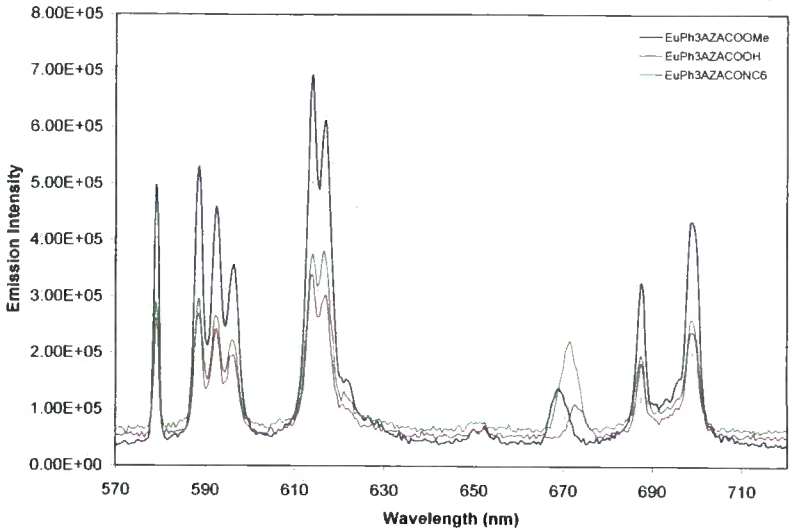

Figure 4.10 – Europium emission spectra for different functional derivatives of the chromophore carboxylic acid functional group (H_2O, 295 K)

No significant change in the form of the spectra can be detected. Thus, these functional group conversions cannot be detected by ratiometric changes in Eu^{3+} emission.

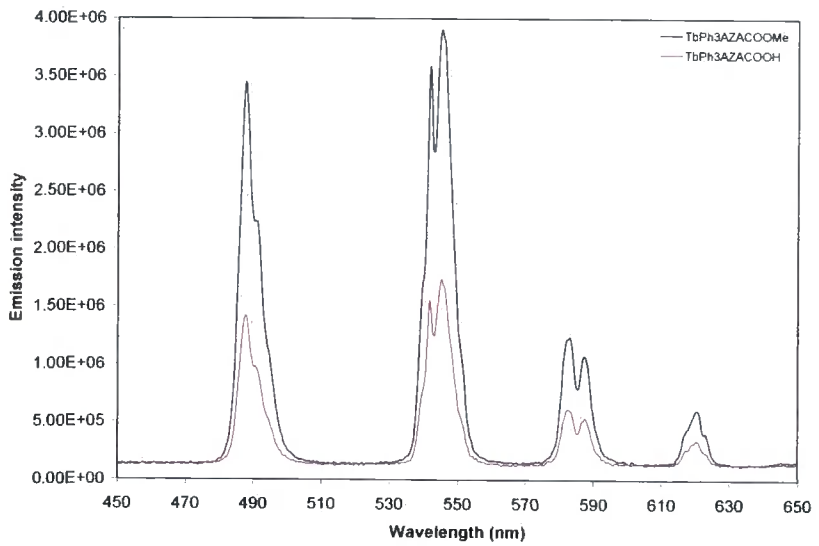

Figure 4.11 – Comparison of emission spectra for $[TbL^8]^{3+}$ and $[TbL^{30}]^{3+}$ (H_2O, 295 K)

Another possibility for ratiometric measurement could be based on differential changes in the Tb and Eu spectra with respect to a given variable, as has been demonstrated in the experiments for uric acid concentration measurement. Inspection

of **Figure 4.11** however shows that the change in the emission intensity is the same for the Tb^{3+} complexes as for the Eu^{3+} ones.

It had been noted during the synthetic work on these complexes that the emission intensity of the carboxylic acid complexes $[LnL^{30}]^{3+}$ was pH dependent

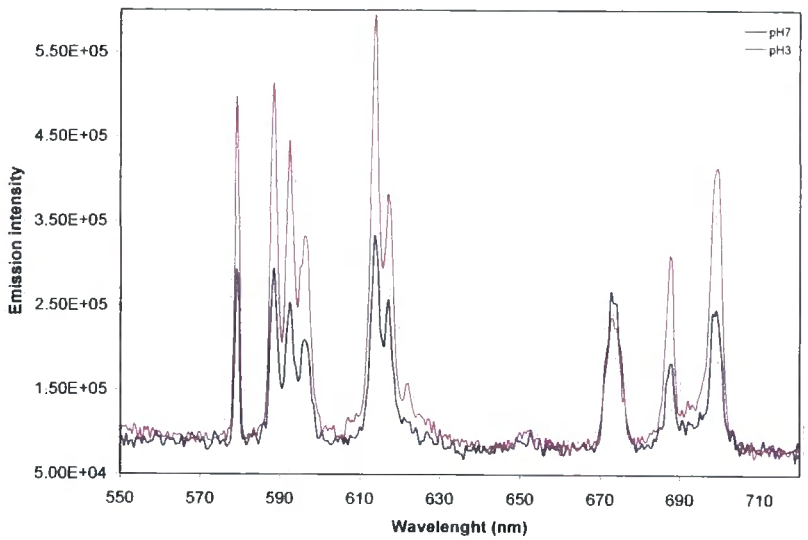

Figure 4.12 – Emission spectra of $[EuL^{30}]^{3+}$ at different pH (H_2O, 295 K)

This pH sensitivity is linked to the protonation equilibrium of the carboxylic acid group of the chromophore and as can be seen (**Fig. 4.12**) it does not result in a change in the form of the Eu^{3+} emission profile; only a decrease in emission intensity is observed, consistent with charge transfer quenching of the chromophore singlet excited state.

4.1.11 Quantum yield differentiation

As noted in the sections discussing the synthesis of the individual conjugates, the meassured lifetime variation was very small (1.38-1.75 ms for Tb^{3+}). However, this was not true for the variation of quantum yields. These differ substantially and could be observed even by inspection of HPLC chromatograms obtained with fluorescence detection. To further quantify these differences, the dependence of the total integrated emission against absorbance was measured for several Tb^{3+} complexes.

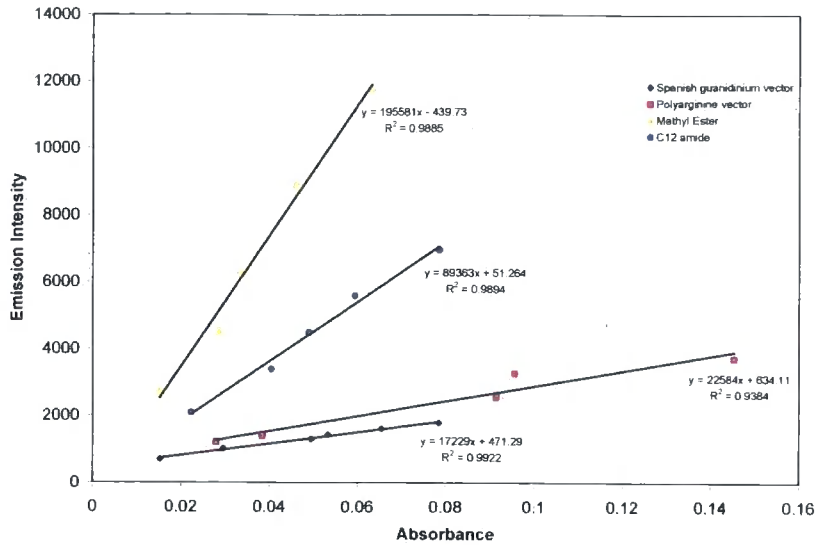

Figure 4.13 – Plot of integrated emission intensity against absorbance for selected Tb^{3+} complexes (295 K, H_2O)

The quantum yield differences can be inferred from the gradients of such plots, **Figure 4.13**. It can be seen that the relative difference of quantum yield of the methyl ester complex, $[TbL^{8}]^{3+}$ and the oligoguanidinium complex $[TbL^{40}]^{3+}$ is an order of magnitude. The two-fold difference with the C_{12} amide complex $[TbL^{37}]^{3+}$ mirrors observations made by analysis of the emission spectra.

Substituent:	*OMe*	*NHC_{12}*	*$HN(Arg)_7$*	*Guanidinium*
φ_{em}^{rel}	1.0	0.46	0.11	0.09

Table 4.1 – Relative overall emission quantum yields, relative to $[TbL^{8}]^{3+}$ ($\varphi_{Tb}^{H_2O}$ 19%)

The modest changes of the quantum yield between the ester and the amide are probably due to small changes of the energies of the singlet and triplet state of the chromophore, which can affect the rate of energy or electron transfer. The large decrease of the quantum yield for the two guanidinium containing complexes is more likely to be a result of static quenching of the singlet excited state, probably involving a charge transfer interaction with these groups. Similar obsevations were

made also for the complexes containing the 3,4-methylene dioxybenzylamine group, the PAMAM dendrimer conjugate and the protein conjugate.

4.2 Cellular imaging studies and further relevant experiments

Fluorescence microscopy experiments were undertaken to assess the characteristics of the synthesised complexes for cellular imaging purposes. These observations were accompanied by supporting experiments establishing, for example, cytotoxicity and the nature of the non-covalent binding to protein, for selected examples

4.2.1 Cell uptake experiments with azaxanthone complexes in NIH 3T3 and CHO cells

The initial cellular uptake experiments were carried out with six Tb^{3+} complexes bearing phenylamide pendant arms and a differently substituted azaxanthone chromophore (**Figure 4.14**).

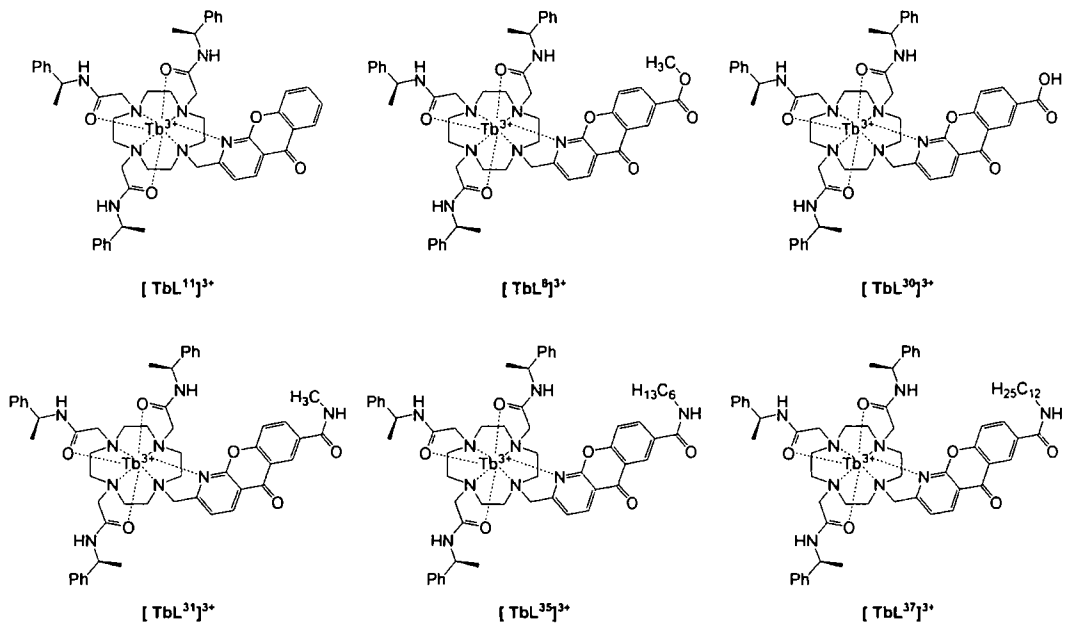

Figure 4.14 – Complexes used in initial cell uptake experiments to investigate the effect of differential substitution on the azaxanthone chromophore

The experiments were carried out with mouse skin fibroblasts (NIH 3T3) and Chinese hamster ovarian (CHO) cells. These were grown on microscope cover-slips in 6-24 well plates using DMEM and F-12 HAM media (penicillin streptomycin, foetal calf serum) for NIH 3T3 and CHO cells respectively. The cells were incubated with 100 μM solutions of the complexes for 18-20 h at 37°C and under an atmosphere of 5% CO_2. The cover-slips were washed with phosphate buffered saline (PBS) prior to mounting onto microscope slides and imaging on a Zeiss Axiovert 200 inverted microscope, using the 40 × oil contact objective. The Zeiss G365 and BP 546/12 filters were used in excitation and emission channels respectively. The images are presented in yellow, as opposed to the green corresponding to Tb emission, to improve the image contrast.

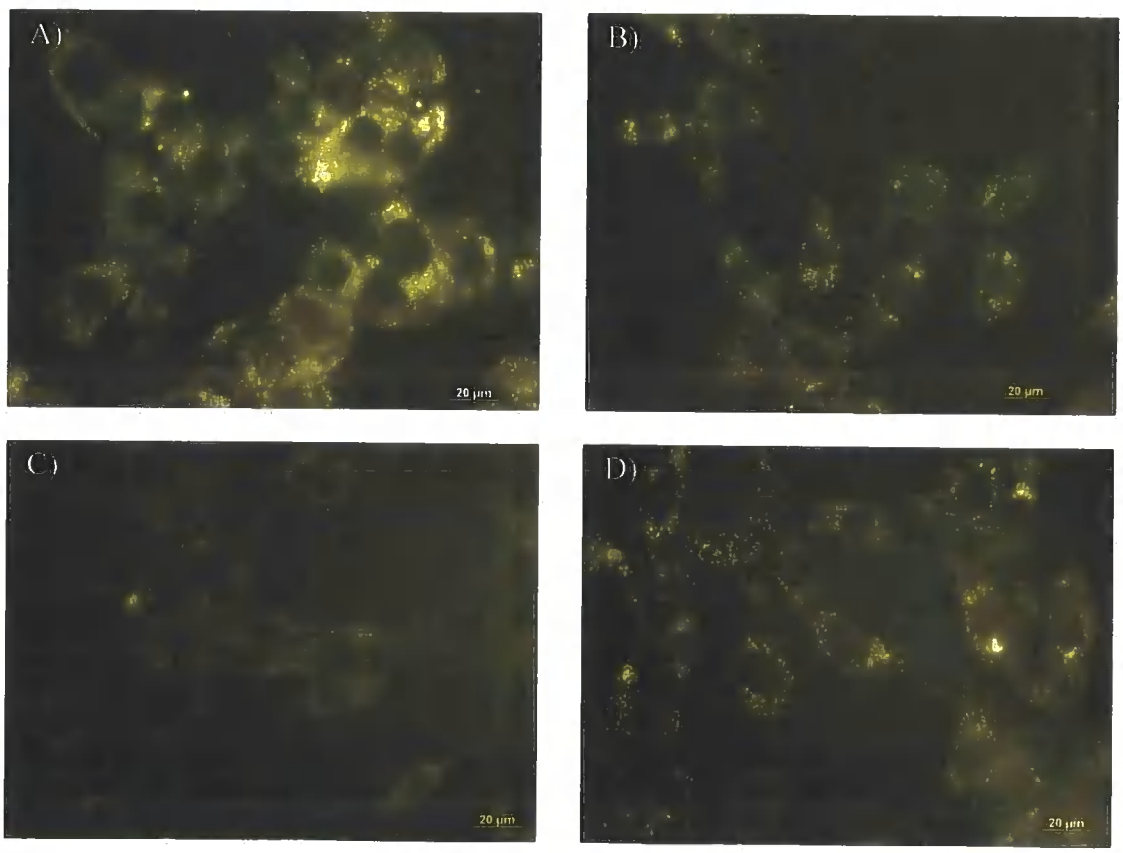

Figure 4.15 – Fluorescence microscopy images of NIH 3T3 cells loaded with: A) $[TbL^{11}]^{3+}$ R = H, B) $[TbL^{8}]^{3+}$ R = COOMe , C) $[TbL^{30}]^{3+}$ R = COOH and D) $[TbL^{35}]^{3+}$ R = $CONC_6H_{13}$

The images in **Figure 4.15** show localisation of the complexes in well defined spots in the cytosol clustered mostly in the perinuclear region for the parent azaxanthone

complex $[TbL^{11}]^{3+}$, the methyl ester complex $[TbL^{8}]^{3+}$ and the hexylamide complex $[TbL^{35}]^{3+}$. It is presumed that this pattern is consistent with late endosomal/lysosomal localisation. The images of cells loaded with the carboxylic acid complex $[TbL^{30}]^{3+}$ showed very little fluorescence and were not significantly different from cells that had not been treated with any complex at all. A similar result was observed for the methyl amide complex $[TbL^{31}]^{3+}$. The dodecylamide complex $[TbL^{37}]^{3+}$ was also loaded into cells but could not be imaged successfully, as this complex was very cytotoxic and tended to kill most of the cells being examined.

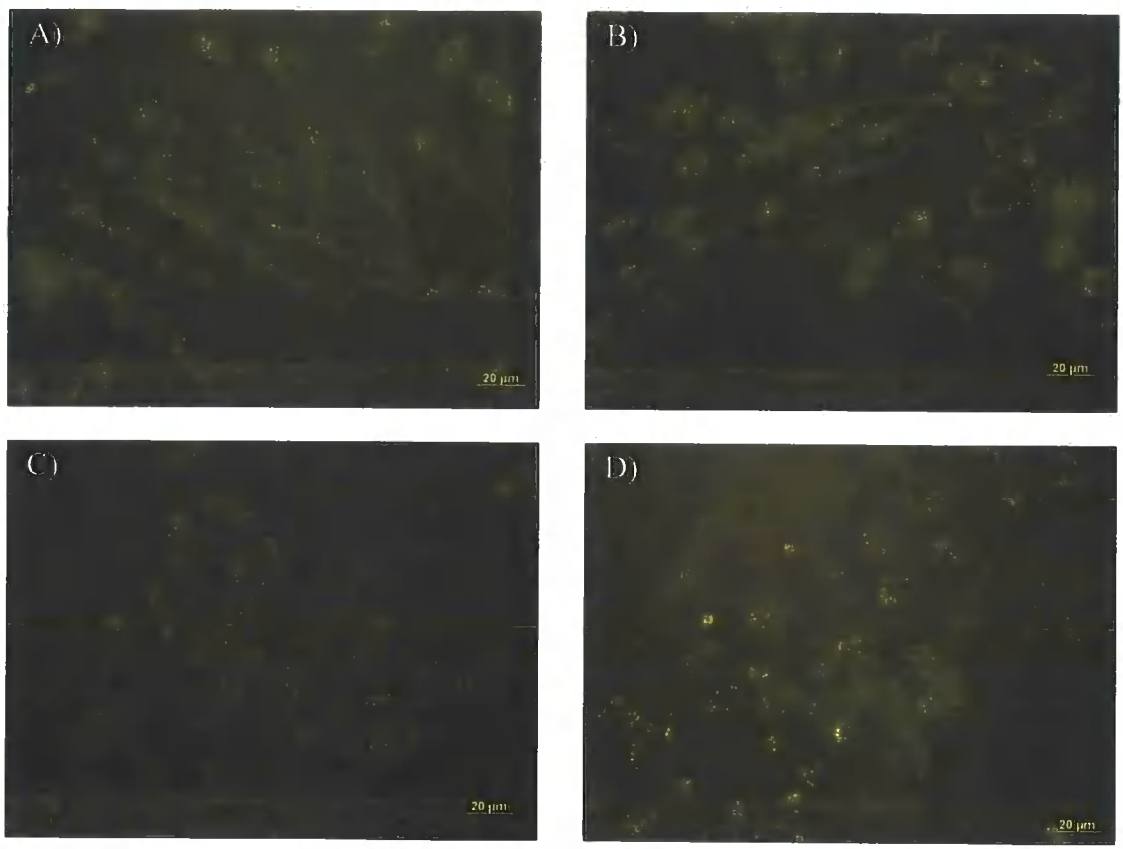

Figure 4.16 – Fluorescence microscopy images of CHO cells loaded with: A) $[TbL^{11}]^{3+}$ R = H, B) $[TbL^{8}]^{3+}$ R = COOMe, C) $[TbL^{30}]^{3+}$ R = COOH and D) $[TbL^{37}]^{3+}$ R = $CONC_{12}H_{25}$

Similar results were obtained in CHO cells. The images for the parent azaxanthone, $[TbL^{11}]^{3+}$ and especially the methyl ester, $[TbL^{8}]^{3+}$ complexes were not as clear as in the case of NIH 3T3 cells, with significantly fewer well defined, strongly fluorescent spots in the cytosol. A similar situation was observed for the hexylamide complex $[TbL^{35}]^{3+}$. The internalisation of the carboxylic acid, $[TbL^{30}]^{3+}$, and methyl

amide, $[TbL^{31}]^{3+}$, complexes was virtually not observed, as in the case of the NIH 3T3 cells. The dodecylamide complex, $[TbL^{37}]^{3+}$, however, proved to be much less cytotoxic to CHO cells than to the NIH 3T3 cells. Thus, fluorescence images could be recorded and revealed a punctate localisation with well defined spots in the cytosol, distinctly different to that observed for the other complexes. Localisation to highly membranous organelles, such as the Golgi apparatus or endoplasmic reticulum could be assumed, based on the long aliphatic chain of the dodecylamide complex $[TbL^{37}]^{3+}$; this needs to be proved by further co-localisation studies.

4.2.2 Two photon fluorescence imaging of NIH 3T3 and HeLa cells

Further cellular experiments were carried out in collaboration with Drs. Ga-Lai Law and Ka-Leung Wang in Hong Kong. The images were recorded with two photon excitation (λ_{ex} = 720 nm). The cells were grown in culture dishes allowing the cells to attach overnight. The cell medium in each well was changed to fresh medium (no added complex) immediately prior to image acquisition.

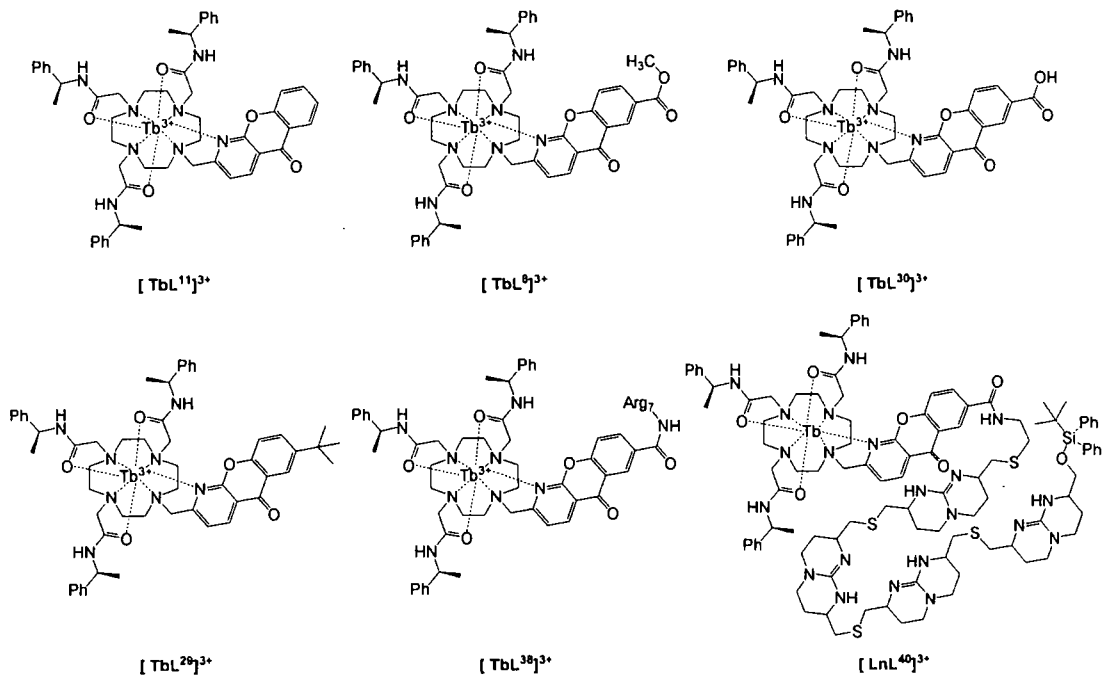

Figure 4.17 – Complexes used in cellular imaging experiments using two photon excitation

The images were taken at different time intervals whilst, the cells were kept in a chamber at 37°C under 5% CO_2 atmosphere.

Complexes based on the triphenyl amide pendant arm ligand system with differently substituted azaxanthone chromophores were used in this study (20 μM). The conjugates with the hepta-arginine, $[TbL^{38}]^{3+}$, and the oligoguanidinium vector, $[TbL^{40}]^{3+}$ were used, as well as some of the complexes used in the previous study, (**Figure 4.17**).

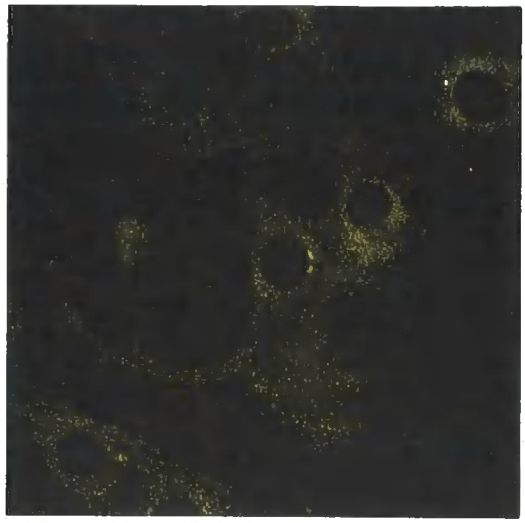

Figure 4.18 – Fluorescence microscopy image of NIH 3T3 cells stained with $[TbL^{11}]^{3+}$, R = H, recorded 3 h after loading

The NIH 3T3 cells loaded with the unsubstituted azaxanthone complex $[TbL^{11}]^{3+}$ were examined 3h after the addition of the complex to the growth medium. The complex was observed distributed throughout the cytosol, with some tendency to be localised in endosomes/lysosomes of the perinuclear region.

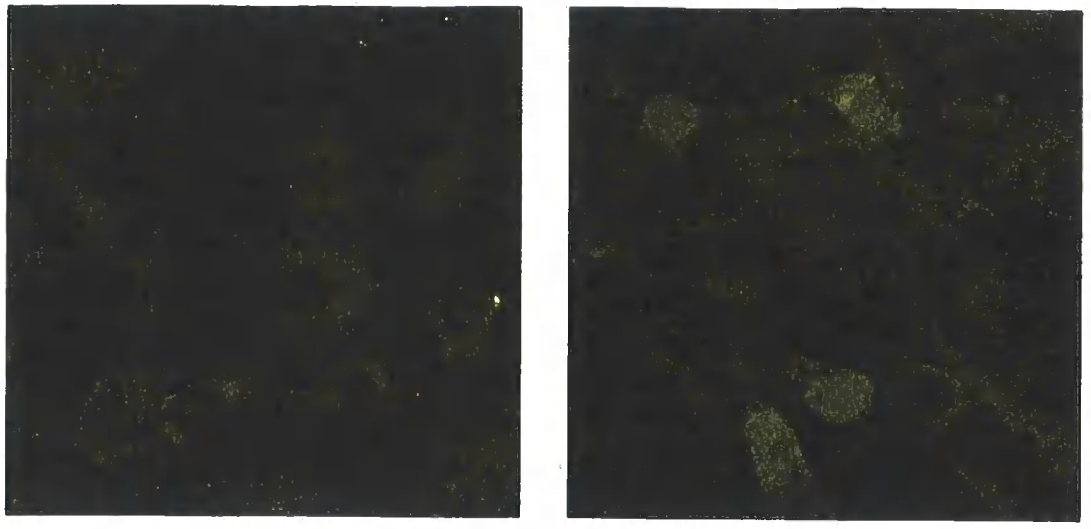

Figure 4.19 – Fluorescence microscopy images of NIH 3T3 cells stained with $[TbL^8]^{3+}$, R = COOMe, recorded 3h after loading

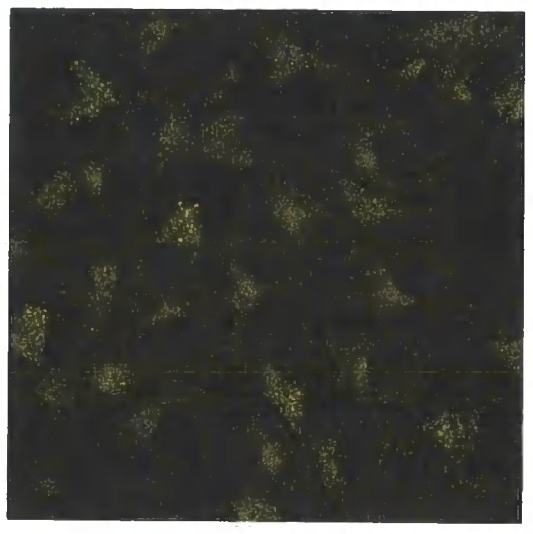

Figure 4.20 – Fluorescence microscopy images of NIH 3T3 cells stained with $[TbL^8]^{3+}$, R = COOMe, recorded 5h after loading

The methyl ester complex $[TbL^8]^{3+}$ was observed to internalize in the NIH 3T3 cells rapidly and was highly emissive. A degree of nuclear staining was observed in some instances, but staining of the cytosol was the most common feature observed. A more localized (compartmental) localization was apparent in images obtained 5h after loading.

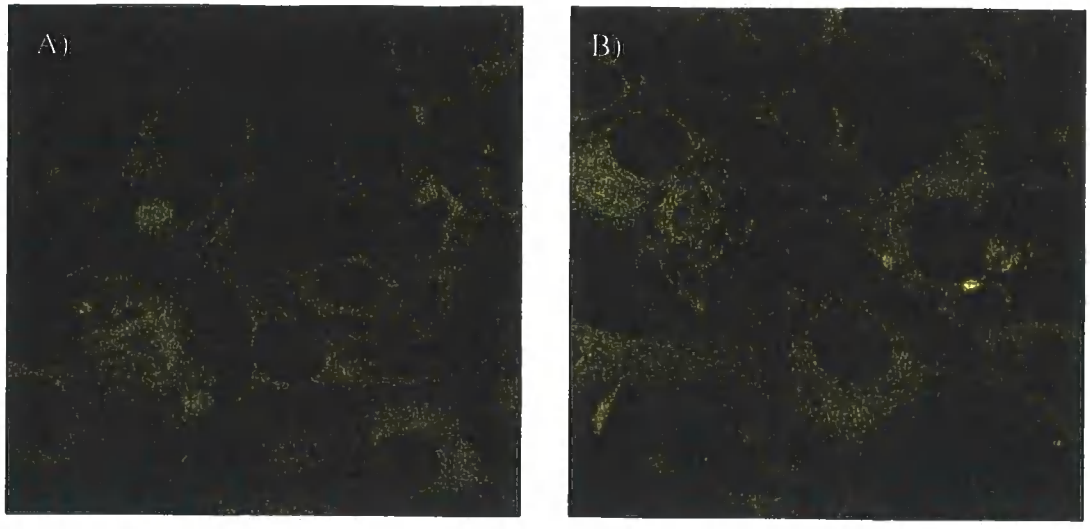

Figure 4.21 – Fluorescence microscopy images of NIH 3T3 cells stained with $[TbL^{30}]^{3+}$, R = COOH, recorded 2 h (A) and 3h (B) after loading

The carboxylic acid complex $[TbL^{30}]^{3+}$ was taken up much more slowly by the NIH 3T3 cells compared to the other complexes. The complex luminescence was observable within a few minutes after loading for each of the other complexes, but it took 45 min for the acid complex to be observable. The images obtained using this complex, were also less bright in comparison to others.

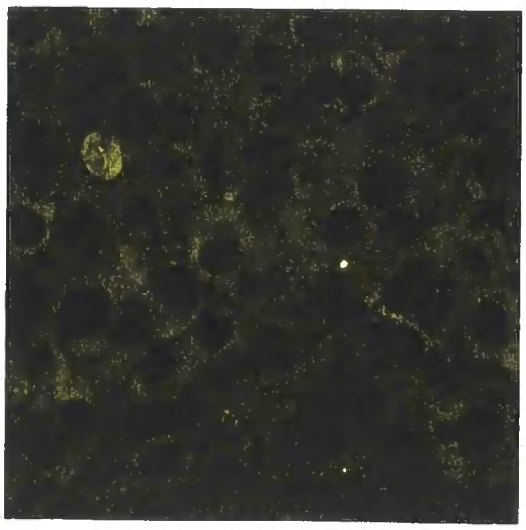

Figure 4.22 – Fluorescence image of NIH 3T3 cells stained with $[TbL^{29}]^{3+}$, R = *t*-Bu, recorded 3h after loading

The complex containing an azaxanthone chromophore substituted with a *t*-Bu group, $[TbL^{29}]^{3+}$, was found to enter the NIH 3T3 cells rapidly and stain the cytoplasm. The staining appears to consist of distinct spots rather than a uniform distribution. The morphology changes in the cells observed during these experiments suggest that this complex is more cytotoxic than the others.

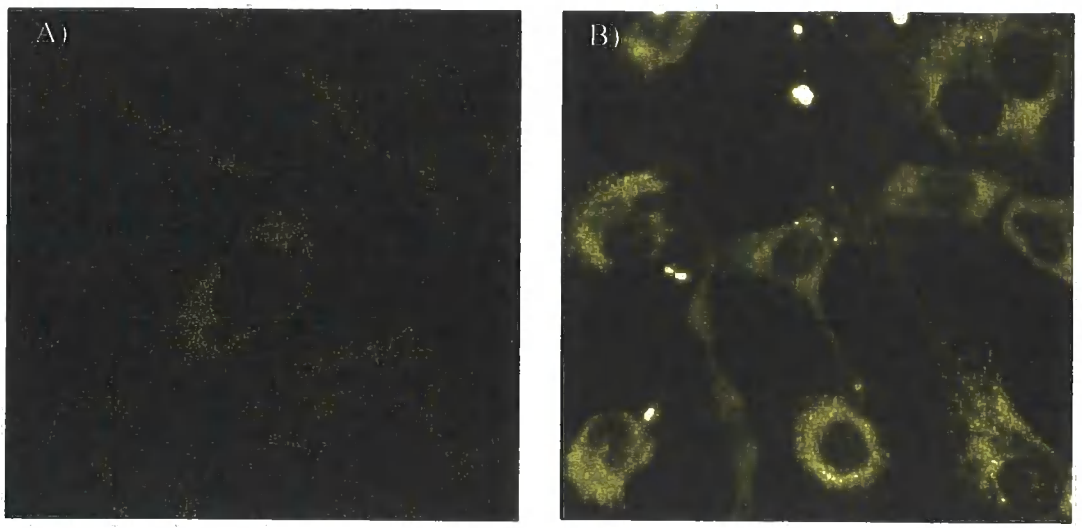

Figure 4.23 – Fluorescence images of NIH 3T3 cells stained with $[TbL^{38}]^{3+}$, R = Arg_7, recorded (A) a few minutes after loading and (B) after overnight loading

The hepatarginine conjugate complex $[TbL^{38}]^{3+}$ was found to translocate rapidly across (of the order of 5-10 minutes) the cellular membrane early after loading. Bright images could be obtained after an overnight staining period, giving a profile strongly reminiscent of a lysosomal distribution.

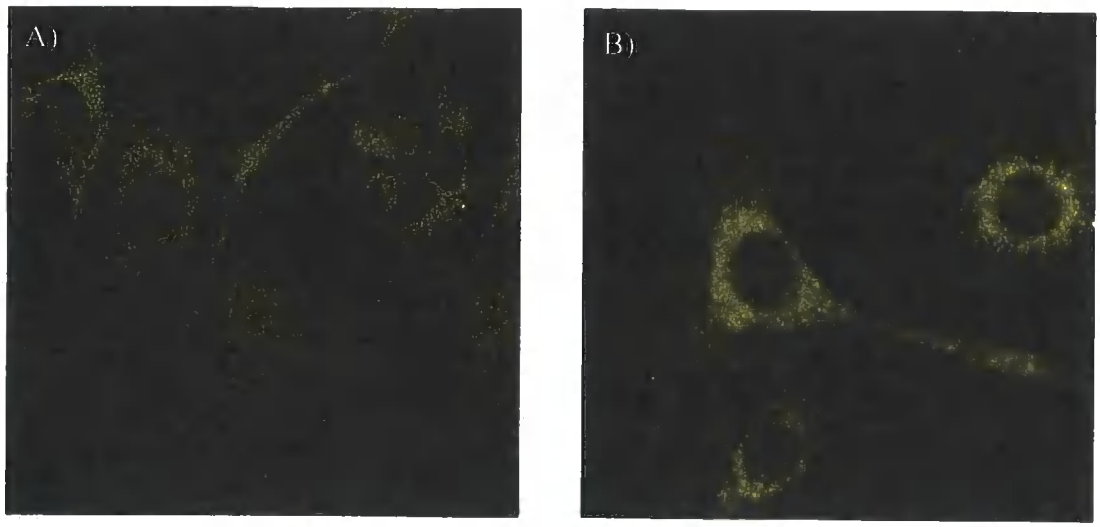

Figure 4.24 – Fluorescence microscopy images of NIH 3T3 cells stained with $[TbL^{40}]^{3+}$, R = guanidinium, recorded (A) 3h after loading and after (B) overnight loading

Observation of NIH 3T3 cells loaded with the oligoguanidinium conjugate complex $[TbL^{40}]^{3+}$ showed fast crossing of the dye across the cellular membrane, resulting in rather weak images at early observation times. More intense staining was observed after overnight loading. The suspected mitochondrial localization, at the earlier time points, needs confirmation by a co-localization study with MitoTracker dyes.

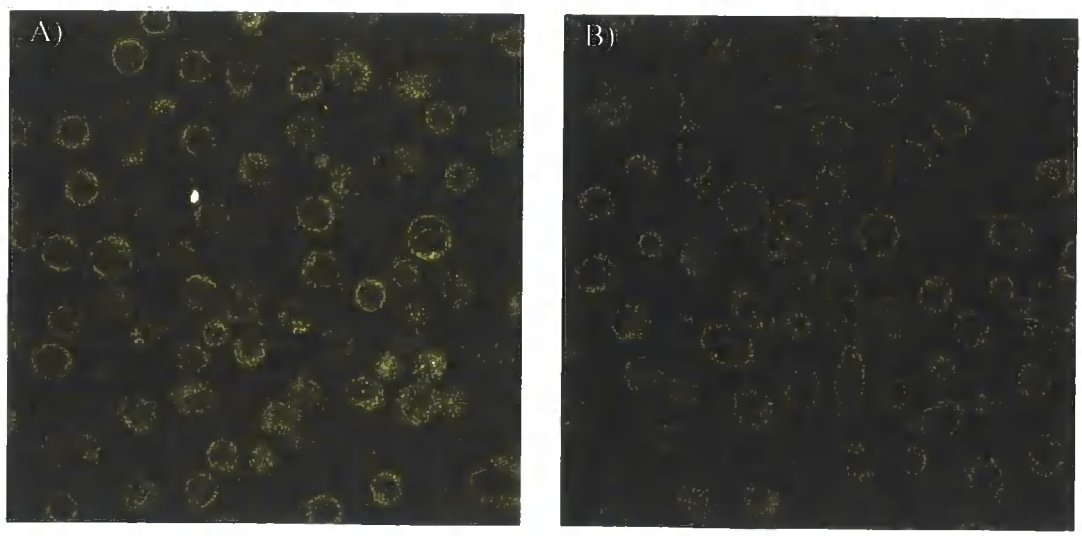

Figure 4.25 – Fluorescence images of HeLa cells stained with (A) $[TbL^{8}]^{3+}$, R = COOMe, and (B) $[TbL^{38}]^{3+}$, R = Arg_7, recorded 1h after loading

The methyl ester $[TbL^{8}]^{3+}$ and heptaarginine conjugate $[TbL^{38}]^{3+}$ complexes were also loaded into HeLa cells. The ester complex again resulted in significantly brighter images. The localization seems mainly perinuclear, in each case.

4.2.3 Protein binding

As discussed in Chapter 3, protein binding of the complexes can have a significant impact on the results obtained in cellular imaging experiments using the lanthanide complexes. Protein binding can shield the lanthanide complexes from local quenching species, ensuring that the complex will actually be emissive *in cellulo*. Protein binding binding experiments were therefore undertaken with the parent azaxanthone $[LnL^{11}]^{3+}$, methyl ester $[LnL^{8}]^{3+}$, carboxylic acid $[LnL^{30}]^{3+}$ and *t*-butyl $[LnL^{29}]^{3+}$ complexes.

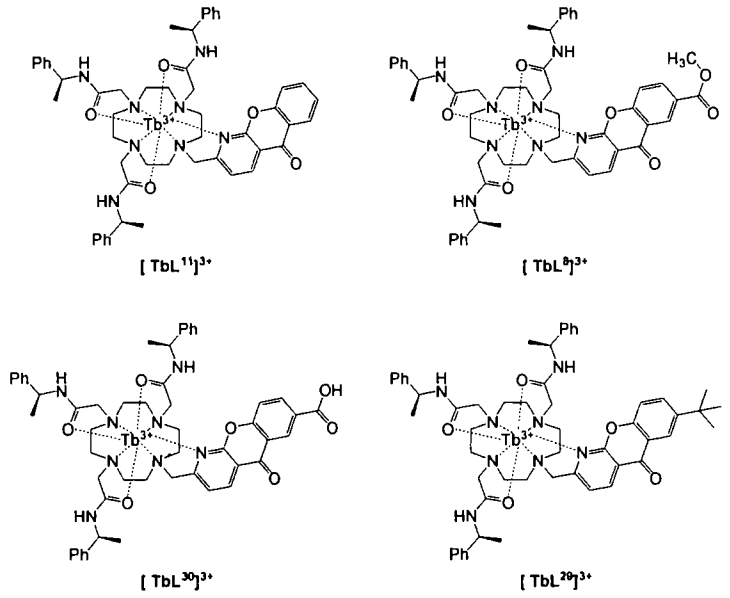

Figure 4.26 – Structures of complexes used in the protein binding study

The most common experiment investigating the binding of a lanthanide complex to a protein is a protein titration of the Gd^{3+} complex monitoring changes in the relaxivity value of the complex r_{1p}.[15, 16] This measurement is based on the dependence of

relaxivity on the rotational correlation time of the complex in solution, which increases significantly upon binding to a protein.

A solution of human serum albumin (HSA) was added to the solutions of the four studied complexes and changes in relaxivity were monitored. The starting relaxivity values of 2.5-3 $mM^{-1}s^{-1}$ were in line with expectation for cationic complexes, where slow exchange of the bound water molecule is anticipated.[17, 18] The limiting relaxivity values reached following addition of excess of HSA were 9 $mM^{-1}s^{-1}$ for complex $[GdL^{11}]^{3+}$, 8.5 $mM^{-1}s^{-1}$ for complex $[GdL^{8}]^{3+}$, 8 $mM^{-1}s^{-1}$ for complex $[GdL^{29}]^{3+}$ and 11.5 $s^{-1}mM^{-1}$ for $[GdL^{30}]^{3+}$.

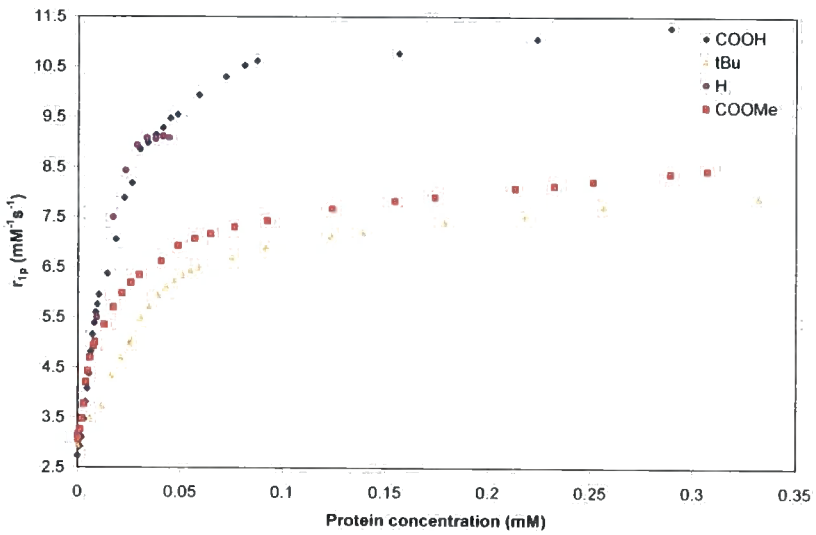

Figure 4.27 – Variation of relaxivity with added protein for complexes $[GdL^{11}]^{3+}$ (purple circles), $[GdL^{8}]^{3+}$ (red squares), $[GdL^{30}]^{3+}$ (blue squares) and $[GdL^{29}]^{3+}$ (yellow triangles) (310 K, H_2O, [complex] = 0.25 mM)

Fitting of the binding curves was attempted to estimate the equilibrium constant. This, however, was not possible as further analysis has shown that there are at least 3-4 complexes bound to a protein molecule. These results are similar to the observations made with the phenylamide arm complex bearing a tetraazatriphenylene chromophore $[GdL^{1}]^{3+}$, and are consistent with 'non-specific' binding of the relatively lipophilic complex.[7]

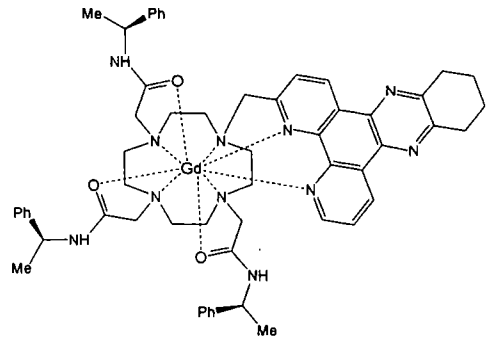

$[GdL^1]^{3+}$

Figure 4.28 – Structure of tetrazatriphenylene complex used in protein titration experiment

An estimate of the relative binding affinity was derived by considering the protein concentration needed to achieve 50% of the observed relaxivity change.

Substituent	*H*	*COOMe*	*COOH*	*t-Bu*
HSA concentration (mM)	0.011	0.016	0.019	0.029

Table 4.2 – HSA concentrations required to achieve 50 % of the total observed relaxivity change in the protein binding experiment

Using this estimation of the protein affinity the complexes may be ranked in the following order of decreasing protein affinity: $\mathbf{[GdL^{11}]^{3+}} > \mathbf{[GdL^{8}]^{3+}} \sim \mathbf{[GdL^{30}]^{3+}} > \mathbf{[GdL^{29}]^{3+}}$.

Protein binding can in principle be monitored also by its effect on the luminescence properties of Eu^{3+} and Tb^{3+}. Changes in the emission spectral form of the Eu^{3+} complexes constitute one of the more useful tools for such an investigation.

The emission spectra of the Eu^{3+} analogues of the complexes used in the relaxivity measurements were recorded in pure H_2O, and in the presence of a 10-fold excess of HSA. Unfortunately, only luminescence intensity reductions were recorded and no significant changes in spectral form could be discerned. Thus, protein association does not affect the local coordination environment of the lanthanide ion.

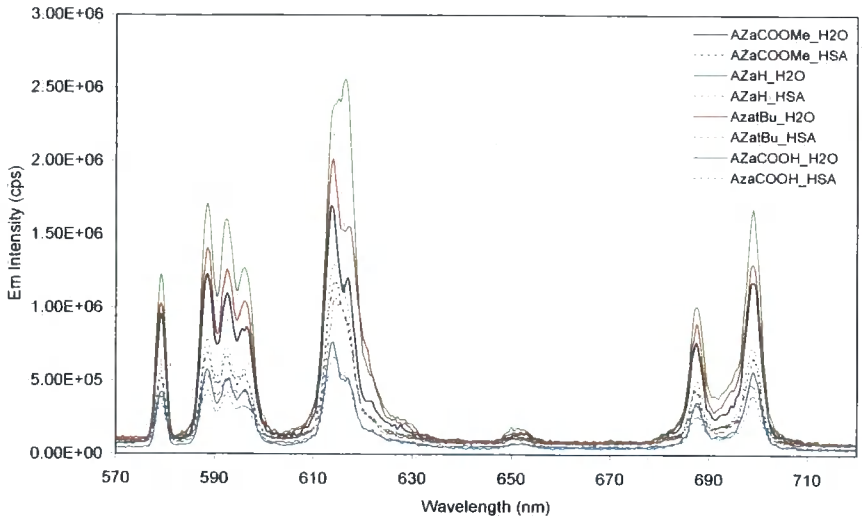

Figure 4.29 – Emission spectra of selected complexes in the absence and presence of added HSA (295 K, H_2O, [complex] = 17 μM)

4.2.4 Cytotoxicity studies

It became apparent during the fluorescence microscopy experiments that there exist significant differences in the cytoxicity levels of the lanthanide complexes used. The complexes were usually added to the cell growth medium at 100 μM concentration and in most cases a preliminary assessment of cell viability by examination of cell morphology in brightfield microscopy did not suggest significant cytotoxicity. Some exceptions were, however, noted, such as the dodecylamide complex $[TbL^{37}]^{3+}$ and the oligoguanidinium conjugate complex $[TbL^{40}]^{3+}$. Thus, a more systematic approach was adopted to establish the relative cytotoxicity of the complexes. The IC_{50} values were measured, indicating the concentration of a substance needed to induce cell death to 50% of the cells.

The measurement of the IC_{50} values was done using an MTT assay[19] by Ms. Elizabeth J. New (Durham). This procedure uses the conversion of MTT (3-(4,5-dimethylthiazol-2-yl)-2,5-diphenyltetrazolium bromide) to a purple formazan product in the mitochondria of viable cells. The product formazan compound is insoluble in water and the spectrophotometrical measurement is done after

dissolution in DMSO. In a typical set up 5000 NIH 3T3 cells would be dosed into the wells of 96 well plates for a plate reader in 100 µl of DMEM growth medium. The cells would be then dosed with complex concentrations ranging from 0-100 µM and incubated for 24 h. Triplicate measurements were carried out. The MTT would be added and a further 4h incubation would follow. The growth medium was then removed and replaced with DMSO (150 µl). The absorbance at 540 nm was measured immediately after 20 s shaking period. The IC_{50} value corresponds to the concentration resulting in 50% absorbance, compared to control cells.

Complex	*IC_{50} (µM)*
$[TbL^{8}]^{3+}$ R = COOMe	95 (±17)
$[GdL^{30}]^{3+}$ R = COOH	150 (±3)
$[TbL^{37}]^{3+}$ R = $CONHC_{12}$	7.2 (±0.5)
$[TbL^{40}]^{3+}$ R = CONGuan	13 (±5)
$[GdL^{29}]^{3+}$ R = *t*-Bu	58 (±0.3)

Table 4.3 – IC_{50} values (errors in parentheses) in NIH 3T3 cells for selected complexes, as measured by the MTT assay

The measured IC_{50} values are in good agreement with observations made in microscopy measurements. Thus the methyl ester **$[TbL^{8}]^{3+}$** and carboxylic acid complexes **$[TbL^{30}]^{3+}$** did not show significant cytotoxicity at the concentrations used, but the other complexes did. The cytotoxicity suggested by the microscopy experiments was most noticeable for the dodecylamide **$[TbL^{37}]^{3+}$** and oligoguanidinium conjugate **$[TbL^{40}]^{3+}$** complexes; indeed the IC_{50} values (**Table 4.3**) are very low. The IC_{50} value for the oligoguanidinum conjugate complex, **$[TbL^{40}]^{3+}$**, is also in good agreement with the literature value (8 µM) determined for a conjugate of this vector to fluorescein.[20]

4.2.4.1 Distinguishing apoptosis and necrosis

Mitochondrial localization was also observed in previous work[19] with a fluorescein conjugate of the oligoguanidinium vector used in complex $[\mathbf{TbL^{40}}]^{3+}$. Thus, apoptosis was hypothesized to be the mechanism by which $[\mathbf{TbL^{40}}]^{3+}$ induced cell death. To prove this and how the dodecylamide complex, $[\mathbf{TbL^{37}}]^{3+}$, exhibits its high cytotoxicity, an apoptosis/necrosis differentiation experiment was carried out. The experiment uses flow-cytometry and the Annexin V-FITC Apoptosis Detection Kit, supplied by SIGMA.[21]

To carry out the experiment, cells were grown to confluence in 6-well plates. Immediately prior to dosing, medium was removed and fresh medium (1 mL) was added. Cells were treated with complex for 4h and 24h at concentrations above the previously-determined IC_{50} values. An apoptotic control was prepared by incubating with 1 μg/mL staurosporine for 3 hours. The control for necrosis was prepared by incubating cells on ice for three hours with 70% ethanol. After incubation, cells were harvested by trypsinisation and centrifugation, and were re-suspended in 500 μL binding buffer (10 mM HEPES, pH 7.5 containing140 mM NaCl and 2.5 mM $CaCl_2$). The suspension was incubated at room temperature in the dark for 10 minutes with annexin V-FITC (0.5 μg/mL) and propidium iodide (5 μg/mL). The fluorescence of the cells was immediately determined by flow cytometry. Results were compared to an untreated control, and to established literature controls for necrosis and apoptosis.

The experiment was carried out in both NIH 3T3 and CHO cell lines. The flow-cytometry images correlate fluorescence of the Annexin-FITC conjugate, as the apoptosis marker, on the x-axis and the propidium iodide fluorescence, which indicates necrosis, on the y-axis. The plot area is divided into four sections R_2, R_3, R_4 and R_5. Where viable cells are present in section R_4, early apoptotic cells are in section R_5, late apoptotic cells are in section R_3 and necrotic cells are in section R_2.

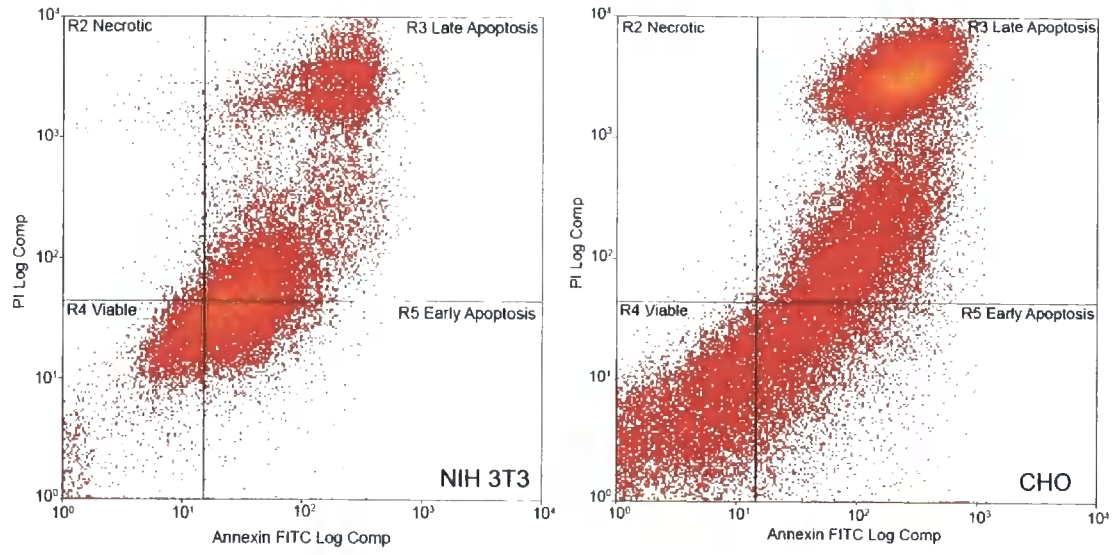

Figure 4.30 – A flow-cytometry plots of NIH 3T3 and CHO cells obtained 24 h after treating the cells with the oligoguanidinium conjugate complex, $[TbL^{40}]^{3+}$

The oligoguanidinium conjugate complex $[TbL^{40}]^{3+}$ exhibits apoptosis as the mode of action in each cell line as can be seen from the flow-cytometry diagrams (**Figure 4.30**).

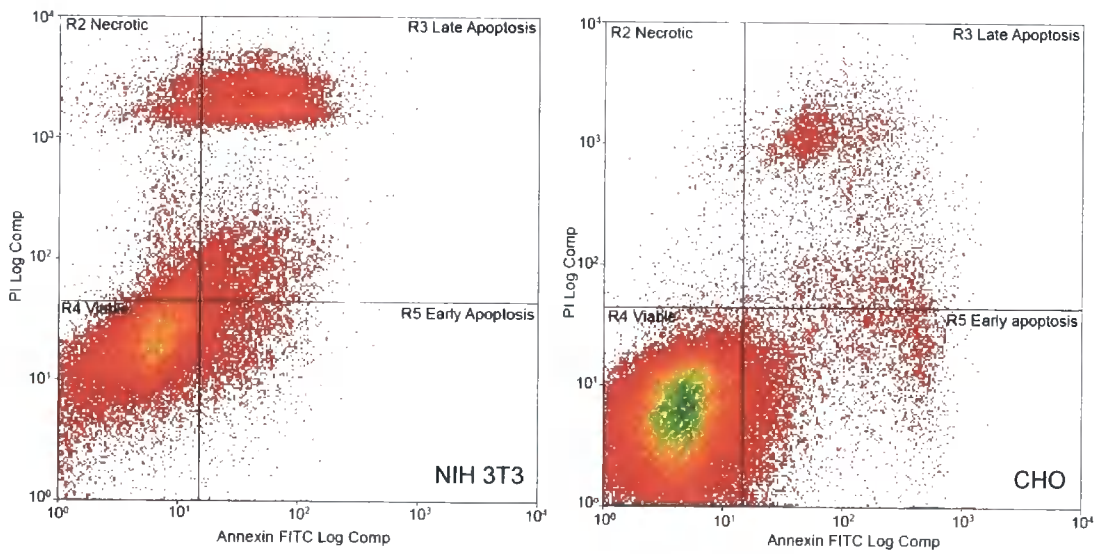

Figure 4.31 – A flow-cytometry plots of NIH 3T3 and CHO cells obtained 24 h after treating the cells with the dodecylamide complex, $[TbL^{37}]^{3+}$

It can be seen from **Fig. 4.31** that the dodecylamide complex $[TbL^{37}]^{3+}$ is not cytotoxic towards CHO cells and comparison to **Figure 4.30** shows also a larger population of viable NIH 3T3 cells. The distribution of the cells is different in the case of NIH 3T3 cells, in comparison to the oligoguanidinium complex $[TbL^{40}]^{3+}$, but the dead cells fall into segment R3 indicating late apoptosis. The necrotic character of the cell death in the case of the dodecylamide complex $[TbL^{37}]^{3+}$ is better demonstrated with cells observed only 4h after dosing with the complex (**Figure 4.32**).

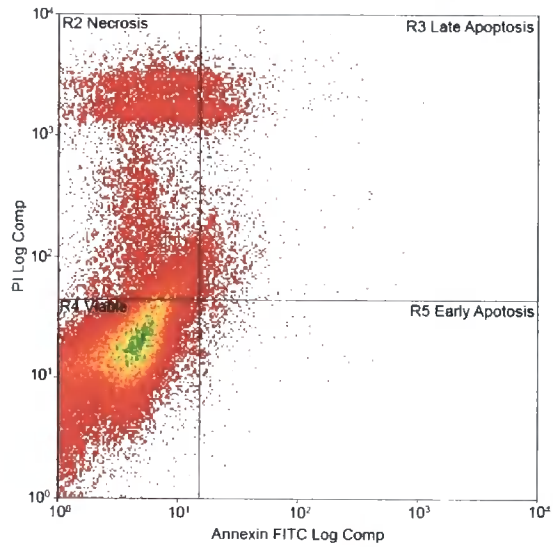

Figure 4.32 – A flow-cytometry plot of NIH 3T3 cells obtained 4 h after treating the cells with the dodecylamide complex, $[TbL^{34}]^{3+}$

The necrotic pathway is clearly shown in **Figure 4.33** for the dodecylamide complex $[TbL^{37}]^{3+}$. The late apoptotic character is observed as a result of longer exposure (**Figure 4.31**), when apoptotic processes can be initiated in cells already undergoing primarily necrosis.

These results are consistent with the expectations for the mode of action of these complexes. Furthermore, the differential sensitivity of NIH 3T3 and CHO cells treated with the dodecylamide complex $[TbL^{37}]^{3+}$ is in line with the observations made in microscopy experiments.

4.3 Conclusions and future work

A conjugation method has been established for complexes containing azaxanthone chromophore with a carboxylic acid function. The preliminary work has been carried out on complexes containing amide pendant arms. Coupling reactions were successfully undertaken with several amine reactants, including Arg-rich peptide sequences, a PAMAM dendrimer and a protein (HSA). It has been demonstrated that the conversions to different derivatives, of the incorporated carboxylate function, do not significantly affect the luminescence properties of the complexes. Some of the conjugates did however seem to exhibit static quenching of the chromophore excited state by amine and guanidinium groups.

It has also been demonstrated that changing the substituent on the chromophore can result in significant changes in the cellular localisation behaviour, with respect to cell penetration, distribution and relative cytotoxicity.

Thus, it has been demonstrated that the approach of using a single luminescent lanthanide complex, conjugated to an appropriate vector can in principle result in a selective probe. The complexes already synthesised need to be more extensively studied to achieve a deeper understanding of their interactions with biological systems. Use of different pendant arms, chomophores and vectors needs to be investigated as well. An interesting option is the synthesis of conjugates where the vector would be able to recognise a tag on a specific protein molecule and label it. Another option is the creation of a targeted complex conjugate with the coordination sphere designed as a responsive one, which would lead to targeted probes. A further interesting option could be synthesis of 'lipid-like' molecules, labelled with luminescent lanthanide complexes based on DO3A. Such an approach could be beneficial as only the complexes within the interior of a membrane, shielded from local quenching, should be highly luminescent.

Literature

[1]) J. C. G. Bünzli, C. Piguet, *Chemical Society Reviews*, 2005, **34**, 1048.
[2]) S. Pandya, J. Yu, D. Parker, *Dalton Transactions*, 2006, 2757.
[3]) R. A. Poole, C. P. Montgomery, E. J. New, A. Congreve, D. Parker, M. Botta, *Organic and Biomolecular Chemistry*, 2007, **5**, 2055.
[4]) J. Yu, D. Parker, R. Pal. R. A. Poole, M. J. Cann, *Journal of the American Chemical Society*, 2006, **128**, 2294.
[5]) Y. Bretonniere, M. J. Cann, D. Parker, R. Slater, *Organic and Biomolecular Chemistry*, 2004, **2**, 1624.
[6]) R. A. Poole, G. Bobba, M. J. Cann, J. C. Frias, D. Parker, R. D. Peacok, *Organic and Biomolecular Chemistry*, 2005, **3**, 1013.
[7]) R. Poole, *Highly Emissive Tetraazatriphenylene Complexes*, PhD. Thesis, University of Durham, 2006.
[8]) V. P. Trochilin, *Annual Reviews of Biomedical Engineering*, 2006, **8**, 343.
[9]) M. Kosuae, T. Takeuchi, I. Nakase, A. T. Jones, S. Futaki, *Bioconjugate Chemistry*, online published.
[10]) J. Rudovský, M. Botta, P. Hermann, K. I. Hardcastle, I. Lukeš, S. Aime, *Bioconjugate Chemistry*, 2006, **17**, 975.
[11]) S. L. Richardson, *MSc. Thesis*, Durham University, 2008.
[12]) D. Wüstner, *Chemistry and Physics of Lipids*, 2007, **146**, 1.
[13]) P. Muhr, W. Likussar, M. Shubert-Zsilavecz, *Magnetic Resonance in Chemistry*, 1996, **34**, 137.
[14]) D. Parker, J. Yu, *Chemical Communications*, 2005, 3141.
[15]) R. B. Lauffer, *Chemical Reviews*, 1987, **87**, 901.
[16]) P. Caravan, N. J. Cloutier, M. T. Greenfield, S. A. McDermid, S. U. Dunham, J. W. M. Bulte, J. C. Amedio Jr., R. J. Looby, R. M. Supkowski, W. DeW. Horrocks Jr., T. J. McMurry, R. B. Lauffer, *Journal of the American Chemical Society*, 2001, **124**, 3152.
[17]) S. Aime, A. Barge, M. Botta, D. Parker, A. S. De Sousa, *Journal of the American Chemical Society*, 1997, **119**, 4767.
[18]) A. S. Batsanov, A. Beeby, J. I. Bruce, J. A. K. Howard, A. M. Kenwright, D. Parker, *Chemical Communications*, 1999, 1011.
[19]) J. Carmichael, W. G. DeGraff, A. F. Gazdar, J. D. Minna, J. B. Mitchell, *Cancer Research*, 1987, **47**, 936.
[20]) J. Fernádez-Carneado, M. Van Gool, V. Martos, S. Castel, P. Prados, J. De Mendoza, E. Giralt, *Journal of the American Chemical Society*, 2005, **127**, 869.
[21]) S. J. Martin, C. P. M. Reutelingsperger, A. J. McGahon, J. A. Rader, R. C. A. A. van Schie, D. M. LaFace, D. R. Green, *Journal of Experimental Medicine*, 1995, **182**, 1545.

CHAPTER 5

Experimental

5 Experimental

All reactants were used as supplied from commercial sources unless stated otherwise. Reactions requiring exclusion of moisture were carried out under an argon atmosphere. Water and H_2O refer to high purity water with conductivity of 0.04 μScm^{-1}, obtained from the "PuriteSTILL Plus" purification system.

Thin-layer chromatography was carried out on neutral alumina plates (Merck Art 5550) or silica plates (Merck 5554) and visualised under UV (254 nm). Preparative column chromatography was carried out using neutral alumina (Merck Aluminium Oxice 90, activity II-III, 70-230 mesh), pre-soaked in ethyl acetate, or silica (Merck Silica Gel 60, 230 ± 400 mesh).

^1H and ^{13}C NMR spectra were recorded on a Varian Mercury 200 (^1H at 199.975 MHz, ^{13}C at 50.289 MHz), Varian Unity 300 (^1H at 299.908 MHz, ^{13}C at 75.412 MHz), Varian VXR 400 (^1H at 399.968, ^{13}C at 100.572 MHz), or a Bruker AMX 500 spectrometer. Chemical shifts are reported relative to TMS and were referenced using the residual protio solvent resonances. Chemical shifts are reported in ppm and coupling constants in Hz. Splitting patterns are described as singlet (s), doublet (d), triplet (t), quartet (q), or multiplet (m).

Mass spectra with electrospray ionisation (ES) were recorded on a VG Platform II (Fisons instruments), operating in positive or negative ion mode, with methanol as the carrier solvent. Accurate masses were recorded on a Thermo Finnigan LTQ instrument.

Melting points were measured using a Reichart-Köfler block and are uncorrected.

Measurements of pH were performed using a Jenway 3320 pH meter and Aldrich Chemical Company micro-pH combination electrode, calibrated using pH 4, pH 7 and pH 10 buffer solutions.

UV/Vis absorbance spectra were recorded on a Perkin Elmer Lambda 900 UV/Vis/NIR spectrometer. Emission Spectra and Lifetimes were measured on a Perkin Elmer LS55 luminescence spectrometer and Instruments SA Fluorolog 3-11 spectrometer and DataMax v2.1 for Windows.

Phosphorescence emission spectra were recorded at 77 K using an Oxford Instruments optical cryostat and LS 55B spectrometer, with EPA (diethyl ether, isopentane and ethanol, 5:5:2) as solvent.

The HPLC analysis and separation was carried out on a Perkin Elmer system comprising of Perkin Elmer Series 200 Pump, Perkin Elmer Series 200 Autosampler, Perkin Elmer Series 200 Diode array detector and Perkin Elmer Series 200 Fluorescence detector. GILSON-FC203B fraction collector was used in separation procedures. The stationary phase used was the Phenomenex Synergi 4μ Fusion-RP 80, and the columns used came in two different sizes; 150x4.6 mm (flow rate 1ml/min) and 250x10 mm (flow rate 5 ml/min). The gradients used are described in Appendix 1.

Lifteime values were measured following excitation of the sample by a short pulse of light, monitoring the integrated intensity of light (546 nm for terbium, 613 nm for europium) emitted during a fixed gate time, t_g, a delay time, t_d, later. A gate time of 0.1 ms was used. The data obtained follow the exponential decay:

$$I = A_0 e^{(-kt)}$$

where I = intensity at time t after the flash
A_0 = a pre-exponential factor
k = rate constant for the decay of the excited state

A linear form of the relationship was obtained:

$$\ln I = \ln A_0 - kt$$

The data were fitted with this equation in Microsoft Excel. The excited state lifetime, τ, is the inverse of the rate constant, k

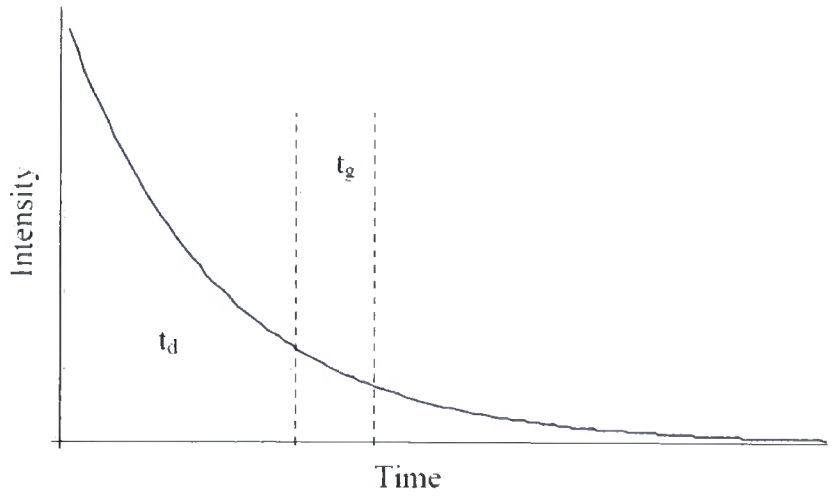

Measured parameters for lifetime measurements

The quantum yield for a given process is defined as the total number of photons emitted by that process divided by the total number of photons absorbed. The techniques and equipment necessary for an absolute determination of quantum yields are not commonly available. Therefore the usual method is to determine a relative quantum yield where the compound of unknown quantum yield is compared to a compound of known quantum yield. The unknown quantum yield can be calculated using the following equation.

$$\Phi_x = \Phi_r \cdot \frac{A_r}{A_x} \cdot \frac{E_x}{E_r} \cdot \frac{I_r}{I_x} \cdot \frac{\eta_x^2}{\eta_r^2}$$

Where r and x refer to reference and unknown respectively

A = absorbance at λ_{ex}

E = corrected integrated emission intensity

I = corrected intensity of excitation light

η = refractive index of solution

The reference complexes used, unless stated otherwise, were $TbPh_3dpqC$ and $EuPh_3dpqC$. For each of the standard and unknown samples solutions of absorbance between 0.02 and 0.1 were prepared. The absorbance and total integrated emission intensity was determined for each sample. A plot of integrated emission against absorbance gives a straight line with slope E/A. The quantum yield of an unknown

sample can thus be determined from the following equation, assuming identical excitation conditions and refractive indices.

$$\Phi_x = \Phi_r \cdot \frac{slope_x}{slope_r}$$

Errors in quantum yield measurements can arise due to the inner filter effect or errors in the amount of absorbed light. This effect can be minimised by only using samples with absorbances below 0.2. Errors in the amount of light absorbed by each sample can be minimised by choosing the excitation wavelength in the flat part of the absorption curve and by using a small bandpass for excitation.

Epifluorescence images were taken on a Zeiss Axiovert 200M epifluorescence microscope with a digital camera. CPL spectra were measured at the University of Glasgow, with the assistance of Dr. R. D. Peacock. Inductively coupled plasma mass spectrometry determinations of europium, gadolinium and terbium concentrations were made by Dr. C. Ottley in the Department of Earth Sciences at Durham University. Relaxivity measurements were made at 37 °C and 60 MHz on a Bruker Minispec mq60 instrument.

5.1 Ligand and Complex synthesis

2-Methyl-1,10-phenanthroline[1] (6)

A solution of 1,10-phenanthroline (10 g, 55 mmol) in dry THF (100 ml) was added to a stirred solution of methyl lithium (1.6 mol dm^{-3} in Et_2O, 34.5 ml, 55 mmol) in dry THF (150 ml) at 0°C under argon. The mixture was stirred overnight at room temperature under argon to give a dark green solution. The reaction was quenched by careful addition of water (100 ml) at 0°C. THF was removed under reduced pressure using a rotary evaporator and the product extracted into diethyl ether (3 × 150 ml) Activated manganese dioxide (53 g, 0.61 mol) was added and the solution was stirred for 1.5 h. Magnesium sulphate was added and the solution stirred for a further 2h. Filtration through a Celite plug yielded a clear yellow solution. The solvent was evaporated to dryness to yield the crude product, which was purified by recrystallisation from ethyl acetate/hexane to give the product as a pale yellow solid (3.60 g, 19 mmol, 35 %), mp 75-76°C (lit[1]. 78°C). ^{1}H NMR (300 MHz, $CDCl_3$): δ 2.93 (3H, s, CH_3), 7.48 (1 H, d, J = 8.1, H3), 7.57 (1 H, dd, J = 8.1, 4.2, H8) , 7.69 (1 H, d, J = 8.7, H6), 7.71 (1 H, d, J = 8.7, H5), 8.09 (1 H, d, J = 8.1, H4), 8.19 (1 H, dd, J = 8.1, 1.8, H7), 9.18 (1 H, dd, J = 4.2, 1.8, H9). ^{13}C NMR (75 MHz, $CDCl_3$): δ 22.9 (CH_3), 122.8 (C8), 123.7 (C3), 125.5 (C6), 126.5 (C5), 126.7 (qAr), 128.8 (qAr), 136.1 (C7), 136.2 (C4), 145.7 (qAr), 146.0 (qAr), 150.3 (C9), 159.5 (C2). m/z (ES^+) 195 (MH^+), 217 (MNa^+), 411 (M_2Na^+).

2-Methyl-1,10-phenanthroline-5,6-dione[1] (7)

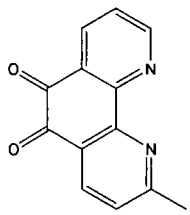

A mixture of 2-methyl-1,10-phenanthroline (2.00 g, 10.3 mmol) and potassium bromide (12.25 g, 102.9 mmol) was placed in an ice bath. Cold sulphuric acid (43 ml) was added carefully to the flask in a dropwise fashion, which turned the solution to a dark reddish colour. Concentrated nitric acid was then added in a similar way and the solution was boiled under reflux overnight. The mixture was cooled, poured into water (500 ml) and neutralised by addition of potassium hydroxide pellets. The product was extracted into dichloromethane (4 × 300 ml), which was dried over

K_2CO_3 and removed under reduced pressure to yield a yellow solid. Purification was achieved by chromatography on silica (gradient elution: CH_2Cl_2 to 1% CH_3OH-CH_2Cl_2, R_f = 0.34 (5% MeOH-CH_2Cl_2) to yield the product as a yellow solid (1.55 g, 67%), m.p. 98-100°C (lit[1]. 98-100°C). ^{1}H NMR (300 MHz, $CDCl_3$): δ 2.84 (3 H, s, CH_3), 7.43 (1 H, d, J = 8.1, H3), 7.56 (1 H, dd, J = 7.8, 4.8, H8), 8.38 (1 H, d, J = 8.1, H4), 8.48 (1 H, dd, J = 8.1, 2.1, H7), 9.13 (1H, dd, J = 4.8, 1.8, H9). ^{13}C (75 MHz, $CDCl_3$): δ 26.2 (CH_3), 125.6 (C8), 125.9 (C3), 126.2(q Ar), 128.3 (q Ar), 137.5 (C7), 137.7 (C4), 152.7 (q Ar), 153.2 (q Ar), 156.6 C9, 167.4 (C2), 178.7 (C5), 192.2 (C6). m/z (ES^+) 246 (MNa^+).

Diethyl-2,3-diaminobutane-1,4-dicarboxylate dihydrochloride[2] (11)

A suspension of 2,3-diamino-1,4-butanedioic acid (2.5 g, 16.9 mmol) in dry ethanol was saturated with HCl. The reaction mixture was boiled under reflux for 48 h. The product was obtained as white solid by removing part of the solvent under reduced pressure and filtration of the obtained precipitate. The product was obtained as a white solid (2.37 g, 8.6 mmol, 51%), m.p. 181-183°C (lit[2]. 178°C). ^{1}H NMR (300 MHz, d_6-DMSO): 1.21 (6H, t, J = 7.2, $OCH_2C\underline{H_3}$), 4.22 (4H, q, J = 7.2, OCH_2), 4.843 (2H, s, CH), 9.24 (6H, bs, NH_3^+). ^{13}C NMR (75 MHz, DMSO): δ 19.1 (CH_3), 57.7 (CH), 68.5 (CH_2), 170.3 (CO).

Diethyl 7-methyldipyrido[3,2-a:2',3'-c]quinoxaline-2,3-dicarboxylate (12)

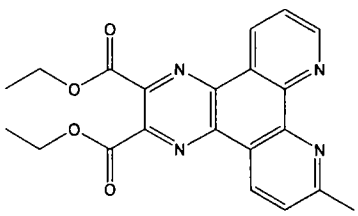

A solution of 2-methyl-1,10-phenanthroline-5,6-dione (1.5 g, 6.7 mmol) and the dihydrochloride of diethyl-2,3-diamino-butane-1,4-dicarboxylate (1.9 g, 6.9 mmol) in dry EtOH (150 ml) was boiled under reflux overnight. The reaction mixture was allowed to cool to 20°C and activated MnO_2 (13 g, 150 mmol) was added. The reaction mixture was stirred at room temperature for 5 h. Solvent was removed under reduced pressure. The residue was dissolved in an aqueous solution of EDTA (pH 7) and CH_2Cl_2. Layers were separated and the aqueous solution was extracted with CH_2Cl_2 (3 × 100 ml). The combined organic extracts were dried over Na_2SO_4 and

solvent was removed under reduced pressure to give the crude product. Purification was achieved by chromatography on alumina (CH_2Cl_2). The product was obtained as a light yellow solid (900 mg, 2.3 mmol, 34%), m.p. > 225°C (decomp). ^{1}H NMR (300 MHz, $CDCl_3$): δ 1.50 (6H, t, J = 7.2, $OCH_2C\underline{H}_3$), 3.02 (3H, s, CH_3), 4.59 (4H, q, J = 7.2, OCH_2), 7.71 (1H, d, J = 8.4, H6), 7.83 (1H, dd, J = 8.1, 4.5, H11), 9.38 (1H, dd, J = 4.5, 1.5, H10), 9.42 (1H, d, J = 8.4, H5), 9.57 (1H, dd, J = 8.1, 1.5, H12). ^{13}C NMR (75 MHz, $CDCl_3$): δ 14.2 ($OCH_2C\underline{H}_3$), 26.1 (CH_3), 63.1 (OCH_2), 124.1 (q Ar), 124.3 (C6), 124.6 (C11), 134.5 (C12), 134.6 (C5), 139.9 (q Ar), 140.6 (q Ar), 143.6 (q Ar), 144.4 (q Ar), 147.9 (q Ar), 148.2 (q Ar), 153.5 (C10), 163.6 (C7), 165.0 (CO), 165.1 (CO). m/z (ES^+) 391 (MH^+), 413 (MNa^+). HRMS (ES^+) 391.1399 ($C_{21}H_{19}N_4O_4$ requires: 391.1401) (MH^+).

Diethyl-7-carboxaldehyde-dipyrido[3,2-f:2',3'-h]quinoxaline-2,3-dicarboxylate (13)

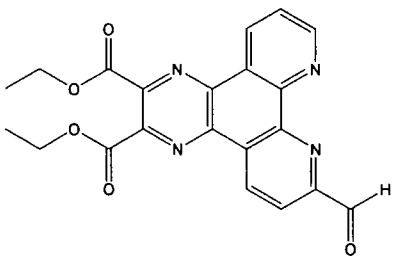

Selenium dioxide (480 mg, 4.33 mmol) was added to a solution of diethyl 7-methyldipyrido[3,2-a:2',3'-c]quinoxaline-2,3-dicarboxylate (810 mg, 2.07 mmol) in dioxane (170 ml). The mixture was boiled under reflux for 4 h and was allowed to cool down afterwards. The reaction mixture was filtered through a Celite plug. The solvent was removed under reduced pressure to give the crude product, which was used without further purification. ^{1}H NMR (200 NMR, $CDCl_3$): δ1.52 (6H, t, J = 7.2, $OCH_2C\underline{H}_3$), 4.60 (4H, q, J = 7.2, OCH_2), 7.92 (1H, dd, J = 8.4, 4.6, H11), 8.46 (1H, d, J = 8.2, H5), 9.43 (1H, dd, J = 4.6, 1.8, H10), 9.61 (1H, dd, J = 8.4, 1.8, H12), 9.74 (1H, dd, J = 8.4, 0.8, H6), 10.60 (1H, d, J = 0.8, COH). ^{13}C NMR (75 MHz, $CDCl_3$): δ 14.2 (CH_3), 63.3 (CH_2), 121.7 (C5), 125.0 (C11), 126.8 (q Ar), 129.2 (q Ar), 134.7 (C12), 136.0 (C6), 139.5 (q Ar), 141.2 (q Ar), 144.5 (q Ar), 145.3 (q Ar), 147.8 (q Ar), 148.4 (q Ar), 153.9 (C10), 154.8 (C7), 164.6 (CO ester), 164.7 (CO ester), 193.7 (CO aldehyde). m/z (ES^+) 459 (MNa^+ + MeOH). HRMS (ES^+) 437.1454 ($C_{22}H_{21}N_4O_6$ requires: 437.1456) (MH^++MeOH).

Diethyl 7-(hydroxymethyl)dipyrido[3,2-f:2',3'-h]quinoxaline-2,3-dicarboxylate (14)

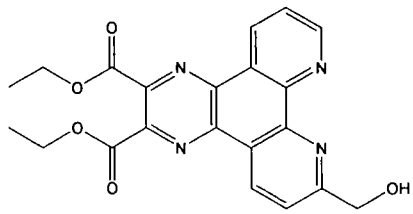

Sodium cyanoborohydride (130 mg, 2.07) was added to a solution of diethyl 7-carboxaldehyde-dipyrido[3,2-f:2',3'-h]quinoxaline-2,3-dicarboxylate (840 mg, 2.07 mmol) in $CHCl_3$-EtOH 7 : 1 (105 ml). The reaction mixture was boiled under reflux for 4h. The reaction mixture was poured into concentrated Na_2CO_3 (150 ml). The organic phase was separated and the aqueous layer was extracted with $CHCl_3$ (4 × 120 ml). The organic layer was dried over K_2CO_3, filtered an the solvent removed under reduced pressure to give the crude product, which was purified by recrystallisation from $CHCl_3$/hexane to yield a pale yellow-green solid (400 mg, 0.98 mmol, 48%), m.p. > 195°C (decomp). ^{1}H NMR (300 MHz, $CDCl_3$): δ 1.51 (6 H, t, J = 7.2, $OCH_2C\underline{H}_3$), 4.59 (4H, q, J = 7.2, OCH_2), 5.24 (2H, s, CH_2OH), 7.83 (1H, dd, J = 8.1, 4.5, H11), 7.94 (1H, d, J = 8.4, H6), 9.30 (1H, dd, J=4.5, 1.8, H10), 9.53 (1H, d, J = 8.4, H5), 9.60 (1H, dd, J = 8.1, 1.8, H12). ^{13}C NMR (75 MHz, $CDCl_3$): δ 14.4 (CH_3), 63.1 (OCH_2), 66.0 (CH_2OH), 121.9 (C6), 124.5 (C11), 125.3 (qAr), 126.5 (qAr), 134.6 (C12), 135.1 (C5), 140.0 (q Ar), 140.4 (q Ar), 144.0 (q Ar), 144.4 (q Ar), 147.5 (q Ar), 148.0 (q Ar), 153.4 (C10), 164.7 (C7), 164.9 (CO), 165.0 (CO). m/z (ES^+) 429 (MNa^+). HRMS (ES^+) 407.1350 ($C_{21}H_{19}N_4O_5$ requires: 407.1350) (MH^+).

Diethyl 7-(chloromethyl)dipyrido[3,2-f:2',3'-h]quinoxaline-3,2-dicarboxylate (15)

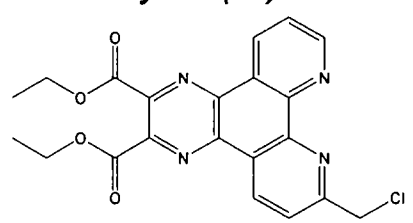

Phosphorus trichloride (473 mg, 3.44 mmol) was added to a solution diethyl 7-(hydroxymethyl)dipyrido[3,2-f:2',3'-h]quinoxaline-2,3-dicarboxylate (350 mg, 0.86 mmol) in $CHCl_3$ (150 ml). The reaction mixture was heated under reflux for 6 h and allowed to cool down to room temperature afterwards. The reaction was quenched by addition of concentrated aqueous Na_2CO_3 solution (150 ml). The layers were

separated and the water was extracted with CH_2Cl_2 (3 × 150ml) and $CHCl_3$ (1 × 150 ml). The organic layer was dried by K_2CO_3. The solvent was removed under reduced pressure to give the crude product. Purification was achieved by chromatography on alumina (gradient elution: CH_2Cl_2 to 2% CH_3OH-CH_2Cl_2) The product was obtained as a yellow glass (95 mg, 0.22 mmol, 26 %). ^{1}H NMR (300 MHz, $CDCl_3$): δ 1.45 (6H, t, J = 7.2, $OCH_2C\underline{H}_3$), 4.53 (4H, q, J = 7.2, OCH_2), 5.07 (2H, s, CH_2Cl), 7.78 (1H, dd, J = 8.1, 4.5, H11), 8.05 (1H, d, J = 8.4, H6), 9.31 (1H, dd, J = 4.5, 1.8, H10), 9.50 (1H, dd, J = 8.1, 1.8, H12), 9.53 (1H, d, J = 8.7, H5). ^{13}C NMR (75 MHz, $CDCl_3$): δ 14.4 (CH_3), 47.3 (CH_2Cl), 63.2 (OCH_2), 123.8 (C11), 124.6 (C6), 125.6 (q Ar), 126.6 (q Ar), 134.5 (C12), 135.7 (C5), 140.1 (q Ar), 140.4 (q Ar), 144.3 (q Ar), 144.4 (q Ar), 147.6 (q Ar), 148.1 (q Ar), 153.8 (C10), 161.0 (C7), 165.0 (CO), 165.1 (CO). m/z (ES^+) 447 (MNa^+). HRMS (ES^+) 425.1012 ($C_{21}H_{18}ClN_4O_4$ requires: 425.1011) (MH^+).

1,4,7-Tris(tert-butoxycarbonylmethyl)-1,4,7,10-tetraazacyclododecane[3] (33)

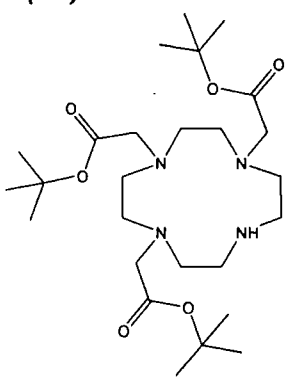

A solution of *t*-butyl bromoacetate (10.3 g, 52.8 mmol) in acetonitrile (82 ml) was added dropwise to a stirred mixture of 1,4,7,10-tetraazacyclododecane (3 g, 17.4 mmol), $NaHCO_3$ (4.42 g, 52.6 mmol) and 4 Å molecular sieves in acetonitrile (15 ml). The reaction mixture was stirred overnight at room temperature, filtered and the solvent was removed under reduced pressure. The residue was purified by chromatography on silica (CH_2Cl_2 followed by CH_2Cl_2, THF 7:3 to Ammonia, MeOH, THF, DCM 1:1:12:6). The product was obtained as white solid (2.45 g, 4.76 mmol, 27%), m.p. 189-192°C (lit[4]. 166-168°C). ^{1}H NMR (300 MHz, $CDCl_3$): δ 1.45 (27 H, CH_3), 2.90 (12H, br m, CH_2 ring), 3.85 (4H, br m, CH_2 ring), 3.28 (2H, s, CH_2), 3.37 (4H, s, CH_2). m/z (ES^+) 515.6 (MH^+).

1-(Diethyl-7'-methyldipyrido[3,2-f:2',3'-h]quinoxaline-2,3-dicarboxylate)-4,7,10-tris-tert-butoxycarbonylmethyl-1,4,7,10-tetraazacyclododecane (34)

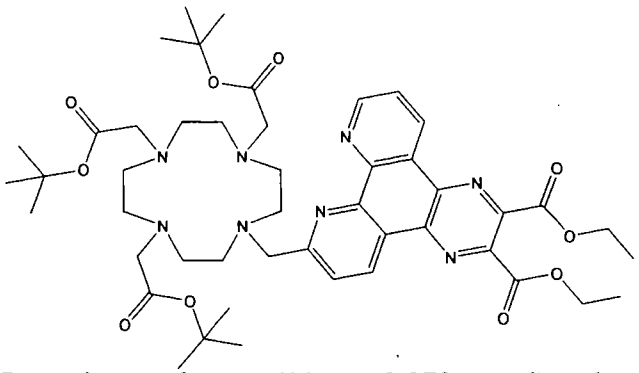

Potassium carbonate (11 mg, 0.079 mmol) and a catalytic amount of KI were added to a solution of 1,4,7-tris-*tert*-butoxycarbonylmethyl-1,4,7,10-tetratacyclododecane (40 mg, 0.077 mmol) and diethyl-7-(chloromethyl)dipyrido[3,2-f:2',3'-h]quinoxaline-2,3-dicarboxylate (35 mg, 0.083 mmol) in acetonitrile (5 ml). The mixture was heated under reflux overnight, under argon. The solution was filtered and the salts were washed with CH_2Cl_2. The solvent was removed under reduced pressure to give the crude product. Purification was achieved by chromatography on alumina (gradient elution: CH_2Cl_2 to 2% CH_3OH-CH_2Cl_2). The product was obtained as a yellow glass (40 mg, 0.44 mmol, 56%). ^{1}H NMR (200 MHz, $CDCl_3$): δ 1.08 (18 H, s, CH_3), 1.43 (9 H, s, CH_3), 1.50 (3H, t, *J* = 7.2, CH_3), 1.51 (3H , t, *J* = 7.2, CH_3), 2.25-3.58 (24 H, br m, CH_2 ring, NCH_2), 4.58 (2H, q, *J* = 7.2, OCH_2), 4.59 (2H, q, *J* = 7.2, OCH_2), 7.84 (1H, d, J = 8.4, H6), 7.86 (1H, dd, *J* = 8.2, 4.4, H11), 8.98 (1H, dd, *J* = 4.4, 1.8, H 10), 9.53 (1H, d, *J* = 8.4, H5), 9.59 (1H, dd, *J* = 8.2, 1.8, H12). ^{13}C NMR (75 MHz, $CDCl_3$): δ 14.4 ($OCH_2\underline{C}H_3$), 28.0 (CH_3), 28.3 (CH_3), 56.4-60.8 (CH_2 ring), 63.3 (OCH_2), 81.9-82.8 (CH_2CO,CH_2), 124.5 (C6), 124.7 (C11), 125.2 (q Ar), 126.7 (q Ar), 134.9 (C12), 135.2 (C5), 139.9 (q Ar), 140.2 (q Ar), 144.2 (q Ar), 144.7 (q Ar), 147.3 (q Ar), 147.7 (q Ar), 153.3 (C10), 163.2 (C7), 164.8 (COOEt), 164.9 (COOEt), 173.0 (CO). m/z (ES^+) 926 (MNa^+). HRMS (ES^+) 903.4963 ($C_{47}H_{67}N_8O_{10}$ requires 903.4975) (MH^+).

[TbL^3], TbDO3Adpq(COOH)$_2$

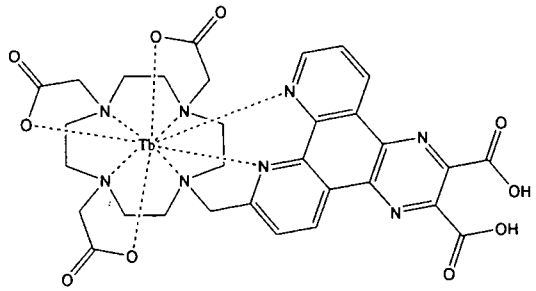

A solution of 1-(diethyl-7'-methyldipyrido[3,2-f:2',3'-h]quinoxaline-2,3-dicarboxylate)-4,7,10-tris(*tert*-butoxycarbonylmethyl)-1,4,7,10tetraazacyclododecane (20 mg, 0.022 mmol) in 6 M HCl (10 ml) was heated under reflux overnight. The solvent was removed under reduced pressure to give the hydrochloride salt of the ligand. The product was checked by ^{1}H NMR to ensure complete ester hydrolysis, and was used for complexation immediately. ^{1}H NMR (300 MHz, CD_3OD): δ 2.90-4.00 (24 H, br m, CH_2), 8.62 (2H, m, C6, C11), 9.57 (2H, m, C5, C12), 10.34 (H, d, J = 8.1, H10).

The ligand was dissolved in a mixture of methanol and water (1:1, 6 ml) and the pH was raised to 5.5 by addition of an aqueous solution of KOH (1 M). $TbCl_3.6H_2O$ (10 mg, 0.027 mmol) was added and the mixture heated at 90°C for 48 h. The pH was readjusted to 5.5 after 24 h. The solvents were removed under reduced pressure and the residue was dissolved water and the pH was adjusted to 7.0 and ion exchange (Dowex 50WH$^+$) was performed using a weakly acidic resin. The solution was freeze-dried to yield a white solid, which was purified by reverse phase HPLC (Method H, Appendix). $\lambda_{abs}(H_2O)$ 347 nm; $\tau_{Tb}(H_2O)$ 2.26 ms. HRMS (ES$^-$) 833.1339 ($C_{31}H_{30}N_8O_{10}{}^{159}Tb$ requires: 833.1344) (M-H$^-$).

[EuL^3], EuDO3Adpq(COOH)$_2$

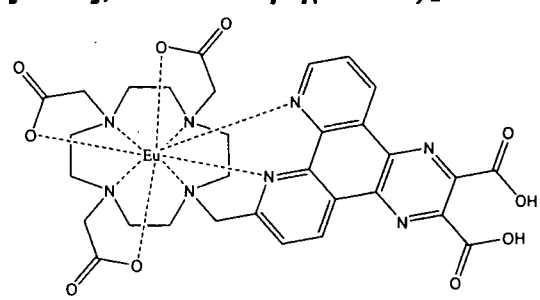

The europium complex was prepared in an analogous manner to the Tb example. The product was obtained as a white solid (10 mg, 12 μmol, 22 %). $\lambda_{abs}(H_2O)$ 347 nm; $\tau_{Eu}(H_2O)$ 1.07 ms. HRMS (ES^-) 825.1285 ($C_{31}H_{30}N_8O_{10}{}^{151}Eu$ requires: 825.1289) ($M-H^-$).

Thiobenzoic acid[5] (21)

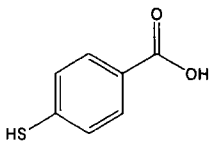

Concentrated hydrochloric acid (14.2 ml) was added to an ice cooled mixture of 4-aminobenzoic acid (10.0 g, 72.9 mmol) and ice (32.0 g). A solution of sodium nitrite (5.03 g, 72.9 mmol) in water (32 ml) was added slowly keeping the temperature below 5°C. A solution of potassium ethyl xanthate (11.7 g, 7.30) in water (15 ml) was added to a stirred solution of Na_2CO_3 (9.50 g, 89.6 mmol) in water (63 ml). The resulting solution was heated up to 70°C. The suspension from the diazotisation reaction was added slowly to the xanthate. The resulting mixture was kept under argon and was stirred at 70°C for 1 h. A solution of sodium hydroxide (11.7 g, 0.29 mol) in water (32 ml) was added, and reaction mixture was heated to reflux for 2 h and then allowed to cool down to room temperature. The reaction mixture was acidified to pH 2 with concentrated HCl. The precipitate formed was filtered off, washed with 1 M HCl and dried under reduced pressure to give the product as a white solid (10.5 g, 68.2 mmol, 94%), which was analysed by ^1H NMR and used without further purification, m.p. 219-222°C (lit[5]. 219-220°C). ^1H NMR (200 MHz, $CDCl_3$): 3.65 (1H, s, SH), 7.32 (2H, d, J = 8.4, H3, H5), 7.96 (2H, d, J = 8.2, H2, H6). ^{13}C NMR (75 MHz, $CDCl_3$): δ 126.3 (C1), 128.3 (C3, C5), 130.7 (C2, C6), 140.0 (C4), 171.5 (CO). m/z (ES^-) 153 ($M-H^-$). HRMS (ES^-) 153.0015 ($C_7H_5O_2S$ requires: 153.0016) ($M-H^-$).

Methyl-4-thiobenzoate[6] (25)

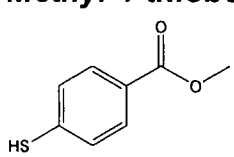

A solution of 4-thiobenzoic acid (5 g, 32.4 mmol) in dry MeOH (150 ml) was saturated with HCl. The reaction mixture was heated under reflux, under argon for 48 h. The solvent was removed under reduced pressure to give the product as a colourless solid (5.45 g, 32.4 mmol, 100%) which was used without further purification. ^{1}H NMR (300 MHz, $CDCl_3$): δ 3.60 (1H, s, SH), 3.88 (3H, s, CH_3), 7.27 (2H, d, J = 7.8, H3, H5), 7.88 (2H, d, J = 7.8, H2, H6). ^{13}C NMR (50 MHz, $CDCl_3$): δ 52.3 (CH_3), 127.4 (C1), 128.4 (C3, C5), 130.7 (C2, C6), 138.5 (C4), 166.8 (CO).

2-(4'-Methoxycarbonylphenylthio)-6-methyl-nicotinic acid (27)

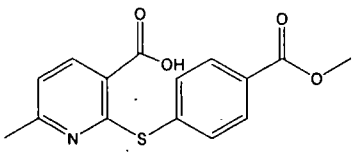

To a stirred solution of methyl-4-thiobenzoate (5 g, 29.7 mmol) and 2-chloro-6-methyl-nicotinic acid (4.25 g, 24.8 mmol) in DMF (28 ml) was added copper (I) bromide (220 mg, 1.53 mmol) and the resulting mixture was heated at 120°C for 10 minutes. K_2CO_3 (5.21 g, 37.7 mmol) was added, followed by DMF (20 ml). The reaction mixture was heated to 150°C overnight. The reaction mixture was allowed to cool down and diluted by water (150 ml). The resulting solution was washed with ether (4 × 150ml). The pH of the solution was adjusted to 4 by addition of acetic acid. The precipitated product was collected by filtration and dried under reduced pressure to yield the *title compound* as a pale yellow solid (4.8, 64 %), m.p. 190-192 °C; (Found: C, 59.23; H, 4.25; N, 4.47. $C_{15}H_{13}NO_4S$ requires: C, 59.39; H, 4.32; N, 4.62%); δ_H (DMSO, 500 MHz) 2.23 (3H, s, CH_3), 3.86 (3H, s, OCH_3), 7.11 (1H, d, J 7.8, H^5), 7.61 (2 H, d, J 8.1, $H^{2'}$, $H^{6'}$), 7.95 (2H, d, J 8.1, $H^{3'}$, $H^{5'}$), 8.13 (1H, d, J 7.8, H^4); δ_C (DMSO, 125 MHz) 24.7 (CH_3), 52.9 (OCH_3), 120.3 (C^5), 121.4 (C^3), 129.9 ($C^{4'}$), 129.9 ($C^{3'}$, $C^{5'}$), 135.5 ($C^{2'}$, $C^{6'}$), 138.4 ($C^{1'}$), 140.1 (C^4), 159.4 (C^2), 162.1 (C^6), 166.6 ($COOCH_3$), 167.7 (COOH); m/z (ESMS$^-$) 302 ([M-H]$^-$, 100%).

7-Methoxycarbonyl-2-methylazathioxanthone (30)

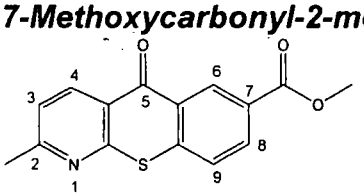

A mixture of 2-(4'-methoxycarbonylphenylthio)-6-methyl-nicotinic acid (4 g, 13.2 mmol) and polyphosphoric acid (120 ml) was heated to 120°C and vigorously stirred

for 24 h. The reaction was allowed to cool down to room temperature and was diluted by dry methanol (300 ml). The reaction mixture was heated under reflux for a further 16 h. The majority of methanol was removed under reduced pressure to give a sticky syrup, which was diluted by water to give 1 l of solution. The pH of the solution was adjusted to 7 by the addition of NaOH pellets and was extracted with $CHCl_3$ (3 × 300 ml). The solvent was removed under reduced pressure to yield the *title compound* as a greenish solid (3.25 g, 86 %), sublimes 190-194 °C. (Found: C, 62.38; H, 3.71; N, 4.81. $C_{15}H_{11}NO_3S$:0.25 H_2O requires: C, 62.36; H, 3.98; N, 4.85%); δ_H ($CDCl_3$) 2.69 (3H, s, CH_3), 3.99 (3H, s, OCH_3), 7.32 (1H, d, *J* 8.0, H^3), 7.70 (1H, d, *J* 8.5, H^9), 8.25 (1H, dd, *J* 8.5, 2.0, H^8), 8.58 (1H, d, *J* 8.0, H^4), 8.88 (1H, d, J 2.0, H^6); δ_C ($CDCl_3$, 125 MHZ) 25.2 (CH_3), 52.7 (OCH_3), 122.7 (C^3), 124.4 ($C^{4'}$), 127.0 (C^9), 128.8 ($C^{6'}$), 129.0 (C^7), 131.7 (C^6), 132.8 (C^8), 138.1 (C^4), 142.6 ($C^{9'}$), 157.8 ($C^{1'}$), 164.3 (C^2), 166.2 ($COOCH_3$), 180.1 (C^5); m/z ($ESMS^+$) 286 ($[M+H]^+$, 30%), 308 ($[M+Na]^+$, 100%), 593 ($[2M+Na]^+$, 15%).

3-Bromomethyl-7-methoxycarbonylazathioxanthone (31)

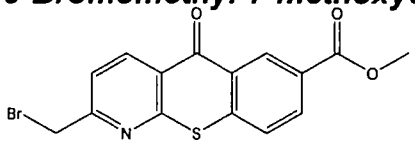

N-Bromosuccinimide (NBS) (175 mg, 0.98 mmol) and dibenzoyl peroxide (10 mg, 0.04 mmol) were added to a solution 7-methoxycarbonyl-2-methylazathioxanthone (500 mg, 1.75 mmol) in CCl_4 (30 ml). The reaction mixture was heated under reflux for 2 h after which NBS (175 mg, 0.98 mmol) and dibenzoyl peroxide (10 mg, 0.04 mmol) were added again. The reaction mixture was heated under reflux for a further 34 h. Further additions of dibenzoyl peroxide were made at 4 h (10 mg, 0.04 mmol), 6.5 h (10 mg, 0.04 mmol), 9.5 h (20 mg, 0.08 mmol), 24 h (10 mg, 0.04 mmol) and 29.5 h (10 mg, mmol) after the reaction start. Further additions of NBS (90 mg, 0.51 mmol) were made at 24 h and 29.5 h after the reaction start. The reaction mixture was allowed to cool down, filtered and the solvent was removed under reduced pressure to give the crude product. The residue was purified by chromatography on silica (gradient elution: CH_2Cl_2-Toluene 1:1 to 2% CH_3OH-49% CH_2Cl_2-49% toluene) to yield the *title compound* as a light yellow solid (90 mg, 25%), R_f 0.42 (Silica, 2% MeOH : 49% toluene : 49% CH_2Cl_2), sublimes 186-190 °C. (Found: C, 49.19; H, 2.70; N, 3.84. $C_{15}H_{10}BrNO_3S$, requires: C, 49.47; H, 2.77; N, 3.85%); δ_H ($CDCl_3$, 500 MHz)

4.00 (3H, s, CH_3), 4.61 (2H, s, CH_2), 7.61 (1H, d, *J* 8.5, H^3), 7.71 (1H, d, *J* 8.5, H^9), 8.28 (1H, dd, *J* 8.5, 1.5, H^8), 8.82 (1H, d, *J* 8.5, H^4), 9.20 (1H, d, *J* 1.5, H^6); δ_C ($CDCl_3$, 125 MHz) 32.4 (CH_2), 52.8 (CH_3), 122.3 (C^3), 125.8 ($C^{4'}$), 127.1 (C^9), 128.9 ($C^{6'}$), 129.2 (C^7), 131.8 (C^6), 133.2 (C^8), 139.3 (C^4), 142.3 ($C^{9'}$), 157.8 ($C^{1'}$), 161.5 (C^2), 166.1 ($COOCH_3$), 179.8 (C^5); m/z ($ESMS^+$) 364 ($[M+H]^+$, 20%), 386 ($[M+Na]^+$, 100%), 749 ($[2M+Na]^+$, 55%).

1-(7-Methoxycarbonylazathioxanthone)-4,7,10-tris-tert-butoxycarbonylmethyl-1,4,7,10-tetraazacyclododecane (35)

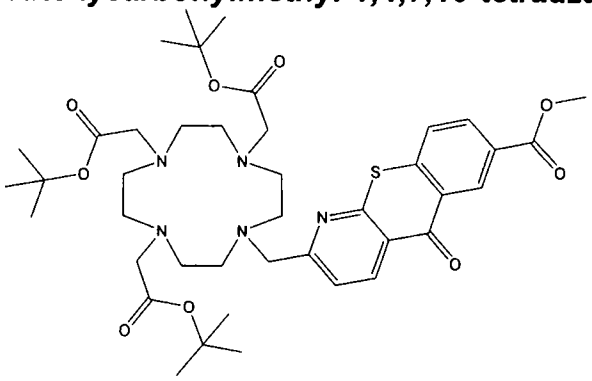

A solution of 4-aza-3-bromomethyl-8-methoxycarbonylthioxanthone (90 mg, 0.25 mmol), 1,4,7-tris-*tert*-butoxycarbonylmethyl-1,4,7,10-tetraazacyclododecane (130 mg, 0.25 mmol) and Cs_2CO_3 (84 mg, 0.26 mmol) in acetonitrile (5 ml) was heated under reflux for 20 h. The solvent was removed under reduced pressure, the residue was dissolved in CH_2Cl_2 (20 ml) and the solvent was removed under reduced pressure again. The residue was dissolved in CH_2Cl_2 (20 ml), the suspension was filtered to remove the salts and the solvent was removed under reduced pressure. The purification was achieved by chromatography on alumina (gradient elution: CH_2Cl_2 to 5% CH_3OH-CH_2Cl_2) to give the desired product as a pale yellow glass (60 mg, 0.075 mmol, 30 %) R_f 0.48 (Alumina, 5% MeOH:CH_2Cl_2). δ_H ($CDCl_3$, 500 MHz) 1.32 (18 H, s, CH_3), 1.59 (9H, s, CH_3), 2.05-3.90 (24H, br m, CH_2 ring, CH_2CO, CH_2), 3.99 (3H, s, OCH_3), 7.44 (1H, d, *J* 8.5, H^9), 7.52 (1H, d, *J* 8.5, H^3), 8.26 (1H, dd, *J* 8.5, 1.5, H^8), 8.81 (1H, d, *J* 8.5, H^4), 9.21 (1H, d, *J* 1.5, H^6); δ_C ($CDCl_3$, 125 MHz) 21.6 (CH_2), 28.3 (CH_3), 52.9 (OCH_3), 49.5-58.2 (CH_2 ring, CH_2CO), 82.4 (C^{tbutyl}), 123.0 (C^3), 125.4 ($C^{4'}$), 126.3 (C^9), 128.8 ($C^{6'}$), 129.1 (C^7), 131.8 (C^6), 133.2 (C^8), 138.9 (C^4), 142.3 ($C^{9'}$), 158.4 ($C^{1'}$), 164.5 (C^2), 166.0 (COOMe), 173.2 (COO*t*Bu), 179.9 (C^5); m/z ($ESMS^+$) 798 ($[M+H]^+$, 20%), 820 ($[M+Na]^+$, 100%). Found: (ES^+) 820.3952 ($C_{41}H_{59}N_5O_9SNa$ requires 820.3926, $[M+Na]^+$).

[TbL^5], TbDO3AthxCOOMe

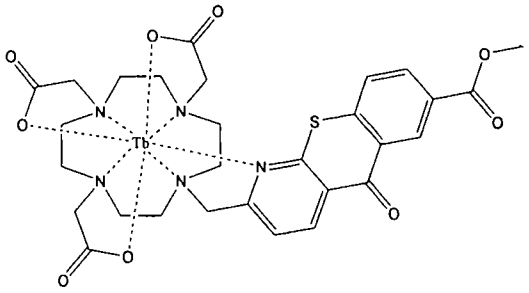

The solution of 1-(4-aza-8-methoxycarbonylthioxanthone)-4,7,10-tris-*tert*-butoxycarbonylmethyl-1,4,7,10-tetraazacyclododecane (42 mg, 0.053 mmol) in TFA (2 ml) and CH_2Cl_2 (0.1 ml) was stirred at room temperature for 18 h. The solvents were removed under reduced pressure. The residue was repeatedly (3 ×) dissolved in CH_2Cl_2 and the solvent removed under reduced pressure. The residue was analysed by NMR and the reaction mixture was stirred on for a further 12 h to ensure completion. Solvents were removed under reduced pressure and the same procedure was used to remove any excess of TFA. The residue was dissolved in water (5 ml) and MeOH (5 ml) and $TbCl_3.6H_2O$ (18 mg, 0.049 mmol) was added. The pH of the solution was adjusted to 5.5 by the addition of aqueous KOH solution (1 M). The reaction mixture was stirred at 65°C overnight. The pH dropped to 2.8 and was adjusted back to 5.5 and the mixture was stirred at 65°C for further 2 h. Methanol was removed under reduced pressure and the remaining solution was diluted with water (10 ml). The reaction mixture was filtered. Water was removed by freeze drying and the residue was purified by HPLC (Method G, Appendix) to yield the *title compound* (9 mg, 0.011 mmol, 22 %). λ_{abs}(MeOH) 372 nm; ε(MeOH) 5360 M^{-1} cm^{-1}, τ_{Tb} (H_2O) 0.53 ms, τ_{Tb}(D_2O) 0.62 ms. HRMS (ES^-) 784.1078 ($C_{29}H_{31}N_5O_9{}^{32}S^{159}Tb$ requires: 784.1091) ($M-H^-$)

[EuL^5], EuDO3AthxCOOMe

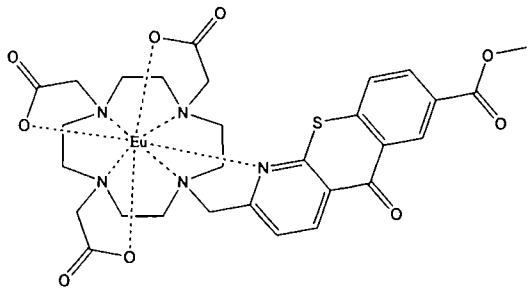

The europium complex was prepared in an analogous manner to the Tb example. The product was obtained as a white solid. (10 mg, 17%). λ_{abs}(MeOH) 372 nm; ε(MeOH) 5360 M^{-1} cm^{-1}, $\tau_{Eu}(H_2O)$ 0.51 ms, $\tau_{Eu}(D_2O)$ 1.62ms; q^{Eu} = 1.31. Found: (ES^-) 778.1060 ($C_{29}H_{31}EuN_5O_9S$ requires: 778.1061) ($M\text{-}H^-$).

2-Phenoxy-6-methyl-nicotinic acid (62)

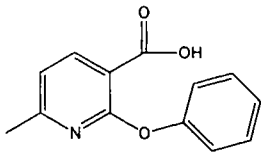

2-Chloro-6-methyl-nicotinic acid (3 g, 17.5 mmol) and phenol (7.8 g, 83.2 mmol) were added to a solution of NaOMe, freshly made from sodium (0.84 g, 36.5 mmol) and dry MeOH (20 ml). The reaction was stirred under an argon atmosphere for 15 minutes and the solvent was removed under reduced pressure. The residue, a yellow oil, was heated to 180°C for 12 h. The reaction mixture was allowed to cool down and dissolved in water. The aqueous solution was washed with Et_2O. The pH of the solution was decreased to 4 by the addition of acetic acid and the precipitated product was collected by filtration. The product was dried under a high vacuum (0.5 g, 2.18 mmol, 12%), mp 108-110 °C. ^{1}H NMR (300 MHz, $CDCl_3$): δ 2.40 (3H, s, CH_3), 7.03 (1H, d, *J* 7.8, H^5), 7.18 (2 H, d, *J* 7.6, $H^{2'}$), 7.29 (1H, t, *J* 7.6, $H^{4'}$), 7.44 (2H, t, *J* 7.6, $H^{3'}$), 8.41 (1H, d, *J* 7.8, H^4). ^{13}C NMR (75 MHz, $CDCl_3$): δ 24.4 (CH_3), 110.0 (C^3), 119.4 (C^5), 121.8 ($C^{2'}$), 125.8 ($C^{4'}$), 129.6 ($C^{3'}$), 143.6 (C^4), 152.0 ($C^{1'}$), 160.2 (C^2), 163.2 (C^6), 164.7 (COOH). m/z (ES^-) 228.0 (M-H). HRMS (ES^+) 230.0805 ($C_{13}H_{12}NO_3$ requires: 230.0812) (MH^+).

2-Methyl-1-azaxanthone (55)

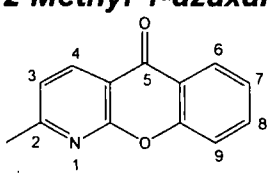

The mixture of 2-phenyloxy-6-methyl-nicotinic acid (1.2 g, 5.23 mmol) and polyphosphoric acid (50 g) was stirred at 120°C for 22 hours. The reaction mixture was dissolved in water (250 ml) and the pH of the resulting solution was increased to 12 using KOH pellets. The aqueous solution was extracted with $CHCl_3$ (3 × 200 ml).

The combined organic extracts were dried over Na_2SO_4 and the solvent was removed under reduced pressure to give the product as an off white solid (1.02 g, 4.83 mmol, 92.4 %), m.p. 110-112 °C. ^{1}H NMR (300 MHz, $CDCl_3$): δ 2.71 (3H, s, CH_3), 7.30 (1H, d, *J* 7.8, H^3), 7.43 (1 H, ddd, *J* 8, 7, 0.9, H^7), 7.61 (1H, dd, *J* 8, 0.9, H^9), 7.77 (1H, ddd, *J* 8, 7, 1.5, H^8), 8.32 (1H, dd, *J* 8, 1.5, H^6), 8.60 (1H, d, *J* 7.8, H^4). ^{13}C NMR (75 MHz, $CDCl_3$): δ 25.2 (CH_3), 114.3 ($C^{4'}$), 118.6 (C^9), 121.3 (C^3), 121.8 ($C^{6'}$), 124.7 (C^7), 126.7 (C^6), 135.5 (C^8), 137.4 (C^4), 155.8 ($C^{9'}$), 160.0 ($C^{1'}$), 165.2 (C^2), 177.7 (C^5). m/z (ES^+) 233.7 ($M+Na^+$). HRMS (ES^+) 212.0707 ($C_{13}H_{10}NO_2$ requires: 212.0706) (MH^+).

2-Bromomethyl-1-azaxanthone (63)

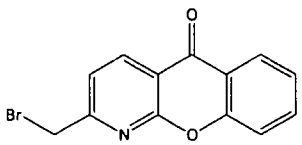

N-Bromosuccinimide (450 mg, 2.53 mmol) and dibenzoylperoxide (20 mg, 82.6 μmol) were added to a solution of 2-methylazaxanthone (1.02 g, 4.83 mmol) in CCl_4 (50 ml). The reaction mixture was refluxed for 18 hours. Further additions of N-bromosuccinimide (2 × 450 mg) and dibenzoylperoxide (20 mg and 30 mg) were made after 2.5 and 5.5 hours from the start of the reaction. The reaction mixture was filtered and the solvent was removed under reduced pressure. The residue was purified by chromatography on silica (CH_2Cl_2/toluene 1:1 to 1% MeOH) to give the product as an off-white solid (380 mg, 1.31 mmol, 27%), mp 169-171°C. ^{1}H NMR (300 MHz, $CDCl_3$): δ 4.61 (3H, s, CH_2Br), 7.45 (1H, ddd, *J* 8, 7.2, 1.0, H^7), 7.58 (1 H, d, *J* 8, H^3), 7.62 (1H, d, *J* 8, H^9), 7.80 (1H, ddd, *J* 8, 7.2, 1.6, H^8), 8.31 (1H, dd, *J* 8, 1.6, H^6), 8.72 (1H, d, *J* 8, H^4). ^{13}C NMR (75 MHz, $CDCl_3$): δ 32.3 (CH_2Br), 116.1 ($C^{4'}$), 118.6 (C^9), 120.9 (C^3), 121.7 ($C^{6'}$), 125.0 (C^7), 126.8 (C^6), 135.9 (C^8), 138.8 (C^4), 155.8 ($C^{9'}$), 158.8 (C'^1), 162.1 (C^2), 177.2 (C^5). m/z (ES^+) 290.1 (MH^+). HRMS (ES^+) 289.9809 ($C_{13}H_9BrNO_2$ requires: 289.9811) (MH^+).

1-(2-Azaxanthonylmethyl)4,7,10-tris(tert-butoxycarbonylmethyl)-1,4,7,10-tetraazacyclododecane (64)

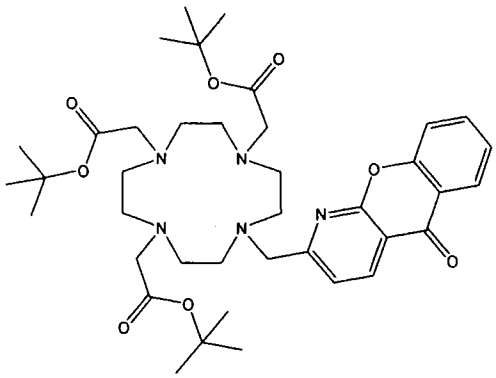

A solution of 2-bromomethylazaxanthone (200 mg, 0.69 mmol), 1,4,7-tris(*tert*-butoxycarbonylmethyl)-1,4,7,-tetraazacyclododecane (319 mg, 0.62 mmol) and Cs_2CO_3 (210 mg, 0.65 mmol) in acetonitrile (15 ml) was heated to reflux under argon atmosphere for 16 h. The solvent was removed in vacuo. The residue was dissolved in DCM, filtered and the solvent was removed in vacuo. The residue was purified by column chromatography on alumina (CH_2Cl_2 to 2% MeOH) to give the product as a yellow glass (300 mg, 0.41 mmol, 66%). ^{1}H NMR (300 MHz, $CDCl_3$): δ 1.46 (27 H, s, *t*-Bu), 3.15 (16 H, br m, ring), 3.45 (2H, s, CH_2 arm), 3.59 (4H, s, CH_2 arm), 4.59 (2H, s, CH_2), 7.45 (1H, t, *J* 8, H^7), 7.53 (1H, d, *J* 8, H^3), 7.60 (1H, d, *J* 8, H^9), 7.77 (1 H, t, *J* 8, H^8), 8.31 (1H, d, *J* 8, H^6), 8.67 (1 H, d, *J* 8, H^4). ^{13}C (125 MHz, $CDCl_3$): δ 28.7 (CH_3), 48.0 (ring C), 50.2 (ring C), 54.8 (ring C), 55.6 (ring C), 58.5 (CH_2-AzaH), 79.8 (^{t}Bu), 115.4 ($C^{9'}$), 118.7 (C^9), 121.9 (C^3), 124.9 (C^7), 126.9 (C^6), 135.8 (C^8), 137.4 (C^4), 155.9 ($C^{6'}$), 156.5 ($C^{4'}$), 159.9 ($C^{1'}$), 161.1 (C^2), 165.3 (COO*t*Bu), 177.7 (C^5). m/z (ES^+) 746.4 ($M+Na^+$), 724.4 (MH^+). HRMS (ES^+) 724.4279 ($C_{39}H_{58}N_5O_8$ requires: 724.4280) (MH^+).

[TbL^{19}], TbDO3AAzaHNOx

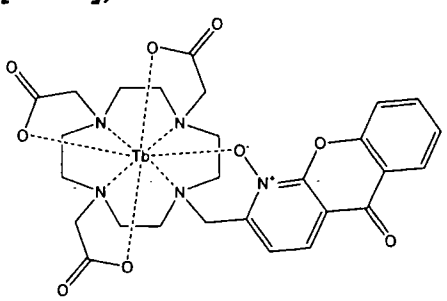

The solution of 1-(2-azaxanthonylmethyl)-4,7,10-tris(*tert*-butoxycarbonylmethyl)-1,4,7,10-tetraazacyclododecane (50 mg, 0.069 mmol) in TFA (2 ml) and DCM (1 ml)

was stirred under an argon atmosphere at room temperature overnight. The solvent was removed under reduced pressure and the removal of *t*-butyl esters was verified by ^{1}H NMR. The residue was dissolved in TFA (0.5 ml) and H_2O_2 (0.15 ml). The reaction mixture was heated to reflux under argon atmosphere. Further three additions of TFA (0.5 ml) and H_2O_2 (0.15 ml) were made. Reaction carried on for 8h. The solvents were removed under reduced pressure. $TbCl_3.6H_2O$ (50 mg) was added to the solution of the residue in H_2O (2 ml) and MeOH (1.5 ml). The pH was adjusted to 6 and the reaction mixture was heated to 60°C stirring under argon atmosphere. The pH dropped and was raised back to 6 during the course of the reaction. A precipitate formed during the reaction, which was removed by centrifugation. The solvent was removed under reduced pressure to give the product as a yellowish solid. $\lambda_{abs}(H_2O)$ 348 nm; λ_{abs}(MeCN) 344 nm; τ_{Tb}(MeCN) 1.08 ms.

[EuL^{19}], EuDO3AAzaHNOx

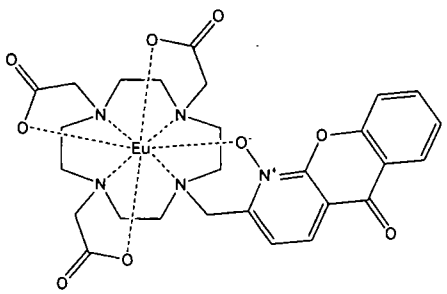

The europium complex was prepared in an analogous manner to the Tb example. The product was obtained as a yellowish solid. $\lambda_{abs}(H_2O)$ 348 nm; λ_{abs}(MeCN) 344 nm; τ_{Eu}(MeCN) 0.78 ms.

1,4,7-Tris(trifluoroethanoyl)-1,4,7,10-tetraazacyclododecane[7]

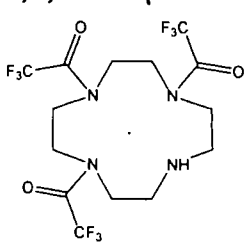

Ethyl trifluoroacetate (16.5 g, 13.8 ml, 0.12 mol) was added dropwise to a solution of cyclen (5g, 0.029 mol) and triethylamine (4.04 ml) in dry MeOH (25 ml) cooled to

0°C. The reaction mixture was stirred at room temperature under argon for 4 h. The solvent was removed under reduced pressure. The residue was purified by column chromatography on silica (CH_2Cl_2 to 5% MeOH) to give the product as a white solid (11.7 g, 0.025 mol, 86%), mp 77-80 °C. ^{1}H NMR (300 MHz, $CDCl_3$): δ 2.96 (4 H, m, NCH_2), 3.55 (8 H, m, NCH_2), 3.91 (4 H, m, CH_2). ^{13}C NMR (75 MHz, $CDCl_3$): δ 43.26-52.91 (NCH_2), 116.21 (q, CF_3, J_{CF} = 210), 157.12-157.96 (m, CO). ^{19}F NMR (188 MHz, $CDCl_3$): δ -69.36 (m, CF_3) . m/z (ES^+) 483.3 (MH^+).

1,4,7-Tris(trifluoroacetyl)-10-tert-butoxycarbonyl-1,4,7,10-tetraazacyclododecane[8]

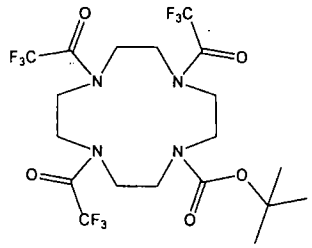

Di*tert*-butyl dicarbonate (1.42 g, 6.51 mmol) was added to a solution of 1,4,7-tris(trifluoroacetyl)-1,4,7,10-tetraazacyclododecane (2 g, 4.34 mmol) and triethylamine (0.3 ml) in dry MeOH (20 ml). The reaction mixture was stirred under argon at room temperature for 24 h after which further di*tert*butyl dicarbonate (1 g) was added. Further additions of di*tert*butyl carbonate (1 g) were made after 48 and 72 hours. The reaction was carried out over the period of 100 h. The solvent was removed under reduced pressure. The residue was purified by column chromatography on silica (CH_2Cl_2 to 7% ethyl acetate) to give the product as a white solid (540 mg, 0.96 mmol, 11%), mp 119-122 °C. ^{1}H NMR (300 MHz, $CDCl_3$): δ 1.47 (9 H, s, $C(CH_3)_3$), 3.20-3.95 (16 H, bm, NCH_2). ^{13}C NMR (75 MHz, $CDCl_3$): δ 27.98 (CH_3), 48.54-50.70 (NCH_2), 81.04 (C), 116.03 (q, CF_3, J_{CF} = 210), 156.67-158.70 (m, CO). ^{19}F NMR (188 MHz, $CDCl_3$): δ -69.70 (m, CF_3) . m/z (ES^+) 583.3 (MH^+).

1-Tertbutyloxycarbonyl-1,4,7,10-tetraazacyclododecane (71)

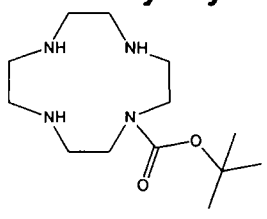

An aqueous solution of KOH (2 M, 6 ml) was added to a solution of 1,4,7-*tris*(trifluoroacetyl)-10-*tert*butoxycarbonyl-1,4,7,10-tetraazacyclododecane (3.0 g, 5.35 mmol) in a mixture of MeOH (30 ml) and water (12 ml). The reaction mixture was stirred at room temperature under argon for 8 h. The solvent was removed under reduced pressure. The residue was dissolved in CH_2Cl_2 (20 ml) and washed with concentrated aqueous Na_2CO_3 and NaCl solutions respectively. The organic phase was dried over K_2CO_3 and solvent was removed to yield the product as a glassy solid (1.0 g, 69%). ^{1}H NMR (300 MHz, $CDCl_3$): δ 1.39 (9 H, s, $C(CH_3)_3$), 2.64 (4 H, t, J = 4.5, NCH_2), 2.74 (8 H, q, J = 5.4, NCH_2), 3.35 (4 H, t, J = 5.4 Hz, NCH_2). m/z (ES^+) 273.3 (MH^+).

Benzyl diethoxyphosphine (72)

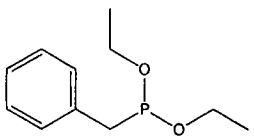

A solution of chlorodiethoxyphosphine (5 g, 31.9 mmol) in dry Et_2O (50 ml) was added dropwise to a solution of benzylmagnesium chloride in Et_2O (1 M, 32 ml) cooled to -15°C. The reaction mixture was warmed up and heated to reflux overnight. The reaction mixture was filtered and solvent was removed by distillation. The residue was purified by vacuum distillation (0.15 mbar, 52-56°C) to yield the product as a colourless liquid (2.5 g, 37 %). ^{1}H NMR (300 MHz, $CDCl_3$): δ 1.22 (6 H, t, J = 7.2, CH_3), 2.98 (2 H, d, J = 3.9, CH_2), 3.89 (4 H, m, OCH_2), 7.24 (5 H, m, phenyl). ^{31}P NMR (120 MHz): δ 171.0.

1,4,7-Tris(ethoxybenzylphosphinatomethyl)-10-tertbutoxycarbonyl-1,4,7,10-tetraazacyclododecane (73)

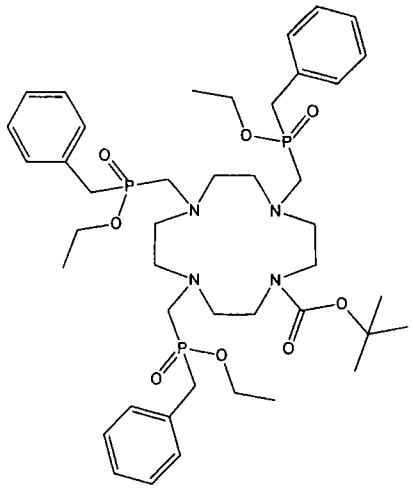

Benzyl diethoxyphosphine (1.4 g, 6.6 mmol) was added to a mixture of 1-*tert*butyloxycarbonyl-1,4,7,10-tetraazacyclododecane (0.4 g, 1.47 mmol) and paraformaldehyde (0.3 g) in dry THF (23 ml). The reaction mixture was heated to reflux for 8 h. The reaction mixture was filtered and the solvent was removed under reduced pressure. The residue was purified by column chromatography on alumina (CH_2Cl_2 to 6% MeOH) to yield the product as an oil (0.3 g, 24%). ^{1}H NMR (300 MHz, $CDCl_3$): δ 1.18 (9 H, m, CH_3), 1.39 (9H, s, $C(CH_3)_3$), 2.60-3.80 (28 H, m, NCH_2,PCH_2), 3.95 (6 H, m, OCH_2), 7.30 (15 H, m, Phenyl). ^{31}P NMR (120 MHz): δ 50.31. m/z (ES^+) 883.4 ($M+Na^+$).

1,4,7-Tris(ethoxybenzylphosphinatomethyl)-1,4,7,10-tetraazacyclododecane (74)

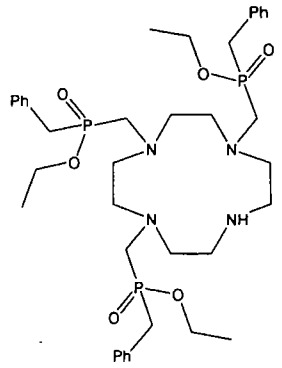

A solution of 1,4,7-*tris*(ethoxybenzylphosphinatomethyl)-10-*tert*butyloxycarbonyl-1,4,7,10-tetraazacyclododecane (450 mg, 0.523 mmol) in CH_2Cl_2 (10 ml) and TFA (20 ml) was stirred at room temperature under an argon atmosphere overnight. The

solvent was removed under reduced pressure. The residue was dissolved in CH_2Cl_2 (10 ml) and treated with saturated aqueous K_2CO_3 solution (10 ml). The product was extracted into CH_2Cl_2 and the combined organic extracts were dried over K_2CO_3. Solvent was removed under reduced pressure to give the product as a pale brown oil (330 mg, 0.434 mmol, 83%). ^1H NMR (300 MHz, $CDCl_3$): δ 1.18 (9 H, m, CH_3), 2.60-3.40 (28 H, m, NCH_2, PCH_2), 3.90 (6 H, m, OCH_2), 7.25 (15 H, m, Phenyl). ^{31}P NMR (120 MHz): δ 51.45. m/z (ES^+) 761.3 (MH^+).

1-(2-Methylazaxanthone)-4,7,10-tris(ethoxybenzylphosphinatomethyl)-1,4,7,10-tetraazacyclododecane (75)

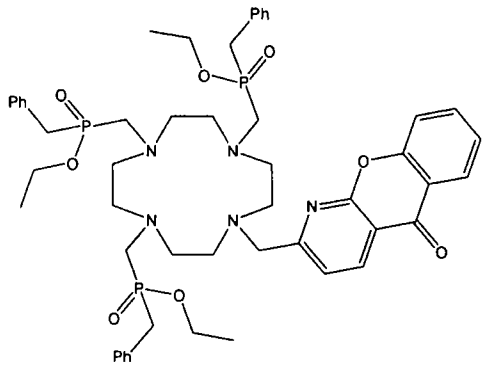

A solution of 1,4,7-*tris*(ethoxybenzylphosphinatomethyl)-1,4,7,10-tetraazacyclododecane (180 mg, 0.237 mmol), 2-bromomethyl-1-azaxanthone (76 mg, 0.262 mmol) and Cs_2CO_3 (77 mg, 0.236 mmol) in acetonitrile (20 ml) was heated to reflux under an argon atmosphere for 6 h. The reaction mixture was filtered and the solvent was removed under reduced pressure. The residue was purified by chromatography on alumina (CH_2Cl_2 to 2% MeOH) to give the product as a brown glass (120 mg, 0.124 mmol, 52%). ^1H NMR (300 MHz, $CDCl_3$): δ 1.13 (9H, s, CH_3), 2.4-3.4 (28H, br. m, macrocycle, PCH_2, $PhCH_2$), 3.70-4.15 (8H, br. m, OCH_2, CH_2), 7.26 (15 H, m, Ph), 7.41 (1H, m, H^7), 7.55 (2 H, m, H^3, H^9), 7.70 (1H, m, H^8), 8.28 (1H, m, H^6), 8.68 (1H, m, H^4). ^{31}P NMR (120 MHz): δ 49.87. m/z (ES^+) 970.4 (MH^+), 992.5 ($M+Na^+$).

[TbL^{22}], TbP$_3$Bn$_3$AzaH

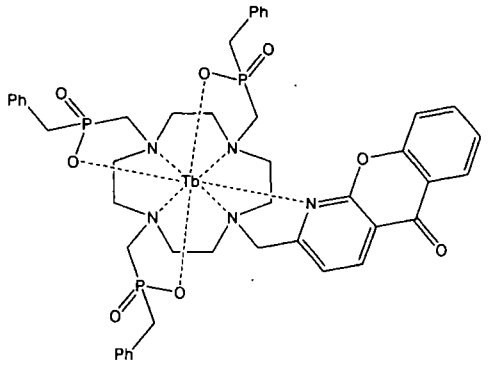

A solution of 1-(2-methylazaxanthone)-4,7,10-*tris*(ethoxybenzylphosphinatomethyl)-1,4,7,10-tetraazacyclododecane (35 mg, 36.1 μmol) in 6 M HCl (7 ml) was heated to reflux for 24 hours. The progress of the ester hydrolysis was monitored by ^{1}H and ^{31}P NMR. The solvent was removed under reduced pressure. The residue was dissolved in water (3 ml) and MeOH (3 ml) and $TbCl_3.6H_2O$ (15 mg, 40.2 μmol) was added. The pH of the reaction mixture was increased to 5.5 by the addition aqueous KOH solution (1 M). The reaction mixture was heated to 60°C overnight. The solvents were removed under reduced pressure and the residue was purified by column chromatography on alumina (CH_2Cl_2 to 10% MeOH) to give the product as a light yellow solid (10 mg, 9.6 μmol, 27%). $\lambda_{abs}(H_2O)$ 335 nm; $\tau_{Tb}(H_2O)$ 3.63 ms, $\tau_{Tb}(D_2O)$ 3.58 ms, ϕ_{Tb} (H_2O) 44%; m/z (ES^+) 1043 (MH^+), 1065 ($M+Na^+$).

[EuL^{22}], EuP$_3$Bn$_3$AzaH

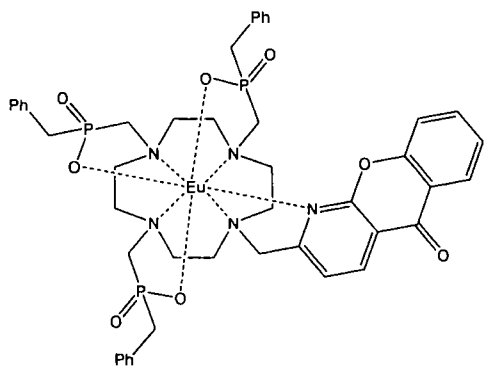

The europium complex was prepared in an analogous manner to the Tb example. The product was obtained as lightly brown solid (9 mg, 8.7 μmol, 21 %). $\lambda_{abs}(H_2O)$ 335 nm; $\tau_{Eu}(H_2O)$ 1.25 ms.

1,4,7-Tris(tert-butoxycarbonyl)-1,4,7,10-tetraazacyclododecane[9] *(66)*

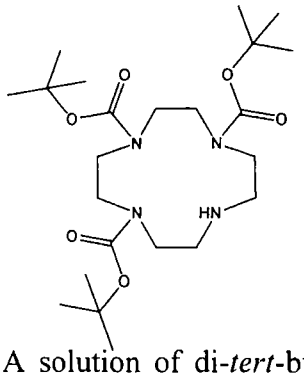

A solution of di-*tert*-butoxycarbonate (6.1 g, 27.9 mmol) in CH_2Cl_2 (140 ml) was added dropwise to a stirred solution of 1,4,7,10-tetraazacyclododecane (2 g, 11.6 mmol). The reaction mixture was stirred at room temperature under argon atmosphere for 3 hours. The solvent was removed under reduced pressure and the residue was purified by chromatography on silica (CH_2Cl_2 to 7% MeOH) to give the product as a white solid (2.95 g, 6.24 mmol, 67%), m.p. 76-78°C (lit[9]. 72-73°C). ^{1}H NMR (300 MHz, $CDCl_3$): δ 1.42 (18H, s, CH_3), 1.44 (9H, s, CH_3), 2.81 (4H, br m, CH_2), 3.26-3.35 (8H, br m, CH_2), 3.60 (4H, m, CH_2). ^{13}C NMR (75 MHz, $CDCl_3$): δ 28.9 (CH_3), 29.0 (CH_3), 46.1 (CH_2), 49.9 (CH_2), 51.2 (CH_2), 79.4 (C), 79.6 (C), 155.8 (C=O), 156.0 (C=O). m/z (ES^+): 495 (MNa^+), 967 (M_2Na^+).

10-(2-Azaxanthonylmethyl)-1,4,7-tris(tertbutoxycarbonyl)-1,4,7,10-tetraazacyclododecane (67)

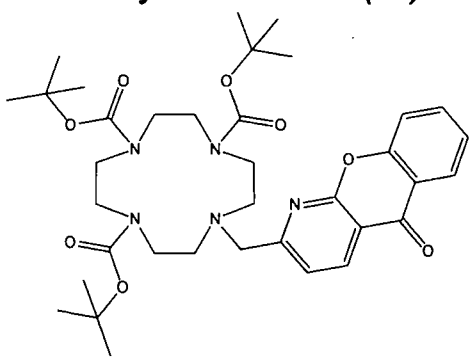

A solution of 2-bromo-metyl-azaxanthone (50 mg, 0.172 mmol), 1,4,7-tris(*tert*butoxycarbonyl)-1,4,7,10-tetraazacyclododecane (81 mg, 0.171 mmol), K_2CO_3 (95 mg, 0.687 mmol) and a catalytic amount of KI in acetonitrile (5 ml) was heated to reflux overnight. The reaction mixture was filtered and salts were washed with CH_2Cl_2. The solvents were removed under reduced pressure. The residue was purified by chromatography on alumina (CH_2Cl_2 to 2% MeOH) to give the product as pale yellow solid (115 mg, 0.169 mmol, 99%), m.p. 170-171 °C. ^{1}H NMR (300 MHz,

$CDCl_3$): δ 1.39 (9H, s, CH_3), 1.46 (18H, s, CH_3), 2.81 (4H, br m, ring CH_2), 3.20-3.70 (12H, br m, ring CH_2), 3.96 (2H, s, CH_2), 7.45 (1H, ddd, *J* 8, 7.2, 1.0, H^7), 7.50 (1 H, d, *J* 8, H^3), 7.59 (1H, dd, *J* 8, 1.0, H^9), 7.75 (1H, ddd, *J* 8, 7.2, 1.6, H^8), 8.28 (1H, dd, *J* 8, 1.6, H^6), 8.59 (1H, d, *J* 8, H^4). ^{13}C NMR (125 MHz, $CDCl_3$): δ 28.7 (CH_3), 48.0 (ring C), 50.2 (ring C), 54.8 (ring C), 55.6 (ring C), 58.5 (CH_2-AzaH), 79.8 (^tBu), 115.4 ($C^{9'}$), 118.7 (C^9), 121.9 (C^3), 124.9 (C^7), 126.9 (C^6), 135.8 (C^8), 137.4 (C^4), 155.9 ($C^{6'}$), 156.5 ($C^{4'}$), 159.9 ($C^{1'}$), 161.1 (C^2), 165.3 (COO*t*Bu), 177.7 (C^5). *m/z* ($ESMS^+$) 682 (M + H, 50%), 704 (M + Na, 100%). HRMS (ES^+) 682.3811 ($C_{36}H_{52}N_5O_8$ requires: 682.3810) (MH^+).

1-Azaxanthonylmethyl-1,4,7,10-tetraazacyclododecane (68)

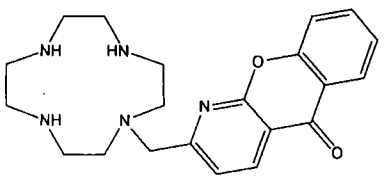

A solution of 1-(2-azaxanthonylmethyl)-4,7,10-*tris*(*tert*butoxycarbonyl)-1,4,7,10-tetraazacyclododecane (115 mg, 0.169 mmol) in TFA (3 ml) and CH_2Cl_2 (3 ml) was stirred at room temperature under an argon atmosphere overnight. The solvents were removed under reduced pressure. The residue was dissolved in CH_2Cl_2 (20 ml) and the solvent was removed. This procedure was repeated three times. The residue was dissolved in aqueous KOH solution (1 M) and the product was extracted into CH_2Cl_2 (20 ml). The combined organic extracts were dried over K_2CO_3 and the solvent was removed to yield the product as a pale red glass (58 mg, 0.152 mmol, 90%), mp 137-139 °C. ^1H NMR (300 MHz, $CDCl_3$): δ 2.56 (4H, m, ring CH_2), 2.69 (8H, s, ring CH_2), 2.80 (4H, m, ring CH_2), 3.87 (2H, s, CH_2), 7.38 (1H, ddd, *J* 8, 7.2, 1.0, H^7), 7.56 (1 H, dd, *J* 8, 1.0, H^9), 7.62 (1H, d, *J* 8, H^3), 7.74 (1H, ddd, *J* 8, 7.2, 1.6, H^8), 8.27 (1H, dd, *J* 8, 1.6, H^6), 8.65 (1H, d, *J* 8, H^4). ^{13}C NMR (125 MHz, $CDCl_3$): δ 45.3 (cyclen C), 46.5 (cyclen C), 47.3 (cyclen C), 52.2 (cyclen C), 61.2 (CH_2-AzaH), 115.4 ($C^{4'}$), 118.6 (C^9), 120.5 (C^3), 121.8 ($C^{6'}$), 124.7 (C^7), 126.8 (C^6), 135.6 (C^8), 138.0 (C^4), 155.8 ($C^{9'}$), 159.8 ($C^{1'}$), 166.5 (C^2), 177.5 (C^5). *m/z* ($ESMS^+$) 382 (M + H, 100%). HRMS (ES^+) 382.2237 ($C_{21}H_{28}N_5O_2$ requires: 382.2238)

1-(2-Azaxanthonylmethyl)-4,7,10-tris(ethoxymethylphosphinatomethyl)-1,4,7,10-tetraazacyclododecane (70)

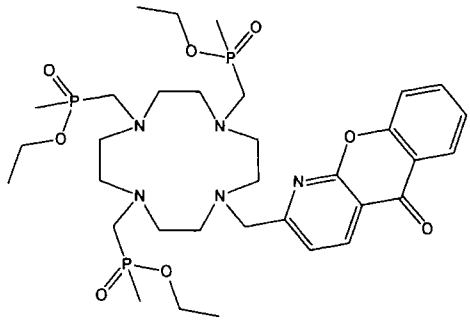

Diethoxymethyl phosphine (130 mg, 0.955 mmol) was added to a mixture of 1-(2-azaxanthonylmethyl)-1,4,7,10-tetraazacyclododecane (90 mg, 0.236 mmol) and parafomaldehyde (60 mg) in THF (5 ml). The reaction mixture was heated to reflux under argon atmosphere overnight. The reaction mixture was filtered and solvent was removed under reduced pressure. The residue was purified by chromatography on silica (CH_2Cl_2 to 2% MeOH) to yield the product as a brown glass (90 mg, 0.121 mmol, 13 %).^{1}H NMR (300 MHz, $CDCl_3$): δ 1.26 (9H, m, CH_2CH_3), 1.53 (9H, m, CH_3), 2.5-3.3 (22 H, br m, ring CH_2, PCH_2), 4.03 (8H, m, OCH_2, CH_2), 7.41 (1H, ddd, *J* 8, 7.2, 1.0, H^7), 7.58 (1 H, d, *J* 8, H^3), 7.74 (2H, m, *J* 8, H^9, H^8) , 8.29 (1H, dd, *J* 8, 1.6, H^6), 8.64 (1H, d, *J* 8, H^4). ^{31}P NMR (120 MHz): δ 53.58.

[TbL^{21}], TbP$_3$Me$_3$AzaH

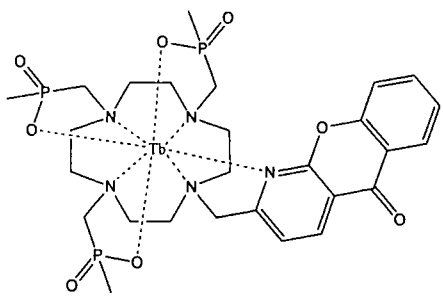

A solution of 1-(2-azaxanthonylmethyl)-4,7,10-*tris*(ethoxymethylphosphinatomethyl)-1,4,7,10-tetraazacyclododecane (45 mg, 60.7 μmol) in 6 M HCl (2 ml) was heated to reflux for 24 hours. The progress of the ester hydrolysis was monitored by ^{1}H and ^{31}P NMR. The solvent was removed under reduced pressure and the residue was dissolved in water (2 ml) and MeOH (2 ml) and $TbCl_3.6H_2O$ (30 mg, 80.3 μmol) was added. The pH of the reaction mixture was increased to 5.5 by the addition of aqueous KOH solution (1 M). The reaction mixture

was heated to 60°C overnight. The solvents were removed and the residue was purified by column chromatography on alumina (69 % CH_2Cl_2, 30 % MeOH and 1 % ammonia solution). $\lambda_{abs}(H_2O)$ 335 nm; $\tau_{Tb}(H_2O)$ 3.57 ms.

[EuL^{21}], EuP$_3$Me$_3$AzaH

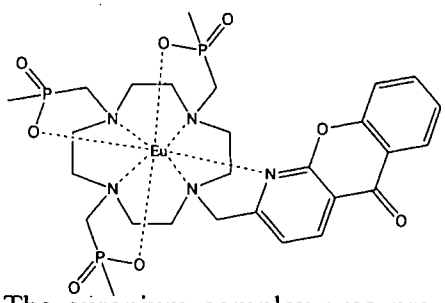

The europium complex was prepared in an analogous manner to the Tb example. $\lambda_{abs}(H_2O)$ 335 nm; $\tau_{Eu}(H_2O)$ 1.16 ms.

2-(4'-Methoxycarbonyl)phenoxy-6-methyl-nicotinic acid (40)

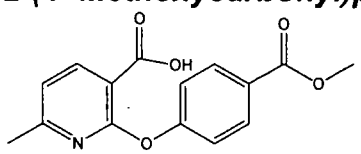

Methyl-4-hydroxy benzoate (10 g, 65.7 mmol) was added to a freshly made solution of sodium methoxide prepared from sodium metal (681 mg, 29.6 mmol) dissolved in dry MeOH (20 ml). The solvent was removed and 2-chloro-6-methyl-nicotinic acid (2.26 g, 13.2 mmol) was added to the residue. The reaction mixture was heated to 150°C overnight. The reaction mixture was cooled down, dissolved in water and the resulting solution was washed with Et_2O (3 × 20 ml). The pH of the aqueous solution was adjusted to 4 by the addition of acetic acid and the precipitate that formed was collected by filtration. The collected precipitate was dried under vacuum and purified by crystallisation from $CHCl_3$/hexane mixture to give the product as a white solid (2.3 g, 8.01 mmol, 61 %), mp 139-141°C. ^{1}H NMR (300 MHz, $CDCl_3$): δ 2.41 (3H, s, CH_3), 3.91 (3H, s, OCH_3), 7.02 (1H, d, *J* 8, H^5), 7.18 (2 H, d, *J* 9, $H^{2'}$), 8.07 (2H, d, *J* 9, $H^{3'}$), 8.32 (1H, d, *J* 8, H^4). ^{13}C NMR (75 MHz, $CDCl_3$): δ 24.4 (CH_3), 52.3 (OCH_3), 111.3 (C^3), 119.3 (C^5), 121.0 ($C^{2'}$), 126.6 ($C^{4'}$), 131.4 ($C^{3'}$), 143.4 (C^4), 157.6 ($C^{1'}$), 160.6 (C^2), 163.2 (C^6), 166.7 ($COOCH_3$), 168.2 (COOH). m/z (ES^-) 286.0 (M-H). HRMS (ES^+) 288.0869 ($C_{13}H_{12}NO_3$ requires: 288.0866) (MH^+).

2-Methyl-7-methoxycarbonyl-1-azaxanthone (41)

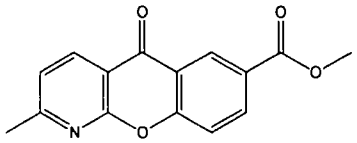

A mixture of 2-(4'-methoxycarbonyl)phenoxy-6-methyl-nicotinic acid (2.3 g, 8.01 mmol) and polyphosphoric acid was heated to 120°C overnight. The reaction mixture was allowed to cool down and was dissolved in MeOH (150 ml). The pH of the resulting solution was increased to 7 by addition of concentrated aqueous NaOH solution. The aqueous solution was extracted with $CHCl_3$ (3 × 200 ml). The combined organic extracts were dried over K_2CO_3 and the solvent was removed under reduced pressure to yield the product as a off-white solid (0.8 g, 2.97 mmol, 37 %), m.p. 194-196 °C. ^{1}H NMR (300 MHz, $CDCl_3$): δ 2.73 (3H, s, CH_3), 3.98 (3H, s, OCH_3), 7.24 (1H, d, *J* 9, H^3), 7.65 (1 H, d, *J* 9, H^9), 8.41 (1H, d, *J* 9, H^8), 8.61 (1H, d, *J* 9, H^4), 9.00 (1H, s, H^6). ^{13}C NMR (75 MHz, $CDCl_3$): δ 25.2 (CH_3), 52.6 (OCH_3), 114.4 ($C^{4'}$), 118.9 (C^9), 121.4 ($C^{6'}$), 121.8 (C^3), 126.8 (C^7), 129.2 (C^6), 136.0 (C^8), 137.6 (C^4), 158.3 ($C^{9'}$), 160.0 ($C^{1'}$), 165.72 ($COOCH_3$), 165.75 (C^2), 176.9 (CO). m/z (ES^+) 269.7 (MH^+). HRMS (ES^+) found: 270.0760 ($C_{13}H_{12}NO_3$ requires: 270.0761) (MH^+).

2-Bromomethyl-7-methoxycarbonyl-1-azaxanthone (42)

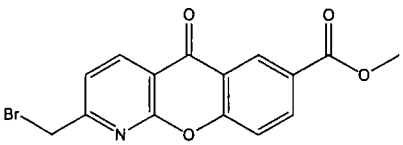

A solution of 2-methyl-7-methoxycarbonyl-1-azaxanthone (0.8 g, 2.97 mmol), N-bromosuccinimide (0.25 g, 1.40 mmol) and dibenzoylperoxide (5 mg, 20.6 μmol) in CCl_4 (10 ml) was heated to reflux. Further additions of NBS (0.25g,) were made after 4.5, 8.5 and 48 h. Dibenzoylperoxide (5 mg) was added after 2, 4.5 and 7 h; (10 mg) after 8.5, 24, 27.5, 32 and 48 h. The reaction was carried out for a total of 55 h. The reaction mixture was filtered and the solvent was removed under reduced pressure. The residue was purified by chromatography on silica (CH_2Cl_2/toluene 1:1 to 1 % MeOH) to give the product as a light yellow solid (140 mg, 0.402 mmol, 13.5 %), . Found: C, 51.64; H, 2.96; N, 3.96%; ($C_{15}H_{10}NO_4Br$ requires: C, 51.75; H, 2.90; N, 4.02%). ^{1}H NMR (300 MHz, $CDCl_3$): δ 3.98 (3H, s, OCH_3), 4.62 (2H, s, CH_2Br), 7.62 (1H, d, *J* 8, H^3), 7.68 (1 H, d, *J* 8.5, H^9), 8.44 (1H, dd, *J* 8.5, 2, H^8), 8.74 (1H, d,

J 8, H^4), 9.00 (1H, d, *J* 2, H^6). ^{13}C NMR (75 MHz, $CDCl_3$): δ 32.3 (CH_2Br), 52.8 (OCH_3), 116.2 ($C^{4'}$), 119.2 (C^9), 121.5 ($C^{6'}$), 121.6 (C^3), 127.3 (C^7), 129.4 (C^6), 136.6 (C^8), 139.0 (C^4), 158.4 ($C^{9'}$), 159.8 ($C^{1'}$), 162.7 (C^2), 165.8 ($COOCH_3$), 176.7 (C^5). m/z (ES^+) 348.1 (MH^+).

10-(7-Methoxycarbonyl-2-azaxanthonylmethyl)-1,4,7-tris(tertbutoxycarbonyl)-1,4,7,10-tetraazacyclododecane (48)

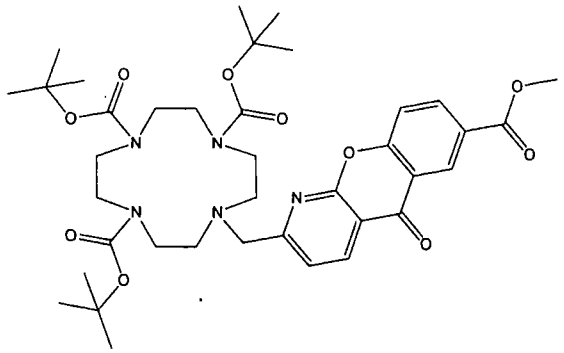

A solution of 2-bromomethyl-7-methoxycarbonyl-1-azaxanthone (140 mg, 0.402 mmol), 1,4,7-*tris*(*tert*butoxycarbonyl)-1,4,7,10-tetraazacyclododecane (190 mg, 0.402 mmol), K_2CO_3 (220 mg, 1.59 mmol) and a catalytic amount of KI in acetonitrile (15 ml) was heated to reflux overnight. The reaction mixture was filtered and salts were washed with CH_2Cl_2 (3 × 20 ml). The solvents were removed under reduced pressure and the residue was purified by chromatography on alumina (CH_2Cl_2 to 2% MeOH) to give the product as a pale yellow solid (200 mg, 0.270 mmol, 67%). ^1H NMR (300 MHz, $CDCl_3$): δ 1.40 (9H, s, CH_3), 1.47 (18H, s, CH_3), 2.81 (4H, br s, ring CH_2), 3.20-3.70 (12H, br m, ring CH_2), 3.97 (3H, s, CH_3), 4.00 (2H, s, CH_2), 7.57 (1H, d, *J* 8, H^3), 7.65 (1 H, d, *J* 8.5, H^9), 8.41 (1H, dd, *J* 8.5, 2, H^8), 8.61 (1H, d, *J* 8, H^4), 8.98 (1H, d, *J* 2, H^6). ^{13}C NMR (75 MHz, $CDCl_3$): δ 28.7 (CH_3), 46.5-50.8 (C ring), 52.7 (OCH_3) 58.5-59 (CH_2AZA), 79.9 (C_q-*tBu*), 115.4 ($C^{4'}$), 119.1 (C^9), 121.6 ($C^{6'}$), 122.0 (C^3), 127.0 (C^7), 129.4 (C^6), 136.2 (C^8), 137.7 (C^4), 158.4 ($C^{9'}$), 159.8 ($C^{1'}$), 160.1 (C^2), 165.9 ($COOCH_3$, $COOtBu$), 177.1 (C^5). m/z (ES^+) (MH^+) 740.2 (MH^+), 762.2 (MNa^+). HRMS (ES^+) 740.3860 ($C_{38}H_{54}N_5O_{10}$ requires: 740.3865) (MH^+).

1-(7-Methoxycarbonyl-azaxanthonylmethyl)-1,4,7,10-tetraazacyclododecane (50)

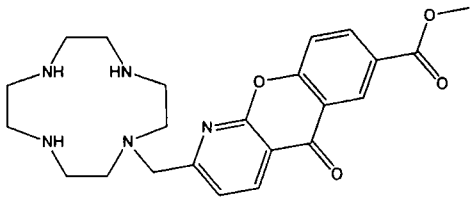

A solution of 1-(2-methyl-7-methoxycarbonyl-1-azaxanthonyl)-4,7,10-*tris*(*tert*butoxycarbonyl)-1,4,7,10-tetraazacyclododecane (200 mg, 0.270 mmol) in TFA (7 ml) and CH_2Cl_2 (5 ml) was stirred at room temperature under an argon atmosphere overnight. The solvents were removed under reduced pressure and the residue was dissolved in CH_2Cl_2 (50 ml) and the solvent was removed. This procedure was repeated three times. The residue was dissolved in aqueous KOH solution (1 M) and the product was extracted into CH_2Cl_2 (3 × 20ml). The combined organic extracts were dried over K_2CO_3 and the solvent was removed to yield the product as a red glass (100 mg, 0.228 mmol, 85 %). ^{1}H NMR (300 MHz, $CDCl_3$): δ 2.59 (4H, m, ring CH_2), 2.71 (8H, s, ring CH_2), 2.82 (4H, m, ring CH_2), 3.89 (2H, s, CH_2), 3.95 (3H, s, OCH_3), 7.62 (1H, d, *J* 8.5, H^9), 7.69 (1 H, d, *J* 8, H^3), 8.38 (1H, dd, *J* 8.5, 2, H^8), 8.67 (1H, d, *J* 8, H^4), 8.95 (1H, d, *J* 2, H^6). ^{13}C NMR (75 MHz, $CDCl_3$): δ 45.4, 46.5, 47.4, 52.3 (C ring), 52.8 (OCH_3), 61.2 (CH_2AZA), 115.5 ($C^{4'}$), 119.1 (C^9), 121.6 ($C^{6'}$), 122.0 (C^3), 127.0 (C^7), 129.4 (C^6), 136.2 (C^8), 137.7 (C^4), 158.4 ($C^{9'}$), 159.8 ($C^{1'}$), 160.0 (C^2), 165.9 ($COOCH_3$), 177.1 (C^5). m/z (ES^+) 440.3 (MH^+). HRMS (ES^+) 440.2288 ($C_{23}H_{30}O_4N_5$ requires: 440.2292) (MH^+).

(S)-N-Chloroethanoyl-1-phenylethylamine[10] (51)

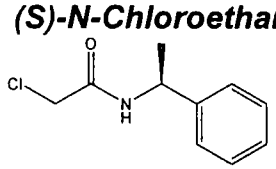

A solution of chloroacetyl chloride (12.5 ml, 17.7 g, 157 mmol) in dry diethyl ether (50 ml) was added dropwise to the stirred solution of (*S*)-1-phenylethylamine (10.6 ml, 9.96 g, 82.2 mmol) and triethyl amine (12.6 ml, 9.15 g, 90.4 mmol) in dry diethyl ether (200 ml) kept at -5°C under argon atmosphere. The reaction mixture was allowed to warm up to room temperature and was stirred for a further 4h. The reaction mixture was washed with 0.1 M HCl solution and dried over K_2CO_3. The solvent was partially removed under reduced pressure yielding crystals of the product. Further

portions of product were obtained by cooling the mother liquors in the refrigerator overnight. The product was obtained as white needles (6.5 g, 32.9 mmol, 40 %), mp 101-103°C (lit[10]. 95-96°C). ^{1}H NMR (300 MHz, $CDCl_3$) δ 1.54 (d, 3H, J 7.0 Hz, CH_3), 4.04 (d, 1H, J 16.5 Hz, CH_2Cl), 4.10 (d, 1H, J 16.5 Hz, CH_2Cl), 5.14 (m, 1H, CH), 6.78 (br, 1H, CONH), 7.40–7.20 (m, 5H, Ph). ^{13}C NMR (75.4 MHz, $CDCl_3$) δ 21.6 (CH_3), 42.6 (CH_2Cl), 49.2 (CH), 126.1 ($Ph_{(o)}$), 127.6 ($Ph_{(p)}$), 128.7 ($Ph_{(m)}$), 142.4 ($Ph_{(q)}$), 165.1 (C=O). m/z (ESMS$^+$) 198 ([M+H]$^+$, 10%), 220 ([M+Na]$^+$, 100%).

1-(2-Methyl-7-methoxycarbonyl-1-azaxanthone)-4,7,10-tris[(S)-1-(1-phenyl)ethylcarbamoylmethyl]-1,4,7,10-tetraazacyclododecane (53)

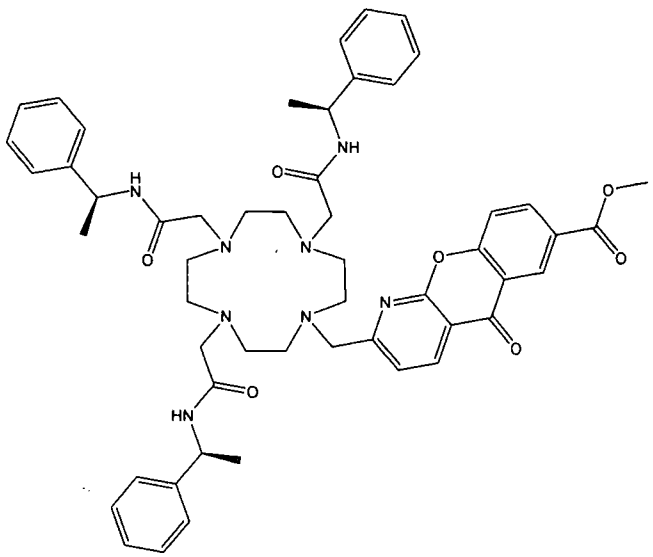

A solution of 1-(2-methyl-7-methoxycarbonyl-1-azaxanthone)-1,4,7,10-tetraaacyclododecane (190 mg, 0.43 mmol), (*S*)-N-chloroacetyl-1-phenylethylamine (285 mg, 1.44 mmol), K_2CO_3 (178 mg,) and KI in acetonitrile (10 ml) was heated to reflux overnight. The reaction mixture was filtered and the salts collected were washed with CH_2Cl_2. The solvents were removed under reduced pressure and the residue was purified by chromatography on alumina (CH_2Cl_2 to 2 % MeOH) to yield the product as a pale brown glass (300 mg, 0.32 mmol, 74%). ^{1}H NMR (300 MHz, $CDCl_3$): δ 1.43 (9 H, m, CH_3), 2.3-3.5 (22H, m, ring and arm CH_2), 3.79 (2H, s, CH_2), 3.95 (3H, s, OCH_3), 4.7-4.95 (3H, m, CH), 7.0-7.4 (15, m, Ph), 7.58 (1H, d, J 8.5, H^9), 7.65 (1 H, d, J 8, H^3), 8.36 (1H, dd, J 8.5, 2, H^8), 8.46 (1H, d, J 8, H^4), 8.93 (1H, d, J 2, H^6). m/z (ES$^+$) 923.4 (MH$^+$), 945.4 (MNa$^+$). HRMS (ES$^+$) 923.4818 ($C_{53}H_{63}O_7N_8$ requires: 923.4814) (MH$^+$).

[TbL^8]Cl$_3$, TbPh$_3$AZACOOMe

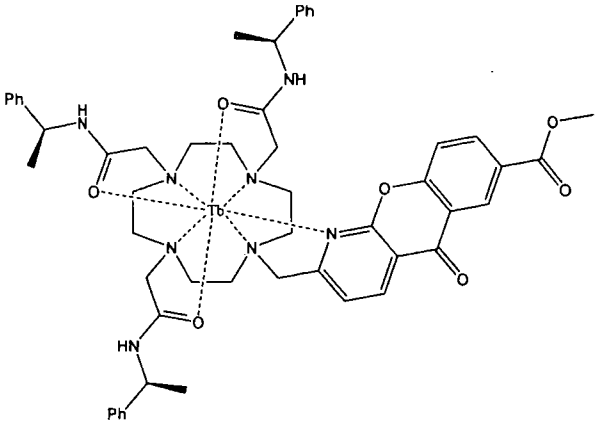

A solution of 1-(2-methyl-7-methoxycarbonyl-1-azaxanthone)-4,7,10-*tris*[(*S*)-1-(1-phenyl)ethylcarbamoylmethyl]-1,4,7,10-tetraazacyclododecane (100 mg, 0.108 mmol) and $Tb(OTf)_3$ (64 mg, 0.106 mmol) in acetonitrile (6 ml) was stirred at 60 °C overnight. The solvent was removed under reduced pressure and the residue redisolved in the minimum volume of acetonitrile. The solution was dropped onto Et_2O (15 ml) and the precipitate was collected by centrifugation. This procedure was repeated three times. The residue was dissolved in $MeOH/H_2O$ mixture and the triflate counter-ions were exchanged for chloride using a strongly basic anion exchange resin. The solvent was removed to yield the product as an off white solid (70 mg). m/z (MALDI-TOF$^+$) 1079.4 (M-2H$^+$). HPLC: t_R 8.01 min (Method A, Appendix). τ_{Tb} (H_2O) 1.53 ms.

[EuL^8]Cl$_3$, EuPh$_3$AZACOOMe

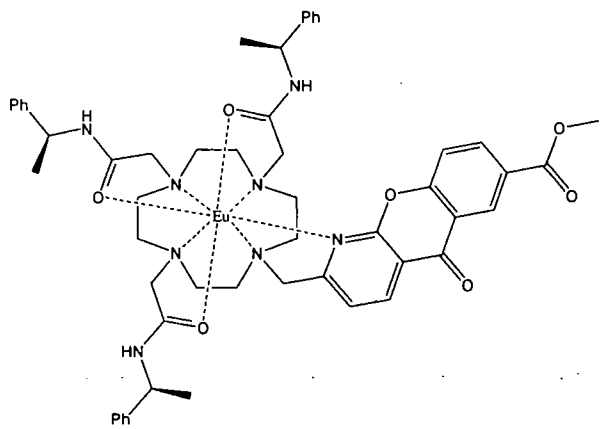

The europium complex was prepared in an analogous manner to the Tb example. The product was obtained as an off-white solid (190 mg). m/z (MALDI-TOF$^+$) 1073.3 (M-2H$^+$). HPLC: t_R 8.01 min (Method A, Appendix). τ_{Eu} (H_2O) 0.58 ms.

$[GdL^{8}]Cl_3$, $GdPh_3AZACOOMe$

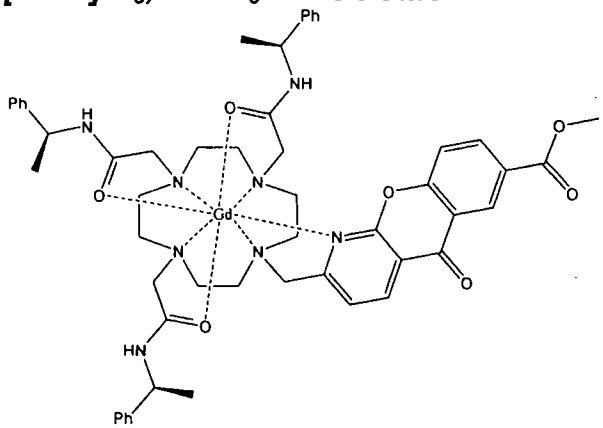

The gadolinium complex was prepared in an analogous manner to the Tb example. The product was obtained as an off-white solid (90 mg). m/z (MALDI-TOF$^+$) 1078.5 (M-2H$^+$). HRMS (MALDI-TOF$^+$) 1078.3825 ($C_{53}H_{60}GdN_8O_7$ requires 1078.3833) (M-2H$^+$), HPLC: t_R 8.01 min (Method A, Appendix).

$[TbL^{30}]Cl_3$, $TbPh_3AZACOOH$

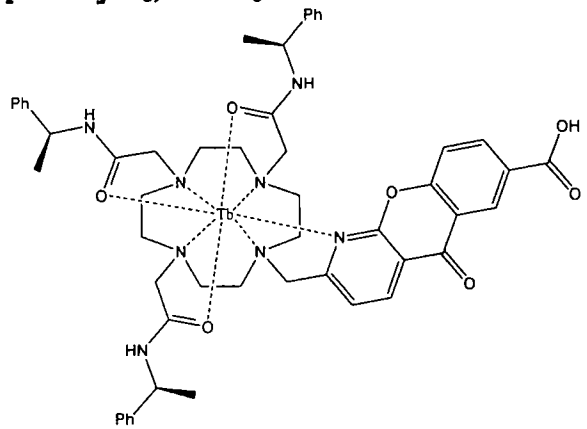

A solution of $TbPh_3AZACOOMe$ (85 mg) in the mixture of H_2O (4 ml) and MeOH (4 ml) was stirred at room temperature for 24 h, maintaining the pH at 10 by the addition of aqueous KOH solution (1M). The reaction progress was monitored by HPLC (Method A, Appendix). The pH was adjusted to 7 with HCl solution (1 M). The solution was syringe filtered and the solvent was removed. The residue was purified by reverse phase HPLC (Method B, Appendix). The solvent was removed to yield the product as a white powder (30 mg). m/z (MALDI-TOF$^+$) 1065.4 (M-2H$^+$). HPLC: t_R 7.68 min (Method A, Appendix). τ_{Tb} (H_2O) 1.62 ms.

[EuL^{30}]Cl$_3$, EuPh$_3$AZACOOH

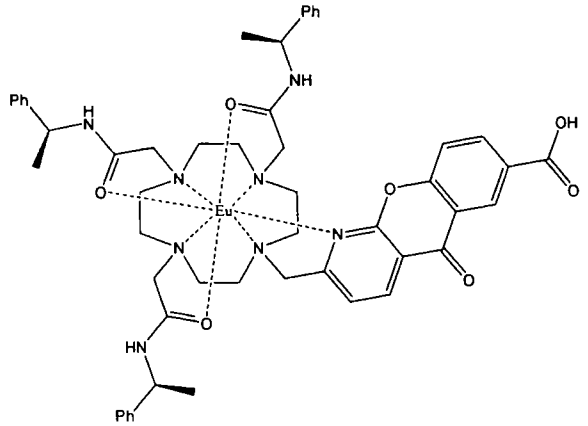

The europium complex was prepared in an analogous manner to the Tb example, but it was used in further experiments without HPLC purification. The product was obtained as an off-white powder (100 mg). m/z (MALDI-TOF$^+$) 1059.3 (M-2H$^+$). HPLC: t_R 7.68 min (Method A, Appendix). τ_{Eu} (H_2O) 0.51 ms.

[GdL^{30}]Cl$_3$, GdPh$_3$AZACOOH

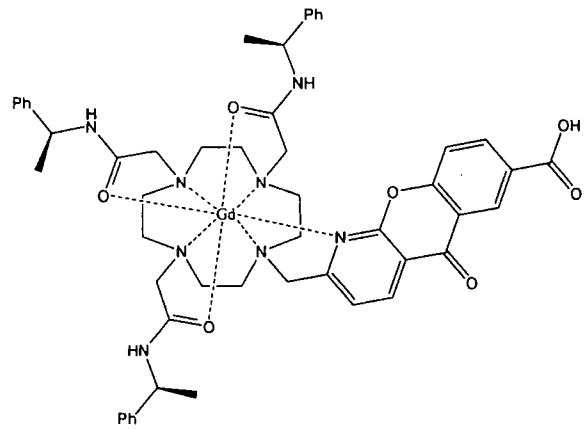

The gadolinium complex was prepared in an analogous manner to the Eu analogue. The solvent was removed under reduced pressure to yield the product as an off white powder (45 mg). m/z (MALDI-TOF$^+$) 1064.1 (M-2H$^+$).HPLC: t_R7.68 min (Method A, Appendix).

[TbL^{36}]Cl$_3$, TbPh$_3$AZACONHS

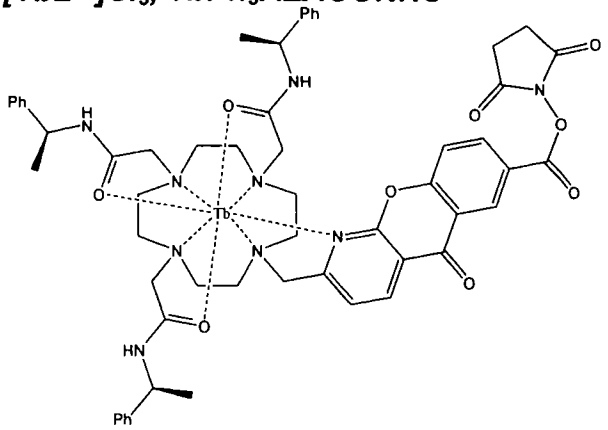

EDC (120 mg, 0.404 mmol) and N-hydroxy succinimde (80 mg, 0.695 mmol) were added to the stirred solution of TbPh$_3$AZACOOH (150 mg, worked up reaction mixture without HPLC purification) in dry DMSO (10 ml). The reaction mixture was stirred overnight at room temperature. The reaction progress was monitored by HPLC (Method A, Appendix). The product was precipitated by dropping the DMSO solution onto dry diethyl ether (30 ml). The residue was triturated with acetonitrile and was redissolved in H_2O. The solvent was removed by freeze-drying to yield the product as a white solid (100 mg). m/z (ES^+) 639.5 ($M+NHS-H^{2+}$), 1277.1 ($M+NHS-2H^+$). HRMS (ES^+): found 639.210 ($M+NHS-H^{2+}$); $C_{60}H_{67}N_{10}O_{12}{}^{159}Tb$ requires 639.209, found 1277.415 ($M+NHS-2H^+$); $C_{60}H_{66}N_{10}O_{12}{}^{159}Tb$ requires 1277.411. HPLC: t_R 8.06 min (Method A, Appendix).

[EuL^{36}]Cl$_3$, EuPh$_3$AZACONHS

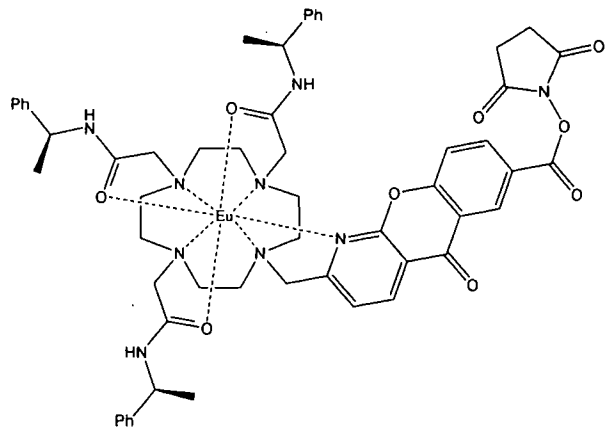

The europium complex was prepared in an analogous manner as the Tb analogue. The solvent was removed by freeze drying to obtain the product as a white solid (130 mg). HPLC: t_R 8.06 min (Method A, Appendix). τ_{Eu} (H_2O) 0.53 ms.

[TbL^{31}]Cl$_3$, TbPh$_3$AZACONC$_1$

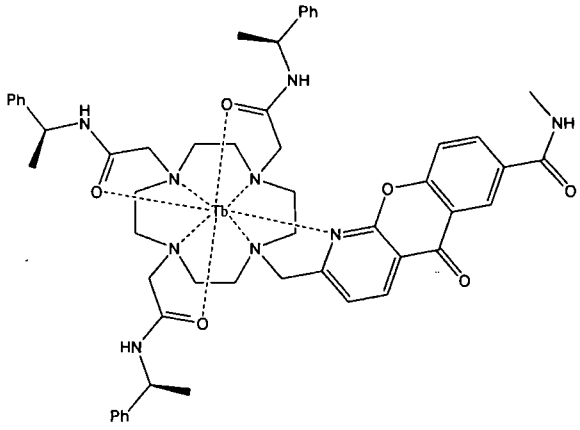

Methylamine (5 µl, 33% wt in absolute ethanol, 0.040 mmol) was added to a stirred solution of TbPh$_3$AZACONHS (20 mg) in dry DMF (2 ml). The reaction mixture was stirred at room temperature under an argon atmosphere overnight and the reaction progress was monitored by HPLC. The reaction mixture was dropped onto diethyl ether (2 ml) and the product was collected by centrifugation. The residue was redissolved in H_2O and the solvent was removed by freeze-drying to yield the product as a white solid (10 mg). m/z (MALDI-TOF$^+$) 1078.4 (M-2H$^+$). HPLC: t_R 7.52 min (Method A, Appendix). τ_{Tb} (H_2O) 1.52 ms.

[TbL^{35}]Cl$_3$, TbPh3AZACONC6

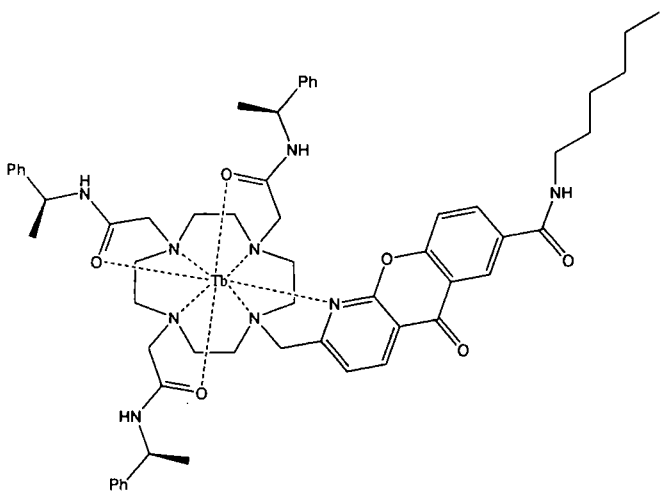

The hexyl amide complex was prepared in an analogous manner to the methyl amide analogue. The crude product was purified by HPLC (Method A, Appendix). The solvent was removed by freezedrying to obtain the product as a white solid (8 mg). m/z (MALDI-TOF$^+$) 1148.4 (M-2H$^+$). HRMS (MALDI-TOF$^+$) 1148.4770

($C_{58}H_{71}N_9O_6Tb$ requires: 1148.4775) ($M\text{-}2H^+$). HPLC: t_R 8.68 min (Method A, Appendix). τ_{Tb} (H_2O) 1.55 ms.

[EuL^{35}]Cl$_3$, EuPh3AZACONC6

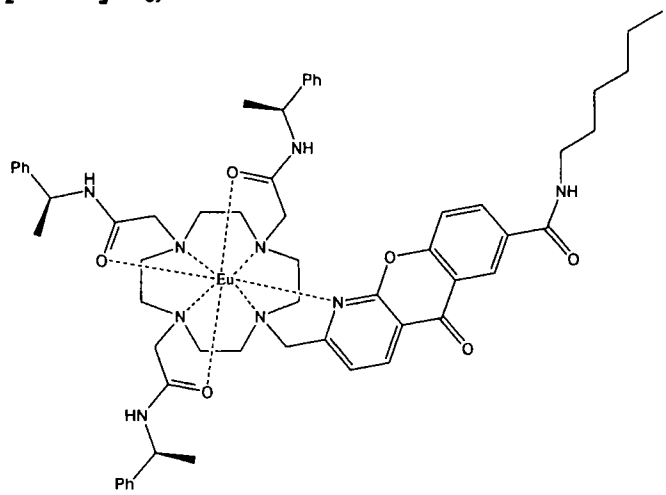

The europium complex was prepared in an analogous manner to the terbium analogue, but was not purified by HPLC. The product was obtained as a white solid (9 mg). HPLC: t_R 8.68 min (Method A, Appendix).

[TbL^{37}]Cl$_3$, TbPh3AZACONC12

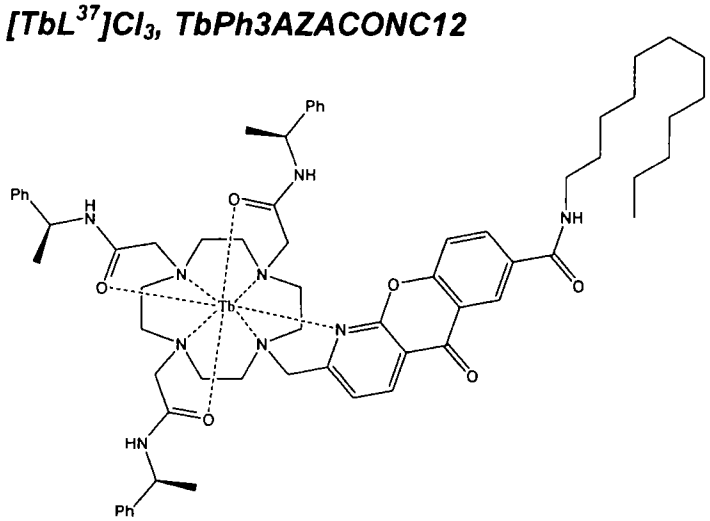

The dodecyl amide complex was prepared in an analogous manner to the hexylamide analogue. The product was obtained as a white solid (7 mg). m/z (MALDI-TOF$^+$) 1232.5 ($M\text{-}2H^+$). HRMS (ES^+) 1232.5725 ($C_{64}H_{83}N_9O_6Tb$ requires: 1232.5714) ($M\text{-}2H^+$); 1278.5800 ($C_{65}H_{85}N_9O_8Tb$ requires: 1278.5769) ($M+HCOOH\text{-}2H^+$); 639.7926 ($C_{65}H_{86}N_9O_8Tb$ requires: 639.7921) ($M+HCOOH\text{-}H^{2+}$). HPLC: t_R 10.30 min (Method A, Appendix). τ_{Tb} (H_2O) 1.71 ms.

[TbL^{45}]Cl$_3$, TbPh3AZACONQN

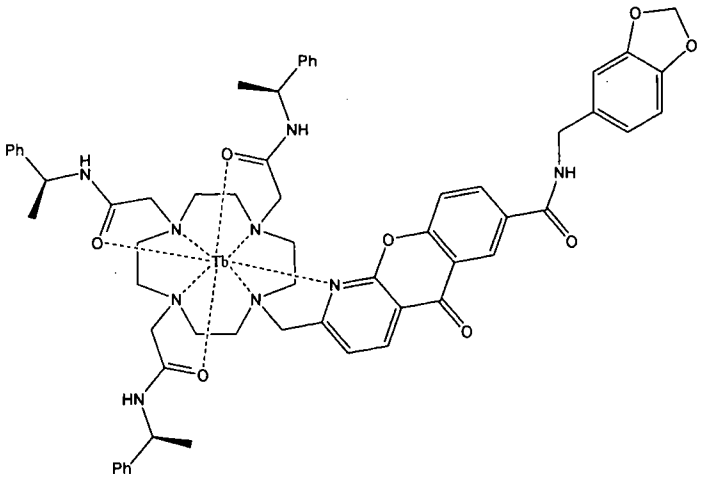

3,4-Methylenedioxybenzylamine (6 µl, 7 mg, 0.048 mmol) was added to the stirred solution of TbPh$_3$AZACONHS (20 mg) in dry DMF (1 ml). The reaction mixture was stirred at room temperature under an argon atmosphere overnight and the reaction progress was monitored by HPLC (Method A, Appendix). The reaction mixture was dropped onto diethyl ether (10 ml) and the product was collected by centrifugation. The residue was redisolved and purified by HPLC (Method E). The solvent was removed by freeze drying to give the product as white powder (5 mg). m/z (MALDI-TOF$^+$) 1198.5 (M-2H$^+$).HPLC: t_R 8.21 min (Method A, Appendix). τ_{Tb} (H_2O) 1.38 ms.

[EuL^{45}]Cl$_3$, EuPh$_3$AZACONQN

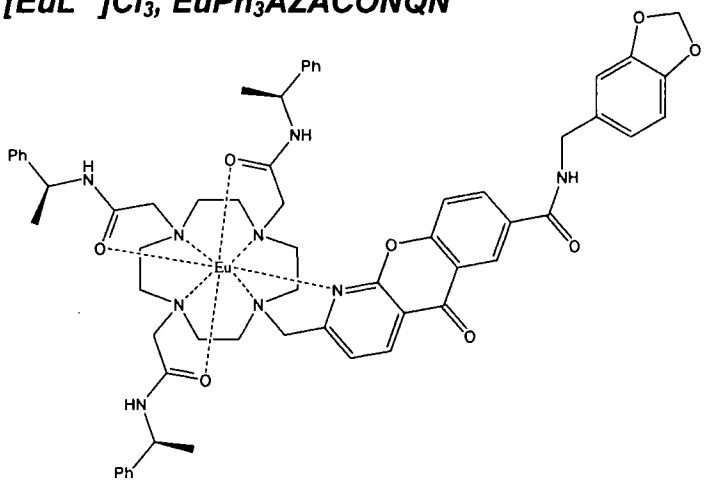

The europium complex was prepared in an analogous manner to the Tb analogue. The product was obtained as a white solid (5 mg). m/z (MALDI-TOF$^+$) 1192.3 (M-2H$^+$). HPLC retention time: 8.21 min (Method A, Appendix). τ_{Eu} (H_2O) 0.52 ms.

Boc Gama amino Cholest (85)

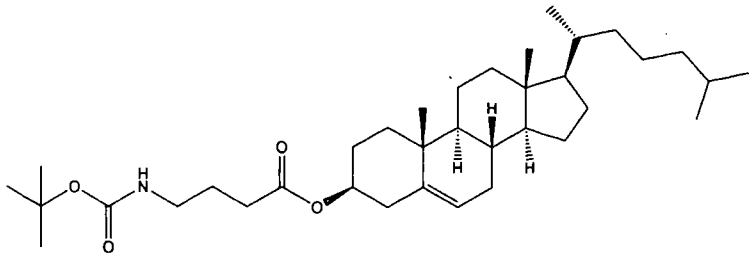

EDC (50 mg), HOBT (35 mg) and DMAP (16 mg) were added to a solution of cholesterol (50 mg) and 4-N-*tert*-butylcarboxyaminobutanoic acid (55 mg) in dry acetonitrile (5 ml). The reaction mixture was stirred at room temperature under argon overnight. The solvent was removed under reduced pressure and the product was obtained by crystallization from MeOH/DCM. m/z ($ESMS^+$) 594.4 (MNa^+). The NMR data is discussed in section 4.1.8 and displayed in Appendix 3.

Gama amino Cholest (86)

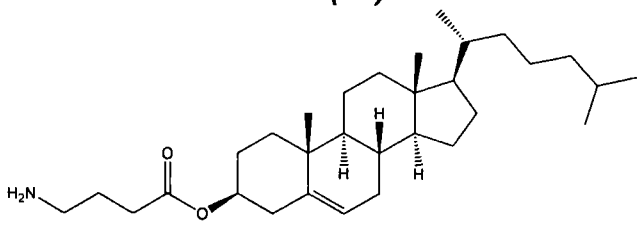

A solution of the *t*-butyl carboxy protected cholesterol derivative (30 mg) in TFA (2ml) and DCM (2ml) was stirred at room temperature under argon atmosphere overnight. The solvent was removed under reduced pressure. The crude product was used immediately in the next step of the reaction sequence. ^1H NMR spectrum is displayed in Appendix 3.

[TbL^{46}]Cl$_3$, TbPh3AZACONCholest

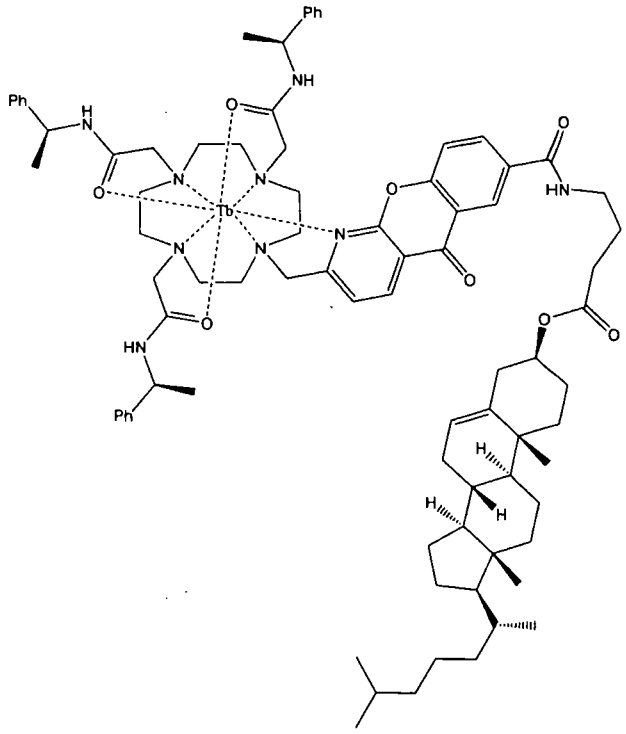

Cholest-3-yl-4-aminobutanoate (10 mg) was added to the stirred solution of $TbPh_3$AZACONHS (5 mg) and DMAP (2 mg) in dry DMF (1 ml). The reaction mixture was stirred at room temperature under argon atmosphere overnight and the reaction progress was monitored by HPLC (Method A, Appendix). The reaction mixture was dropped onto diethyl ether and the product was collected by centrifugation. The residue was purified by HPLC (Method F, Appendix). The solvent was removed by freeze drying to yield the product as a white powder (1 mg) m/z (MALDI-TOF$^+$) 1518.8 (M-2H$^+$). HPLC: t_R 12.69 min (Method A, Appendix). τ_{Tb} (H_2O) 1.42 ms.

[TbL^{40}]Cl$_3$, TbPh$_3$AZACOSpanish

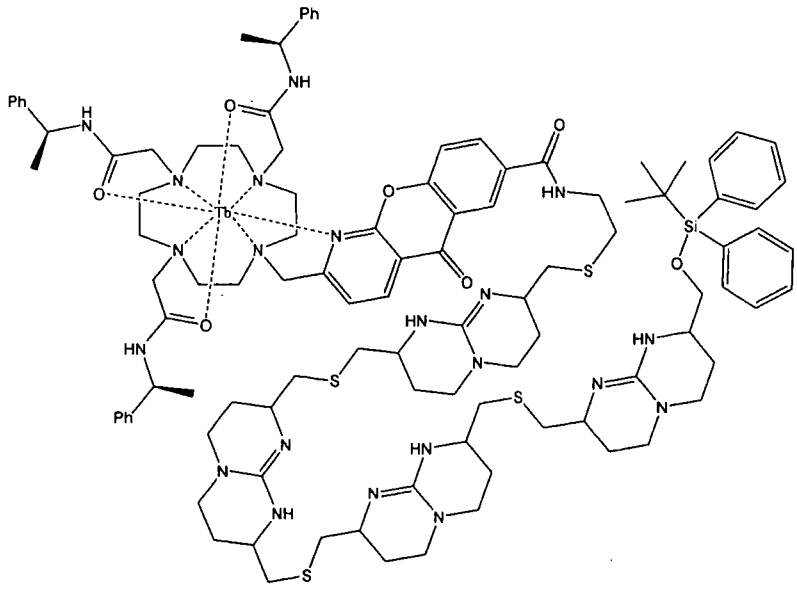

The tetraguanidinium vector **80** (10 mg, 6.4 μmol) was added to a stirred solution of TbPh$_3$AZACONHS (10 mg) in dry DMF (1 ml). The reaction mixture was stirred at room temperature under an argon atmosphere overnight and the reaction progress was monitored by HPLC (Method A, Appendix). The reaction mixture was dropped onto diethyl ether (10 ml) and the product was collected by centrifugation. The residue was purified by HPLC (Method C, Appendix). The product was obtained as a white powder (3 mg). m/z (MALDI-TOF$^+$) 2134.7 (M-2H$^+$). HPLC: t_R 8.29 min (Method A, Appendix). τ_{Tb} (H_2O) 1.63 ms.

[TbL^{38}], TbPh$_3$AZACON(Arg)$_7$OH

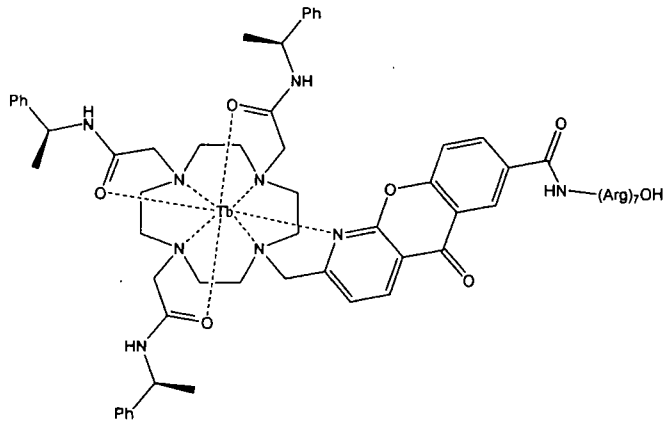

TbPh$_3$AZACONHS (3 mg) was added to a stirred solution of Arg$_7$ (1 mg) in aqueous HEPES buffer (0.1 ml, 0.1 M, pH 7.4). The reaction mixture was stirred at room

temperature for 24 h. The reaction progress was monitored by HPLC (Method A, Appendix) and further two additions of $TbPh_3AZACONHS$ (3 mg) were made. The solvent was removed under reduced pressure and the residue was purified by HPLC (Method A, Appendix), to give the product as a white solid (1 mg). m/z (MALDI-TOF^+) 2160.0 ($M\text{-}2H^+$). HPLC: t_R 6.09 min (Method A, Appendix). τ_{Tb} (H_2O) 1.53 ms.

[TbL^{39}], TbPh3AZACONLys(Arg)$_7$OH

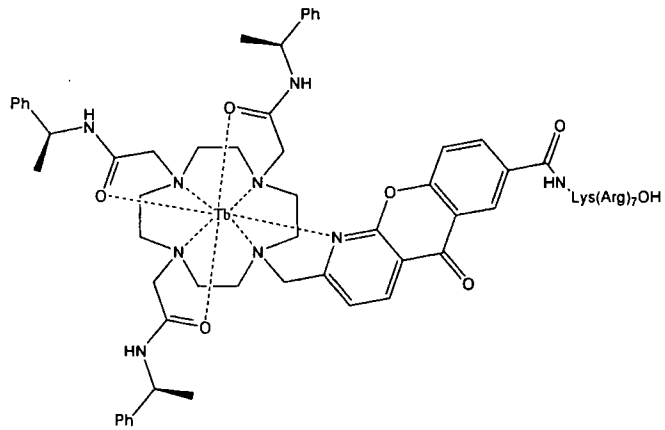

$TbPh_3AZACONHS$ (5 mg) was added to the stirred solution of $LysArg_7$ (1 mg) in aqueous HEPES buffer (0.1 ml, 0.1 M, pH 7.4). The reaction mixture was stirred at room temperature for 24 h. The reaction progress was monitored by HPLC (Method A, Appendix) and further two additions of $TbPh_3AZACONHS$ (5 mg) were made. The solvent was removed under reduced pressure and the residue was purified by HPLC (Method A, Appendix), to give the product as a white solid (1 mg). m/z (MALDI-TOF^+) 2286.2 ($M\text{-}2H^+$) HPLC: t_R 6.09 min (Method A, Appendix). τ_{Tb} (H_2O) 1.53 ms.

[TbL^{41}], TbPh$_3$AZACONG$_2$PAMAM

$TbPh_3AZACONHS$ (20 mg) was added to the stirred solution of G_2PAMAM dendrimer (250 µl, 20% w /w in MeOH, 43 mg, 0.013 mmol) in DMF (2 ml) and MeOH (2 ml). The reaction mixture was stirred at room temperature for 24 h. The reaction progress was monitored by HPLC (Method A, Appendix). The solvent was removed under reduced pressure and the residue was purified by dialysis (Dialysis Tubing: Sigma Aldrich D2272-FT, Benzoylated cellulose, cut off 1200 g/mol) to give the product as a white solid (30 mg). τ_{H20} (1.45 ms).

TbPh$_3$AZACONHSA

TbPh$_3$AZACONHS (6.7 mg) was added to the stirred solution of human serum albumin (20 mg) in H_2O (3 ml). The reaction mixture was stirred at room temperature for 24 h. The solvent was removedunder reuced pressure and the residue was purified by dialysis (Dialysis Tubing: BDH D102, biodesing dialysis tubing, cellulose, cut off 8000 g/mol) to give the product as a white solid (15 mg). τ_{H20} (1.63 ms).

10-(7-Methoxycarbonyl-2-azathioxanthonylmethyl)-1,4,7-tris(tertbutoxycarbonyl)-1,4,7,10-tetraazacyclododecane (47)

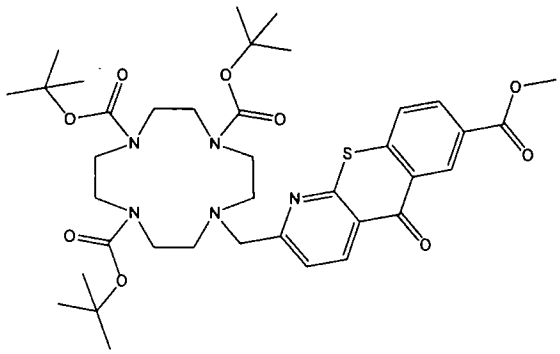

A solution of 2-bromo-7-methoxycarbonyl-1-azathioxanthone (230 mg, 0.661 mmol), 1,4,7-*tris*(*tert*butoxycarbonyl)-1,4,7,10-tetraazacyclododecane (300 mg, 0.635 mmol), K_2CO_3 (320 mg, 2.32 mmol) and a catalytic amount of KI in acetonitrile (23 ml) was heated to reflux overnight. The reaction mixture was filtered and salts were washed with CH_2Cl_2. The solvents were removed under reduced pressure. The residue was purified by chromatography on alumina (CH_2Cl_2 to 2% MeOH) to give the product as a light-yellow solid (340 mg, 0.450 mmol, 71%). ^{1}H NMR (300 MHz, $CDCl_3$): δ 1.38 (9H, s, CH_3), 1.46 (18H, s, CH_3), 2.75 (4H, br s, ring CH_2), 3.20-3.70 (12H, br m, ring CH_2), 3.97 (5H, s, OCH_3, CH_2), 7.48 (1H, d, *J* 8, H^3), 7.68 (1 H, d, *J* 8.5, H^9), 8.25 (1H, dd, *J* 8.5, 2, H^8), 8.72 (1H, d, *J* 8, H^4), 9.19 (1H, d, *J* 2, H^6). m/z (ES^+) 756.3 (MH^+), 778.4 ($M+Na^+$), 1533.0 ($2M+Na^+$). HRMS (ES^+) 756.3649 ($C_{38}H_{54}N_5O_9S$ requires: 756.3637) (MH^+); 778.3464 ($C_{38}H_{53}N_5O_9SNa$ requires: 778.3456) ($M+Na^+$).

1-(7-Methoxycarbonyl-azathioxanthonylmethyl)-1,4,7,10-tetraazacyclododecane (49)

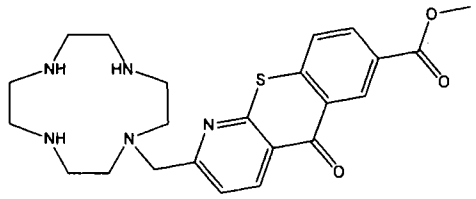

A solution of 1-(2-methyl-7-methoxycarbonyl-1-azathioxanthone)-4,7,10-*tris*(*tert*butoxycarbonyl)-1,4,7,10-tetraazacyclododecane (300 mg, 0.397 mmol) in TFA (10 ml) and CH_2Cl_2 (7 ml) was stirred at room temperature under an argon atmosphere overnight. The solvents were removed under reduced pressure and the residue was dissolved in CH_2Cl_2 (10 ml) and the solvent was removed. This procedure was repeated three times. The residue was dissolved in aqueous KOH solution (1 M) and the product was extracted into CH_2Cl_2 (3 × 25ml). The combined organic extracts were dried over K_2CO_3 and the solvent was removed to yield the product as a red glass (120 mg, 0.263 mmol, 66%). ^{1}H NMR (300 MHz, $CDCl_3$): δ 2.59 (4H, m, ring CH_2), 2.69 (8H, s, ring CH_2), 2.82 (4H, m, ring CH_2), 3.87 (2H, s, CH_2), 3.97 (3H, s, OCH_3), 7.62 (1H, d, *J* 8, H^3), 7.68 (1 H, d, *J* 8.5, H^9), 8.24 (1H, dd, *J* 8.5, 2, H^8), 8.78 (1H, d, *J* 8, H^4), 9.19 (1H, d, *J* 2, H^6). m/z (ES^+) 456.3 (MH^+). HRMS (ES^+) 456.2062 ($C_{23}H_{30}N_5O_3S$ requires: 456.2064) (MH^+).

1-(2-Methyl-7-methoxycarbonyl-1-azathioxanthone)-4,7,10-tris[(S)-1-(1-phenyl)ethylcarbamoylmethyl]-1,4,7,10-tetraazacyclododecane (52)

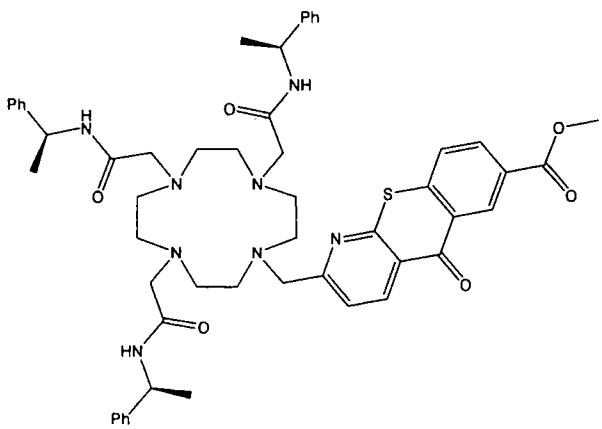

A solution of 1-(2-methyl-7-methoxycarbonyl-1-azathioxanthone)-1,4,7,10-tetraazacyclododecane (80 mg, 0.176 mmol), *N*-chloroacetyl-1-phenylethylamine (106 mg, 0.538 mmol), K_2CO_3 (125 mg, 0.904 mmol) and KI in acetonitrile was heated to reflux overnight. The reaction mixture was filtered and the salts collected

were washed with CH_2Cl_2. The combined organic washings were evaporated and the residue was purified by chromatography on alumina (CH_2Cl_2 to 2 % MeOH) to yield the product as a brown glass (40 mg, 43 μmol, 24 %). ^1H NMR (300 MHz, $CDCl_3$): δ 1.48 (9H, m, CH_3), 2.40-3.95 (24H, br m, ring CH_2, CH_2), 3.99 (3H, s, OCH_3), 4.95 (3H, br m, CH), 7.62 (1H, d, *J* 8, H^3), 7.71 (1 H, d, *J* 8.5, H^9), 8.27 (1H, dd, *J* 8.5, 2, H^8), 8.73 (1H, d, *J* 8, H^4), 9.18 (1H, d, *J* 2, H^6). m/z (ES^+) 939.5 (MH^+), 961.4 (MNa^+). HRMS (ES^+) 939.4595 ($C_{53}H_{63}N_8O_6S$ requires: 939.4586) (MH^+), 961.4412 ($C_{53}H_{62}N_8O_6SNa$ requires: 961.4405) ($M+Na^+$).

[EuL^7]Cl$_3$, EuPh$_3$THAZACOOMe

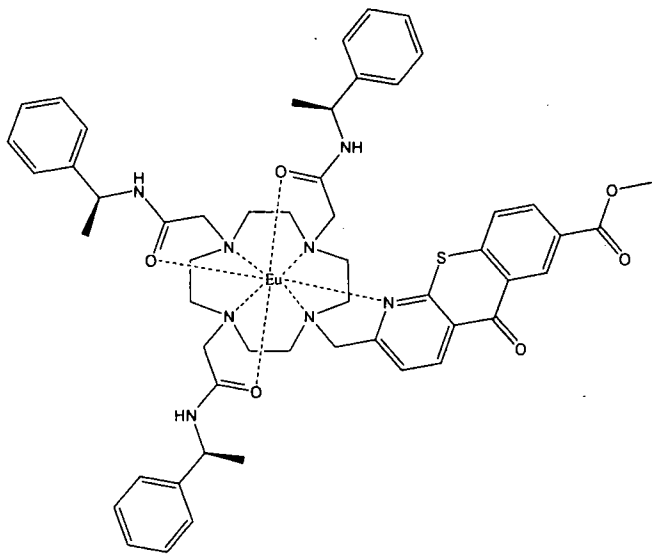

A solution of 1-(2-methyl-7-methoxycarbonyl-1-azathioxanthone)-4,7,10-tris[(S)-1-(1-phenyl)ethylcarbamoylmethyl]-1,4,7,10-tetraazacyclododecane (30 mg, 31.9 μmol) and $Eu(OTf)_3$ (20 mg, 28.3 μmol) in acetonitrile (2 ml) was heated to reflux overnight. The solvent was removed and the residue dissolved in the minimum amount of acetonitrile and was added dropwise to Et_2O (30 ml). The precipitate formed was separated by centrifugation and the procedure was repeated. The product was dried under vacuum. The counter anion was exchanged for chloride using an anion exchange resin and the solvent was removed to give the product as a light yellow solid (25 mg, 20.8 μmol, 73.4%). m/z (MALDI-TOF$^+$) 1089.3 ($M-2H^+$). $\lambda_{abs}(H_2O)$ 370 nm; $\tau_{Eu}(H_2O)$ 0.53 ms,

[EuL^{33}]Cl$_3$, EuPh$_3$THAZACOOH

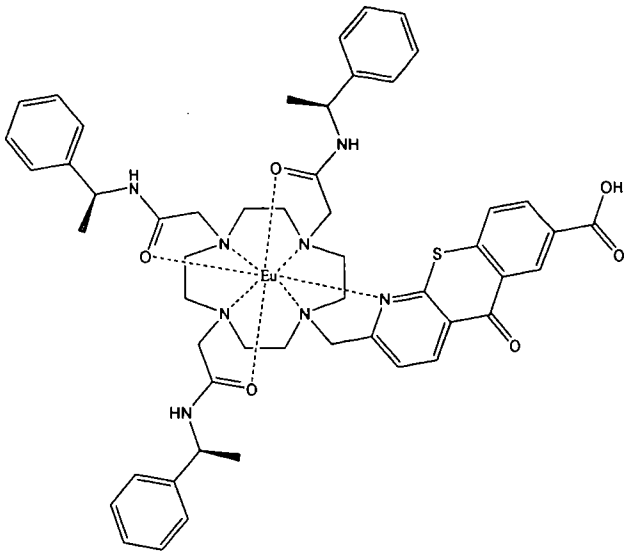

A solution of EuPh$_3$THAZACOOMe (10 mg) in 0.02 M KOH solution (2 ml) was stirred at room temperature for 3 h. The reaction progress was monitored by HPLC. The pH of the reaction mixture was adjusted to 6 by addition of 1 M HCl solution. The precipitate was removed by syringe filtration. The reaction mixture was freeze dried to give the product as a white solid.

Literature

[1]) R. A. Poole, G. Bobba, M. J. Cann, J. C. Frias, D. Parker, R. D. Peacock, *Organic and Biomolecular Chemistry*, 2005, **3**, 1013.
[2]) J. Tamura, *Journal of Biochemistry (Tokyo)*, 1938, **27**, 335.
[3]) O. Reany, T. Gunnlaugsson, D. Parker, *Journal of the Chemical Society Perkin Transactions 2*, 2000, 1819.
[4]) Mark Woods, *Chiral Gadolinium Complexes as Potential Contrast Agents*, 1998, PhD. Thesis, Durham University.
[5]) R. Schwarzenbach, *Helvetica Chimica Acta*, 1939, **22**, 360.
[6]) R. Grice, L. N. Owen, *Journal of the Chemical Society*, 1963, 1947.
[7]) R. S. Dickins, J. A. K. Howard, C. L. Maupin, J. M. Moloney, D. Parker, J. P. Riehl, G. Siligardi and J. A. G. Williams, *Chem. Eur. J.*, 1999, **5**, 1095.
[8]) P. Atkinson, *Chemoselective Phopho-Anion Binding Studies*, 2005, PhD. Thesis, Durham University
[9]) S. Brandes, C. Gros, F. Denat, P. Pullumbi, R. Guilard, *Bull. Soc. Chim. Fr.*, 1996, **133**, 65.
[10]) R. S. Dickins, J. A. K. Howard, C. L. Maupin, J. M. Moloney, D. Parker, J. P. Riehl, G. Siligardi and J. A. G. Williams, *Chem. Eur. J.*, 1999, **5**, 1095.

APPENDICES

6 Appendixes

6.1 Appendix 1: HPLC Conditions

6.1.1 Method A (Basic analytical gradient)

Solvent A: H_2O/0.1% HCOOH (TFA or no added acid)

Solvent B: ACN/0.1% HCOOH (TFA or no added acid)

Flow: 1 ml/min

Time (min)	Solvent A (%)	Solvent B (%)	Curvature
0	100	0	0
15	0	100	1
20	0	100	0
25	100	0	-3
27	100	0	0

6.1.2 Method B

Solvent A: H_2O/0.1% HCOOH

Solvent B: ACN/0.1% HCOOH

Flow: 5 ml/min

Time (min)	Solvent A (%)	Solvent B (%)	Curvature
0	100	0	0
11	50	100	1
13	0	100	-3
16	0	100	0
16	100	0	-3
22	100	0	0

6.1.3 Method C

Solvent A: H_2O/0.1% HCOOH

Solvent B: ACN/0.1% HCOOH

Flow: 1 ml/min

Time (min)	Solvent A (%)	Solvent B (%)	Curvature
0	100	0	0
6	60	40	1
11	60	40	0
13	0	100	-3
15	0	100	0
18	100	0	-3
20	100	0	0

6.1.4 Method D

Solvent A: H_2O/0.1% HCOOH

Solvent B: ACN/0.1% HCOOH

Flow: 1 ml/min

Time (min)	Solvent A (%)	Solvent B (%)	Curvature
0	80	20	0
2	80	20	0
4	40	60	1
6	40	60	0
7	0	100	-3
9	0	100	0
10	80	20	-3
12	80	20	0

6.1.5 Method E

Solvent A: H_2O/0.1% HCOOH

Solvent B: ACN/0.1% HCOOH

Flow: 5 ml/min

Time (min)	Solvent A (%)	Solvent B (%)	Curvature
0	80	20	0
3	80	20	0
6	40	60	1
9	40	60	0
10.5	0	100	-3
13.5	0	100	0
15	80	20	-3
18	80	20	0

6.1.6 Method F

Solvent A: H_2O/0.1% HCOOH

Solvent B: ACN/0.1% HCOOH

Flow: 1 ml/min

Time (min)	Solvent A (%)	Solvent B (%)	Curvature
0	55	45	0
1.5	55	45	0
3	5	95	1
6	5	95	0
7.5	0	100	-3
9	0	100	0
10.5	55	45	-3
12	55	45	0

6.1.7 Method G

Solvent A: H_2O

Solvent B: ACN

Flow: 5 ml/min

Time (min)	Solvent A (%)	Solvent B (%)	Curvature
0	100	0	0
3	80	20	1
4	40	60	1
9	20	80	1
10.5	0	100	1
12	0	100	0
13.5	100	0	-3
15	100	0	0

6.1.8 Method H

Solvent A: H_2O/0.1% TFA

Solvent B: ACN/0.1% TFA

Flow: 5 ml/min

Time (min)	Solvent A (%)	Solvent B (%)	Curvature
0	95	5	0
4.5	75	25	1
6.5	75	25	0
7.5	0	100	1
9	0	100	0
10	95	5	-3
12	95	5	0

6.2 Appendix 2: Selected chromatograms

6.2.1 Chromatogram of methyl ester complex $[LnL^{8}]^{3+}$

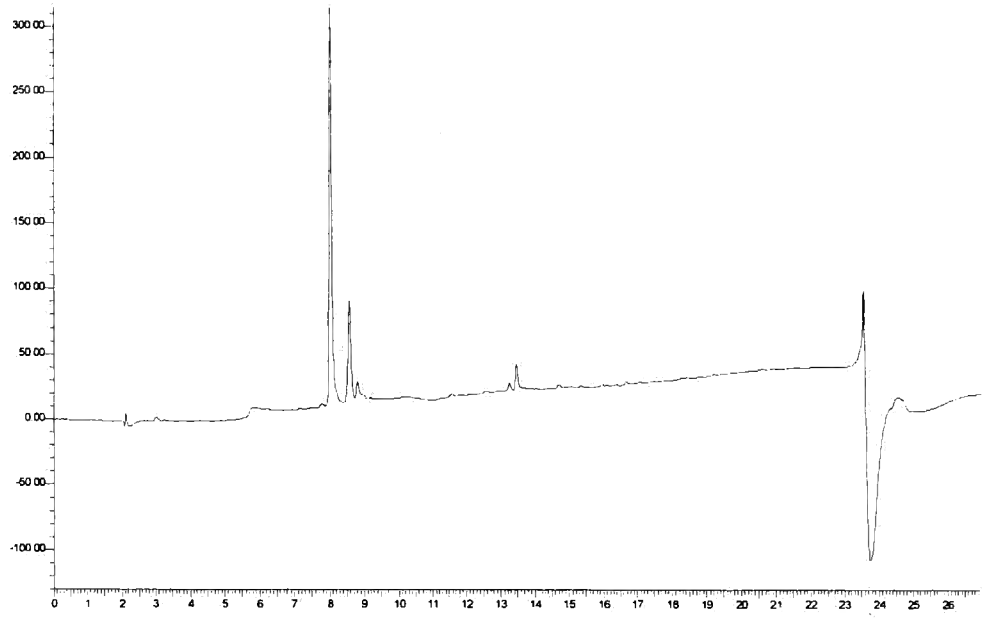

6.2.2 Chromatogram of carboxylic acid complex

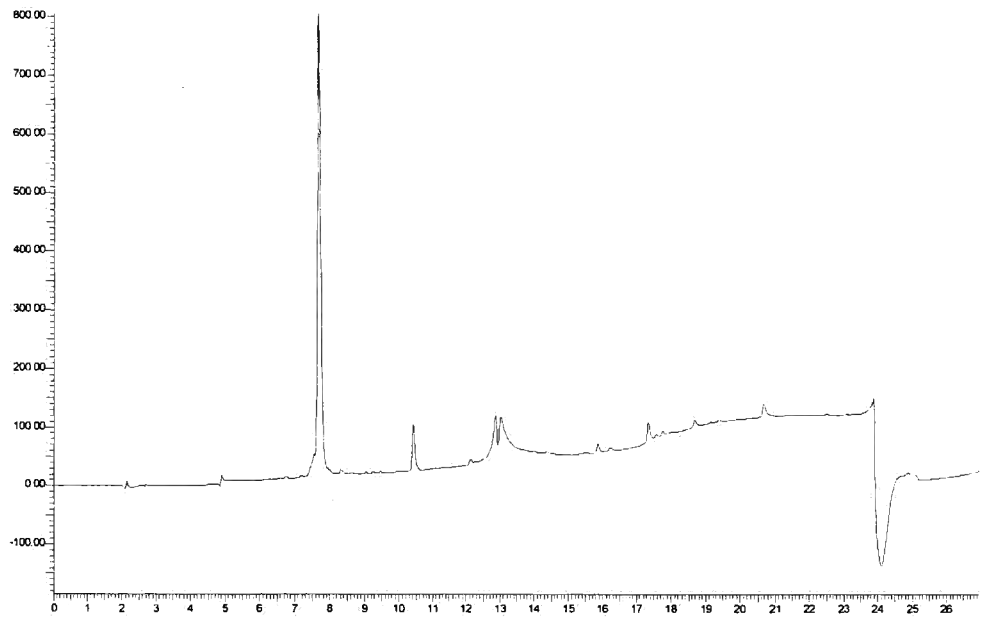

6.2.3 Chromatogram of NHS ester comples formation

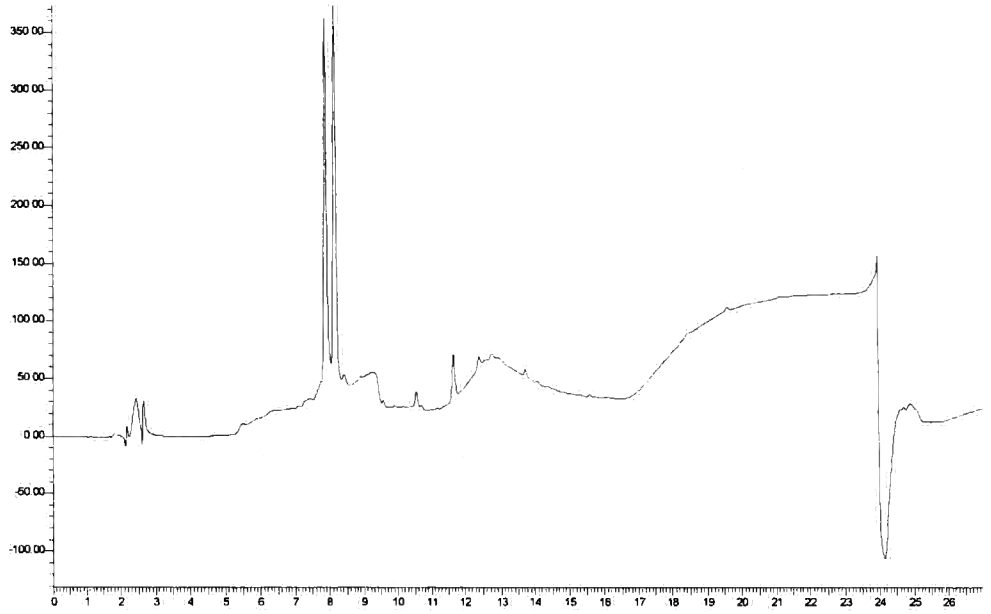

6.2.4 Chromatogram of methyl amide complex

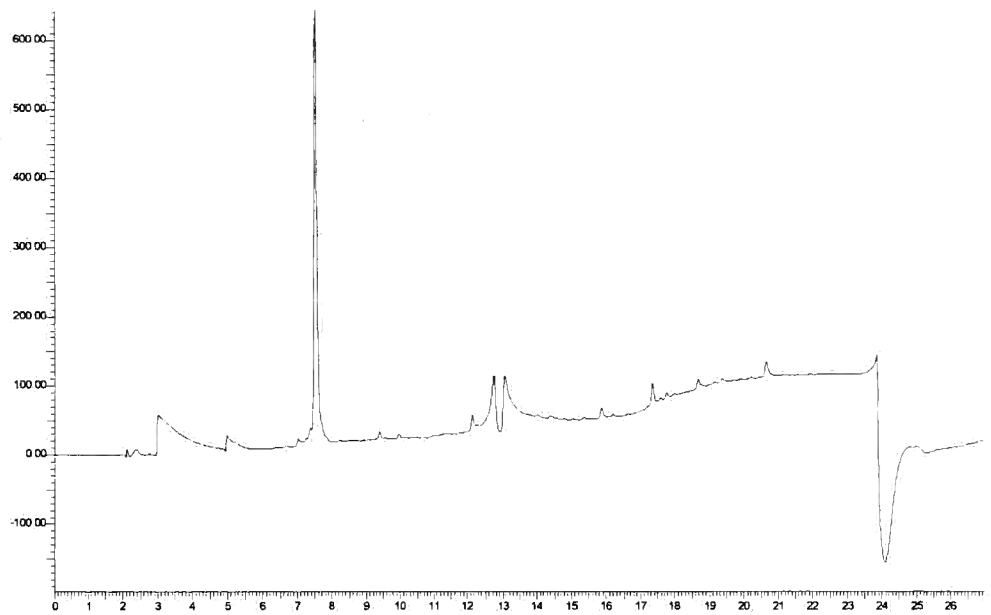

6.2.5 Chromatogram of the hexyl amide complex

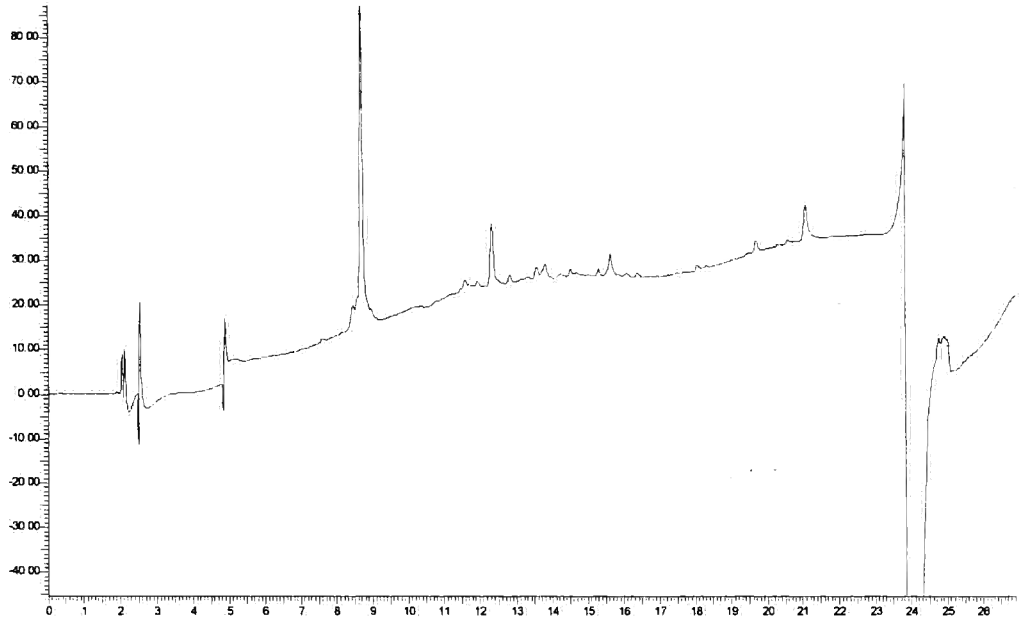

6.2.6 Chromatogram of the dodecyl amide complex

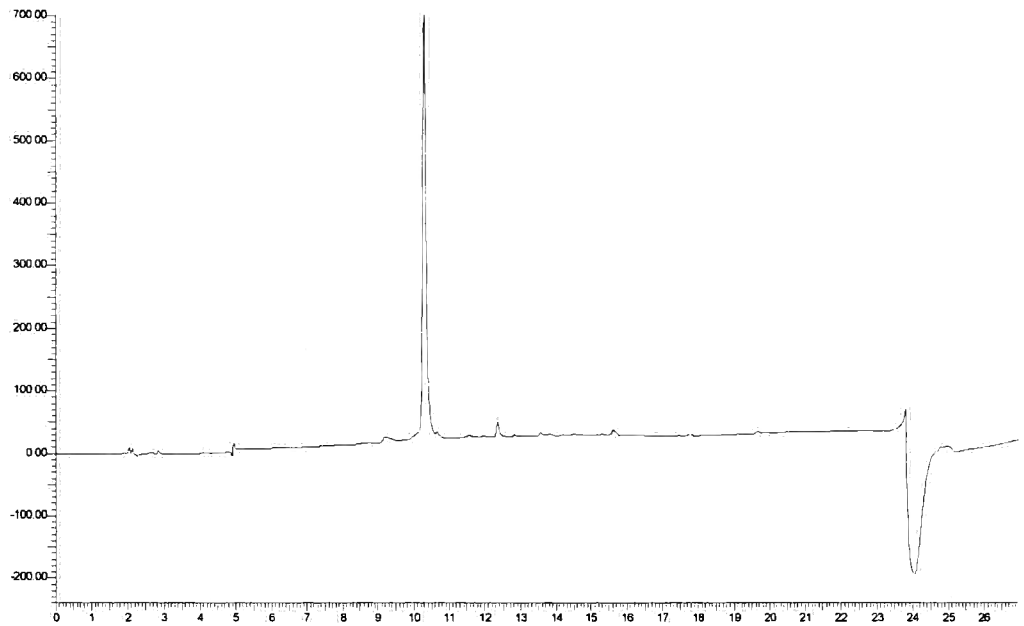

6.2.7 Chromatogram of the coupling reaction mixture for oligoarginine peptides

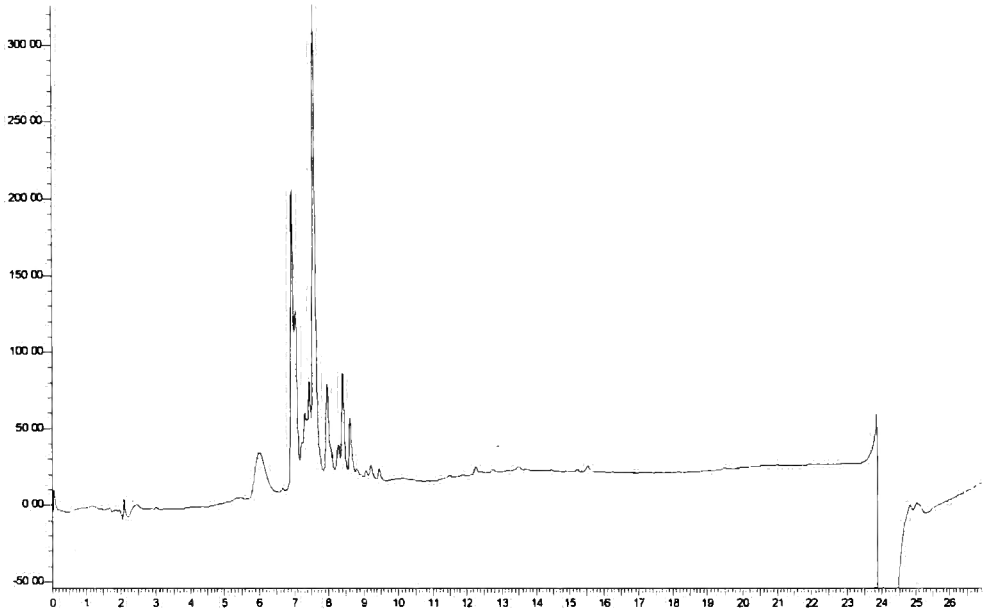

6.2.8 Chromatogram for the purified conjugate with the oligoarginine peptide

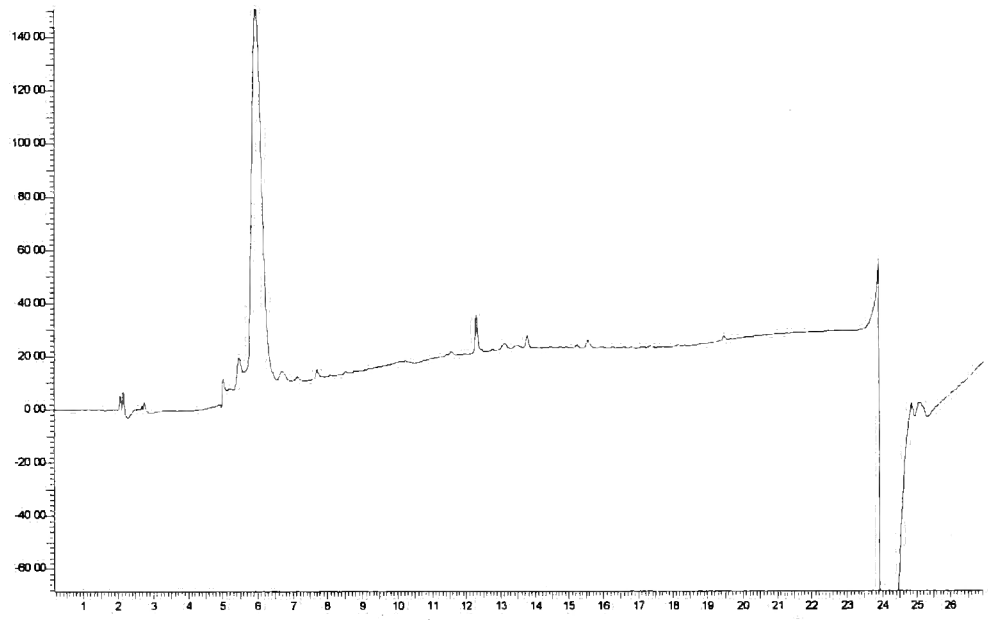

6.2.9 Chromatogram of the oligoguanidinium vector conjugation reaction mixture

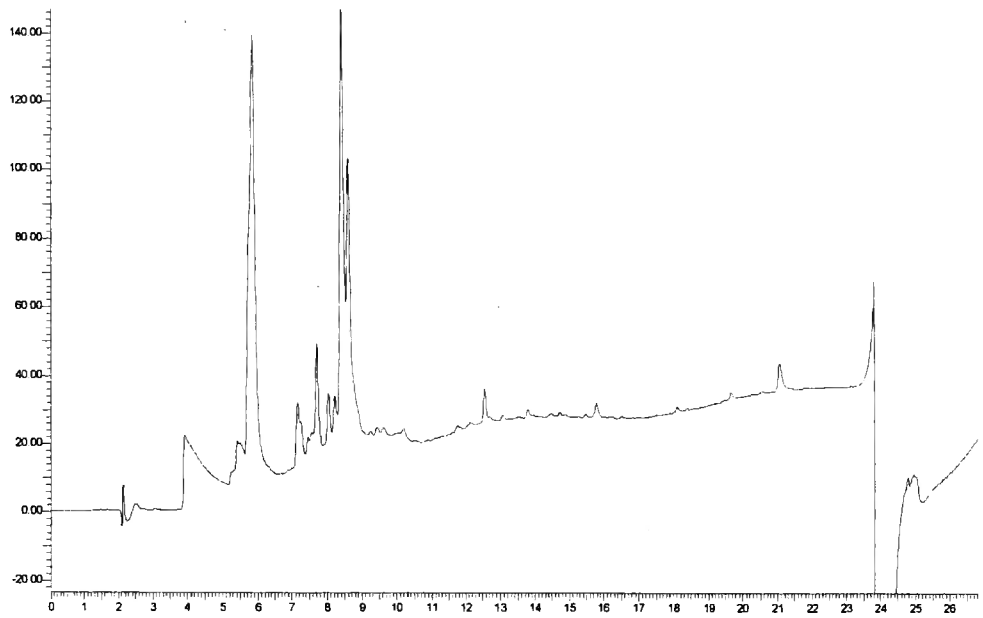

6.2.10 Chromatogram of the purified oligoguanidinium conjugate

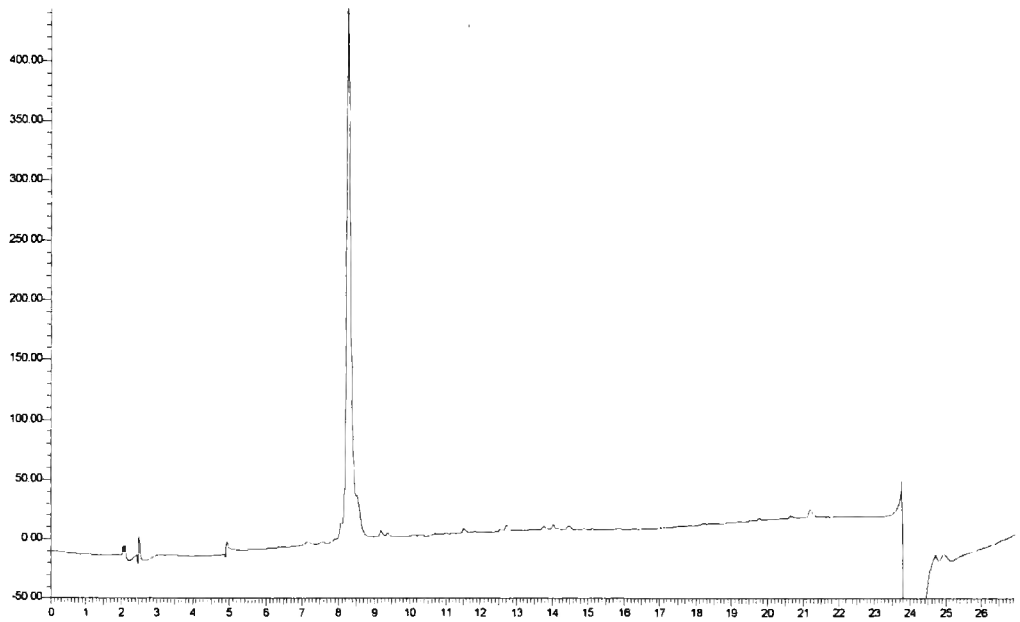

6.2.11 Chromatogram of reaction mixture of coupling to PAMAM dendrimer

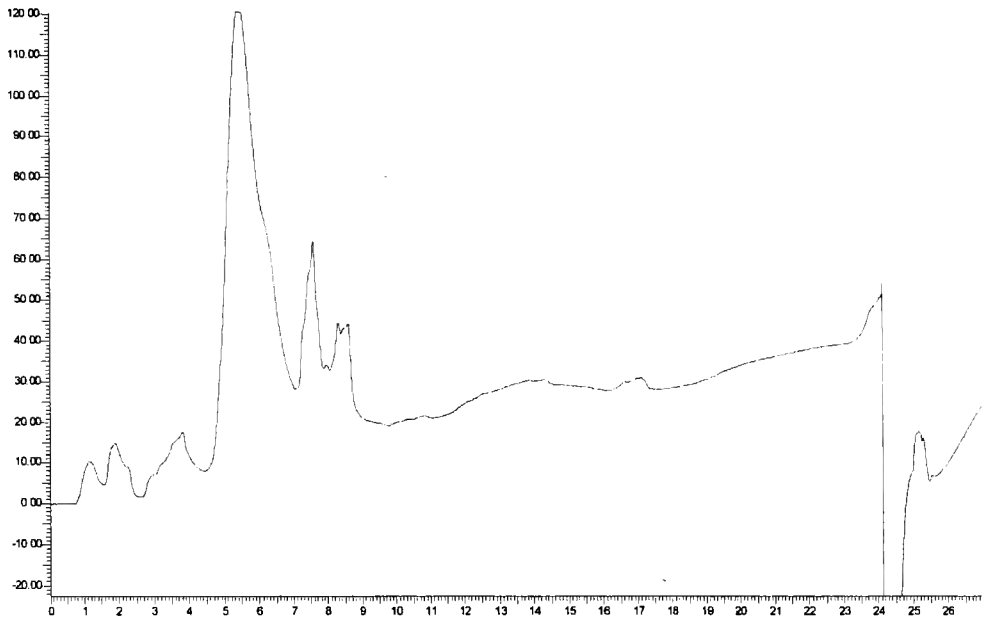

6.2.12 Chromatogram of reaction mixture of coupling to PAMAM dendrimer (fluorescence detection)

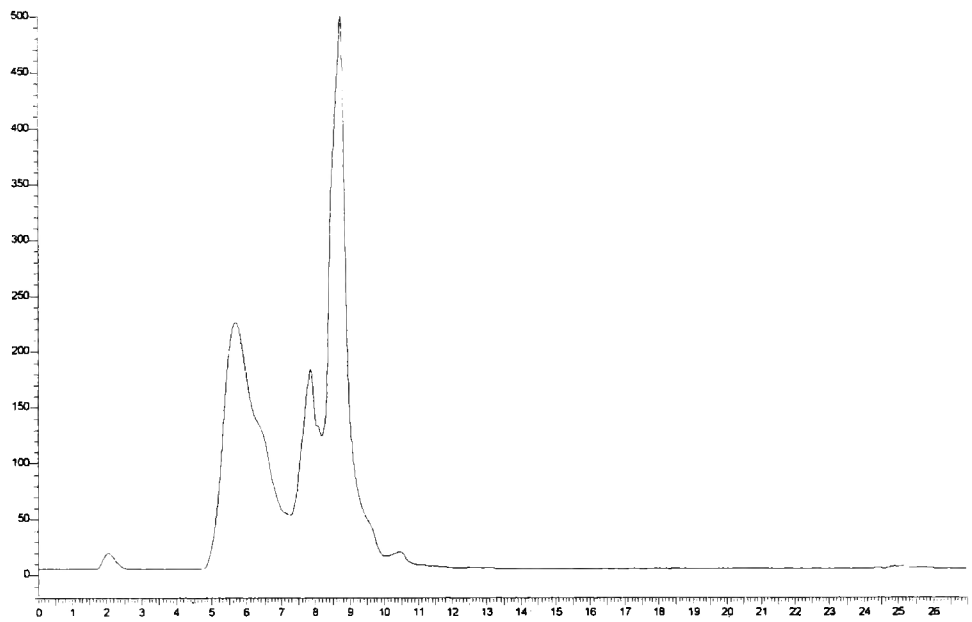

6.2.13 Chromatogram of purified conjugate with PAMAM dendrimer

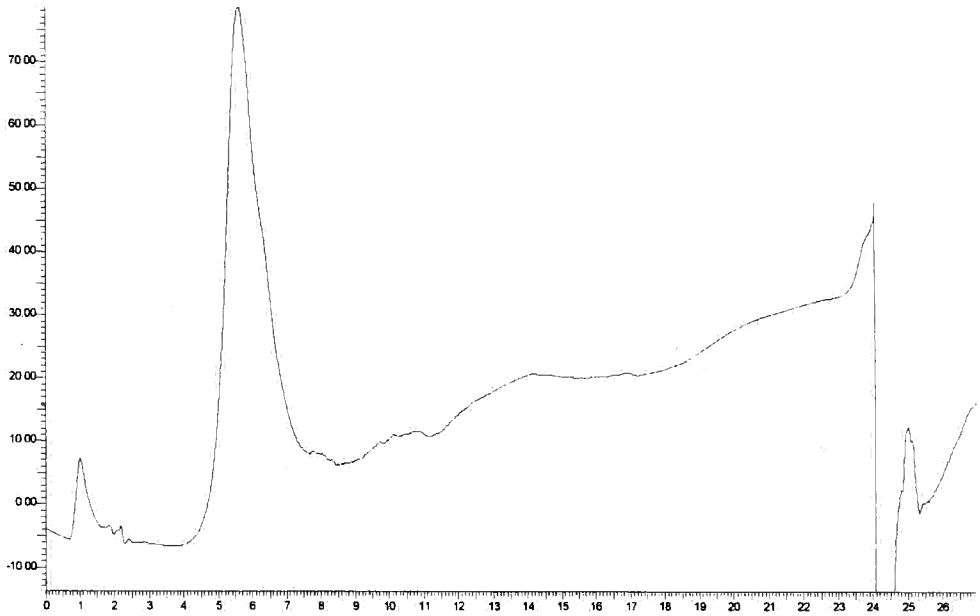

6.2.14 Chromatogram of purified conjugate with PAMAM dendrimer (fluorescence detection)

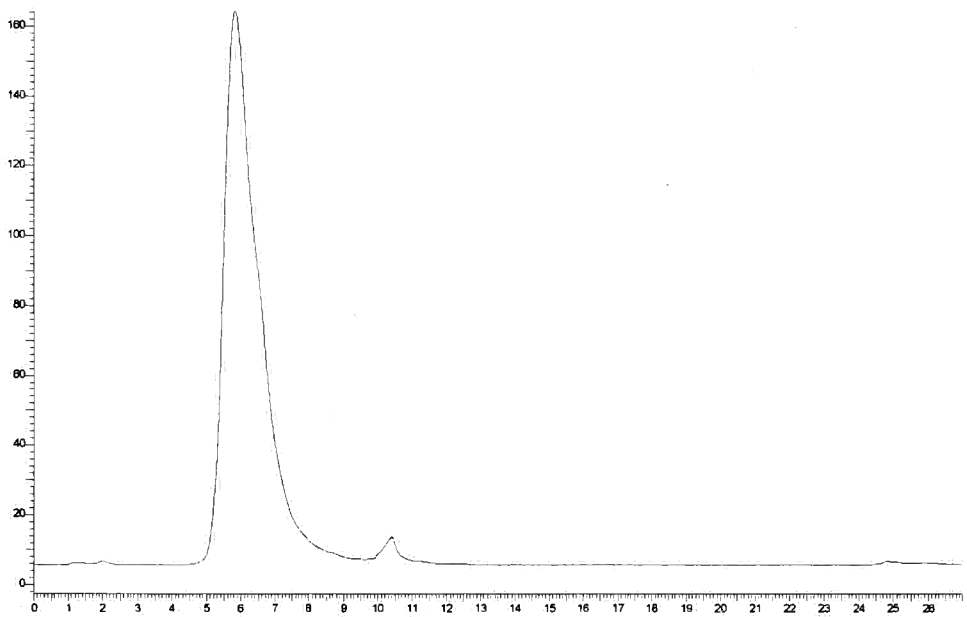

6.2.15 Chromatogram of purified quencher conjugate (Chromatography method D)

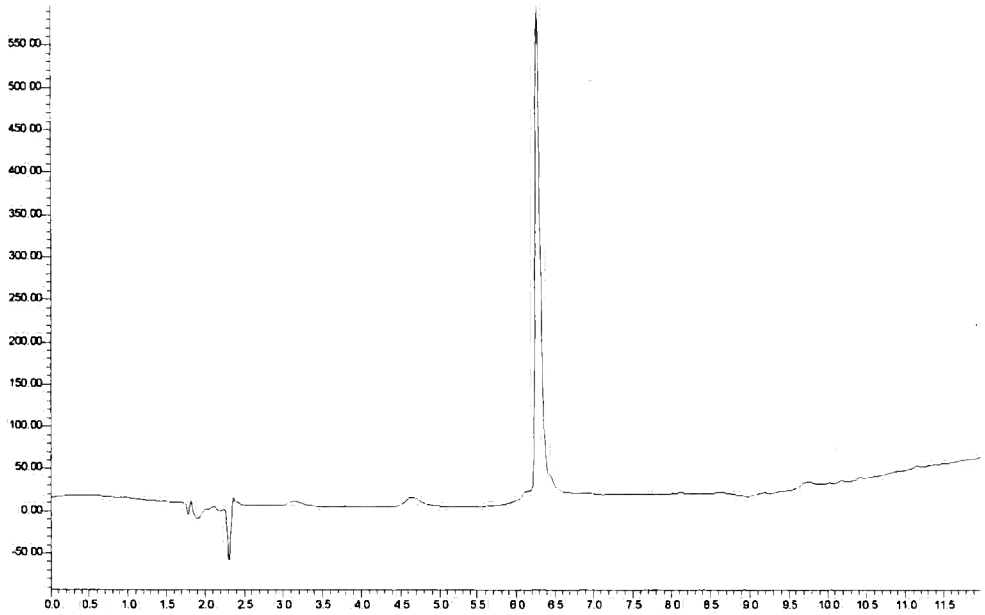

6.2.16 Chromatogram of cholesterol derivative conjugation reaction mixture

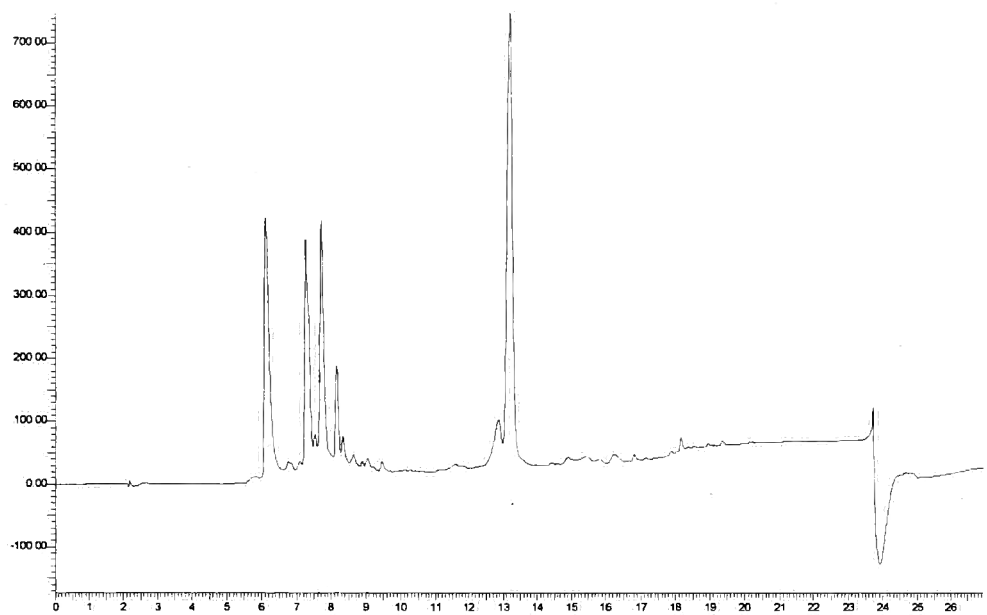

6.2.17 Chromatogram of purified cholesterol conjugate

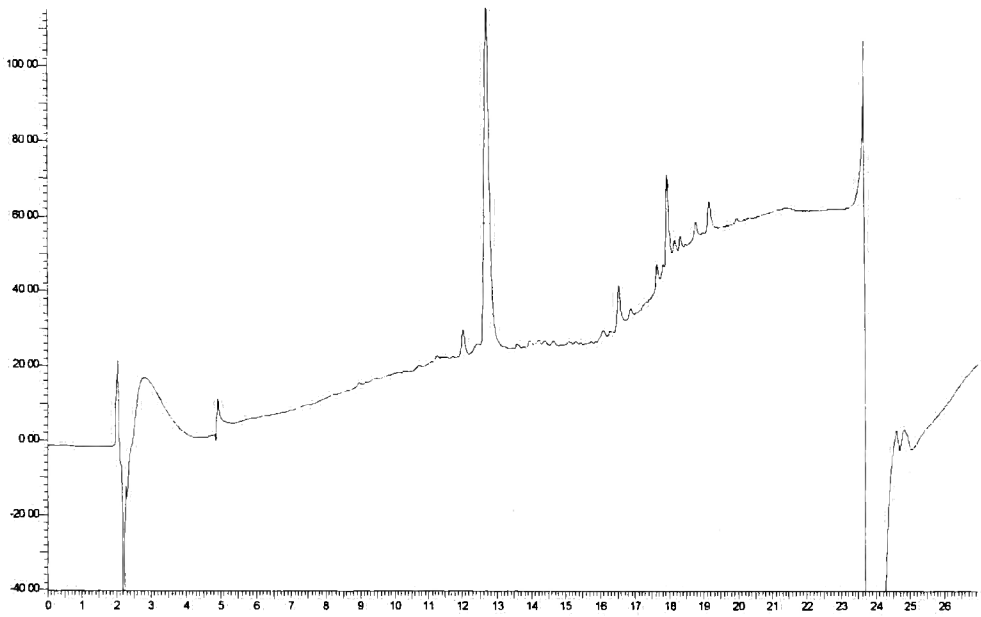

6.3 NMR data for cholesterol and its derivatives

All spectra were recorded in $CDCl_3$ at 295 K unless stated otherwise

6.3.1 ^{1}H NMR spectrum of Cholesterol

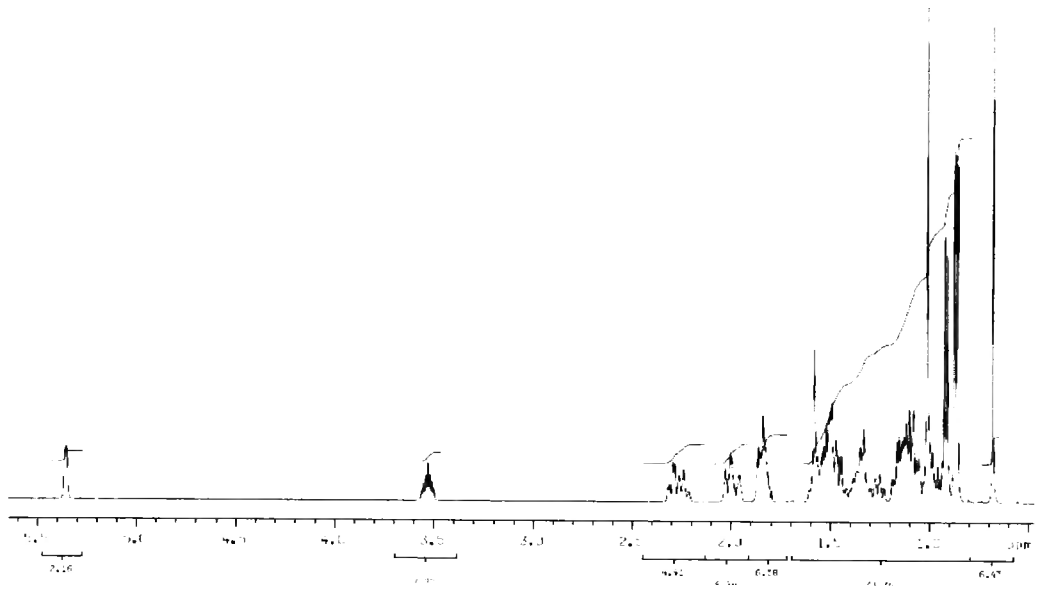

6.3.2 ^{1}H NMR spectrum of Boc protected cholesteryl ester 85

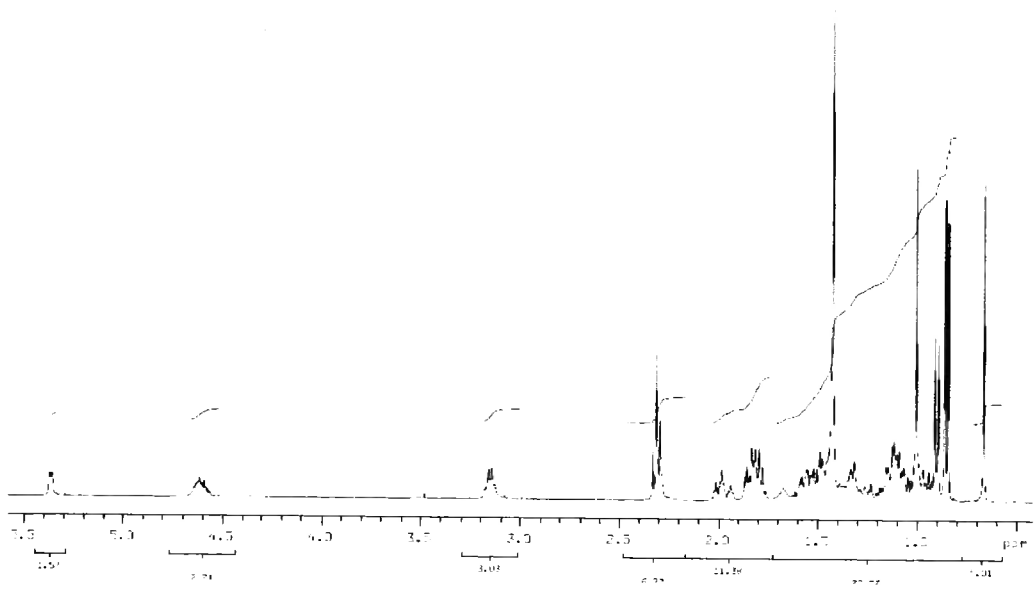

6.3.3 ^{1}H NMR spectrum of deprotected cholesteryl ester 86 (d_6-DMSO)

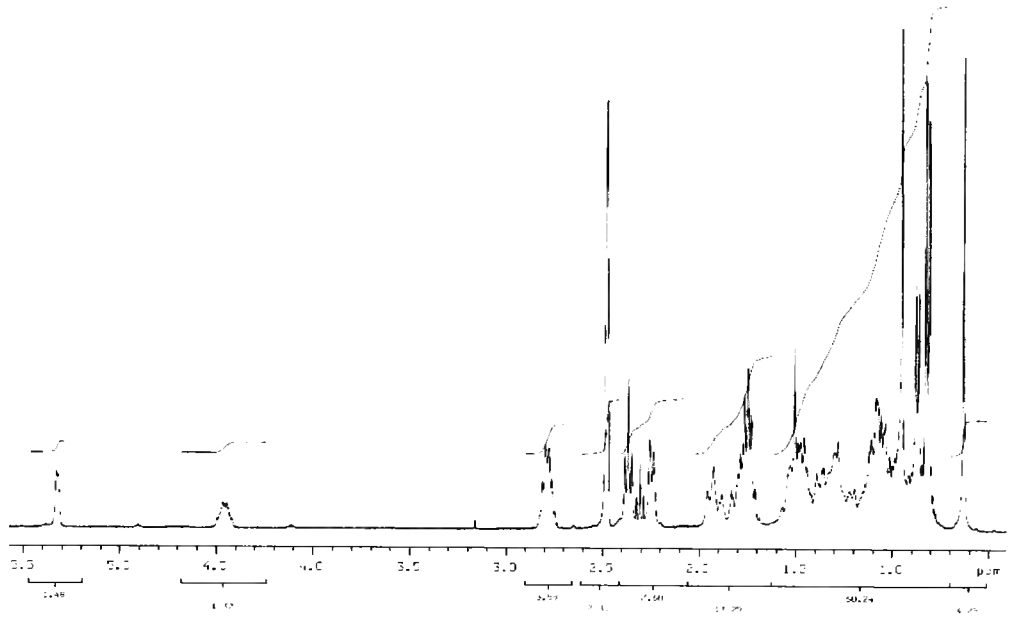

6.3.4 Expansion of ^{1}H NMR spectrum for the Boc protected cholestery ester 85

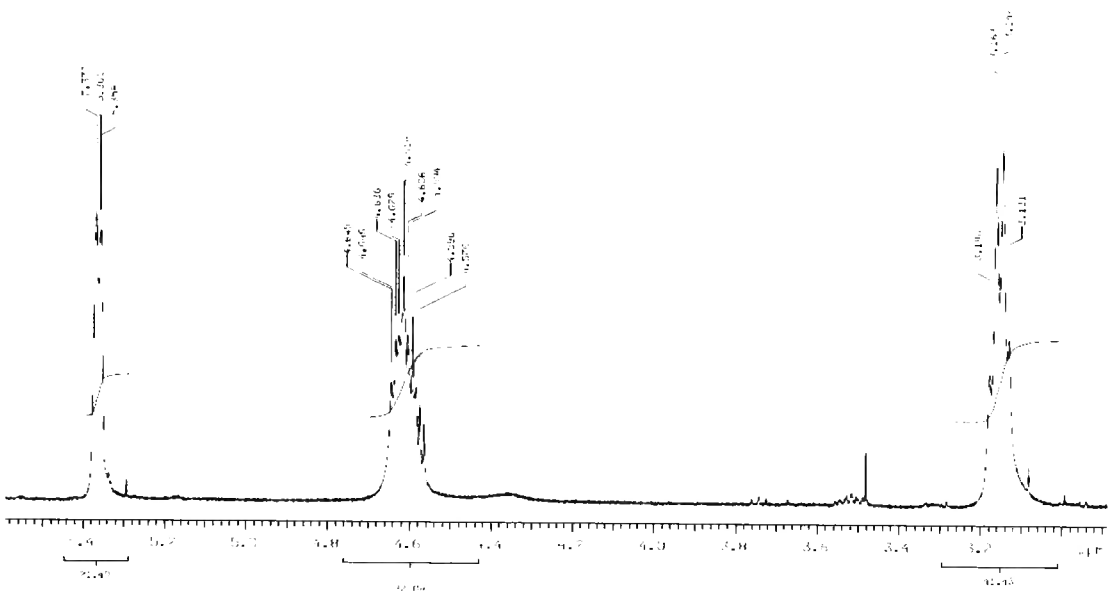

6.3.5 ^{13}C NMR spectrum of Cholesterol

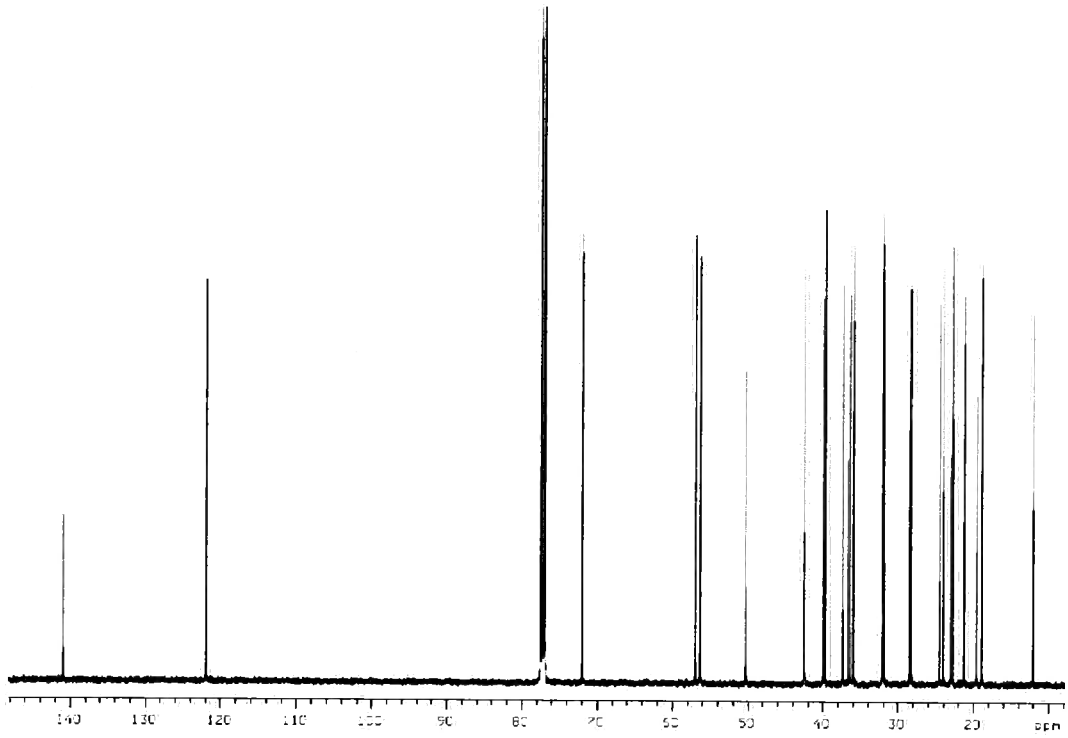

6.3.6 ^{13}C NMR spectrum of Boc protected cholesteryl ester 85

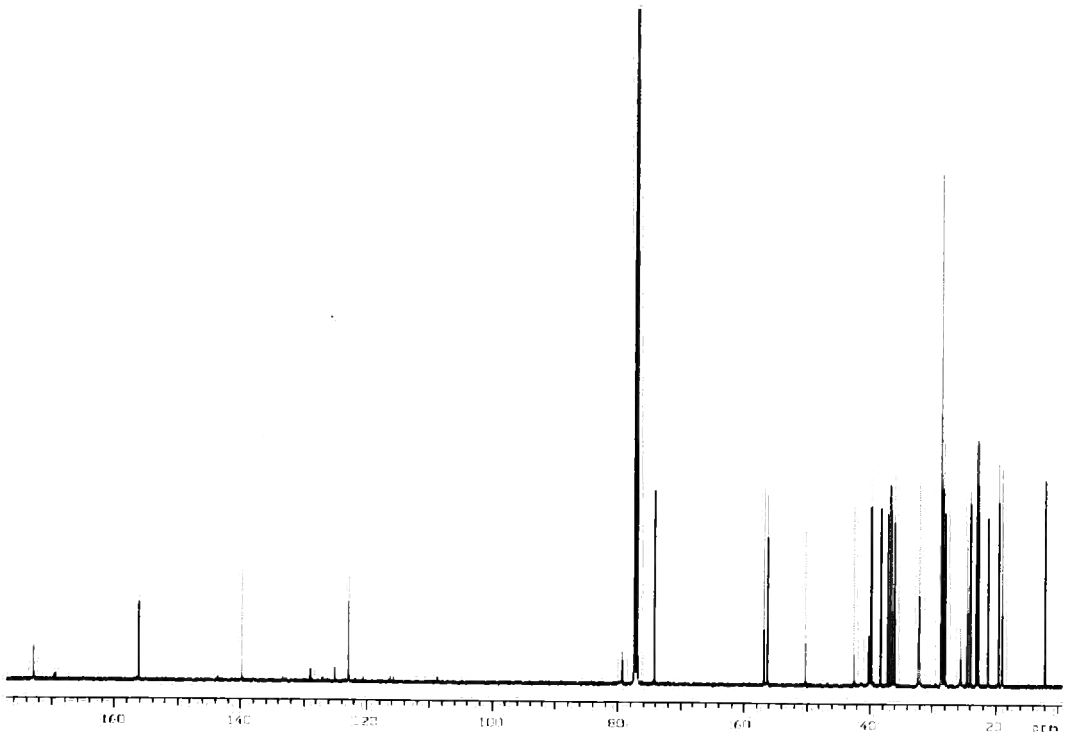

6.3.7 Aliphatic region of the ^{13}C spectrum of Cholesterol

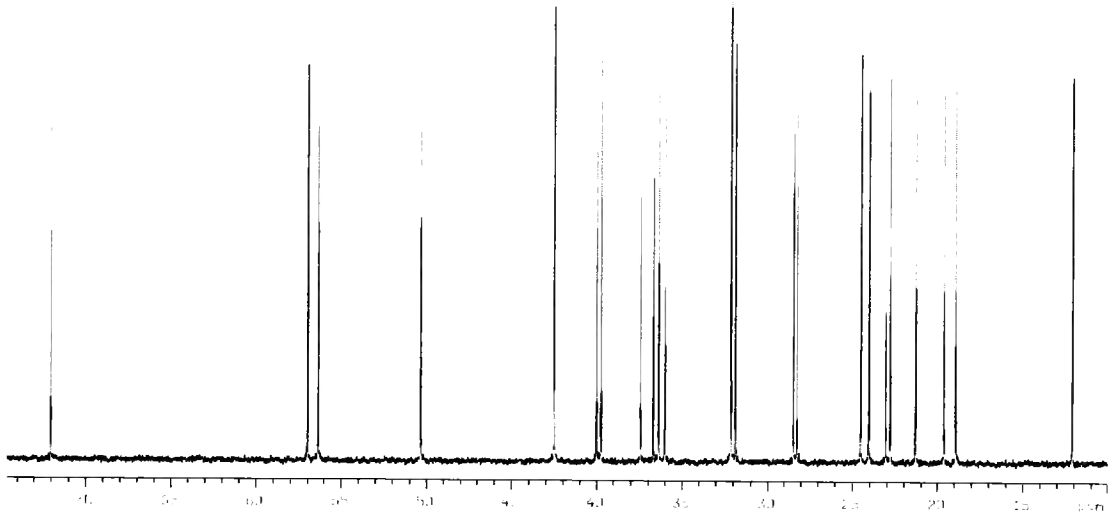

6.3.8 Aliphatic region of the ^{13}C spectrum of the Boc protected cholesteryl ester 85

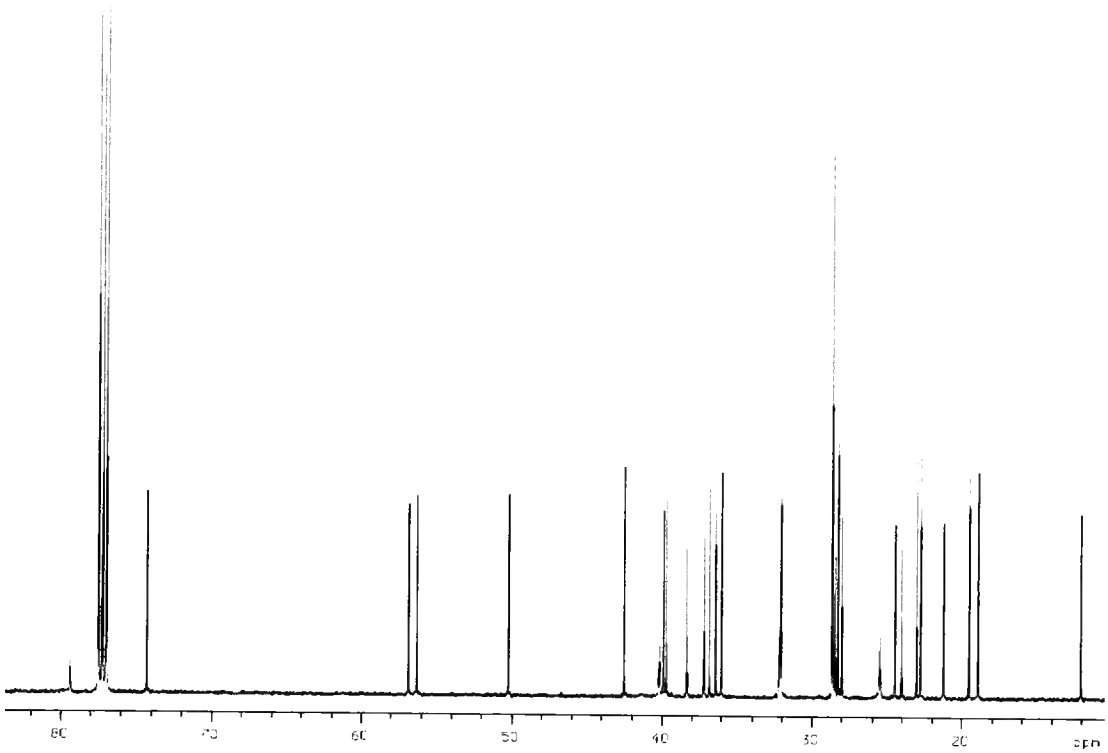

6.3.9 COSY spectrum of Cholesterol

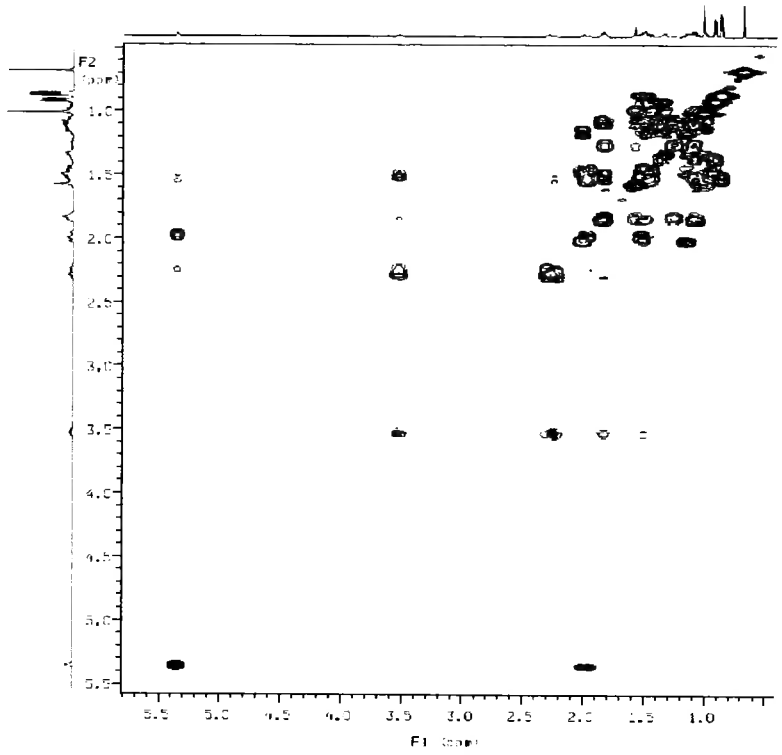

6.3.10 COSY spectrum of the Boc protected cholesteryl ester 85

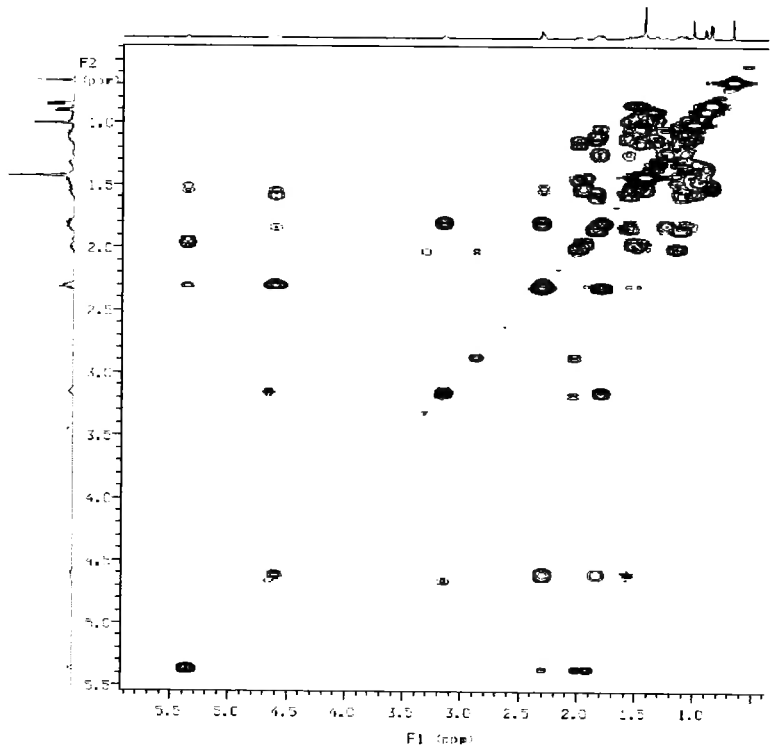

6.3.11 HSQC spectrum of Cholesterol

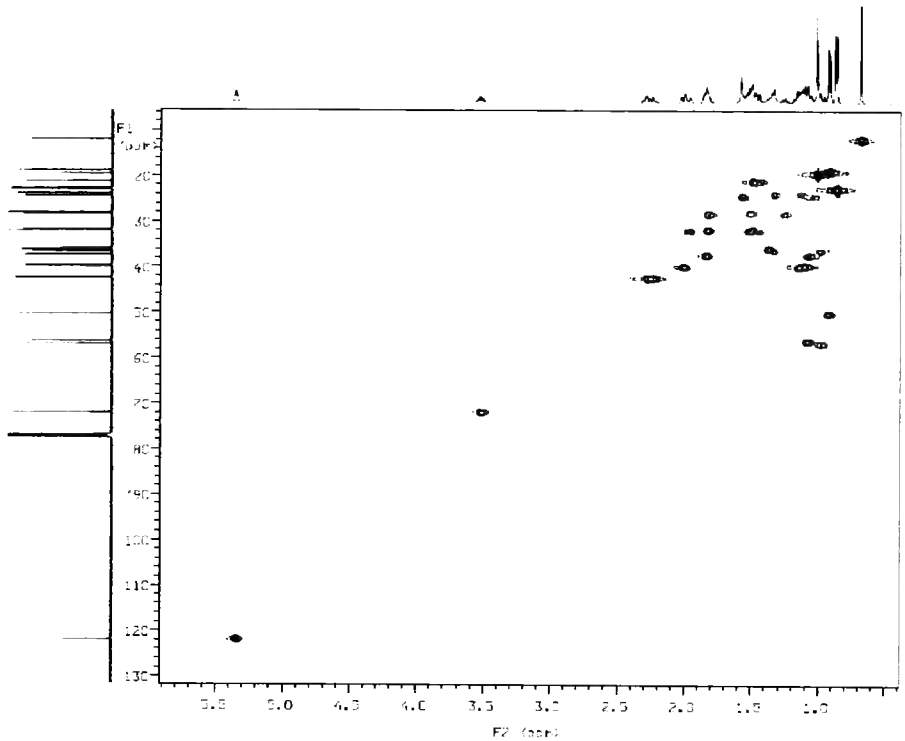

6.3.12 HSQC spectrum of the Boc protected cholesteryl ester 85

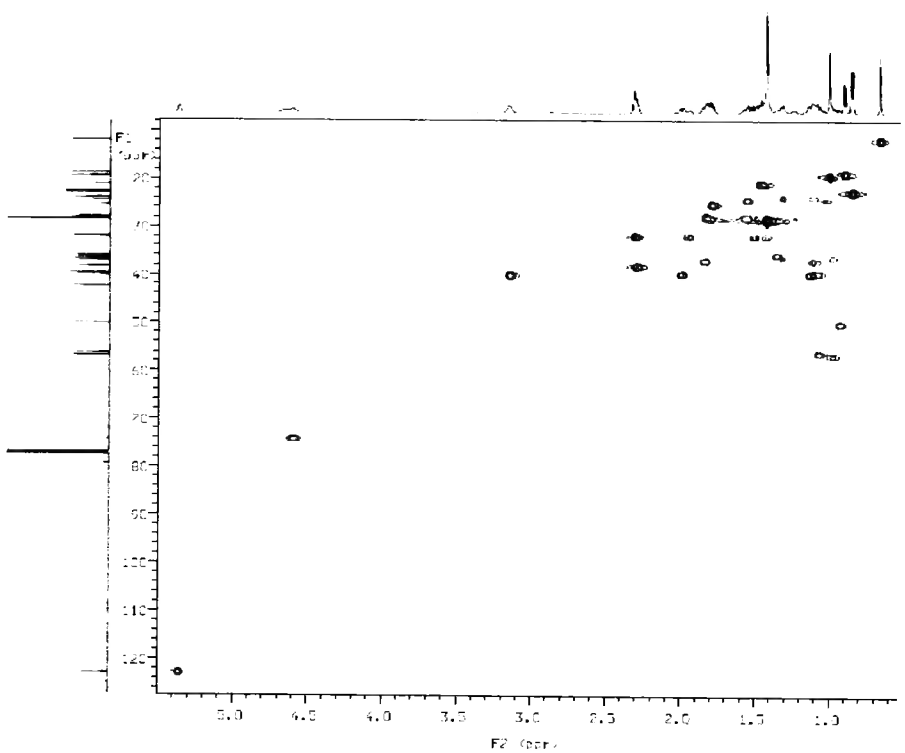

6.3.13 HMBC spectrum of Cholesterol

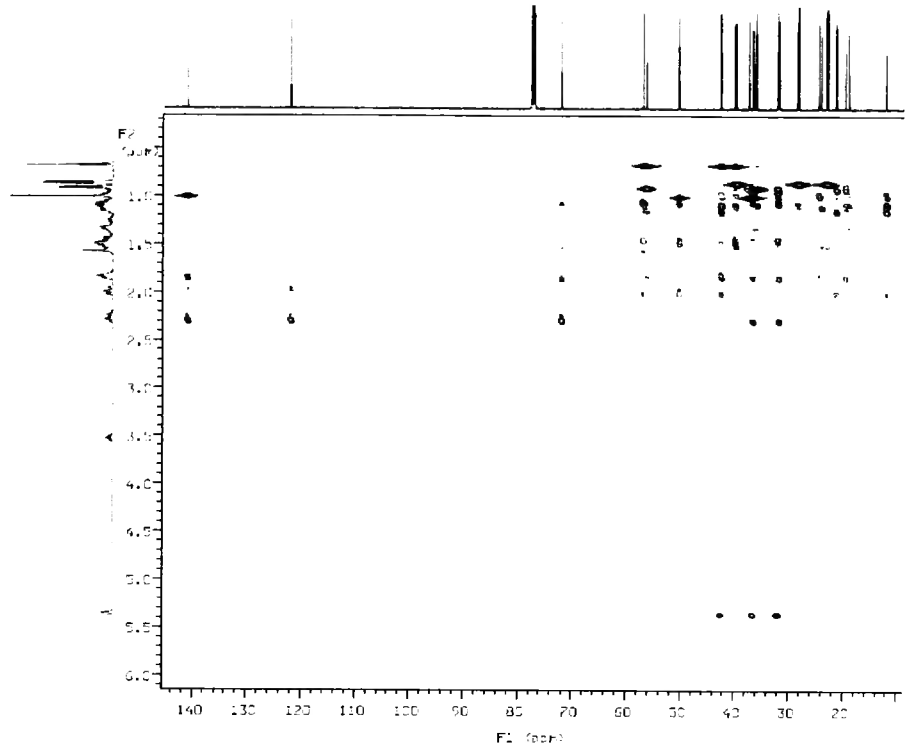

6.3.14 HMBC spectrum of the Boc protected cholesteryl ester 85

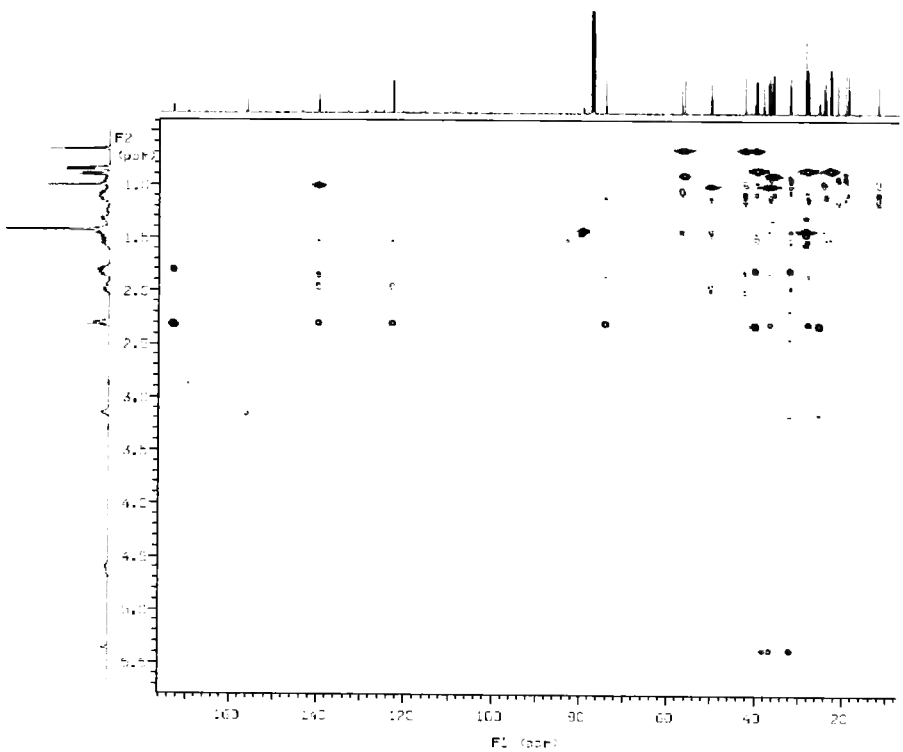

6.3 NMR data for cholesterol and its derivatives

All spectra were recorded in $CDCl_3$ at 295 K unless stated otherwise

6.3.1 ^{1}H NMR spectrum of Cholesterol

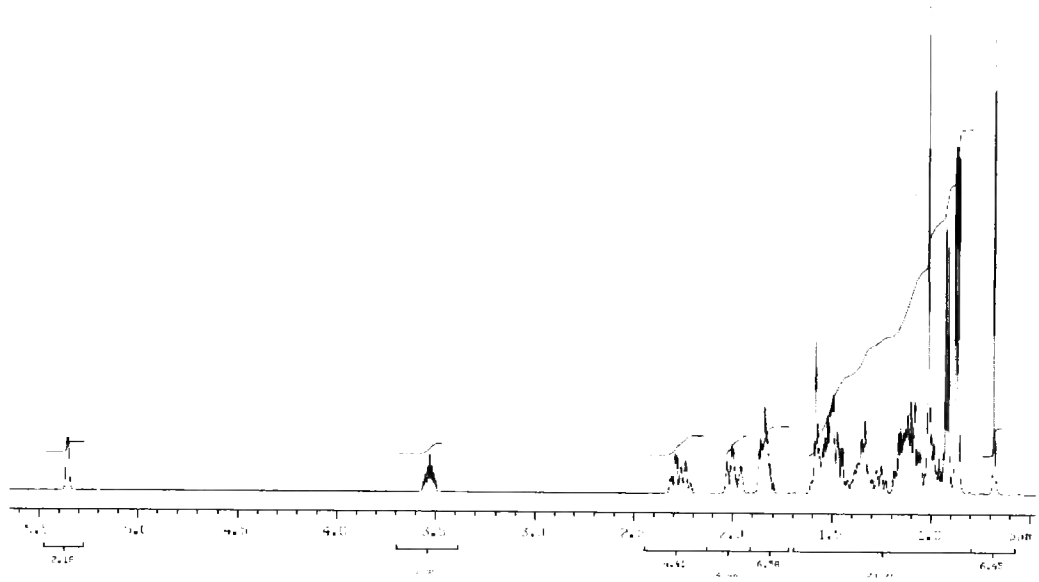

6.3.2 ^{1}H NMR spectrum of Boc protected cholesteryl ester 85

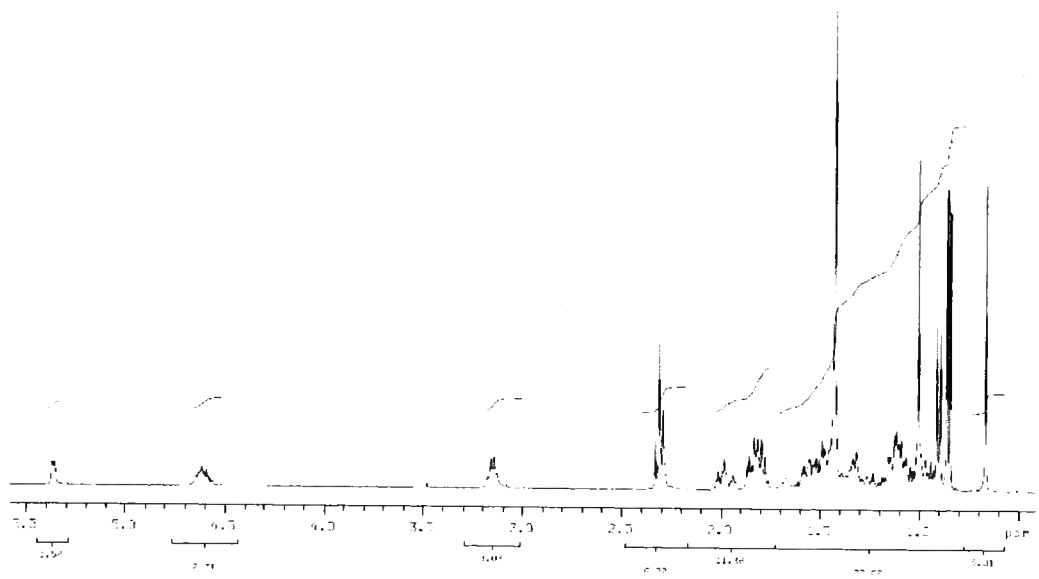

6.3.3 ^{1}H NMR spectrum of deprotected cholesteryl ester 86 (d_6-DMSO)

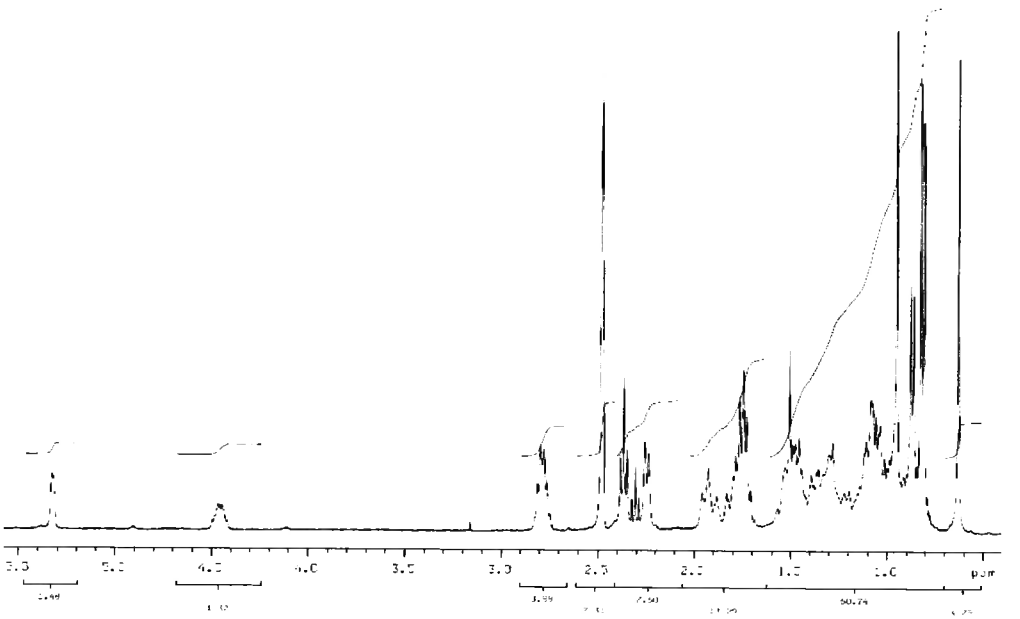

6.3.4 Expansion of ^{1}H NMR spectrum for the Boc protected cholestery ester 85

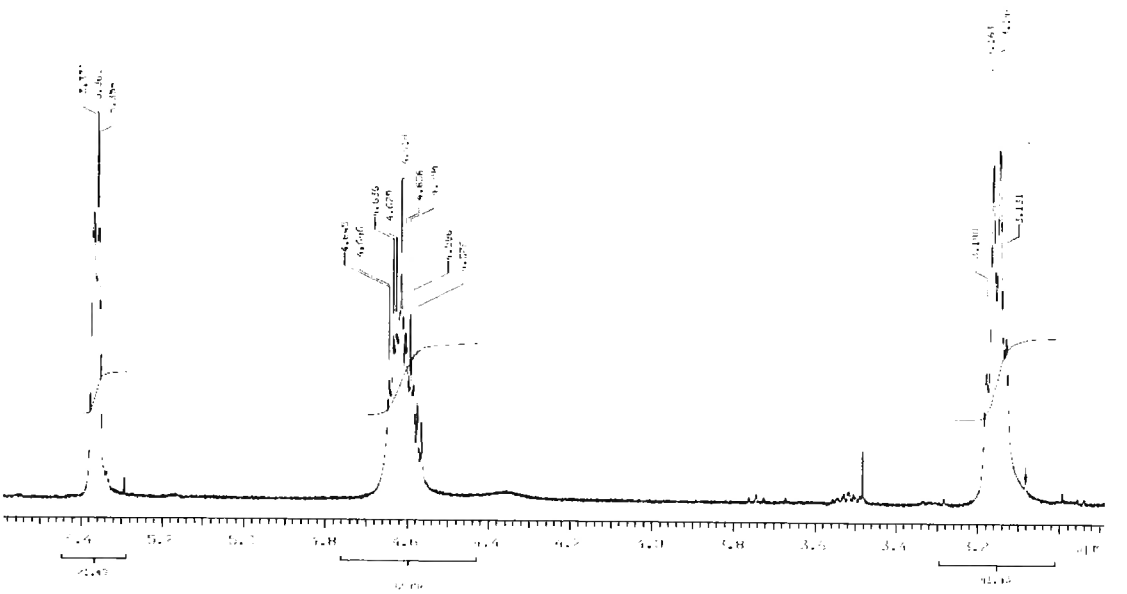

6.3.5 ^{13}C NMR spectrum of Cholesterol

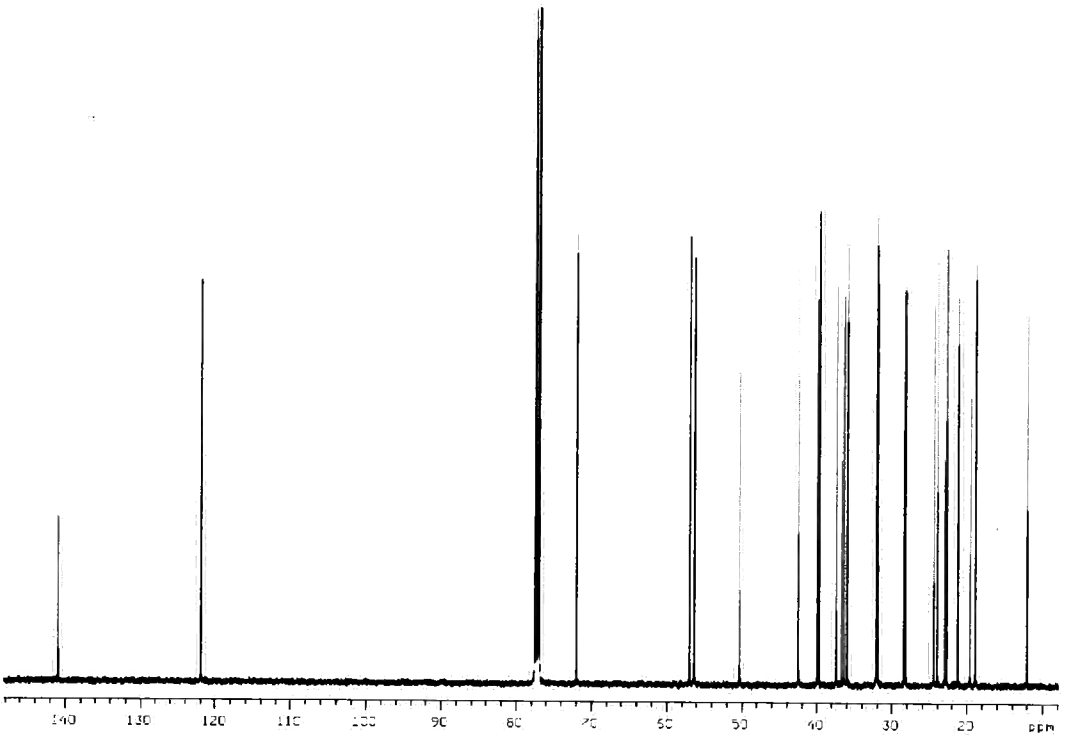

6.3.6 ^{13}C NMR spectrum of Boc protected cholesteryl ester 85

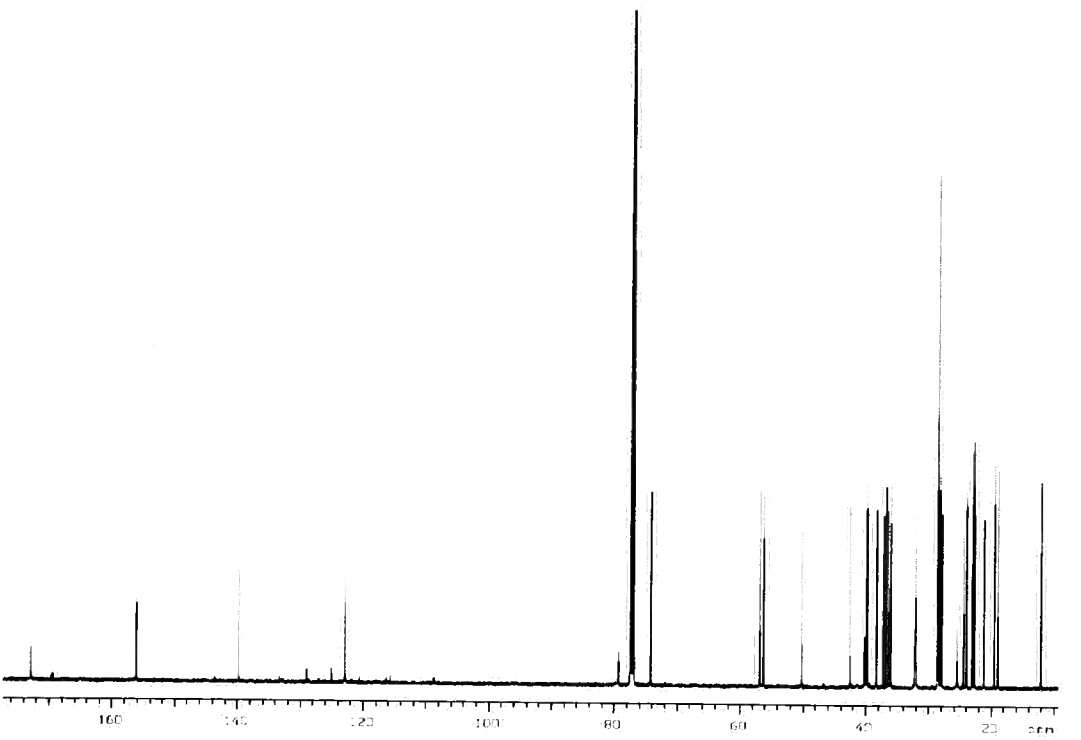

6.3.7 Aliphatic region of the ^{13}C spectrum of Cholesterol

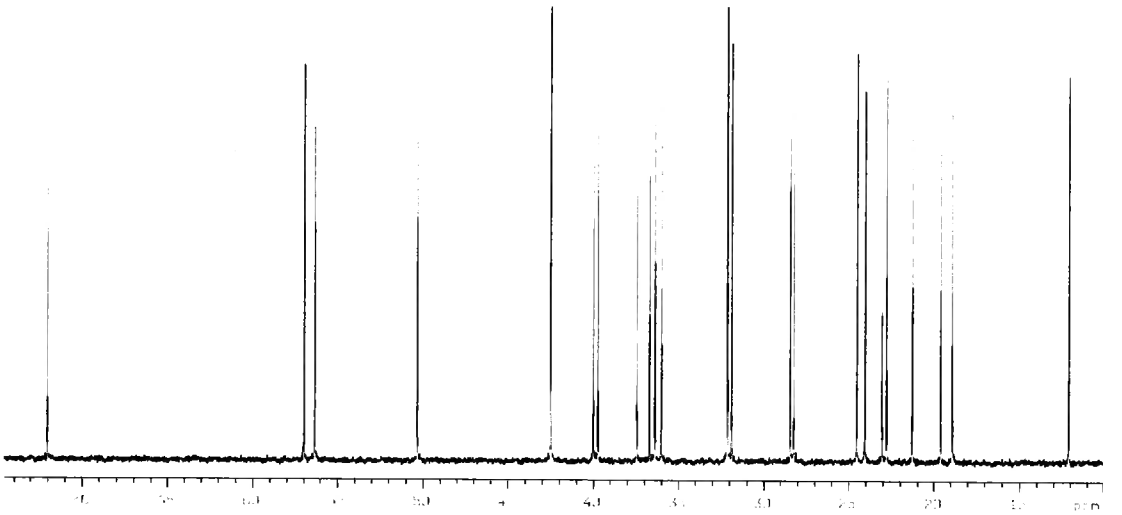

6.3.8 Aliphatic region of the ^{13}C spectrum of the Boc protected cholesteryl ester 85

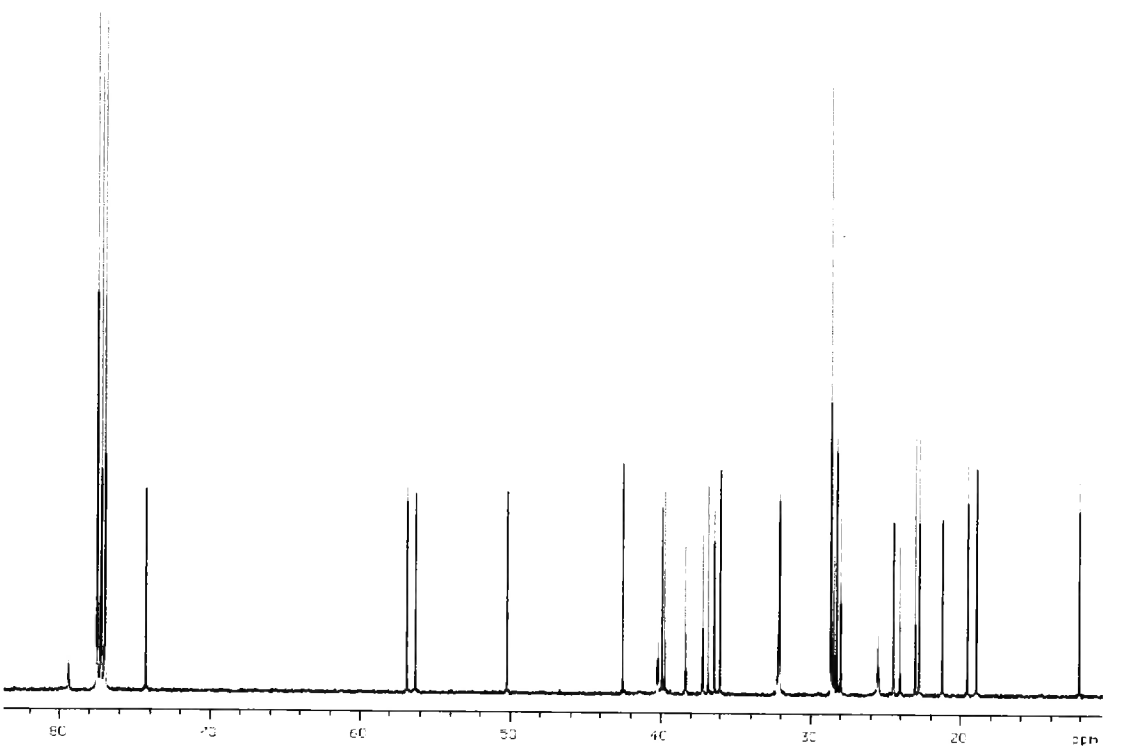

6.3.9 COSY spectrum of Cholesterol

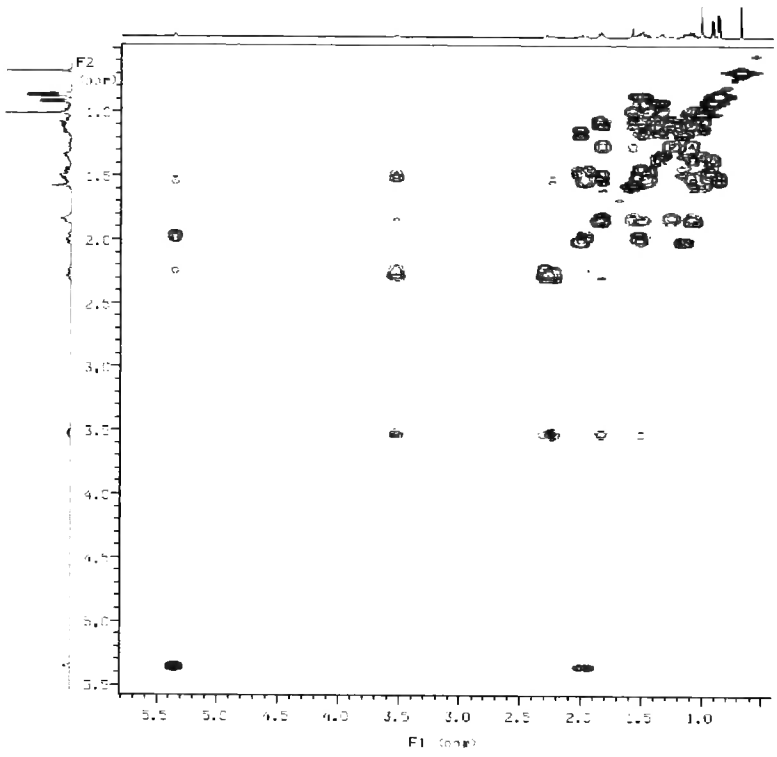

6.3.10 COSY spectrum of the Boc protected cholesteryl ester 85

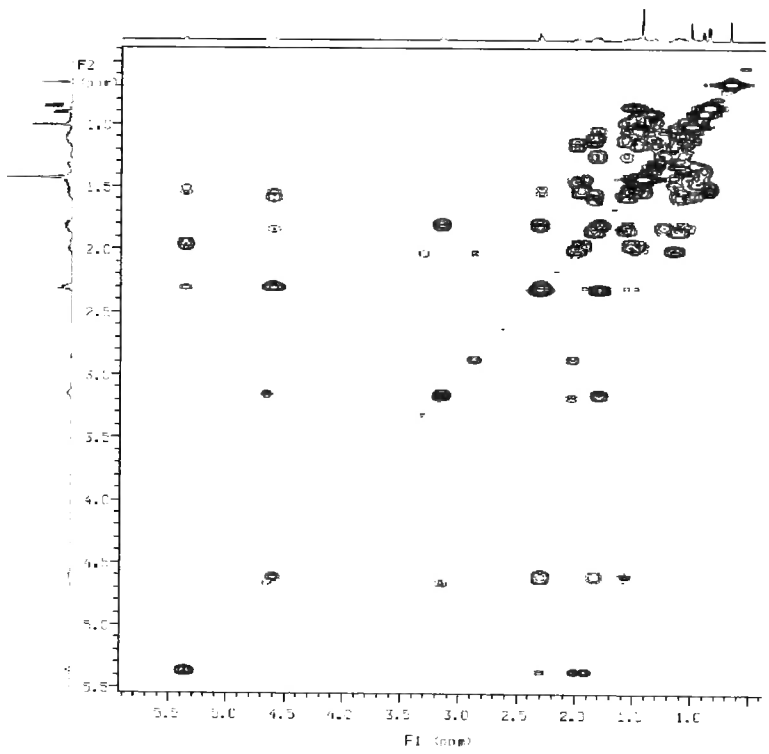

6.3.11 HSQC spectrum of Cholesterol

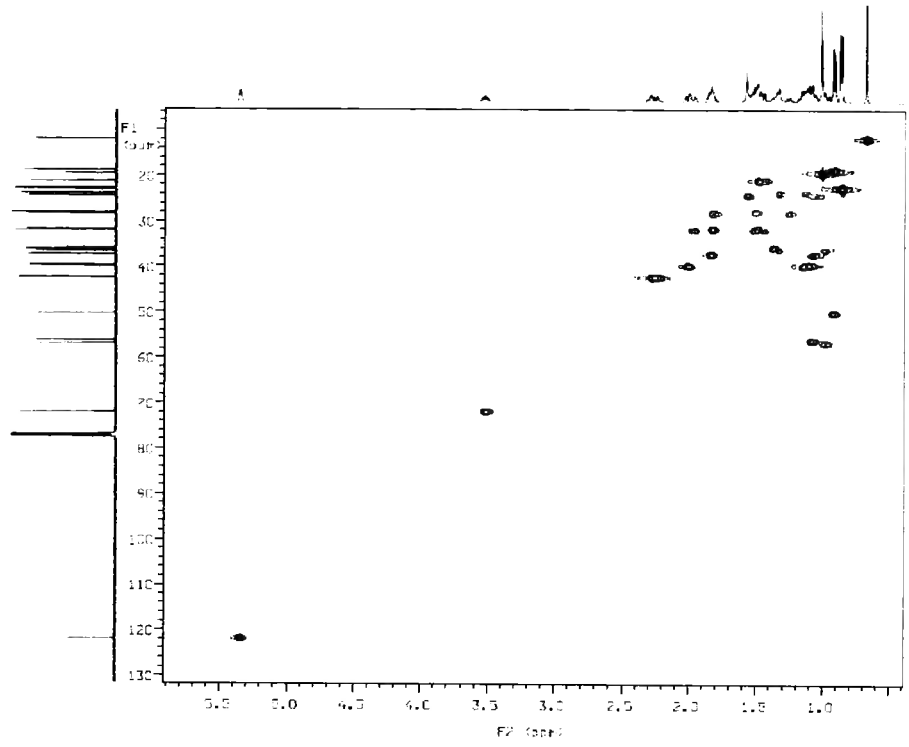

6.3.12 HSQC spectrum of the Boc protected cholesteryl ester 85

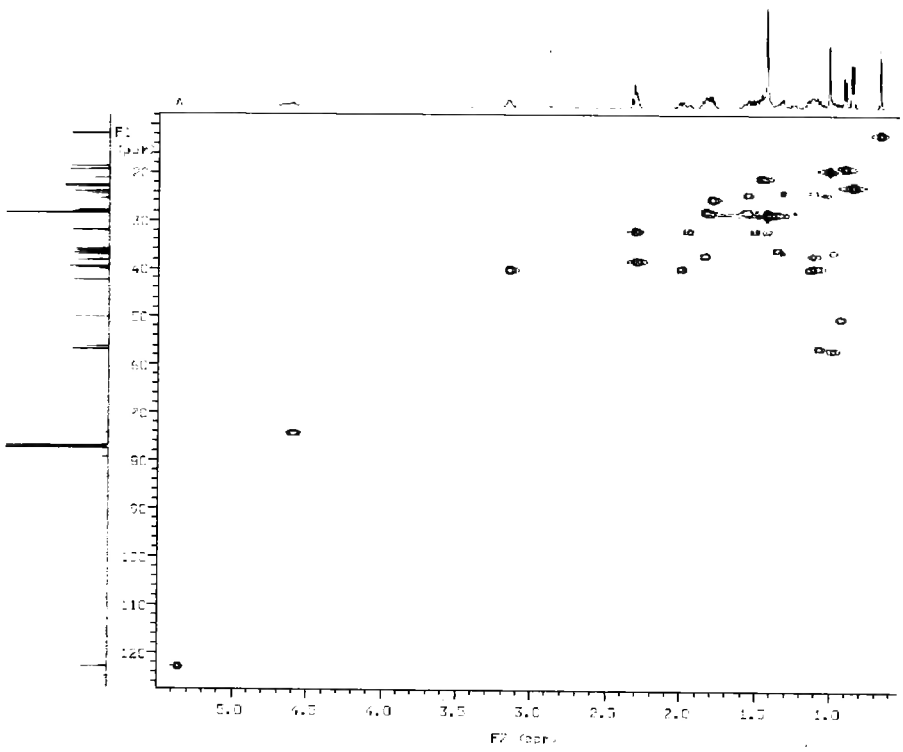

6.3.13 HMBC spectrum of Cholesterol

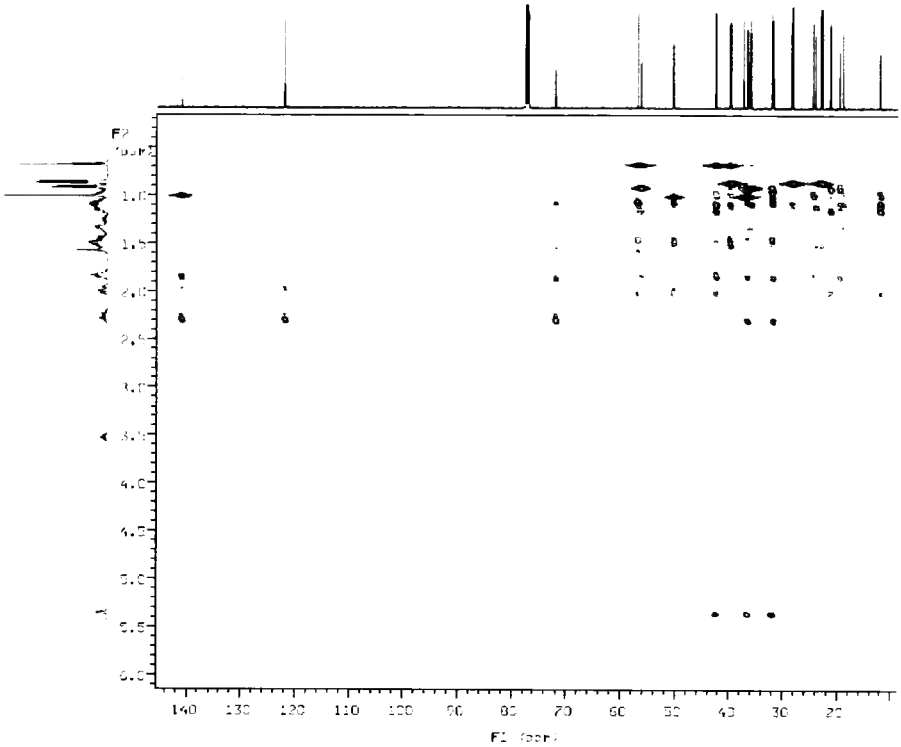

6.3.14 HMBC spectrum of the Boc protected cholesteryl ester 85